Spine: 5 mm

Volume 73 • Issue 2 • April-June 2024

Journal of The Anatomical Society of India • Volume 73 • Issue 2 • April-June 2024 • Pages 101-196

ISSN : 0003-2778

Scopus Indexed

JOURNAL OF THE ANATOMICAL SOCIETY OF INDIA

An International Journal

An Official Publication of Anatomical Society of India

Full text online at **https://journals.lww.com/joai**
Submit articles online at **https://review.jow.medknow.com/jasi**

Editor-in-Chief
Dr. Vishram Singh

Wolters Kluwer

Medknow

Journal of the Anatomical Society of India

Print ISSN: 0003-2778

GENERAL INFORMATION

About the Journal

Journal of the Anatomical Society of India (ISSN: Print 0003-2778) is peer-reviewed journal. The journal is owned and run by Anatomical Society of India. The journal publishes research articles related to all aspects of Anatomy and allied medical/surgical sciences. Pre-Publication Peer Review and Post-Publication Peer Review Online Manuscript Submission System Selection of articles on the basis of MRS system Eminent academicians across the globe as the Editorial board members Electronic Table of Contents alerts Available in both online and print form. The journal is published quarterly in the months of January, April, July and October.

Scope of the Journal

The aim of the *Journal of the Anatomical Society of India* is to enhance and upgrade the research work in the field of anatomy and allied clinical subjects. It provides an integrative forum for anatomists across the globe to exchange their knowledge and views. It also helps to promote communication among fellow academicians and researchers worldwide. The Journal is devoted to publish recent original research work and recent advances in the field of Anatomical Sciences and allied clinical subjects. It provides an opportunity to academicians to disseminate their knowledge that is directly relevant to all domains of health sciences.

The Editorial Board comprises of academicians across the globe.

JASI is indexed in Scopus, available in Science Direct.

Abstracting and Indexing Information

The journal is registered with the following abstracting partners:

Baidu Scholar, CNKI (China National Knowledge Infrastructure), EBSCO Publishing's Electronic Databases, Ex Libris – Primo Central, Google Scholar, Hinari, Infotrieve, Netherlands ISSN center, ProQuest, TdNet, Wanfang Data

The journal is indexed with, or included in, the following:

SCOPUS, Science Citation Index Expanded, IndMed, MedInd, Scimago Journal Ranking, Emerging Sources Citation Index.

Impact Factor® as reported in the 2023 Journal Citation Reports® (Clarivate Analytics, 2024): 0.2

Information for Authors

Article processing and publication charges will be communicated by the editorial office. All manuscripts must be submitted online at https://review.jow.medknow.com/jasi.

Subscription Information

A subscription to JASI comprises 4 issues. Prices include postage. Annual Subscription Rate for non-members-		
Rates of Membership (with effect from 1.1.2022)		
	India	**International**
Ordinary membership	INR 1500	US $ 100
Couple membership	INR 2250	
Life membership	INR 8000	US $ 900
Subscription Rates (till 31st August)		
Individual	INR 6000	US $ 650
Library/Institutional Trade discount of 10% for agencies only	INR 12000	US $ 1000
Subscription Rates (after 31st August)		
Individual	INR 6500	US $ 700
Library/Institutional	INR 12500	US $ 1050
The Journal of Anatomical Society of India (ISSN: 0003-2778) is published quarterly **Subscriptions** are accepted on a prepaid basis only and are entered on a calendar year basis. Issues are sent by standard mail Priority rates are available upon request.		

Information to Members/Subscribers

All members and existing subscribers of the Anatomical Society of India are requested to send their membership/existing subscription fee for the current year to the Treasurer of the Society on the following address: Prof (Dr.) Punit Manik, Treasurer, ASI, Department of Anatomy, KGMU, Lucknow - 226003. Email: punitamanik@yahoo.co.in. All payments should be made through an account payee bank draft drawn in favor of the **Treasurer, Anatomical Society of India,** payable at **Lucknow** only, preferably for **Allahabad Bank, Medical College Branch, Lucknow.** Outstation cheques/drafts must include INR 70 extra as bank collection charges.

All complaints regarding non-receipt of journal issues should be addressed to the Editor-in-Chief, JASI at editorjasi@gmail.com. The new subscribers may, please contact wkhlrpmedknow_subscriptions@wolterskluwer.com.

Requests of any general information like travel concession forms, venue of next annual conference, etc. should be addressed to the General Secretary of the Anatomical Society of India.

For mode of payment and other details, please visit www.medknow.com/subscribe.asp

Claims for missing issues will be serviced at no charge if received within 60 days of the cover date for domestic subscribers, and 3 months for subscribers outside India. Duplicate copies cannot be sent to replace issues not delivered because of failure to notify publisher of change of address. The journal is published and distributed by Wolters Kluwer India Pvt. Ltd. Copies are sent to subscribers directly from the publisher's address. It is illegal to acquire copies from any other source. If a copy is received for personal use as a member of the association/society, one cannot resale or give-away the copy for commercial or library use.

The copies of the journal to the subscribers are sent by ordinary post. The editorial board, association or publisher will not be responsible for non receipt of copies. If any subscriber wishes to receive the copies by registered post or courier, kindly contact the publisher's office. If a copy returns due to incomplete, incorrect or changed address of a subscriber on two consecutive occasions, the names of such subscribers will be deleted from the mailing list of the journal. Providing complete, correct and up-to-date address is the responsibility of the subscriber.

Nonmembers: Please send change of address information to subscriptions@medknow.com.

Advertising Policies

The journal accepts display and classified advertising. Frequency discounts and special positions are available. Inquiries about advertising should be sent to Wolters Kluwer India Pvt. Ltd, advertise@medknow. com.

The journal reserves the right to reject any advertisement considered unsuitable according to the set policies of the journal.

The appearance of advertising or product information in the various sections in the journal does not constitute an endorsement or approval by the journal and/or its publisher of the quality or value of the said product or of claims made for it by its manufacturer.

Addresses

Editorial Office

Dr. Vishram Singh, Editor-in-Chief, JASI
B5/3 Hahnemann Enclave, Plot No. 40, Sector 6, Dwarka Phase – 2,
New Delhi - 110 075, India.
Email: editorjasi@gmail.com

Published by

Wolters Kluwer India Pvt. Ltd
A-202, 2nd Floor, The Qube,
C.T.S. No.1498A/2 Village Marol, Andheri (East),
Mumbai - 400 059, India.
Phone: 91-22-66491818
Website: www.medknow.com

Printed at

Nikeda Art Printers Pvt. Ltd.,
Building No. C/3 - 14,15,16, Shree Balaji Complex, Vehele Road,
Village Bhatale, Taluka Bhiwandi, District Thane - 421302, India.

Journal of the Anatomical Society of India

Print ISSN: 0003-2778

GENERAL INFORMATION

About the Journal

Journal of the Anatomical Society of India (ISSN: Print 0003-2778) is peer-reviewed journal. The journal is owned and run by Anatomical Society of India. The journal publishes research articles related to all aspects of Anatomy and allied medical/surgical sciences. Pre-Publication Peer Review and Post-Publication Peer Review Online Manuscript Submission System Selection of articles on the basis of MRS system Eminent academicians across the globe as the Editorial board members Electronic Table of Contents alerts Available in both online and print form. The journal is published quarterly in the months of January, April, July and October.

Scope of the Journal

The aim of the *Journal of the Anatomical Society of India* is to enhance and upgrade the research work in the field of anatomy and allied clinical subjects. It provides an integrative forum for anatomists across the globe to exchange their knowledge and views. It also helps to promote communication among fellow academicians and researchers worldwide. The Journal is devoted to publish recent original research work and recent advances in the field of Anatomical Sciences and allied clinical subjects. It provides an opportunity to academicians to disseminate their knowledge that is directly relevant to all domains of health sciences.

The Editorial Board comprises of academicians across the globe.

JASI is indexed in Scopus, available in Science Direct.

Abstracting and Indexing Information

The journal is registered with the following abstracting partners:

Baidu Scholar, CNKI (China National Knowledge Infrastructure), EBSCO Publishing's Electronic Databases, Ex Libris – Primo Central, Google Scholar, Hinari, Infotrieve, Netherlands ISSN center, ProQuest, TdNet, Wanfang Data

The journal is indexed with, or included in, the following:

SCOPUS, Science Citation Index Expanded, IndMed, MedInd, Scimago Journal Ranking, Emerging Sources Citation Index.

Impact Factor® as reported in the 2023 Journal Citation Reports® (Clarivate Analytics, 2024): 0.2

Information for Authors

Article processing and publication charges will be communicated by the editorial office. All manuscripts must be submitted online at https://review.jow.medknow.com/jasi.

Subscription Information

A subscription to JASI comprises 4 issues. Prices include postage. Annual Subscription Rate for non-members-		
Rates of Membership (with effect from 1.1.2022)		
	India	**International**
Ordinary membership	INR 1500	US $ 100
Couple membership	INR 2250	
Life membership	INR 8000	US $ 900
Subscription Rates (till 31st August)		
Individual	INR 6000	US $ 650
Library/Institutional Trade discount of 10% for agencies only	INR 12000	US $ 1000
Subscription Rates (after 31st August)		
Individual	INR 6500	US $ 700
Library/Institutional	INR 12500	US $ 1050
The Journal of Anatomical Society of India (ISSN: 0003-2778) is published quarterly **Subscriptions** are accepted on a prepaid basis only and are entered on a calendar year basis. Issues are sent by standard mail Priority rates are available upon request.		

Information to Members/Subscribers

All members and existing subscribers of the Anatomical Society of India are requested to send their membership/existing subscription fee for the current year to the Treasurer of the Society on the following address: Prof (Dr.) Punit Manik, Treasurer, ASI, Department of Anatomy, KGMU, Lucknow - 226003. Email: punitamanik@yahoo.co.in. All payments should be made through an account payee bank draft drawn in favor of the **Treasurer, Anatomical Society of India,** payable at **Lucknow** only, preferably for **Allahabad Bank, Medical College Branch, Lucknow.** Outstation cheques/drafts must include INR 70 extra as bank collection charges.

All complaints regarding non-receipt of journal issues should be addressed to the Editor-in-Chief, JASI at editorjasi@gmail.com. The new subscribers may, please contact wkhlrpmedknow_subscriptions@wolterskluwer.com.

Requests of any general information like travel concession forms, venue of next annual conference, etc. should be addressed to the General Secretary of the Anatomical Society of India.

For mode of payment and other details, please visit www.medknow.com/subscribe.asp

Claims for missing issues will be serviced at no charge if received within 60 days of the cover date for domestic subscribers, and 3 months for subscribers outside India. Duplicate copies cannot be sent to replace issues not delivered because of failure to notify publisher of change of address. The journal is published and distributed by Wolters Kluwer India Pvt. Ltd. Copies are sent to subscribers directly from the publisher's address. It is illegal to acquire copies from any other source. If a copy is received for personal use as a member of the association/society, one cannot resale or give-away the copy for commercial or library use.

The copies of the journal to the subscribers are sent by ordinary post. The editorial board, association or publisher will not be responsible for non receipt of copies. If any subscriber wishes to receive the copies by registered post or courier, kindly contact the publisher's office. If a copy returns due to incomplete, incorrect or changed address of a subscriber on two consecutive occasions, the names of such subscribers will be deleted from the mailing list of the journal. Providing complete, correct and up-to-date address is the responsibility of the subscriber.

Nonmembers: Please send change of address information to subscriptions@medknow.com.

Advertising Policies

The journal accepts display and classified advertising. Frequency discounts and special positions are available. Inquiries about advertising should be sent to Wolters Kluwer India Pvt. Ltd, advertise@medknow. com.

The journal reserves the right to reject any advertisement considered unsuitable according to the set policies of the journal.

The appearance of advertising or product information in the various sections in the journal does not constitute an endorsement or approval by the journal and/or its publisher of the quality or value of the said product or of claims made for it by its manufacturer.

Addresses

Editorial Office

Dr. Vishram Singh, Editor-in-Chief, JASI
B5/3 Hahnemann Enclave, Plot No. 40, Sector 6, Dwarka Phase – 2,
New Delhi - 110 075, India.
Email: editorjasi@gmail.com

Published by

Wolters Kluwer India Pvt. Ltd
A-202, 2nd Floor, The Qube,
C.T.S. No.1498A/2 Village Marol, Andheri (East),
Mumbai - 400 059, India.
Phone: 91-22-66491818
Website: www.medknow.com

Printed at

Nikeda Art Printers Pvt. Ltd.,
Building No. C/3 - 14,15,16, Shree Balaji Complex, Vehele Road,
Village Bhatale, Taluka Bhiwandi, District Thane - 421302, India.

Journal of the Anatomical Society of India

Print ISSN: 0003-2778

EDITORIAL BOARD

Journal of the Anatomical Society of India

Volume 73 | Issue 2 | April-June 2024

CONTENTS

continued...

JASI

Neuroanatomical Basis of Schizophrenia

Schizophrenia is a chronic and serious mental disorder in which people interpret reality abnormally, i.e. they are not able to think, feel, and behave properly, which makes daily living difficult. It affects 1 million people per year in India and about 24 million people worldwide as reported by the WHO.[1]

Signs and Symptoms

People with schizophrenia present positive, cognitive, and negative symptoms as follows:[2]

A. Positive symptoms
   - Hallucinations: seeing or hearing things that do not exist. The people here strange voices and sounds which could horrify the individual
   - Delusions: False beliefs that are not based on reality. This belief remains unchanged despite the contradicting evidence
   - Disorganized speech and thinking: Impairing effective communication. The answers to questions may be partly or completely unrelated
   - Catatonia: Purposeless motor activity or aggressive behavior
   - Insomnia: Change in sleep patterns, viz., excessive sleeping.

B. Cognitive symptoms
   - Poor executive functioning: Inability to understand information to make proper decisions
   - Poor working memory: Inability to use information immediately after learning.

C. Negative symptoms
   - Flat effect: Reduced expression of emotions
   - Alogia: Reduced speech, i.e., reduction in quality of words spoken.
   - Avolition: Inability to begin and sustain activities due to decreased motivation
   - Anhedonia: Inability to experience pleasure, viz., in eating, touching, or even sex
   - Asociality: Reduced interest in socializing, i.e. engaging in interpersonal relationship
   - Uncleanliness: Poor hygiene, i.e. lack of self-care.

Classification

Based on clinical presentation, schizophrenia is classified into the following types:[3]

a. Paranoid schizophrenia: Dominated by delusion and hallucinations
b. Disorganized or hebephrenic schizophrenia: Disorganized thinking, emotional blunting that does not fit to situation, meaningless behavior
c. Catatonic schizophrenia: Stupor, i.e., no psychomotor activity, no interaction with the environment, motor stereotypes, abnormalities of posture, mutism, i.e., limited verbal response
d. Undifferentiated schizophrenia: Mixed symptoms, hence the person cannot be categorized into any of the above categories
e. Residual schizophrenia: Currently, the person has no positive symptoms of schizophrenia. Diagnosis is only based on the past history of at least one episode of schizophrenia.

However, mental health professionals no longer use the above terms of classification; instead, they use the umbrella term "schizophrenia."

Etiology

The exact cause of schizophrenia is not known, but the scientists think that it involves a combination of genetic, psychological, and environmental factors and altered brain structure and chemistry.[4]

The present account deals with only neuroanatomical basis of schizophrenia.

The anatomical regions of the brain mainly involved in schizophrenia are prefrontal area of the frontal lobe and medial temporal lobe of the temporal lobe.

The prefrontal cortex (PFC) of the brain plays an important role in executive functions, viz., decision-making and stress compatibility. It is, therefore, involved in behavioral flexibility and in extinction of fear responses.

The medial temporal lobe: It is located on the medial aspect of the temporal lobe and is distinct from the rest of the lobe which is composed of neocortex. (The medial temporal lobe includes amygdala, hippocampus, uncus, dentate gyrus, and parahippocampus).

The medial temporal lobe is involved in declarative/narrative memory, i.e., conscious memory of facts and events. Therefore, if damaged, it impairs new learning (anterograde amnesia) as well as memory for information that was required before the damage (retrograde amnesia).

The major changes seen in the brain of schizophrenic patients are:

(a) Volumetric abnormalities in cortical and subcortical structures

The cortical structures include cerebral cortexes of different lobes of the brain, especially those of frontal and temporal lobes.

The subcortical structures include thalamus basal ganglia (caudate nucleus, putamen, pallidum), hippocampus, amygdala and nucleus accumbens, etc

The volumetric abnormalities are as follows:

- Reduction in cortical volume, especially that of PFC and medial temporal lobe
- Reduction in volume of hippocampus, amygdala, and nucleus accumbens
- Increase in volume of caudate nucleus, putamen, and pallidum
- In addition, there is an increase in size of the lateral ventricles and widespread deficiency of tracts of white matter across multiple areas of the brain. The above findings are based on new imaging techniques, viz., magnetic resonance imaging, diffusion tensor imaging, and position emission tomography.

(b) Imbalance of neurotransmitters

In schizophrenia, there occurs an imbalance in following neurotransmitters in brain.

- Dopamine
- Serotonin
- Glutamate
- Gamma-amino-butyric acid (GABA).

Among all neurotransmitters involved in schizophrenia, dopamine plays a major role.

- The increase in dopamine activity in certain parts of the brain causes positive symptoms of schizophrenia, viz., hallucinations and delusions, while its reduced activity in other parts of the brain may affect negative and cognitive symptoms
- The increase in serotonin level causes disturbed behavioral and somatic functions, viz., perception, attention, mood, aggression, sexual drive, appetite, and sleep
- The reduced level of glutamate causes psychotic symptoms, viz., lack of restraint and social isolation
- The reduced level of GABA leads to mood disorder, insomnia, etc.

Treatment

The schizophrenia is not 100% curable, although its treatment can help manage symptoms and improve quality of life. The various modes of treatment are as follows:[5]

- Pharmacotherapy: with antipsychotic drugs, viz., haloperidol, fluphenazine, and chlorpromazine. Recently, a new drug KarXT has been approved, which reduces both positive and negative symptoms
- Cognitive behavioral therapy: It is a common type of psychotherapy/talk therapy by counselors, mental health social workers, etc.
- Electroconvulsive therapy: It can reduce the chances of relapse as long as you undergo follow-up treatment. It should be given preferably by an anesthetist.

Vishram Singh, Rashi Singh[1], Gaurav Singh[2]

Department of Anatomy, Kasturba Medical College, Mangalore, Manipal Academy of Higher Education, Manipal, Karnataka, [1]Department of Pediatric and Preventive Dentistry, Santosh Dental College and Hospital, Ghaziabad, Uttar Pradesh, [2]Clinical Editor, British Medical Journal, Noida, NCR Delhi, India

Address for correspondence: *Prof. Vishram Singh, B5/3 Hahnemann Enclave, Plot No. 40, Sector 6, Dwarka Phase-2, New Delhi - 110 075, India.*
E-mail: drvishramsingh@gmail.com

References

1. World Health Organization. The World Health Report 2001: Mental Health: New Understanding, New Hope. World Health Organization; 2001.
2. Mosolov SN, Yaltonskaya PA. Primary and secondary negative symptoms in schizophrenia. Front Psychiatry 2021;12:766692.
3. McCutcheon RA, Reis Marques T, Howes OD. Schizophrenia-an overview. JAMA Psychiatry 2020;77:201-10.
4. Volkan K. Schizophrenia: Epidemiology, causes, neurobiology, pathophysiology, and treatment. J Health Med Sci 2020;3:487-521.
5. American Psychiatric Association. The American Psychiatric Association Practice Guideline for the Treatment of Patients with Schizophrenia. American Psychiatric Association; 2020.

Article Info

Received: 13 June 2024
Accepted: 13 June 2024
Available online: 27 June 2024

Access this article online

Quick Response Code:

Website: https://journals.lww.com/joai

DOI: 10.4103/jasi.jasi_86_24

How to cite this article: Singh V, Singh R, Singh G. Neuroanatomical basis of schizophrenia. J Anat Soc India 2024;73:101-2.

Original Article

The Distribution of Ectopic Pregnancy in Natural Pregnancy and the Comparison of Diagnostic Efficacy between Transabdominal Ultrasound and Transvaginal Ultrasound

Xiyan Shao[1,2], Qi Xie[1,3], Ming Li[4]

[1]Medical Imaging Center, The First Clinical Medical College, Jinan University, [3]Medical Imaging Department of Nansha, Guangzhou First People's Hospital, Guangzhou, [2]Ultrasound Medicine Department, [4]Health Management Center, The Second Affiliated Hospital, School of Medicine, The Chinese of University of Hong Kong (Shenzhen), Shenzhen, Canton, China

Abstract

Objective: The objective of this study was to analyze the advantages and disadvantages of transabdominal and transvaginal color Doppler ultrasound in the diagnosis of early ectopic pregnancy (EP) and to evaluate the value of two kinds of ultrasonography in the diagnosis of early EP. **Patients and Methods:** One hundred and ten EP patients who underwent preoperative transvaginal and transabdominal ultrasound examinations and were confirmed by surgical pathology were included in the study. The sonographic findings of different methods were analyzed, and the diagnostic effects of the two ultrasound methods were compared. **Results:** The positive rate of transvaginal ultrasound for EP masses was 100%, while the positive rate of transabdominal ultrasound was 67.27%, with a significant difference ($P < 0.0001$). For 53 cases of EP located in the ampulla, the diagnostic rate of transvaginal ultrasound was 100%, while transabdominal ultrasound was only 58.49%, with a significant difference ($P < 0.0001$). The sensitivity, specificity, positive predictive value, and negative predictive value of ultrasound in diagnosing EP rupture were 94.44%, 58.67%, 52.31%, and 58.67%, respectively. **Conclusions:** The diagnostic efficacy of transvaginal ultrasound for EP is significantly better than that of transabdominal ultrasound. Therefore, for patients suspected of EP and without contraindication, transvaginal ultrasound is recommended as the first choice. Both peritoneal effusion by ultrasound and intraoperative abdominal hemorrhagic effusion had low specificity in diagnosing EP rupture. The diagnosis of EP rupture requires intraoperative direct vision.

Keywords: *Diagnosis, early ectopic pregnancy, transabdominal color Doppler ultrasound, transvaginal color Doppler ultrasound*

Introduction

Ectopic pregnancy (EP), also known as extrauterine pregnancy, refers to the implantation and development of the zygote outside the uterine cavity.[1,2] The most common ectopic implantation site is the fallopian tube, and a few patients also have EP in the ovary, cervix, abdominal cavity, and other regions.[1] Hemorrhage caused by EP is an important cause of early pregnancy death. Early and timely diagnosis is the most effective way to reduce the life risk of pregnant women. However, clinically, EP is a disease that is difficult to identify according to the medical history and clinical physical examination. The medical history and physical examination characteristics are not sensitive and specific to diagnosis.[3] It is estimated that 40% of EPs are not diagnosed when they first appear symptoms.[1] Even experienced gynecologists cannot detect more than half of EP masses in physical examination.[4] It can be seen that the diagnosis of EP is difficult only from a clinical perspective. Therefore, the information obtained from laboratory data and imaging examination is an important part of diagnosing EP.[1]

The imaging method for obstetric examination requires minimizing radiation exposure to the greatest extent possible and should be used for all obstetric evaluations in accordance with the "As Low As (is) Reasonably Achievable" practice standard.[5] Therefore, no-radiation, static, and dynamic real-time imaging of human organs and lesions is the preferred imaging method for the diagnosis of EP. At present, there are two kinds of ultrasound methods that can be used to evaluate EP: less invasive transabdominal ultrasound and more invasive but more diagnostic intravaginal ultrasound.[1,2,5-7] There is only one absolute contraindication for transvaginal ultrasound,

How to cite this article: Shao X, Xie Q, Li M. The distribution of ectopic pregnancy in natural pregnancy and the comparison of diagnostic efficacy between transabdominal ultrasound and transvaginal ultrasound. J Anat Soc India 2024;73:103-9.

Article Info

Received: 26 October 2023
Revised: 06 December 2023
Accepted: 17 December 2023
Available online: 27 June 2024

Address for correspondence:
Dr. Qi Xie, Department of Medical Imaging, School of Medicine, Nansha Hospital, Guangzhou First People's Hospital, South China University of Technology, Guangzhou 511457, Guangdong, China.
E-mail: xieqi8@yeah.net

Access this article online

Website: https://journals.lww.com/joai
DOI: 10.4103/jasi.jasi_111_23
Quick Response Code:

i.e., gynecological surgery recently. There are no absolute contraindications for transabdominal ultrasound.[1] However, the diagnosis of early EP by transabdominal ultrasound is vulnerable to obesity and intestinal gas, which may lead to missed diagnosis or misdiagnosis.[4] With the widespread application of transvaginal ultrasound in clinical practice, some studies[2,5] have shown that transvaginal ultrasound is not easily affected by intestinal gases and has high diagnostic accuracy for gynecological and obstetric diseases.

Clinical practice also requires continuous improvement of ultrasonic evaluation of patients with EP to help reduce the mortality related to EP rupture.[8-10] In order to determine the diagnostic efficacy of the two ultrasound methods for EP, we retrospectively collected the patients who were suspected of EP due to acute abdomen from January 1, 2020, to December 31, 2022. Finally, 110 patients with confirmed diagnosis by surgery and pathology were included, and preoperative transvaginal and transabdominal ultrasound examinations were performed simultaneously with complete information. By analyzing the ultrasonographic manifestations of different methods, and comparing the diagnostic value of the two ultrasound methods for EP, we hope to provide experience for clinical timely selection of effective imaging methods for the diagnosis of EP.

Patients and Methods

Study object

From January 1, 2020, to December 31, 2022, 554 female patients with suspected EP due to acute abdomen were collected from the Department of Gynecology, the Second Affiliated Hospital of School of Medicine, the Chinese University of Hong Kong (Shenzhen).

Inclusion criteria

The inclusion criteria of this study were as follows: (1) having complete medical records; (2) laparoscopy or curettage was performed in our hospital, and EP was confirmed by pathology; (3) quantitative detection of serum *β*-human chorionic gonadotropin (β-hCG) was performed before and 24–48 h after surgery; and (4) both vaginal and abdominal ultrasound examinations were performed before surgery.

Exclusion criteria

The exclusion criteria of this study were as follows: (1) concomitant acute pelvic inflammatory disease and threatened abortion and (2) no simultaneous transabdominal and transvaginal ultrasound gynecological ultrasound examinations were performed in this hospital.

Finally, 110 patients with EP were included, all of whom were naturally conceived. The age range is 20–47 years, with an average of 32.5 ± 5.7. At the time of treatment, the patient had a menopause of 32–88 days, with an average of 48.54 days. 23 cases were primiparous women and 87 cases were multiparous women; among them, 20 cases underwent 1 cesarean section, and 11 cases underwent 2 cesarean sections. 110 patients had 1-9 pregnancies with an average of 3.54, and 1-3 deliveries with an average of 1.17. Thirty-eight cases had no history of miscarriage (34.9%), and 72 cases had a history of 1–6 miscarriages. Ninety-six cases (80.7%) had no history of EP. Twelve cases had EP of one time (10.9%), and 2 cases had EP of two times (1.7%). Ten cases underwent fallopian tube surgery: 1 case underwent ligation, 6 cases underwent unilateral fallopian tube resection, and 3 cases underwent unilateral fallopian tube fenestration for fetal retrieval.

Ultrasound examination and image data acquisition

All patients underwent transabdominal and transvaginal color Doppler ultrasound examination before surgical treatment. To ensure consistency in the examination results, transvaginal ultrasound and transabdominal ultrasound examinations are performed by the same group of doctors with more than 10 years of experience in gynecological ultrasound examination and diagnosis.

The examination was conducted using the German SIEMENS S2000 ultrasound diagnostic instrument and a 2–5 MHz phased array probe (transabdominal ultrasound examination) and a 5–7 MHz intracavity probe (transvaginal ultrasound examination).

Before undergoing abdominal ultrasound examination, the patient should drink water and wait for the bladder to be moderately filled before lying on their back. A probe should be used to scan the patient's lower abdominal and pelvic area horizontally and obliquely in multiple sections and directions, and the images should be collected in a standardized manner.

After completing the transabdominal ultrasound examination, the pregnant woman empties the bladder and takes the lithotomy position. After applying gel coupling agent to the probe, put on the latex condom, and apply sterile water-soluble lubricant on the outside of the condom. Place the probe at the far end of the vagina or against the outer opening of the cervix. Change the depth of the ultrasound probe to generate different focal points and obtain different areas of view in the pelvic cavity. After the probe moves left and right from one attachment to another, rotate the probe 90° and scan in the forward and backward directions. Observe the surrounding structures of the uterus, ovaries, and pelvic cavity in multiple directions and sections, and collect typical ultrasound images in a standardized manner.

During the examination, observe whether there were embryos in the uterine cavity, free fluid around the uterus, masses between the uterus and bladder, masses in the appendix, or identifiable signs of pregnancy outside the

uterus (gestational sac, gestational sac with yolk sac, fetal pole, or fetal pole with cardiac activity in the appendix area).

Statistical analysis

The surgical pathological data and ultrasound examination data were organized into counting and measuring data. SPSS 19.0 statistical software (IBM, USA) was used for analysis. The measurement data were shown in mean ± standard deviation. The counting data were expressed as n (%). Chi-squared test was used for analysis of the detection rate of EP with ultrasound examination through two pathways. P <0.05 was considered statistically significant.

Results

Ultrasound findings of ectopic pregnancy through different routes

Abdominal Doppler ultrasound shows a hypoechoic or mixed echoic mass outside the uterine cavity in size of approximately 40 mm × 31 mm × 21 mm ~ 85 mm × 76 mm × 61 mm. Some of which are doughnut shaped. Some lumps have uneven and cystic internal echoes. The pelvic cavity has a liquid dark area with a width between 30 and 70 mm in 65 patients. In some patients, circular congestion of the gestational sac occurs in the accessory area, with a liquid dark area inside [Figure 1]. In some patients, a slightly hyperechoic mass can be seen in the adnexal area. Small cysts can be seen in the mass, and echo of yolk sac can be seen in the cyst [Figure 2]. In some patients, cardiac pulsation of the gestational sac or embryonic tissue can be seen in the pelvic cavity. In some patients, irregular masses which the internal blood flow velocity is significantly reduced can be seen near the uterus, and accompanied by a small amount of pelvic fluid accumulation.

Transvaginal Doppler ultrasound examination revealed a hypoechoic or mixed echoic mass in the accessory area, which was circular in shape [Figure 3]. For most patients, a circular hyperechoic gestational sac can be seen in the adnexal area, with a liquid dark area inside and a portion of doughnut-shaped hyperechogenicity. Heartbeats or embryos can be seen. Color Doppler imaging shows flickering blood flow signals in the attachment area of the gestational sac, and the blood flow around the mass is a semi-circular trophoblast [Figure 4].

Detection and diagnosis of ectopic pregnancy by transabdominal and transvaginal ultrasound

During the surgery, EP was found to occur in the uterine horn, stroma, isthmus, ampulla, umbrella, abdominal cavity, uterine scars, cervix, ovaries, intrauterine and extrauterine complexes, and residual fallopian tubes. There were 82 cases of tubal pregnancy (74.55%), including 16 cases in the interstitial region, 9 cases in the isthmus region, 53 cases in the ampulla region, 3 cases in the fimbriae i.e fimbriated end, and 1 case in the residual fallopian tube. In addition, there were 10 cases of uterine scar pregnancy (9.09%), 7 cases of ovarian pregnancy (6.36%), and 3 cases of abdominal pregnancy (2.73%). There were 5 cases of cornual pregnancy (4.54%), 2 cases of cervical pregnancy (1.82%), and 1 case of intrauterine and intrauterine composite pregnancy (0.91%). The exploration results of transabdominal and transvaginal ultrasound are shown in Table 1.

The positive rate of transvaginal ultrasound for EP masses was 100%, while the positive rate of transabdominal ultrasound was 67.27%, with a significant difference (P < 0.0001). The positive rate of cervical pregnancy and scar pregnancy detected by transvaginal ultrasound and transabdominal ultrasound is the same, while the positive rate of other parts detected by transabdominal ultrasound is lower than that by transvaginal ultrasound. Among them, there were 53 cases of EP located in the ampulla, and the diagnostic rate of transvaginal ultrasound was 100%, while transabdominal ultrasound was only 58.49%. There is a significant difference between the two (P < 0.0001).

The detection rates of extrauterine yolk sac, embryo, and fetal heartbeat were 41.81%, 19.09%, and 18.18%,

Figure 1: Pregnancy in the left adnexal area (arrow) by transabdominal ultrasound ("doughnut" shape). LOV: Left ovary

Figure 2: Pregnancy in the right adnexal area (arrow) by transabdominal ultrasound. ROV: Right ovary

Table 1: Detection of ectopic pregnancy by transvaginal and transabdominal ultrasound – cases, *n* (%)

Intraoperative findings	Ultrasound findings			χ^2	*P*
	Detection	Transvaginal	Transabdominal		
Mass	+	110 (100)	74 (67.27)	43.04	<0.0001
	−	0	36		
Uterine horn	+	5 (100)	5 (100)		
	−	0	0		
Stroma	+	16 (100)	13 (81.25)	3.310	0.0688
	−	0	3		
Isthmus	+	9 (100)	6 (66.67)	3.600	0.0578
	−	0	3		
Ampulla	+	53 (100)	31 (58.49)	27.76	<0.0001
	−	0	22		
Umbrella	+	3 (100)	2 (66.67)	1.200	0.2733
	−	0	1		
Abdominal cavity	+	3 (100)	1 (33.33)	3.000	0.0833
	−	0	2		
Uterine scars	+	10 (100)	10 (100)		
	−	0	0		
Cervix	+	2 (100)	2 (100)		
	−	0	0		
Ovaries	+	7 (100)	5 (71.43)	2.333	0.1266
	−	0	2		
Intrauterine and extrauterine complexes	+	1 (100)	0	2.000	0.1573
	−	0	1		
Residual fallopian tubes	+	1 (100)	1 (100)		
	−	0	0		
Total	+	110	110		

+: Positive detection by ultrasound for Intraoperative findings, −: Negative detection by ultrasound for Intraoperative findings

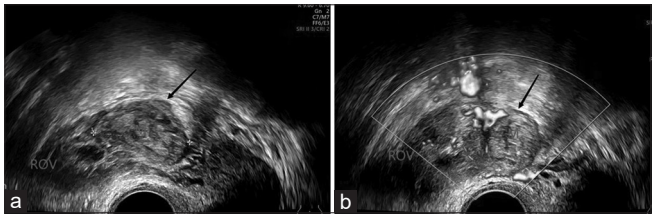

Figure 3: (a) Pregnancy in the right adnexal area (arrow) by transvaginal ultrasound. (b) Color Doppler flow imaging (CDFI) shows blood flow signals within the mass (arrow). ROV: Right ovary

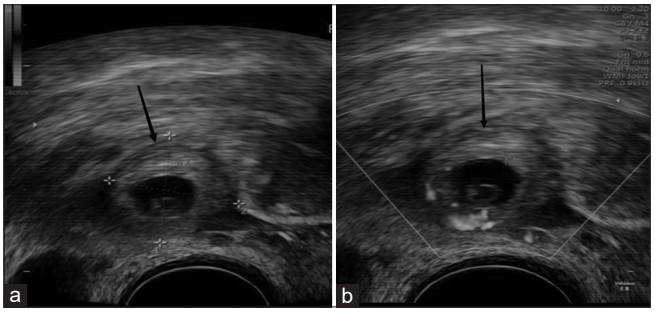

Figure 4: (a) Pregnancy in the right accessory area (showing yolk sac and embryo, arrow) by transvaginal ultrasound. (b) Color Doppler flow imaging (CDFI) displays fetal heartbeat blood flow signals (arrow)

respectively, by transvaginal ultrasound and 11.82%, 7.27%, and 6.36%, respectively, by abdominal ultrasound. Transvaginal ultrasound is significantly superior to transabdominal ultrasound examination, as shown in Table 2.

Comparative analysis of intraoperative intraperitoneal hematocele and ultrasound intraperitoneal effusion in diagnosing EP rupture

During the operation, 74 cases of abdominal hematocele were found, and 65 cases (87.84%) were detected by ultrasound. Among them, 35 cases were confirmed to have ruptured EP. The sensitivity, specificity, positive predictive value, and negative predictive value for diagnosing EP rupture with intraoperative intraperitoneal hematocele were 100%, 48%, 47.3%, and 48%, respectively. The sensitivity, specificity, positive predictive value, and negative predictive value for diagnosing EP rupture with ultrasound intraperitoneal effusion were 94.44%, 58.67%, 52.31%, and 58.67%, respectively.

The rupture of EP in patients with intraoperative abdominal bleeding and peritoneal effusion by ultrasound is shown in Table 3.

Discussion

The most common site of EP is the fallopian tube. According to the literature, the incidence of each position varies depending

Table 2: Ultrasound findings of ectopic embryos, cases (exploration rate, %)

Exploring content	Ultrasound			χ^2	*P*
	Detection	Transvaginal	Transabdominal		
Yolk sac	+	46 (41.81)	13 (11.82)	25.220	<0.0001
	−	64	97		
Embryo	+	21 (19.09)	8 (7.27)	6.712	0.0096
	−	89	102		
Fetal heart pulsation	+	20 (18.18)	7 (6.36)	7.135	0.0076
	−	90	103		
False embryo sac	+	3 (2.73)	3 (2.73)	0.000	1.0000
	−	107	107		

+: Positive detection by ultrasound for exploring content, −: Negative detection by ultrasound for exploring content

Table 3: Peritoneal effusion by ultrasound and intraoperative abdominal hemorrhagic effusion and rupture of extrauterine pregnancy

Observed indicator outcome	Detection	Rupture of EP		total
		+	−	
Intraoperative abdominal hemorrhagic effusion	+	35	39	110
	−	0	36	
Peritoneal effusion by ultrasound	+	34	31	110
	−	1	44	

+: Observation indicator outcome (Intraoperative abdominal hemorrhagic effusion, Peritoneal effusion by ultrasound or Confirmed EP rupture) was positive, −: Observation indicator outcome (Intraoperative abdominal hemorrhagic effusion, Peritoneal effusion by ultrasound or Confirmed EP rupture) was negative

on whether the patient is naturally pregnant or external fertilization and other assisted reproductive technologies.[1,11] In natural pregnancy, 95% of EP is tubal pregnancy, 1.4% is abdominal pregnancy, and <1% is cervical or ovarian pregnancy.[1] After assisted reproductive technology (ART), about 82% of EPs will be tubal pregnancy, mainly ampullary pregnancy, and 11% of EPs will be EP outside the fallopian tube.[1,12-16] The incidence of ovarian EP will increase, which is very different from natural pregnancy.[1,12-16] The cases in this group were all naturally conceived, and the incidence of various positions differs significantly from literature reports. There were 82 cases (74.55%) of tubal pregnancy, of which 66.25% occurred in the ampulla. In addition, there were 10 cases of uterine scar pregnancy (9.09%), 7 cases of ovarian pregnancy (6.36%), and 3 cases of abdominal pregnancy (2.73%). There were 5 cases of cornual pregnancy (4.54%), 2 cases of cervical pregnancy (1.82%), and 1 case of intrauterine and intrauterine composite pregnancy (0.91%).

The etiology and pathological mechanism of EP are unclear. At present, it is believed that risk factors include history of gonorrhea or chlamydia, history of endometriosis, history of intrauterine device (IUD) use, history of pelvic inflammation, pelvic adhesion, and intrauterine surgery and ART.[12-18] Among them, IUD is the most identified risk factor. A 10-year study of 1800 EPs showed that the use of IUD was the only risk factor associated with EP. It is believed that the use of IUD may change the motility of the fallopian tube and cause EP.[18]

The vast majority of EP patients exhibit amenorrhea, abdominal pain, and vaginal bleeding.[1,5,11] When accompanied by a large amount of intraperitoneal bleeding, clinical manifestations of hemorrhagic anemia and hemorrhagic shock can be presented.[19] Urine β-hCG is positive. Further quantification of serum β-hCG increases.[5] However, normal intrauterine pregnancy also manifests as urine-positive β-hCG and a high level of serum β-hCG. Therefore, the most reliable diagnostic indicator of EP is the image visualization of extrauterine pregnancy.[5]

Ultrasound has become the preferred method for imaging diagnosis of gynecological acute abdomen due to its high accessibility and no radiation.[5,11] For suspected patients undergoing ultrasound examination, if obesity and intestinal gas accumulation may limit the diagnostic ability of transabdominal imaging, transvaginal ultrasound examination can be performed.[5] Patients with vaginal trauma may encounter difficulties during the transvaginal approach due to pain. Young patients may not have undergone pelvic examination before, and transvaginal ultrasound examination may cause anxiety in these patients. It may be reasonable to start with transabdominal imaging and use transvaginal imaging as a second-line alternative.[6]

The currently recognized diagnostic criteria for EP ultrasound:[5,11,16,20,21] Ultrasound examination did not detect intrauterine pregnancy in patients but could detect free fluid around the uterus, masses between the uterus and bladder, adnexal masses, or recognizable EP. The ultrasonographical identifiable pregnancies outside the uterus include gestational sac, gestational sac with yolk sac, fetal pole, or fetal pole with cardiac activity in the accessory area.[5,11]

One hundred and ten cases of EP confirmed by surgery and pathology in this group showed hypoechoic or mixed echoic masses in the accessory area on preoperative ultrasound, which were circular in shape. In most patients, a circular hyperechoic gestational sac can be seen in the adnexal area, with a liquid dark area inside and a portion of doughnut-shaped hyperechogenicity. Heartbeats or embryos can be seen. Color Doppler imaging shows flickering blood flow signals near

the gestational sac, and the blood flow around the mass is a semi-circular trophoblast. The positive rate of transvaginal ultrasound for EP masses (100%) was significantly higher than that of transabdominal ultrasound (67.27%) ($P < 0.0001$). The positive rates of cervical pregnancy and scar pregnancy detected by transvaginal ultrasound and transabdominal ultrasound are the same. The positive rate of EP detection in other parts is lower on transabdominal ultrasound than on vaginal ultrasound. Among them, there were 53 cases of EP located in the ampulla, and the diagnostic rate of transvaginal ultrasound was 100%, while transabdominal ultrasound was only 58.49%. There is a significant difference between the two ($P < 0.0001$). It can be seen that the diagnostic effect of transvaginal ultrasound on EP is significantly better than that of transabdominal ultrasound.

Cases in this group showed that 74 cases of abdominal bleeding were found during surgery, and 65 cases (87.84%) were detected by ultrasound. Among them, 35 cases of EP rupture were clearly identified. The sensitivity, specificity, positive predictive value, and negative predictive value for diagnosing EP rupture with abdominal bleeding were 100%, 48%, 47.3%, and 48%, respectively; the sensitivity, specificity, positive predictive value, and negative predictive value of ultrasound in diagnosing EP rupture were 94.44%, 58.67%, 52.31%, and 58.67%, respectively. The specificity of intraoperative abdominal bleeding or ultrasound detection of pelvic fluid accumulation in diagnosing EP rupture is not high.

However, there are some risks in the diagnosis of EP only based on ultrasound examination. First, EP and intrauterine pregnancy may coexist;[22,23] therefore, ultrasound showing intrauterine pregnancy cannot absolutely rule out the possibility of EP. Second, when the gestational sac of ovarian pregnancy does not have a gestational sac, a gestational sac with a yolk sac, a fetal pole, or a fetal pole with cardiac activity in the accessory area and other identifiable pregnancy manifestations, it is similar to the rupture of corpus luteum cyst, endometrioma, or other ovarian cyst torsion, and it is difficult to identify.[13-15,24] In addition, retroperitoneal EP located in the middle or upper abdomen may be inaccessible to transvaginal ultrasound (TVS), which may increase the risk of misdiagnosis and missed diagnosis.[21]

Therefore, the diagnosis of EP requires a clinical medical history combined with the results of serum β-hCG and ultrasound examination.[11] If the patient has menopause, abdominal pain and vaginal bleeding, in addition, her serum β –hCG is >2000 mIU/mL, no intrauterine pregnancy is identified on ultrasound, and her ultrasound images show free fluid around the uterus, mass between the uterus and bladder, mass in the adnexa, or an identifiable pregnancy outside of the uterus, the patient should be considered to have an ectopic pregnancy until proven otherwise.[1,11] If the patient has amenorrhea, abdominal pain, and vaginal bleeding, her serum β hCG is also>2000 mIU/mL, but no extrauterine masses or recognizable extrauterine pregnancy signs on the ultrasound of lower abdomen and pelvis, the patient should be considered to have a rare ectopic pregnancy in the mid and upper abdominal. Besides full abdominal ultrasound, computed tomography scanning, or magnetic resonance imaging would be instrumental for diagnosis as soon as possible.[25-27]

There are still limitations in this study. As a retrospective study, there was no analysis and research on the ultrasound localization diagnosis of EP. This study shows that the specificity of intraperitoneal effusion and bleeding in the diagnosis of EP rupture is not high. Whether we can combine the patient's abdominal pain characteristics with dynamically monitoring of serum quantification β- HCG value to improve the diagnosis of EP rupture may be worth further exploration.

Conclusions

The results of this study confirm that the diagnostic efficacy of transvaginal ultrasound for EP is significantly better than that of transabdominal ultrasound. Therefore, if there is no contraindication for patients suspected of EP, transvaginal ultrasound is recommended as the first choice. Ultrasound detection of pelvic fluid accumulation has low specificity in diagnosing EP rupture, and the diagnosis of EP rupture requires intraoperative observation.

Financial support and sponsorship

This work was supported by the Science and Technology Development Fund of Longgang District, Shenzhen, in 2017 and 2021 (Grant No. 20170405183747348 and LGWJ2021-047).

Conflicts of interest

There are no conflicts of interest.

References

1. Baker M, dela Cruz J. Ectopic pregnancy, ultrasound. In: StatPearls. Treasure Island (FL): StatPearls Publishing; 2023.
2. Levine D. Ectopic pregnancy. Radiology 2007;245:385-97.
3. Chen QL, Weng NZ, Zeng LJ. Comparison of the application value of transabdominal and transvaginal ultrasound in the diagnosis of early ectopic pregnancy in different parts. China Contemp Med 2015;22:108-10.
4. Padilla LA, Radosevich DM, Milad MP. Accuracy of the pelvic examination in detecting adnexal masses. Obstet Gynecol 2000;96:593-8.
5. Pek E, Beyzait F, Siddikoglu D. Is it possible to predict the success of single dose methotrexate in the treatment of tubal ectopic pregnancies? Ginekol Pol 2023;94:249-57.
6. Kaakaji Y, Nghiem HV, Nodell C, Winter TC. Sonography of obstetric and gynecologic emergencies: Part II, gynecologic emergencies. AJR Am J Roentgenol 2000;174:651-6.
7. Juliano ML, Sauter BM. Fetal outcomes in first trimester pregnancies with an indeterminate ultrasound. J Emerg Med 2012;43:417-22.
8. Beals T, Naraghi L, Grossestreuer A, Schafer J, Balk D,

Hoffmann B. Point of care ultrasound is associated with decreased ED length of stay for symptomatic early pregnancy. Am J Emerg Med 2019;37:1165-8.
9. Wang PS, Rodgers SK, Horrow MM. Ultrasound of the first trimester. Radiol Clin North Am 2019;57:617-33.
10. Mukherjee R, Samanta S. Surgical emergencies in pregnancy in the era of modern diagnostics and treatment. Taiwan J Obstet Gynecol 2019;58:177-82.
11. Sosa M, Brancazio S, Drummey A, Nguyen T, Toussaint T. Transvaginal ultrasound diagnosis of Ovarian ectopic pregnancy. Cureus 2023;15:e33536.
12. Hoffman B, editor. Ectopic pregnancy. In: Williams Gynecology. New York: McGraw Hill; 2006. p. 161-79.
13. Gupta S, Kunwar K, Agrawal M, Agrawal N, Mani A. Ovarian ectopic pregnancy with IUCD *in situ*: A rare case report. J Evol Med Dent Sci 2018;7:4926-8.
14. Ko PC, Lo LM, Hsieh TT, Cheng PJ. Twenty-one years of experience with ovarian ectopic pregnancy at one institution in Taiwan. Int J Gynaecol Obstet 2012;119:154-8.
15. Sotelo C. Ovarian ectopic pregnancy: A clinical analysis. J Nurse Pract 2019;15:224-7.
16. Ren F, Liu G, Wang T, Li M, Guo Z. Unruptured ovarian ectopic pregnancy: Two case reports and literature review. Front Physiol 2022;13:1036365. [doi: 10.3389/fphys.2022.1036365].
17. Chunyan P. Analysis of the clinical value of transabdominal ultrasonography, transvaginal ultrasonography and combined diagnosis of ectopic pregnancy. J Clin Ration Use 2017;10:117-8.
18. Sergent F, Mauger-Tinlot F, Gravier A, Verspyck E, Marpeau L. Ovarian pregnancies: Revaluation of diagnostic criteria. J Gynecol Obstet Biol Reprod (Paris) 2002;31:741-6.
19. Resta S, Fuggetta E, D'Itri F, Evangelista S, Ticino A, Porpora MG. Rupture of ovarian pregnancy in a woman with low beta-hCG levels. Case Rep Obstet Gynecol 2012;2012:213169.
20. Kasraei S, Seifollahi A, Aghajani F, Nakhostin-Ansari A, Zarei N, Tehranian A. Successful management of a patient with ovarian ectopic pregnancy by the end of the first trimester: A case report. J Med Case Rep 2022;16:175.
21. Xu H, Cheng D, Yang Q, Wang D. Multidisciplinary treatment of retroperitoneal ectopic pregnancy: A case report and literature review. BMC Pregnancy Childbirth 2022;22:472.
22. Huang J, Jing X, Fan S, Fufan Z, Yiling D, Pixiang P, *et al.* Primary unruptured full term ovarian pregnancy with live female infant: Case report. Arch Gynecol Obstet 2011;283 Suppl 1:31-3.
23. Sehgal A, Goyal LD, Goel P, Sunita BS. Full term ovarian pregnancy: A case report. Aust N Z J Obstet Gynaecol 2005;45:165-6.
24. Shrestha A, Chawla CD, Shrestha RM. Ruptured primary ovarian pregnancy: A rare case report. Kathmandu Univ Med J (KUMJ) 2012;10:76-7.
25. Zhang M, Qin LL. A case of retroperitoneal para-aortic ectopic pregnancy detected by sonography. J Clin Ultrasound 2018;46:412-4.
26. Huang X, Zhong R, Tan X, Zeng L, Jiang K, Mei S, *et al.* Conservative management of retroperitoneal ectopic pregnancy by computed tomographic-guided methotrexate injection in the gestational sac: 2 case reports and literature review. J Minim Invasive Gynecol 2019;26:1187-92.
27. Anh ND, Hai NX, Ha NT, Toan NK, Thuong PH, Duc NM. Retroperitoneal ectopic pregnancy after *in vitro* fertilization: A case report of a patient with bilateral salpingectomy. Radiol Case Rep 2022;17:721-4.

Original Article

Important Morphometric Values and Anatomical Ratios Obtained from Cervical Magnetic Resonance Imaging Images and their Differences from the Literature in Terms of Evaluation of Myelopathy

Sinan Bakirci, Senem Senturk[1]

Department of Anatomy, Faculty of Medicine, Izmir Katip Celebi University, Izmir, [1]Department of Radiology, Faculty of Medicine, Dicle University, Diyarbakir, Turkey

Abstract

Objective: A Torg ratio of 0.80 or less is considered positive support for the diagnosis of cervical spinal canal stenosis. In our study, it was aimed to determine the morphometric values of the spinal cord, spinal canal, and vertebral body, to calculate the subarachnoid distance, and to examine the differences in Torg ratio according to cervical vertebra levels and between genders in young adult individuals belonging to our community. **Materials and Methods:** The study was performed on magnetic resonance imaging (MRI) images (28–35 years, 50 men and 50 women, retrospectively). **Results:** The Torg ratio was found to be <0.80 in 194 of 350 measurements made at 7 levels (55.4%) in men and in 83 of 350 measurements in women (23.7%). The Torg ratio value was found to be higher in women than men at C3–T1 levels ($P < 0.01$). There is a positive and highly significant relationship between the Torg ratio and "canal-cord distance" ($P < 0.01$). Spinal canal diameter was found to be <14 mm in 235 vertebrae (67.1%) in men and 282 vertebrae (80.6%) in women. In addition, it was found below 12 mm in 12.6% of men and 16% of women. **Conclusion:** In our study, the Torg ratio was found below 0.80 in a significant part of our cases. Therefore, it would be appropriate to revise the Torg ratio separately for different populations in MRI measurements. It is clear that there is a need for planning epidemiological studies consisting of control–patient groups in the future, especially for many societies.

Keywords: *Cervical morphometry, Pavlov, spinal canal diameter, spinal cord diameter, torg*

Introduction

Torg ratio is the ratio of the sagittal length of the spinal canal to the sagittal length of the vertebral body on lateral neck radiographs. A ratio of 0.80 and below is used for the evaluation of cervical spinal stenosis. To reduce the errors that may occur due to magnification in radiographs taken from nonstandard distances, the Torg ratio has been used instead of the spinal canal length.[1] In patients with cervical spinal neuropraxia causing transient quadriplegia, a Torg ratio of 0.80 or less is considered an indicator of significant spinal stenosis. Torg ratio has a very high sensitivity of 93% in transient neuropraxia that occurs in football players. However, due to its low positive predictive value (0.2%) Torg ratio, it is not suitable for use as a screening test to determine the fitness of the athlete in football and similar sports branches. When the literature is examined, there are studies conducted in different societies of India, China, Japan, and other Caucasian races, which reported that C4 is the narrowest level of spinal canal diameter in radiography studies.[2-5] There are also studies reporting that the narrowest level is C5 and C6.[6-8] In addition, Bakirci *et al*. reported that the narrowest level for the spinal canal in patients with ankylosing spondylitis was C6 in women and C7 in men.[9] However, apart from these, according to the results of some authors, the spinal canal diameter gradually decreases from top to bottom in the cervical region, and the narrowest level is the C7 level, which is located in the most distal.[10,11]

Vertebral degenerative changes that may occur with age have the potential to affect the cervical spinal canal diameter.[12] Therefore, performing the study in a narrowed age range reduces factors that have the potential to affect anatomical and morphometric evaluation. In an X-ray radiography study performed by Bakirci *et al*. in patients with ankylosing spondylitis,

How to cite this article: Bakirci S, Senturk S. Important morphometric values and anatomical ratios obtained from cervical magnetic resonance imaging images and their differences from the literature in terms of evaluation of myelopathy. J Anat Soc India 2024;73:110-8.

Article Info

Received: 18 July 2023
Revised: 17 April 2024
Accepted: 08 May 2024
Available online: 27 June 2024

Address for correspondence:
Dr. Sinan Bakirci, Department of Anatomy, Faculty of Medicine, Izmir Katip Celebi University, Izmir, Turkey. E-mail: sinan.bakirci@ikcu.edu.tr

Access this article online

Website: https://journals.lww.com/joai

DOI: 10.4103/jasi.jasi_75_23

Quick Response Code:

the Torg ratio at a level of 0.80 or less in females was 25.90% whereas the percentage for males was 21.40%.[9] In addition, in their study, no significant difference was found in Torg ratio values in terms of corresponding vertebral levels between the 4th and 5th decades.

In this study, it was aimed to reveal the standard spinal cord, spinal canal, and subarachnoidal distance (SAD) data of our society, retrospectively, and to examine the gender-related differences in young adults who had neck magnetic resonance imaging (MRI) for any reason. In addition, it has been examined whether the 0.80 ratio, which is accepted as the limit value in the Torg ratio, can be used for our society.

Materials and Methods

The study was performed using standard techniques on sagittal T2-weighted MRI images of the neck of young adults (18–35 years) obtained retrospectively [Figure 1]. A total of 100 neck MR images, 50 male and 50 female, were used in this cross-sectional study. MRI images were evaluated and selected by a radiologist. Cases whose MRI examinations were within normal limits except for cervical lordosis flattening were included in the study. Cases with pathologies that may affect the measurement results such as infection, trauma, congenital anomaly, degeneration, and ligament laxity were excluded from the study. In midsagittal T2-weighted sections, the anteroposterior (AP) vertebral body length of the C2–T1 vertebrae (7 vertebrae in total) from the mid-vertebral part and the spinal canal AP length at the same level (from the vertebra posterior body to the spinolaminar line perpendicular to the spinal canal) were measured. Spinal cord AP length was also measured at the same level. All morphometric measurements were done by a specialist radiologist. Torg ratio was obtained by dividing the spinal canal AP length by the vertebral AP length. The subarachnoid distance was calculated by subtracting the spinal cord length from the spinal canal length (SAD).

Figure 1: Vertebal body, spinal canal, spinal cord measurements on T2-weighted sagittal magnetic resonance images

Statistical analyses

Statistical analyses were done with SPSS Statistics Standard Concurrent User v25 (IBM Corp., Armonk, New York, USA). While evaluating the study data, descriptive statistical methods (mean, standard deviation, median, frequency, ratio, minimum, and maximum) as well as the distribution of the data were evaluated with the Shapiro–Wilk test. The Mann–Whitney *U* test was used to compare the quantitative data between two groups that did not show normal distribution. Spearman's correlation analysis was used to determine the relationship between quantitative data. Significance was evaluated at $P < 0.01$ and $P < 0.05$ levels.

Results

Vertebral body diameter was narrowest at the C3 level (1.66 ± 0.11 cm) in males and at the C5 level (1.45 ± 0.09 cm) in females [Table 1]. Spinal canal diameter was found to be narrowest at the C4 level (1.29 ± 0.12 cm in men; 1.28 ± 0.10 cm in women) in both genders [Table 2]. Spinal canal diameters were found to be <14 mm in 235 (67.1%) of 350 vertebrae in men and in 282 (80.6%) of 350 vertebrae in women. Spinal canal diameter was found to be <11 mm in 9 vertebrae in men and 3 vertebrae in women [Table 3].

The sagittal diameter of the spinal cord decreased linearly from top to bottom in C2–T1 vertebrae in both sexes. In both genders, the diameter of the spinal cord is widest at C2 (0.78 ± 0.05 cm in men; 0.75 ± 0.06 cm in women), and at its narrowest at T1 (0.63 ± 0.05 cm in men, 0.62 ± 0.05 cm in women) [Table 4].

In the cervical region; in women, the smallest Torg ratio is at C4 (0.86 ± 0.1), the smallest cord/canal ratio is at C7 (0.49 ± 0.05), and the smallest canal-cord distance is at C4 (0.55 ± 0.09). In males, the smallest Torg ratio is at C4 (0.78 ± 0.1), the smallest cord/canal ratio is at C7 (0.49 ± 0.05), and the smallest canal-cord distance is at C3 (0.54 ± 0.12) [Table 5]. In the measurements made at seven levels (C2–T1), the Torg ratio was found below 0.80 in 194 of 350 vertebrae in men and in 83 of 350 vertebrae in women (55.4% in men and 23.7% in women). The Torg ratio was below 0.80 in more than half of the vertebrae in men (60.5%) and in 24% of the vertebrae in women in the measurements made between C3 and C6 [Table 6].

When compared according to genders, the "canal/vertebral body" value was found to be higher in women than men at C3–T1 levels ($P < 0.01$). At the C2 level, the Torg value did not show a significant difference between the genders. "Cord/canal" value did not differ significantly in terms of gender at any level of measurement. The differences in the "canal–cord distance" values by gender are not statistically significant at all levels except for C2 ($P > 0.05$). At the C2 level, the "canal–cord distance" value of women is smaller than that of men, and this difference was found to be statistically significant ($P = 0.017$; $P < 0.05$) [Table 7].

Table 1: Average values of vertebral body diameter

Vertebral body diameter	Men		Women		Significant
	Mean±SD	Minimum–maximum (median)	Mean±SD	Minimum–maximum (median)	
C2	1.70±0.12	1.50–2.05 (1.70)	1.55±0.11	1.32–1.76 (1.56)	0.000*
C3	1.66±0.11	1.43–1.88 (1.65)	1.50±0.08	1.27–1.63 (1.51)	0.000*
C4	1.67±0.12	1.43–1.93 (1.67)	1.49±0.09	1.25–1.73 (1.51)	0.000*
C5	1.67±0.12	1.42–1.95 (1.67)	1.45±0.09	1.23–1.66 (1.44)	0.000*
C6	1.70±0.12	1.43–1.99 (1.71)	1.50±0.08	1.26–1.73 (1.49)	0.000*
C7	1.75±0.12	1.48–2.02 (1.74)	1.54±0.08	1.31–1.75 (1.53)	0.000*
T1	1.82±0.12	1.60–2.09 (1.74)	1.63±0.12	1.33–1.98 (1.62)	0.000*

*P<0.05 significance for the gender difference. SD: Standard deviation

Table 2: Average values of spinal canal diameter

Canal diameter	Men		Women		Significant
	Mean±SD	Minimum–maximum (median)	Mean±SD	Minimum–maximum (median)	
C2	1.54±0.13	1.26–1.92 (1.52)	1.45±0.13	1.18–1.82 (1.44)	0.000*
C3	1.30±0.11	1.12–1.56 (1.30)	1.29±0.10	1.10–1.59 (1.29)	0.785
C4	1.29±0.12	1.09–1.59 (1.29)	1.28±0.10	1.07–1.50 (1.29)	0.882
C5	1.32±0.12	1.06–1.60 (1.32)	1.28±0.10	1.07–1.50 (1.30)	0.155
C6	1.32±0.14	1.00–1.72 (1.32)	1.30±0.09	1.11–1.45 (1.31)	0.283
C7	1.36±0.12	1.02–1.65 (1.33)	1.33±0.09	1.15–1.58 (1.33)	0.336
T1	1.36±0.10	1.05–1.56 (1.36)	1.32±0.10	1.15–1.68 (1.31)	0.026*

*P<0.05 significance for the gender difference. SD: Standard deviation

Table 3: Distribution of spinal canal diameters <14 mm

Spinal canal diamater (mm)	C2	C3	C4	C5	C6	C7	T1	Total (%)
Men (n=350)								
13.1–14	4	17	12	15	14	15	21	98 (28.0)
12.1–13	1	16	20	15	16	16	9	93 (26.6)
11.1–12		13	8	5	5	1	3	35 (10.0)
10.1–11			2	2	2	1	1	8 (2.3)
<10					1			1 (0.3)
Total	5	46	42	37	38	33	34	235 (67.1)
Women (n=350)								
13.1–14	16	14	20	15	18	22	18	123 (35.1)
12.1–13	3	21	12	15	18	17	17	103 (29.4)
11.1–12	2	9	14	12	7	3	6	53 (15.1)
10.1–11			1	2				3 (0.9)
<10			-	-				
Total	21	44	47	44	43	42	41	282 (80.6)

There is a positive and highly significant relationship between the Torg ratio and "canal–cord distance" (P < 0.01). The correlation of measurement values at different vertebral levels is given in Table 8.

Discussion

In this study, the Torg ratio was found below 0.80 in both genders in a significant part of the cases [Table 6]. In the evaluation of radiographic measurements, a Torg ratio of 0.80 and below is important in terms of cervical spinal stenosis. However, cases without cervical spinal stenosis were included in our study, and despite this, the Torg ratio was below 0.80 in many measurements in our study. Based on our results, we think that the Torg ratio may differ from society to society and may not be reliable in the diagnosis of spinal stenosis. Ehni reported that if the Torg ratio is between 80% and 85%, the probability of having spondylotic myelopathy increases, and if this rate is between 50% and 75%, cervical myelopathy is almost certain.[13] Pavlov *et al*. reported that when the Torg ratio was accepted as 0.82 as an indicator of stenosis, the accuracy rate was 92% in the diagnosis of patients with cervical myelopathy.[14] Based on the cumulative data from their study (the study was conducted on 195 normal vertebrae and 91 abnormal vertebrae), they reported that a Torg ratio of 0.80 would have an accuracy rate of 96.3% for cervical myelopathy.

In our study, the mean values of the Torg ratio obtained from men were found below the value of 0.80 at all levels (except for the C2 level). In women, the mean Torg values were not below 0.80 at any level. However, in our study, the Torg ratio was found to be <0.80 in 194 out of 350 measurements made at 7 cervical levels in men and in 83 out of 350 measurements in women. The Torg ratio was found to be <0.80 in more than half of the measurements made at C3–C6 levels in men [Table 6]. This shows that in social terms, when the data are analyzed in terms of mean values, although the risk of cervical myelopathy in women seems to be low or absent, when evaluated individually, 83 out of 350 measurements in women have a Torg ratio below 0.80 and there seems to be a risk of cervical myelopathy. In a study in the literature, much different from our study, it was reported that the Torg ratio was below 0.80 in 10% of the measurements in women, at only

Table 4: Average values of spinal cord diameter

Cord diameter	Men		Women		Significant
	Mean±SD	Minimum–maximum (median)	Mean±SD	Minimum–maximum (median)	
C2	0.78±0.05	0.66–0.88 (0.78)	0.75±0.06	0.60–0.90 (0.75)	0.013*
C3	0.76±0.06	0.60–0.86 (0.77)	0.73±0.06	0.60–0.85 (0.72)	0.020*
C4	0.74±0.05	0.61–0.83 (0.75)	0.73±0.06	0.60–0.83 (0.72)	0.174
C5	0.73±0.06	0.62–0.88 (0.74)	0.71±0.06	0.60–0.84 (0.70)	0.046*
C6	0.71±0.06	0.60–0.85 (0.71)	0.69±0.06	0.58–0.81 (0.70)	0.163
C7	0.66±0.05	0.58–0.79 (0.66)	0.64±0.05	0.55–0.78 (0.65)	0.065
T1	0.63±0.05	0.55–0.76 (0.63)	0.62±0.05	0.54–0.74 (0.62)	0.069

*P<0.05 significance for the gender difference. SD: Standard deviation

Table 5: Average values of ratios and results obtained from morphometric measurements

Level	Canal/vertebral body		Cord/canal ratio		Cord–canal distance	
	Mean±SD	Minimum–maximum (median)	Mean±SD	Minimum–maximum (median)	Mean±SD	Minimum–maximum (median)
Women						
C2	0.94±0.13	0.68–1.37 (0.92)	0.52±0.06	0.41–0.63 (0.53)	0.70±0.13	0.48–1.08 (0.68)
C3	0.87±0.09	0.71–1.06 (0.87)	0.57±0.05	0.45–0.68 (0.57)	0.56±0.09	0.37–0.87 (0.56)
C4	0.86±0.1	0.65–1.1 (0.87)	0.57±0.05	0.44–0.67 (0.58)	0.55±0.09	0.35–0.77 (0.54)
C5	0.89±0.1	0.66–1.11 (0.89)	0.55±0.05	0.45–0.7 (0.55)	0.58±0.1	0.32–0.82 (0.58)
C6	0.87±0.09	0.7–1.13 (0.89)	0.53±0.05	0.46–0.63 (0.53)	0.61±0.09	0.41–0.77 (0.62)
C7	0.87±0.08	0.73–1.15 (0.86)	0.49±0.05	0.39–0.6 (0.49)	0.69±0.1	0.51–0.92 (0.69)
T1	0.81±0.09	0.67–1.14 (0.81)	0.47±0.05	0.38–0.58 (0.47)	0.70±0.11	0.50–1.03 (0.69)
Men						
C2	0.91±0.09	0.72–1.15 (0.91)	0.51±0.05	0.39–0.64 (0.51)	0.76±0.14	0.47–1.11 (0.76)
C3	0.79±0.09	0.62–0.97 (0.78)	0.59±0.06	0.47–0.75 (0.59)	0.54±0.12	0.28–0.79 (0.53)
C4	0.78±0.1	0.58–1.01 (0.76)	0.58±0.06	0.44–0.73 (0.58)	0.55±0.13	0.3–0.89 (0.55)
C5	0.79±0.1	0.57–1.05 (0.79)	0.56±0.06	0.45–0.72 (0.56)	0.59±0.12	0.32–0.88 (0.58)
C6	0.79±0.11	0.51–1.08 (0.79)	0.54±0.06	0.38–0.67 (0.54)	0.62±0.14	0.36–1.07 (0.62)
C7	0.78±0.09	0.59–0.99 (0.77)	0.49±0.05	0.40–0.58 (0.50)	0.69±0.12	0.43–0.95 (0.68)
T1	0.75±0.08	0.59–0.95 (0.74)	0.47±0.05	0.37–0.59 (0.47)	0.72±0.11	0.46–0.96 (0.72)

SD: Standard deviation

Table 6: The number, percentage, and levels of vertebrae with Torg ratio below 0.80

	C2, *n* (%)	C3, *n* (%)	C4, *n* (%)	C5, *n* (%)	C6, *n* (%)	C7, *n* (%)	T1, *n* (%)	Total, *n* (%)
Men (*n*=50×7=350)	5 (100)	29 (58)	31 (62)	29 (58)	32 (64)	31 (62)	37 (74)	194 (55.4)
Women (*n*=50×7=350)	4 (80)	14 (28)	16 (32)	9 (18)	9 (18)	10 (20)	21 (41)	83 (23.7)
Total (*n*=100×7=700)	9 (9)	43 (430)	47 (47)	38 (38)	41 (41)	41 (41)	58 (58)	277 (39.6)

one vertebral level in men. In our study, this percentage rate is much higher.[15]

In our study, MR images of patients who were not diagnosed with cervical myelopathy were used. For this reason, the general opinion and rule that a Torg ratio of 0.80 and below will increase the risk of cervical myelopathy may not be valid for our society. It would be appropriate to conduct a larger study on cervical myelopathy risk ratio for our society, similar to that of Pavlov *et al*. (comparing symptomatic patient groups with control groups).[14]

In addition, in the study by Pavlov *et al*., it was reported that there was no statistical difference between the Torg ratios of male and female genders in the control groups.[14] In our study, unlike the study of Pavlov *et al*., a significant difference was found between the sexes in terms of the Torg ratio at all levels (except for the C2 level) $P < 0001$.

For the diagnosis of severe cervical spinal stenosis, the sagittal canal diameter value was accepted as 13 mm by Epstein *et al*. and 14 mm by Countee and Vijayanathan.[16,17] Kessler similarly reported that a canal diameter of <14 mm is important and can cause at least two clinical conditions.[18] Pavlov *et al*. reported the mean value of the sagittal canal diameter as 15.2 mm in their measurements in symptomatic patients, and they reported that if the cervical canal diameter is accepted as 14 mm as an indicator of stenosis, stenotic canal cannot be diagnosed in approximately 65% of all symptomatic patients.[14] Bajwa *et al*. as a result of their study on 1066 cadaver bone samples, reported that the

Table 7: Comparison of variables by genders

	n	Mean±SD	Minimum–maximum (median)	*P*
C2 (canal/vertebral body)				
Women	50	0.94±0.13	0.68–1.37 (0.92)	0.362
Men	50	0.91±0.09	0.72–1.15 (0.91)	
C2 (cord/canal)				
Women	50	0.52±0.06	0.41–0.63 (0.53)	0.221
Men	50	0.51±0.05	0.39–0.64 (0.51)	
C2 (canal–cord)				
Women	50	0.7±0.13	0.48–1.08 (0.68)	0.017*
Men	50	0.76±0.14	0.47–1.11 (0.76)	
C3 (canal/vertebral body)				
Women	50	0.87±0.09	0.71–1.06 (0.87)	0.001**
Men	50	0.79±0.09	0.62–0.97 (0.78)	
C3 (cord/canal)				
Women	50	0.57±0.05	0.45–0.68 (0.57)	0.099
Men	50	0.59±0.06	0.47–0.75 (0.59)	
C3 (canal–cord)				
Women	50	0.56±0.09	0.37–0.87 (0.56)	0.293
Men	50	0.54±0.12	0.28–0.79 (0.53)	
C4 (canal/vertebral body)				
Women	50	0.86±0.1	0.65–1.1 (0.87)	0.001**
Men	50	0.78±0.1	0.58–1.01 (0.76)	
C4 (cord/canal)				
Women	50	0.57±0.05	0.44–0.67 (0.58)	0.365
Men	50	0.58±0.06	0.44–0.73 (0.58)	
C4 (canal–cord)				
Women	50	0.55±0.09	0.35–0.77 (0.54)	0.6
Men	50	0.55±0.13	0.3–0.89 (0.55)	
C5 (canal/vertebral body)				
Women	50	0.89±0.1	0.66–1.11 (0.89)	0.001**
Men	50	0.79±0.1	0.57–1.05 (0.79)	
C5 (cord/canal)				
Women	50	0.55±0.05	0.45–0.7 (0.55)	0.548
Men	50	0.56±0.06	0.45–0.72 (0.56)	
C5 (canal–cord)				
Women	50	0.58±0.1	0.32–0.82 (0.58)	0.817
Men	50	0.59±0.12	0.32–0.88 (0.58)	
C6 (canal/vertebral body)				
Women	50	0.87±0.09	0.7–1.13 (0.89)	0.001**
Men	50	0.79±0.11	0.51–1.08 (0.79)	
C6 (cord/canal)				
Women	50	0.53±0.05	0.46–0.63 (0.53)	0.679
Men	50	0.54±0.06	0.38–0.67 (0.54)	
C6 (canal–cord)				
Women	50	0.61±0.09	0.41–0.77 (0.62)	0.847
Men	50	0.62±0.14	0.36–1.07 (0.62)	
C7 (canal/vertebral body)				
Women	50	0.87±0.08	0.73–1.15 (0.86)	0.001**
Men	50	0.78±0.09	0.59–0.99 (0.77)	
C7 (cord/canal)				
Women	50	0.49±0.05	0.39–0.6 (0.49)	0.431
Men	50	0.49±0.05	0.4–0.58 (0.5)	
C7 (canal–cord)				
Women	50	0.69±0.1	0.51–0.92 (0.69)	0.983

Contd...

Table 7: Contd...

	n	Mean±SD	Minimum–maximum (median)	*P*
Men	50	0.69±0.12	0.43–0.95 (0.68)	
T1 (canal/vertebral body)				
Women	50	0.81±0.09	0.67–1.14 (0.81)	0.001**
Men	50	0.75±0.08	0.59–0.95 (0.74)	
T1 (cord/canal)				
Women	50	0.47±0.05	0.38–0.58 (0.47)	0.887
Men	50	0.47±0.05	0.37–0.59 (0.47)	
T1 (canal–cord)				
Women	50	0.7±0.11	0.5–1.03 (0.69)	0.259
Men	50	0.72±0.11	0.46–0.96 (0.72)	

*P<0.05, **P<0.01 Mann–Whitney U-test. SD: Standard deviation

sagittal spinal canal diameter of 13 mm or less is strongly associated with congenital cervical canal stenosis.[19]

In our study, it was determined that the mean spinal canal diameters were below 14 mm in men and 13.5 mm in women at all measured vertebral levels (except C2). Considering all vertebrae (350 vertebrae), the number of measurements with a spinal canal diameter of 14 mm and less was found to be 235 (67.1%) in men and 282 (80.6%) in women [Table 3]. If the spinal canal diameter is accepted as 12 mm as the limit value, the spinal canal diameter was 12 and below in 44 vertebrae in men (12.6%) and in 56 (16%) in women. In our study, the smallest spinal canal diameter was found to be 10 mm in only one vertebra (male, C6) [Table 3]. We think that accepting 13 or 14 mm as the lower limit of the normal values of sagittal spinal canal diameter would not be appropriate for our society.

In our study, the lowest mean values of spinal canal diameter belong to the C4 vertebrae in men and C4 and C5 vertebrae in women. Isık and Samanci reported the narrowest level of spinal canal diameter as C4 in men and C5 in women in their study in children and young people (2–17 years old). Our study and their study are in different age groups. However, our results are similar. In addition, in the studies of Işık and Samancı, the diameter of the spinal canal was reported to be smaller than 14 mm in men and 12.5 mm in women at all cervical levels (except C1, C2).[20] In a study conducted in Macedonia, the mean spinal canal diameter (C3–C7) was reported as 14.59 mm ± 1.01 in men and 15.26 mm ± 1.11 in women. The narrowest level of spinal canal diameter was reported as C5 in both sexes, and the widest level was reported as C6 and C7.[15] In our study, the narrowest spinal canal diameter was found as C4 in both sexes, and the widest level was found as C2 in both sexes. Matveeva *et al*. found spinal canal diameter below 12 mm in only males (8 males).[15] In our study, the spinal canal diameter in the measurements; it was found below 12 mm in 12.6% of men and 16% of women.

In our study, the lowest level of SAD (spinal canal-spinal cord) values was C3 levels in men and C4 levels in women, and the mean SAD value was found to be 5.4 mm and 5.5 mm, respectively. This rate is higher than the values given in many studies in the literature. Inoue *et al*., Ndubuisi *et al*., and Prasad *et al*. in their study, the lowest level of SAD value was C4, similar to our results, and the SAD value was 4.2; 4.5; They reported that it was 4.0 (respectively).[21-23] Presciutti *et al*. on the other hand reported that the lowest SAD value was C4, but the mean value was 6.5 mm.[24] Matveeva *et al*. showed that a SAD value of 5 mm or less was consistent with a Torg ratio of <0.80 and a spinal canal diameter of <12 mm.[15]

In our study of adults, it was observed that the sagittal diameter of the spinal cord decreased gradually from top to bottom in both genders (C2, 7.5 –C7, 6.4 mm in females; C2, 7.9–C7, 6.6 mm in males). Sherman *et al*. reported that the diameter of the spinal cord decreased gradually at all cervical levels from top to bottom in their study on adults.[11] However, their spinal canal diameter values were reported to be greater than our values at all levels (C2, 8.8–C7, 7.4 mm). It seems not right to talk about a similar situation in children and young people. In a study performed on children younger than 18 years of age, it was reported that the sagittal diameter of the spinal cord did not decrease gradually from top to bottom in the cervical region.[20] Isık and Samancı reported in their study that the sagittal diameter of the spinal cord was the largest at the C4 level (7.9 ± 1.7 mm) in men and at the C5 level (7.8 ± 2.4 mm) in women.[20] Matveeva *et al*. also reported that the sagittal diameter of the spinal cord in adults was the largest between C3 and C5 in both genders due to cervical cord enlargement (7.57 mm ± 0.42 in males and 7.67 mm ± 0.95 in females at C3).[15] The results obtained in these two studies differ from the results of our study. This may be due to two reasons. Isık and Samancı used youth and children in their studies.[20] In addition, the number of participants was low. Matveeva *et al*. conducted their study in a wider age range (50 individuals covering the age range 19–64).[15] Okada *et al*., in an MRI study conducted on 497 healthy individuals, found the incidence of degenerative changes in the elderly (60s) to be 86% in men and 89% in women (such as decrease in signal intensity of disc, anterior compression of dura and spinal cord, posterior disc

Table 8: Correlation analyses

Vertebral level		1	2	3	4	5	6	7	8	9	10	11	12	13	14	15	16	17	18	19	20	21
1. C2 (Canal/	*r*	1																				
Body)	*p*	.																				
2. C2 (Cord/	*r*	-586**	1																			
Canal)	*p*	0	.																			
3. C2	*r*	664**	-943**	1																		
(Canal-Cord)	*p*	0	0	.																		
4. C3 (Canal/	*r*	722**	-302**	365**	1																	
Body)	*p*	0	0.002	0	.																	
5. C3 (Cord/	*r*	-367**	651**	-542**	-513**	1																
Canal)	*p*	0	0	0	0	.																
6. C3	*r*	495**	-609**	608**	703**	-911**	1															
(Canal-Cord)	*p*	0	0	0	0	0	.															
7. C4 (Canal/	*r*	530**	-0.125	0	854**	-357**	531**	1														
Body)	*p*	0	0.216	0.098	0	0	0	.														
8. C4 (Cord/	*r*	-334**	492**	-453**	-546**	766**	-785**	-572**	1													
Canal)	*p*	0.001	0	0	0	0	0	0	.													
9. C4	*r*	387**	-411**	440**	650**	-660**	791**	707**	-940**	1												
(Canal-Cord)	*p*	0	0	0	0	0	0	0	0	.												
10. C5	*r*	392**	-0.041	0.07	754**	-322**	463**	905**	-527**	645**	1											
(Canal/Body)	*p*	0	0.684	0.491	0	0.001	0	0	0	0	.											
11. C5	*r*	-208*	421**	-358**	-372**	630**	-583**	-415**	774**	-712**	-532**	1										
(Cord/Canal)	*p*	0.038	0	0	0	0	0	0	0	0	0	.										
12. C5	*r*	266**	-325**	336**	487**	-536**	609**	561**	-761**	812**	669**	-916**	1									
(Canal-Cord)	*p*	0.008	0.001	0.001	0	0	0	0	0	0	0	0	.									
13. C6	*r*	429**	-0.088	0.114	709**	-309**	422**	803**	-492**	579**	894**	-526**	611**	1								
(Canal/Body)	*p*	0	0.383	0.258	0	0.002	0	0	0	0	0	0	0	.								
14. C6	*r*	-0.18	422**	-371**	-326**	551**	-522**	-320**	674**	-604**	-417**	814**	-736**	-515**	1							
(Cord/Canal)	*p*	0.073	0	0	0.001	0	0	0.001	0	0	0	0	0	0	.							
15. C6	*r*	253*	-309**	335**	457**	-440**	524**	472**	-650**	691**	572**	-761**	823**	672**	-907**	1						
(Canal-Cord)	*p*	0.011	0.002	0.001	0	0	0	0	0	0	0	0	0	0	0	.						

Contd...

Table 8: Contd...

Vertebral level		1	2	3	4	5	6	7	8	9	10	11	12	13	14	15	16	17	18	19	20	21
16. C7	*r*	458**	-231*	200*	677**	-458**	486**	682**	-506**	510**	756**	-529**	527**	834**	-523**	569**	1					
(Canal/Body)	*p*	0	0.021	0.047	0	0	0	0	0	0	0	0	0	0	0	0	.					
17. C7	*r*	-0.174	437**	-358**	-268**	584**	-507**	-251*	601**	-503**	-342**	703**	-601**	-392**	841**	-711**	-587**	1				
(Cord/Canal)	*p*	0.084	0	0	0.007	0	0	0.012	0	0	0	0	0	0	0	0	0	.				
18. C7	*r*	232*	-378**	355**	353**	-524**	527**	326**	-587**	561**	426**	-679**	669**	492**	-795**	783**	662**	-936**	1			
(Canal-Cord)	*p*	0.02	0	0	0	0	0	0.001	0	0	0	0	0	0	0	0	0	0	.			
19. T1	*r*	400**	-0.191	0.174	508**	-344**	365**	507**	-347**	351**	525**	-318**	308**	607**	-299**	329**	758**	-385**	427**	1		
(Canal/Body)	*p*	0	0.057	0.084	0	0	0	0	0	0	0	0.001	0.002	0	0.003	0.001	0	0	0	.		
20. T1 (Cord/	*r*	-0.161	457**	-371**	-0.147	467**	-370**	-0.126	411**	-312**	-0.164	495**	-375**	-223*	628**	-471**	-444**	791**	-723**	-535**	1	
Canal)	*p*	0.11	0	0	0.144	0	0	0.212	0	0.002	0.103	0	0	0.026	0	0	0	0	0	0	.	
21. T1	*r*	218*	-388**	376**	0.185	-345**	345**	0.174	-361**	344**	0.188	-406**	389**	261**	-539**	498**	437**	-681**	716**	619**	-915**	1
(Canal-Cord)	*p*	0.03	0	0	0.065	0	0	0.083	0	0	0.061	0	0	0.009	0	0	0	0	0	0	0	.

protrusion, disc space narrowing, and foraminal stenosis).[12] In order not to be affected by degenerative changes, we conducted our study in young adults (18–35 years old) in a narrower age range. For this reason, one of the reasons for the difference between the results of the studies may be the age range.

Cadaver studies on the spinal cord are also included in the literature. Ko *et al*., in their study on 15 cadavers in Chorea, reported that the sagittal diameter of the spinal cord decreases gradually from the cervical region to the upper thoracic region.[25]

The most important limitation of our study is that it was not conducted on healthy volunteers, but on patients who presented retrospectively with the complaint of neck pain. However, none of our cases had findings compatible with myelopathy, and cases with pathology in MRI were excluded from the study. Considering that pain is also a temporary and relative complaint, we think that it will not affect the results of the study.

Conclusion

Torg ratio is a ratio obtained from cervical X-rays and helps to interpret spinal canal stenosis. However, considering the Torg ratio of 0.80 and below as the limit for cervical stenosis may be misleading for some societies. Again, for the spinal canal sagittal diameter, a clinician's evaluation according to the data of studies conducted in different races and populations (14, 13, and 12 mm are considered limit values) may lead to erroneous inferences. It would be appropriate to interpret the cervical spinal canal measurement results and the lower limit values of the Torg ratio according to race and ethnic groups.

Financial support and sponsorship

Nil.

Conflicts of interest

There are no conflicts of interest.

References

1. Torg JS, Naranja RJ Jr., Pavlov H, Galinat BJ, Warren R, Stine RA. The relationship of developmental narrowing of the cervical spinal canal to reversible and irreversible injury of the cervical spinal cord in football players. J Bone Joint Surg Am 1996;78:1308-14.
2. Hashimoto I, Tak YK. The true sagittal diameter of the cervical spinal canal and its diagnostic significance in cercical myelopathy. J Neurosurg 1977;47:912-6.
3. Herzog RJ, Wiens JJ, Dillingham MF, Sontag MJ. Normal cervical spine morphometry and cervical spinal stenosis in asymptomatic professional football players. Plain film radiography, multiplanar computed tomography, and magnetic resonance imaging. Spine (Phila Pa 1976) 1991;16:S178-86.
4. Lim JK, Wong HK. Variation of the cervical spinal Torg ratio with gender and ethnicity. Spine J 2004;4:396-401.
5. Torg JS, Corcoran TA, Thibault LE, Pavlov H, Sennett BJ, Naranja RJ Jr., *et al.* Cervical cord neurapraxia: Classification,

pathomechanics, morbidity, and management guidelines. J Neurosurg 1997;87:843-50.
6. Boijsen E. The cervical spinal canal in intraspinal expansive processes. Acta radiol 1954;42:101-15.
7. Eismont FJ, Clifford S, Goldberg M, Green B. Cervical sagittal spinal canal size in spine injury. Spine (Phila Pa 1976) 1984;9:663-6.
8. Murone I. The importance of the sagittal diameters of the cervical spinal canal in relation to spondylosis and myelopathy. J Bone Joint Surg Br 1974;56:30-6.
9. Bakirci S, Ataoglu S, Pasin T, Ankarali H. The importance of Torg ratio in patients with ankylosing spondylitis. Ann Med Res 2018;25:330-4.
10. Burrows EH. The sagittal diameter of the spinal canal in cervical spondylosis. Clin Radiol 1963;14:77-86.
11. Sherman JL, Nassaux PY, Citrin CM. Measurements of the normal cervical spinal cord on MR imaging. AJNR Am J Neuroradiol 1990;11:369-72.
12. Okada E, Matsumoto M, Ichihara D, Chiba K, Toyama Y, Fujiwara H, *et al.* Aging of the cervical spine in healthy volunteers: A 10-year longitudinal magnetic resonance imaging study. Spine (Phila Pa 1976) 2009;34:706-12.
13. Ehni C. Cervical Arthrosis: Diseases of Cervical Motion Segments (Spondylosis, Disk Rupture, Radiculopathy, and Myelopathy). Chicago: Year Book Medical; 1984. p. 26-43.
14. Pavlov H, Torg JS, Robie B, Jahre C. Cervical spinal stenosis: Determination with vertebral body ratio method. Radiology 1987;164:771-5.
15. Matveeva N, Janevski P, Nakeva N, Zhivadinovik J, Dodevski A. Morphometric analysis of the cervical spinal canal on MRI. Pril (Makedon Akad Nauk Umet Odd Med Nauki) 2013;34:97-103.
16. Countee RW, Vijayanathan T. Congenital stenosis of the cervical spine: Diagnosis and management. J Natl Med Assoc 1979;71:257-64.
17. Epstein BS, Epstein JA, Jones MD. Cervical spinal stenosis. Radiol Clin North Am 1977;15:215-26.
18. Kessler JT. Congenital narrowing of the cervical spinal canal. J Neurol Neurosurg Psychiatry 1975;38:1218-24.
19. Bajwa NS, Toy JO, Young EY, Ahn NU. Establishment of parameters for congenital stenosis of the cervical spine: An anatomic descriptive analysis of 1,066 cadaveric specimens. Eur Spine J 2012;21:2467-74.
20. Isık S, Samancı M. Analysis of MRI morphometric parameters of the pediatric cervical spine and spinal cord. J Turk Spinal Surg 2019;30:157-61.
21. Inoue H, Ohmori K, Takatsu T, Teramoto T, Ishida Y, Suzuki K. Morphological analysis of the cervical spinal canal, dural tube and spinal cord in normal individuals using CT myelography. Neuroradiology 1996;38:148-51.
22. Ndubuisi CA, Mezue WC, Ohaegbulam SC. Space available for the cervical spinal cord of asymptomatic adult Nigerians. Korean J Spine 2017;14:61-5.
23. Prasad SS, O'Malley M, Caplan M, Shackleford IM, Pydisetty RK. MRI measurements of the cervical spine and their correlation to Pavlov's ratio. Spine (Phila Pa 1976) 2003;28:1263-8.
24. Presciutti SM, DeLuca P, Marchetto P, Wilsey JT, Shaffrey C, Vaccaro AR. Mean subaxial space available for the cord index as a novel method of measuring cervical spine geometry to predict the chronic stinger syndrome in American football players. J Neurosurg Spine 2009;11:264-71.
25. Ko HY, Park JH, Shin YB, Baek SY. Gross quantitative measurements of spinal cord segments in human. Spinal Cord 2004;42:35-40.

Original Article

Histopathological Changes Induced by Exposure of Mosquito Coil Smoke on the Liver of Adult Wistar Albino Rats – An Experimental Study

Masooma Syed, Midhat Syed, Farah Syed, Waqar Akram[1]

Department of Anatomy, Government Medical College, Srinagar, Jammu and Kashmir, [1]Department of Anatomy, Autonomous State Medical College, Fatehpur, Uttar Pradesh, India

Abstract

Background: Mosquito coils are widely used to control mosquitoes due to their low cost. However, their combustion releases harmful pollutants. **Objective:** This study investigates the histological changes in rat liver due to exposure to mosquito coil smoke containing d-trans allethrin. **Methods:** Eighteen Wistar rats were divided into three groups: control (Group A), exposed for 4 weeks (Group B), and exposed for 6 weeks (Group C). The rats were exposed to the smoke for 8 hours daily. Liver tissues were collected, fixed, sectioned, and stained for histological analysis. **Results:** Prolonged exposure to mosquito coil smoke leads to significant liver damage and inflammation due to the release of fine particles and toxic compounds. **Conclusion:** Long-term exposure to mosquito coil smoke is hepatotoxic. Public awareness and measures to minimize exposure are necessary.

Keywords: *Albino rat, liver, mosquito coil*

Introduction

Mosquito repellents and mosquito nets are common measures used to control the mosquito population in residential areas. Mosquito repellents come in the form of coils, vaporizers, mats, and sprays.[1] Mosquito coils (MCs) are the most commonly used method to control the mosquito population due to their economical price. The annual worldwide consumption of MCs is 29 billion units according to the WHO reports.[2]

Pyrethroids, which are the most common active ingredients in MCs, account for only 3%–4% of the coil's mass.[3,4] The bulk of MCs consists of plant-based materials, such as wood powder, coconut shell powder, joss powder, binders, dyes, oxidants (e.g., nitrates), and other additives making controlled smoldering possible during their use of approximately 8 h.

Burning a single MC has health consequences that are comparable to those of burning 75–137 cigarettes in terms of the amount of particulate matter released, as well as emitting an amount of formaldehyde equivalent to that of 51 cigarettes.[5]

Insecticides vaporize with smoke and immobilize mosquitoes. The combustion of the remaining materials generates large amounts of submicrometer particles and gaseous pollutants[4] that can be hazardous. During overnight sleeping, children and adult inhabitants are exposed to inhale these components containing small particles, metal fumes, and vapors that may reach the alveolar region of the lung and cause irritating effects on the respiratory tract.[6,7] Epidemiological studies have shown asthma and persistent wheeze in long-term exposure of children.[8,9]

As liver is the main organ involved in the metabolism of drugs and toxins, it is the primary site of target of these toxins. Thus, in the present study, we intend to conduct a detailed investigation into the histological changes in rat liver induced by exposure to MC smoke containing d-trans allethrin.

Subjects and Methods

The present study was carried out on 18 albino rats of the Wistar strain of both sexes. Rats were divided into three groups of 6 each [Table 1].

The clearance for the use of animals was obtained from the "Institutional Ethics Committee" of the college.

The study was divided into two phases:
1. Acclimatization phase
2. Experimental phase.

How to cite this article: Syed M, Syed M, Syed F, Akram W. Histopathological changes induced by exposure of mosquito coil smoke on the liver of adult Wistar albino rats – An experimental study. J Anat Soc India 2024;73:119-22.

Article Info

Received: 02 August 2023
Revised: 01 May 2024
Accepted: 08 May 2024
Available online: 27 June 2024

Address for correspondence:
Dr. Waqar Akram, Department of Anatomy, Autonomous State Medical College, Near Allipur, GT Road, Fatehpur - 212 601, Uttar Pradesh, India.
E-mail: waqarakram0306@gmail.com

Access this article online

Website: https://journals.lww.com/joai

DOI: 10.4103/jasi.jasi_78_23

Quick Response Code:

- Acclimatization phase: All the groups were acclimatized to the laboratory environment for 2 weeks under standard laboratory condition with access to food and water
- Exposure phase: The animals were exposed to MC smoke for 8 h a day (average period that humans sleep in a day) using a mosquito repellent coil brand containing 0.1% w/w of d-trans allethrin. The MC was placed at a distance of 30 cm from the cage. Group B was exposed for 4 weeks and Group C was exposed for 6 weeks [Table 2].

Dissection of the liver

After the exposure phase, the rats were euthanized by placing them in a jar filled with chloroform-soaked cotton. A midline incision was made in the abdominal wall, and the skin was retracted to open the abdominal cavity. The liver was dissected out. The tissue of 3 mm thickness was excised from the liver using a sharp blade and placed in a 10% formalin solution of the following composition.[10]

I. Formalin: 100 m
II. Tap water: 900 m
III. Sodium chloride: 8.5 g.

The tissue samples were embedded into paraffin wax and sectioned into 8-um thick sections using a microtome. Hematoxylin and eosin were used to stain the tissue sections.

Results

- Group A: Light microscopic examination of liver sections from control group rats revealed hexagonal classic hepatic lobules with radiating hepatic cords, central veins in the lobule's center, and portal areas containing portal triad formed by the portal vein, hepatic arteriole, and bile ductule surrounded by connective tissue at 3–5 corners of the lobule [Figure 1]. The central veins of the classical hepatic lobule were found in the lobule's center and had a thin connective tissue wall lined internally by endothelial cells. Hepatocyte cords radiated from the central veins [Figure 1] towards the lobule's periphery, which included the portal areas, and were one cell thick in most places.
- Group B: The histology of the liver of rats exposed to MC smoke for 4 weeks showed a normal cytoarchitecture with lymphocytic cell infiltration in the periportal area and in the parenchyma [Figure 2].
- Group C: Histological section of the liver of rats exposed to MC smoke for 6 weeks showed dilatation and congestion of the central vein and sinusoids with focal areas of hemorrhage [Figures 3 and 4].

Marked inflammatory cell infiltration in the periportal area and in the parenchyma was noted [Figure 5]. Hepatocytes showed balloon degeneration with intracytoplasmic accumulation of eosinophilic material [Figure 6]. An increase in the nuclear:cytoplasm ratio was reported. Powdery chromatin was reported in some hepatocytes. Areas of spotty necrosis were seen [Figure 7].

MC contains pyrethroid insecticide and is used widely in tropical and subtropical regions including India because of the low cost and easy availability. Upon burning, MC releases over 60 organic compounds, fine and ultrafine particles, and heavy metals, all of which can have toxic effects. In the study, the experimental group exposed to MC smoke for 4 weeks showed preserved liver cytoarchitecture,

Table 1: Division of animals into three groups (A, B, and C)

Groups	Types	Specimen Numbers
A	Control Group	6
B	Experimental Group	6
C	Experimental Group	6

Table 2: Details of exposure of rats to mosquito coil smoke

Group	Duration of Exposure
A	No exposure
B	Exposed for 4 weeks
C	Exposed for 6 weeks

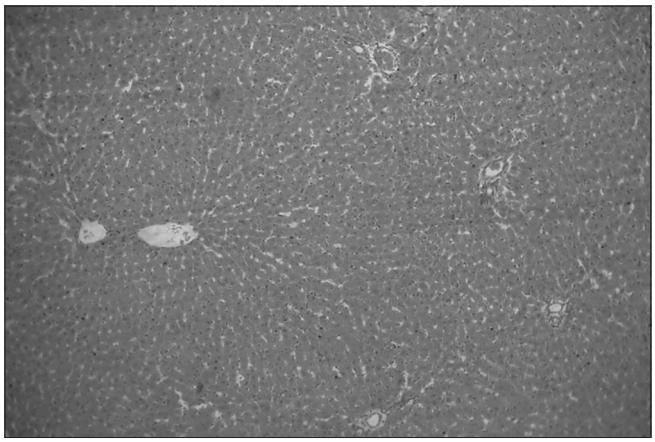

Figure 1: Section of the liver of the control group showing normal architecture (H and E stain, ×50)

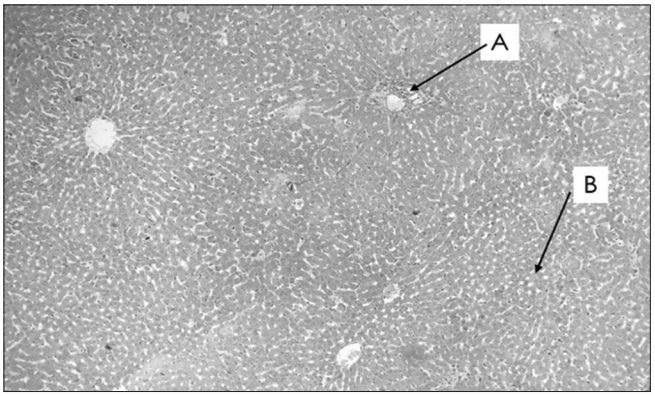

Figure 2: Section of the liver of Group B rats showing periportal inflammatory infiltrates (A) and interstitial infiltration (B) (H and E stain, ×50)

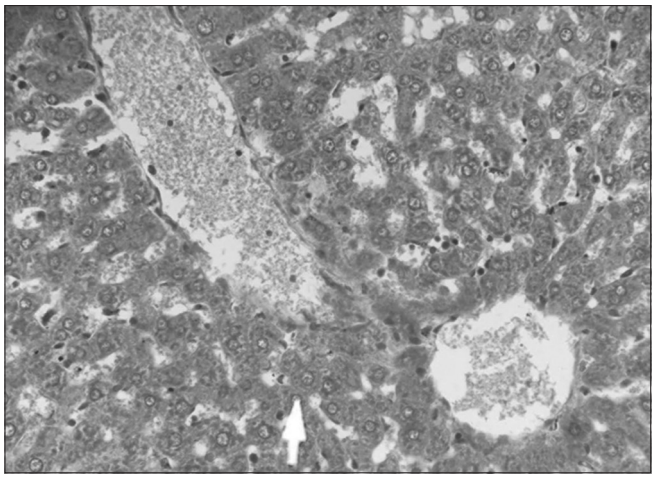

Figure 3: Section of the liver of Group C rats showing dilated and congested central vein, dilated and congested sinusoids (H and E stain, ×400

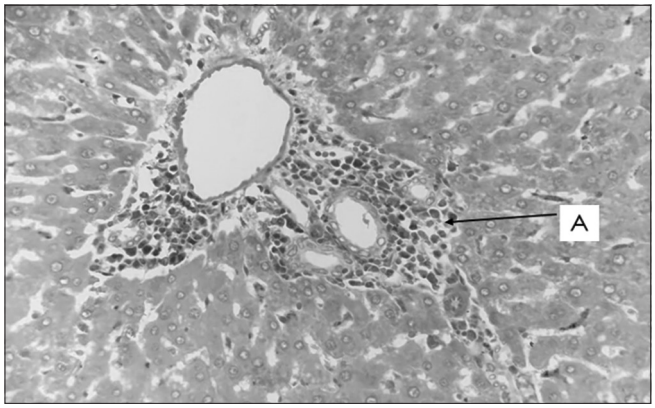

Figure 5: Section of the liver of Group C rats showing periportal inflammatory infiltrates (A) (H and E stain, ×400)

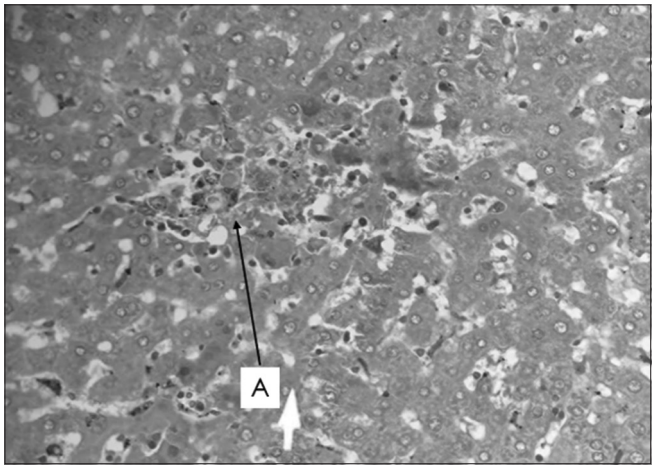

Figure 7: Section of the liver of the experimental group showing foci of necrosis (A) (H and E stain, ×400)

with lymphocytic infiltration in the periportal area and the parenchyma. The rats exposed to coil smoke for 6 weeks showed dilated and congested central vein and sinusoids, lymphocytic infiltration, and changes in the hepatocytes such as ballooning degeneration and focal areas of

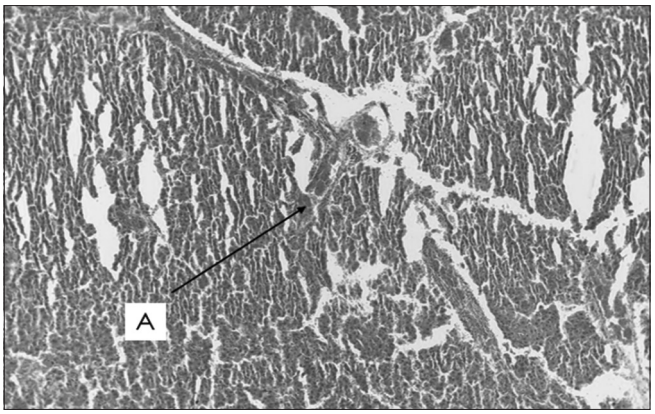

Figure 4: Section of the liver of Group C rats showing hemorrhagic foci (A) (H and E stain, ×100)

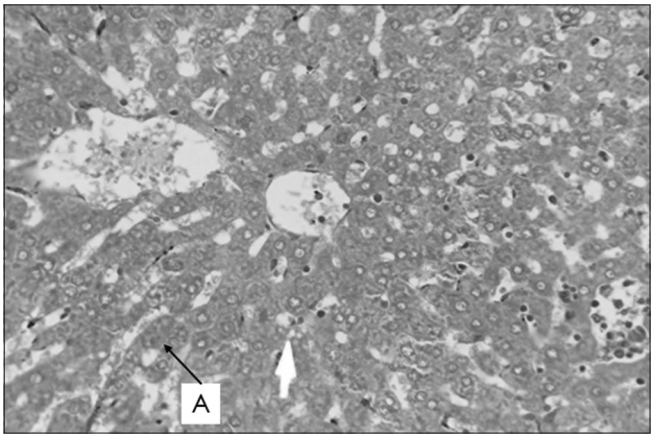

Figure 6: Section of the liver of the experimental group showing balloon degeneration of hepatocytes (A)

necrosis. Intracellular accumulations and severe sinusoidal congestion were also demonstrated by Garba *et al.*, Taiwo *et al.*, Aslam *et al.*, Idowu *et al.*, Abubakar, and Hassan [Table 3].[11-15]

The changes can be attributed to the fact that burning MC produces harmful substances, particularly hydrogen chloride and formaldehyde. The formaldehyde decomposes to form formate and causes an increase in the reactive oxygen species in the cell that can cause damage to the cell. The potential damage to the liver cells evident by an increase in the liver enzymes such as aspartate aminotransferase and alanine aminotransferase was reported by Fetoui *et al.* and Liu and Wong.[16,17]

Conclusion

These results show that exposure to MC smoke is hepatotoxic, thus long-term exposure to MC smoke is a matter of concern.

Based on these results, we recommend that general masses should be made aware about the possible hazards of the overuse of MCs and adequate measures should be taken to ensure minimal exposure to coil smoke during domestic use.

Table 3: Light microscopic changes in the liver of rats exposed to mosquito coil smoke discussion

Parameter	Group A	Group B	Group C
Architecture	Normal	Normal	
Central vein	Normal	Normal	Markedly dilated and congested
Sinusoids	Normal	Normal	Dilated and congested
Nucleus	Normal	Normal	Nuclear pleomorphism
Hepatocytes	Normal	Normal	Cloudy swelling and vacuolated cytoplasm, ill-defined boundaries
Infiltration	Absent	Periportal	Marked inflammatory cell infiltration in the periportal area, around the central vein, and in the parenchyma
Hemorrhage	Absent	No	Focal areas of hemorrhage
Portal triad	Normal	Normal	Inflammatory infiltration
Necrosis	Absent	Absent	Focal areas of necrosis

Financial support and sponsorship

Nil.

Conflicts of interest

There are no conflicts of interest.

References

1. Soderlund DM, Bloomquist JR. Neurotoxic actions of pyrethroid insecticides. Annu Rev Entomol 1989;34:77-96.
2. Mulla MS, Thavara U, Tawatsin A, Kong-Ngamsuk W, Chompoosri J. Mosquito burden and impact on the poor: Measures and costs for personal protection in some communities in Thailand. J Am Mosq Control Assoc 2001;17:153-9.
3. Lukwa N, Chandiwana SK. Efficacy of mosquito coils containing 0.3% and 0.4% pyrethrins against *An.gambiae sensu lato* mosquitoes. Cent Afr J Med 1998;44:104-7.
4. John NA, John J. Prolonged use of mosquito coil, mats, and liquidators: A review of its health implications. Int J Clin Exp Physiol 2015;2:209-13.
5. Chen SC, Wong RH, Shiu LJ, Chiou MC, Lee H. Exposure to mosquito coil smoke may be a risk factor for lung cancer in Taiwan. J Epidemiol 2008;18:19-25.
6. Cheng V, Lee HR, Chen CS. Morphological changes in the respiratory system of mice after inhalation of mosquito-coil smoke. Toxicol Lett 1992;62:163-77.
7. Chang JY, Lin JM. Aliphatic aldehydes and allethrin in mosquito-coil smoke. Chemosphere 1998;36:617-24.
8. Yang TT, Lin ST, Shie RH, Tseng CK, Ku CH. Characterization of volatile organic pollutant emissions from smoldering mosquito coils containing various atomic hydrogen/carbon ratios. Aerosol Air Qual Res 2016;16:2570-80.
9. Taylor ET, Beah JM, Barrie M, James MS, Kaitibi D, Sannoh A. Characterizing emission of particulate matter from combusting different products of mosquito coils in southern Sierra Leone. JSM Environ Sci Ecol 2017;5:1054-9.
10. Drury RA, Wallington EA. General Staining Procedures. Carleton's Histological Techniques. 5th ed. New York: Oxford University Press; 1980. p. 125-50.
11. Garba SH, Shehu MM, Adelaiye AB. Histopathological and biochemical changes in the rats following exposure to a pyrethroid based mosquito coil. J Appl Sci Res 2007;3:1788-93.
12. Taiwo VO, Nwagbara ND, Suleiman R, Angbashim JE, Zarma MJ. Clinical signs and organ pathology in rats exposed to graded dose of pyrethroids containing mosquito smoke and aerosolized insecticidal spray. Afr J Biomed Res 2008;11:97-104.
13. Aslam F, Khan A, Khan MZ, Sharaf S, Gul ST, Saleemi MK. Toxico-pathological changes induced by cypermethrin in broiler chicks: Their attenuation with Vitamin E and selenium. Exp Toxicol Pathol 2010;62:441-50.
14. Idowu ET, Aimufua OJ, Ejovwoke YO, Akinsanya B, Otubanjo OA. Toxicological effects of prolonged and intense use of mosquito coil emission in rats and its implications on malaria control. Rev Biol Trop 2013;61:1463-73.
15. Abubakar M, Hassan L. Toxicological effects of some mosquito coils brands in experimental rats. Int J Toxicol 2006;4:1-4.
16. Fetoui H, Makni M, Garoui el M, Zeghal N. Toxic effects of lambda-cyhalothrin, a synthetic pyrethroid pesticide, on the rat kidney: Involvement of oxidative stress and protective role of ascorbic acid. Exp Toxicol Pathol 2010;62:593-9.
17. Liu WK, Wong MH. Toxic effects of mosquito coil (a mosquito repellent) smoke on rats. II. Morphological changes of the respiratory system. Toxicol Lett 1987;39:231-9.

Original Article

In vitro Preparation of Dry Bones from Remnants of Dissected Cadavers: An Effective Low-cost Method of Recycling Remnants of Human Cadavers

E. A. T. Edirisinghe Sajith, H. K. De Silva Dulmini, P. Dissanayake Harsha, G. Yasawardane Surangi, Adhikarinayake Bhashitha, D. P. De Zoysa Nawodha

Department of Anatomy, Faculty of Medical Sciences, University of Sri Jayawardenapura, Gangodawila, Nugegoda, Sri Lanka

Abstract

Background: Human bones are an essential part of medical education. **Objectives:** This study outlines a new method developed by the Department of Anatomy, Faculty of Medical Sciences, University of Sri Jayewardenepura, for processing human bones from cadaver waste. **Subjects and Methods:** The bones were disarticulated, cleaned of soft tissues, and boiled with potassium hydroxide. Afterward, they were deposited in an aerating system with a water pump, covered with a soil mixture, and were aerated to provide fresh air, and the humidity of the soil was monitored. After 4 months of soil treatment, the bones were exhumed, boiled, air-dried, and varnished. **Results:** This method produced good-quality bones within a shorter time using less resources. It helped generate more bones and halve the cadaver waste cost. **Conclusion:** The technique can easily be adopted to produce human bones, even within a small space, in less time and with less labor force.

Keywords: *Anatomy education, bone preparation, cadaver waste, low cost*

Introduction

The study of anatomy begins at least as early as 1600 BC.[1] The traditional method of teaching anatomy using cadavers is universally practiced and has been considered essential for medical learning.[2] Gaining exposure to the human skeleton in the course of dissection is a crucial necessity in learning anatomy.[3] One of the goals of higher education is to create a quality, student-friendly learning environment.[4] With respect to that, there are ongoing debates in the field of medical education regarding techniques of teaching anatomy to medical students.

Due to the unavailability and high cost of human skeletons, a multitude of synthetic materials have been introduced to create models of the skeleton to teach anatomy. However, these synthetic models are not as effective as real bones in imparting anatomical knowledge regarding the human skeleton.[5] There are both advantages and disadvantages to using natural bones to study anatomy. The main advantage is that natural bones provide the ability to study the exact bony landmarks and points which are not clearly demonstrated on synthetic models. The disadvantage is the difficulty to find natural bones and ethical issues in procuring the bones.[6]

In the past, most medical faculties obtained human skeletons fairly easily by dissection of unclaimed bodies. However, in this day and age, this practice is considered unethical and requires special permission from relevant legal authorities.[7] The bone storage circulating among medical faculties and medical students has declined drastically due to these ethical and legal matters as well as due to wear and tear occurring with continuous use.[8]

Acquiring cadavers for medical teaching is not a difficult task in Sri Lanka due to the prevailing sociocultural and religious background.[9] At present, medical faculties receive cadavers as donations or by conducting excavations with legal permission.[7] However, donation of skeletons to the anatomy department too has dropped drastically during the past few years. In addition, the cost for transportation, maintenance, and disposal of cadaver remains after completion of dissections is a considerable expense that has to be borne by the faculty.[10]

Excavation of cadavers is a complex, time-consuming process with various legal obstacles which include obtaining a special

How to cite this article: Sajith EA, Dulmini HK, Harsha PD, Surangi GY, Bhashitha A, Nawodha DP. *In vitro* preparation of dry bones from remnants of dissected cadavers: An effective low-cost method of recycling remnants of human cadavers. J Anat Soc India 2024;73:123-7.

Article Info

Received: 27 July 2023
Revised: 08 April 2024
Accepted: 08 May 2024
Available online: 27 June 2024

Address for correspondence:
Dr. E. A. T. Edirisinghe Sajith, Department of Anatomy, Faculty of Medical Sciences, University of Sri Jayawardenapura, Gangodawila, Nugegoda, Sri Lanka.
E-mail: edirisinghe@sjp.ac.lk

Access this article online

Website: https://journals.lww.com/joai

DOI: 10.4103/jasi.jasi_77_23

Quick Response Code:

court order and a police report. In addition, the university has to obtain a special license for bone transportation after the excavation.[11] With regard to the excavation process, the relevant technicians need to carry it out carefully to prevent damage to the bones. Since the exact time duration after burial is not usually known, it may lead to the excavation of highly decayed or partially decayed bones which cannot be used for teaching.[12] Therefore, the process could turn out to be a waste of human labor, time, and money.

Medical undergraduate and postgraduate students need natural bones to learn anatomy effectively.[13] With the current legal restrictions, it is difficult to find a human skeleton for their academic purposes as illustrated previously. Furthermore, it is illegal for the general public to excavate buried human remains to obtain bones for academic purposes.[14] In addition to the requirement of medical faculties, there are numerous osteological studies that need to be carried out in the Sri Lankan setting to develop supportive devices for orthopedic surgery and also for forensic studies and archaeological research.[15] Therefore, there is a huge demand for natural bones with a dwindling supply. The aims of this study were to produce dry human bones by recycling the remnants of cadaver dissections via a cost-effective method to teach anatomy and to develop the smart bin for recycling remnants of cadaver dissections.

Subjects and Methods

The human specimens were obtained from cadavers that had been donated to the Department of Anatomy, Faculty of Medical Sciences, University of Sri Jayewardenepura, with complete written consent of donors before death to use the cadaver for medical teaching and research purposes. Once medical students had finished dissecting the relevant region of the body, the bones were obtained for processing. This process is carried out inside the dissection hall within the medical faculty premises.

Initially, the dissection remnants with large bones were disarticulated from the large joints and excess tissues (muscles, tendons, and skin) were removed carefully [Figure 1a and b]. The hand and foot were disarticulated at the wrist and ankle joint, respectively. The dry weight of each of the cleaned bones was measured separately and 10 g of potassium hydroxide pellets was allocated for each kilogram of dry bones, according to a ratio of 100:1. Then, the long bones and small bones were dipped in two separate boiling chambers filled with water six times the volume of the bones, and the measured potassium hydroxide pellets were added to these boiling chambers according to the dry bone weight. The chamber containing long bones was boiled with topping up of water for 6–8 h, while the chamber with small bones was boiled for 3–4 h. This was done to remove the fat in the bone marrow and loosen the attached soft tissues which are difficult to remove manually [Figure 1c]. The boiled bones were taken for burial in the custom-made smart bone bin.

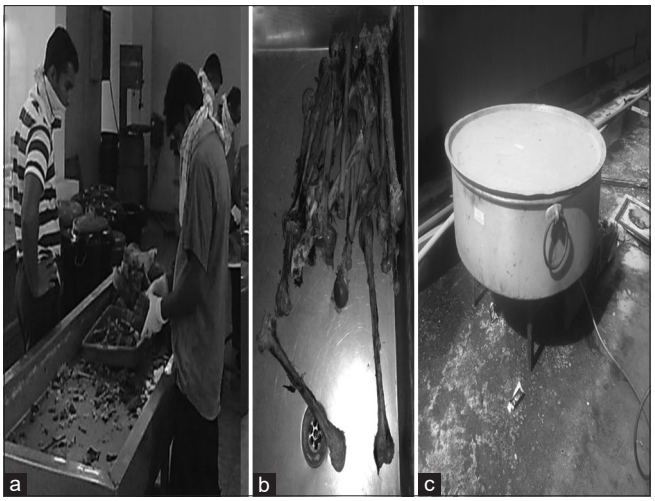

Figure 1: Cleaning of the bones. (a) Removal of excess tissue parts manually. (b) Carefully cleaned bones. (c) Boiling the bones with KOH

Four commercially available capacitive soil moisture detection sensors with analog output were coupled to an Arduino board. The threshold was adjusted to maintain the soil moisture level between 50% and 60%. The sensors were placed halfway along the height of the bin at the four sides [Figure 2a]. An aeration tubing system with four columns was made using one inch PVC tubes which were fitted to a 100 L plastic barrel. Holes which were 3 mm in diameter were drilled one inch apart in a spiral manner. All four tubes were connected at the bottom to a common central line. The central line was brought up to the top of the barrel and was connected to a socket which could connect to a flexible hose coming from the air blower [Figure 2b]. The Arduino board was programmed to pump water containing lactobacillus when the humidity of the soil dropped below 45%. The same board was programmed to switch on the blower when the soil moisture exceeded 65%. Furthermore, a commercially available timer was installed to make the air blower run for 15 min every 12 h to supply adequate air for the decaying process. This was scheduled to take place at 6 a.m. and 6 p.m. daily to avoid disturbance to the academic work at the faculty due to the noise. A few holes were made at the bottom of the bin to remove excess water. The bin was placed in an aluminum tray which was kept on a custom-made trolley with side brake-caster wheels which were 100 mm in diameter. Sand was added to the gap between the aluminum tray and the bin. This helps in the evaporation of excess water seeping out of the bin which in turn prevents mosquito breeding.

A commercially available submersible water pump used in the aquarium industry was employed to pump water containing lactobacillus. The lactobacilli bacteria solution was added to accelerate the decaying process and reduce the odor. The power supply output for the water pump

was taken out of the metal box and fixed to the bottom of the box. The water container was sealed and kept next to the smart bone preparation bin. The Arduino circuit, air blower, and timer were fixed inside a commercially available metal box and wired with a power indicator and was then mounted on a wall [Figure 3A-E].

Red soil, sand, and compost were mixed in 1:2:1 ratio. A layer of the soil mixture was first added to the bottom of the bin. Then, a set of boiled bones were packed around the aeration tubes and another layer of soil mixture was added on top. Similarly, the bones were packed in layers until the bin was filled. Special precautions were taken to prevent damage to the fixed soil moisture sensors. Long bones were buried in a vertical manner and small bones were wrapped in a small stainless-steel mesh [Figure 4a and b]. The bin was placed in the dissection hall at room temperature. The fluctuation of soil moisture, aeration, and the addition of water was graphed, and the data were uploaded to a cloud server. After 5 months, the bones were recovered. They were washed and reboiled in water for disinfection [Figure 4c]. Figure 5 shows the full diagrammatic representation of the system.

Results

The new invention helps prepare real bones from cadaver waste in a small space. This method is easily adaptable by any medical faculty with the use of few resources. It helps in reducing the cost of cadaver waste disposal by the anatomy department. Annually, the Department of Anatomy of the Faculty of Medical Sciences, University of Sri Jayewardenepura, disposes 16 cadavers after dissections. Thereby with this technique, the Department of Anatomy can produce 16 skeletons annually for medical learning and teaching of undergraduates and postgraduates as well as for research purposes. These skeletons are given free of charge to students to carry out their day-to-day studies.

This method reduced the annual load of dissected waste and costs of disposal by 50% and the quality of the bones was better than that of the bones collected from the cemetery. The method produced a higher number of bones using minimum space in a short period of time. A patent application was filed for the process that was employed to prepare bones from remnants of dissected cadavers.

Discussion

Anatomists and medical educators have long attempted to develop effective techniques to prepare bones for anatomical studies in a sustainable manner.[16] In addition, obtaining human bones for such preparation has also proved to be a challenge. Historically, grave robbing and even murder have been recorded as some of the reprehensible methods used to acquire human bones.[17] Dissection of unclaimed bodies and excavation of buried bodies too have been practiced, but these practices are now governed by rules

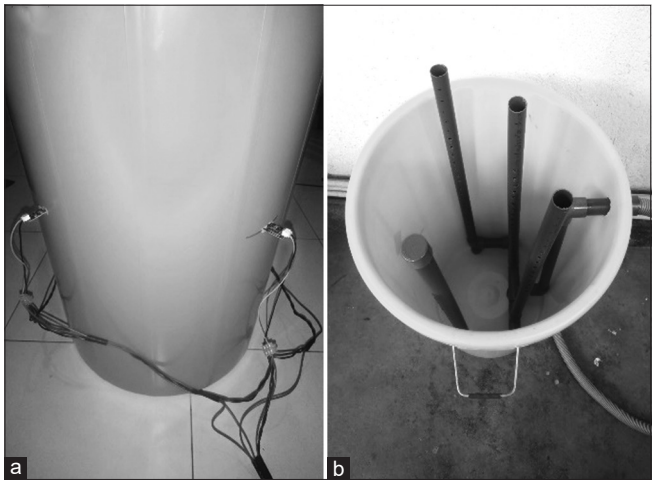

Figure 2: Preparation of the smart bone bin. (a) Positioning of the soil moisture sensors. (b) Aeration tubing system

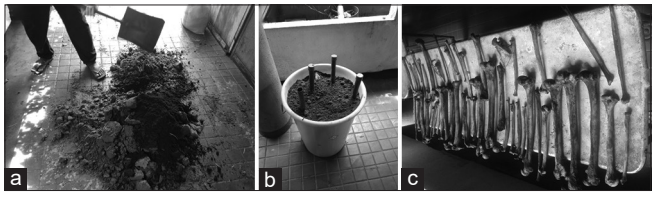

Figure 4: (a) Preparation of soil mixture, (b) packed bones in the soil bin with aeration system, and (c) final product

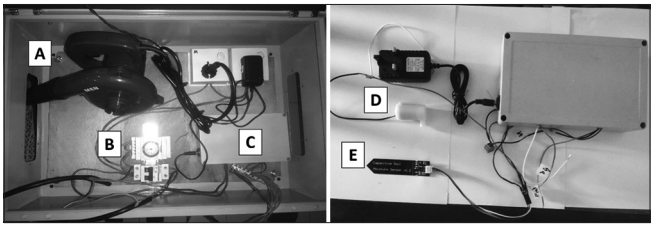

Figure 3: (A) Air blower, (B) timer, (C) control unit with arduino circuit, (D) water pump, (E) soil moisture sensor

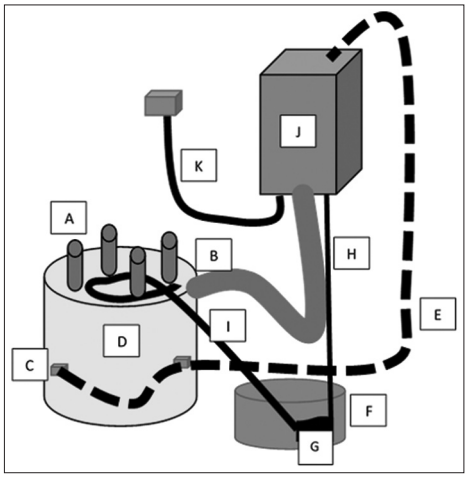

Figure 5: (A) Aerating vertical columns, (B) air inlet, (C) soil moisture sensor, (D) plastic bin, (E) electrical wiring for soil moisture sensors, (F) water storage bin, (G) submersible water pump, (H) electrical input for the water pump, (I) water pump outlet tubing system, (J) controlling unit with Arduino board, (K) main power supply

and regulations to prevent misuse in the name of science.[18] Therefore, utilizing the remains of cadavers donated to the medical faculties is an ethically and legally unobjectionable method as opposed to the other methods mentioned above.

Preparation of skeletal material has three basic steps; maceration or the removal of soft tissues, defatting, and bleaching.[12] Maceration could be carried out via numerous methods including immersion of bones in water, boiling, and insect consumption. Inorganic chemicals such as ammonium hydroxide and sodium hydroxide and organic chemicals such as enzymes and detergents too have been used for maceration purposes.[12] Burial of the bones in soil is also another method that can be used to remove soft tissues.[16] In a study done by Modi *et al*., 2014, it was found that boiling of bones followed by burial under soil is a better method of obtaining good-quality bones compared to the use of detergent and immersion in warm water.[12] These techniques are employed in the present study as well.

A technique for the use of enzymes for the removal of soft tissues and chemical defatting was described by Wang Huaqiao in the Chinese patent number CN1320369A. In a resource-poor setup such as Sri Lanka, getting down such enzymes (proteases) is a logistic and financial challenge. Furthermore, the use of acetone for defatting needs to be carried out under extra precautions due to the high risk of fire. In the current study, a very low amount of chemicals was used.

Wang Jingtao in Chinese patent number CN107361055A disclosed a bone specimen preparation method in medical teaching. In that method, no chemicals were used for boiling and a 30% hydrogen peroxide solution was used for the removal of fat. 30% hydrogen peroxide is a costly acquisition. In the present invention, defatting is done at the time of boiling which reduced the consumption of both chemicals and time. In the patented process, the burial process was not monitored, but, in this study, the burial method was carried out indoors and the soil moisture level and aeration were closely monitored. Therefore, the new method was able to prepare bones in a shorter time period than the method described in the above patent.

The method outlined in this study completely utilizes the remnants of human cadaver after dissections. Once medical students have finished dissecting a certain region of the body, the bones of that region are free for processing. One such advantage in this process is that technicians can proceed systematically with bone processing of different regions of the body according to the academic calendar. This can prevent a heavy workload and minimize the disposal cost of cadaver waste.

The proposed method is highly effective especially for medical faculties located in urban areas where the allocation of space for the burial of cadavers is a problem. The greatest advantage in this process is that it can be conducted entirely in an indoor environment and requires very small space. The ability to develop multiple full skeletons simultaneously within a short period of time using minimal resources and a smaller labor force is an additional advantage. This process also provides an acceptable alternative to obtaining human bones without the accompanying ethical, legal, and social issues of excavating burial sites.

Conclusion

This is an effective method of recycling the remnants of human cadavers *in vitro* and reducing the maintenance and disposal costs of human cadavers. This method can produce an ample number of bones to satisfy the requirements for undergraduate and postgraduate teaching purposes within a short period of time using much less resources.

Financial support and sponsorship

Nonacademic staff of the Department of Anatomy, Faculty of Medical sciences, University of Sri Jayawardenapura, in providing technical support. Dr. Devmini, K.A.M.T, and Dr. Pathmaperuma, S.D.S, for their support in collecting data and editing the manuscript.

Conflicts of interest

There are no conflicts of interest.

References

1. Staden HV. Herophilus: The Art of Medicine in Early Alexandria: Edition, Translation and Essays: Cambridge University Press; 1989.
2. Aly AA, Staden HV. Herophilus: The Art of Medicine in Alexandria: Edition, Translation and Essays. Cambridge: Cambridge University Press; 1989. p. xliii-666.
3. Pujol S, Baldwin M, Nassiri J, Kikinis R, Shaffer K. Using 3D modeling techniques to enhance teaching of difficult anatomical concepts. Acad Radiol 2016;23:507-16.
4. Biggs JL, Sutherell JS, Remus R, Armbrecht ES, King MA. Positive outcomes of optimizing student-preceptor continuity in a traditional block clerkship. Teach Learn Med 2018;30:202-12.
5. Habbal O. The state of human anatomy teaching in the medical schools of gulf cooperation council countries: Present and future perspectives. Sultan Qaboos Univ Med J 2009;9:24-31.
6. Preece D, Williams SB, Lam R, Weller R. "Let's get physical": Advantages of a physical model over 3D computer models and textbooks in learning imaging anatomy. Anat Sci Educ 2013;6:216-24.
7. Habicht JL, Kiessling C, Winkelmann A. Bodies for anatomy education in medical schools: An overview of the sources of cadavers worldwide. Acad Med 2018;93:1293-300.
8. Mekereş F, Buhaş C, Rahotă D, Moga I, Voiță F, Mekereş G. A new approach to exploring human anatomy. Rom J Funct Clin, Macro Microsc Anat Anthropol 2017;16.
9. Subasinghe SK, Jones DG. Human body donation programs in Sri Lanka: Buddhist perspectives. Anat Sci Educ 2015;8:484-9.
10. Ghazanfar H, Rashid S, Hussain A, Ghazanfar M, Ghazanfar A, Javaid A. Cadaveric dissection a thing of the past? The insight of consultants, fellows, and residents. Cureus 2018;10:e2418.

11. Hutchinson EF, Kramer B, Billings BK, Brits DM, Pather N. The law, ethics and body donation: A tale of two bequeathal programs. Anat Sci Educ 2020;13:512-9.
12. Modi B, Puri N, Patnaik VV. Evaluation of techniques for cleaning embalmed cadaver bones. Int J Anat Res 2014;2:810-3.
13. Aggarwal N, Gupta M, Goyal PK, Kaur J. An alternative approach to bone cleaning methods for anatomical purposes. Int J Anat Res. 2016;4:2216-21.
14. Laws of Sri Lanka; 2014. Available from: https://www.srilankalaw.lk/revised-statutes/volume-ii/147-cemeteries-and-burial-grounds-ordiance.html. [Last accessed on 2024 Apr 08].
15. Scheuer L. Application of osteology to forensic medicine. Clin Anat 2002;15:297-312.
16. Ajayi A, Edjomariegwe O, Iselaiye O, TS A. A review of bone preparation techniques for anatomical studies. Malaya J Biosci 2016;3:76-80.
17. Ator GA, Andrews JC, Maxwell DS. Preparation of the human skull for skull base anatomic study. Skull Base Surg 1993;3:1-6.
18. Štrkalj G, El-Haddad J, Hulme A. A global geography of body acquisition for anatomy education: Issues, challenges and prospects. In: Chan LK, Pawlina W, editors. Teaching Anatomy: A Practical Guide. Cham: Springer International Publishing; 2020. p. 223-35.

Original Article

Morphological Variations of the Umbilical Cord of Full-term Fetuses – Correlation with Maternal and Newborn Parameters

Divia Paul Aricatt, Meera Jacob[1], Manisha Rajanand Gaikwad[2], Dane Chandy

Department of Anatomy, Fr. Muller Medical College, Kankanady, [1]Department of Anatomy, Yenepoya Medical College, Mangalore, Karnataka, [2]Department of Anatomy, All India Institute of Medical Sciences, Bhubaneswar, Odisha, India

Abstract

Introduction: Abnormalities in the development and site of insertion of the umbilical cord (UC) can cause problems which have the potential to affect maternal and fetal health. The aim of the present study was to evaluate the gross features of UC of singleton pregnancies and correlate it to the newborn parameters and maternal parameters at term. **Materials and Methods:** An observational, descriptive pilot study was carried out with 100 placentas. All ethical principles for human research were followed and ethical approval was obtained from the institutional ethics committee of the medical college from where data were collected. The inclusion criteria were the adequately preserved placenta with no gross abnormalities. Placenta belonging to hypertensive mothers and mothers with gestational diabetes were excluded. **Results and Conclusion:** The UC morphology was recorded and analyzed. Newborn parameters and maternal parameters were correlated to UC parameters. The present study statistics showed 53% placentas with central insertion, 36% eccentric insertion, 3% furcated and marginal insertions each, and 5% specimens with velamentous insertion. A correlation between the UC insertion site and birth weight was observed. Low birth weight was observed when the cord was inserted eccentrically. Further investigations are required among velamentous insertion to reach a conclusion for maternal blood group correlations.

Keywords: *Fetal growth retardation, maternal parameters, single umbilical artery, umbilical cord design, umbilical cord insertion*

Introduction

The umbilical cord (UC) connects the fetus with the placenta which contains two arteries and one vein surrounded by Wharton's jelly. Normal development and central pattern of insertion UC are expected, any deviation from the morphology can have potential affect maternal and fetal health.[1,2] The UC transfers oxygen and nutrients to the growing fetus throughout pregnancy. Numerous studies have pointed out the importance of normal UC morphology with implications on the insertion site. Abnormal positioning of UC can be associated with numerous maternal complications and fetal distress.[2-7] Variations in the site of insertion of UC are thought to result from the process known as trophotropism in which the chorionic frondosum or the early placenta "migrates" with advancing gestation to ensure a better blood supply from a more richly vascularized area.[3,8] The UC insertion site can be subdivided into four categories: central, paracentral, marginal/battledore, and velamentous/membranous. The central/paracentral category is considered the normal condition. It is well accepted that UC insertion is considered aberrant when attached within 2 cm of the edge of the placental disk (marginal/battledore) or when it is inserted into the chorioamniotic membranes (velamentous/membranous), which often leads to fetal death. The incidence of velamentous is 1.1% in singleton births and 8. 7%–16% in twin deliveries.[9] Thus UC insertion to the placenta is divided as central, eccentric, marginal, and velamentous, as it is related to the chorionic plates. Another type of variation is a furcate insertion, in which UC branch before its insertion into the placenta.[3,10-13]

Complications during delivery and other pathologies, i.e., intrauterine growth restriction, preterm labor, and trophotropism can be the outcome of peripherally inserted UC.[14] Furcate placenta (0.5%–1%) has more volume of villi, villous trophoblast, and syncytial knots.[10] Early impaired

How to cite this article: Aricatt DP, Jacob M, Gaikwad MR, Chandy D. Morphological variations of the umbilical cord of full-term fetuses – Correlation with maternal and newborn parameters. J Anat Soc India 2024;73:128-32.

Article Info

Received: 03 April 2023
Accepted: 12 January 2024
Available online: 27 June 2024

Address for correspondence:
Dr. Divia Paul Aricatt, Department of Anatomy, Fr. Muller Medical College, Kankanady, Mangalore - 575 008, Karnataka, India.
E-mail: divia_manoj@yahoo.com

Access this article online

Website: https://journals.lww.com/joai
DOI: 10.4103/jasi.jasi_34_23
Quick Response Code:

fetal development can be correlated with genetic and environmental-associated mechanisms which are associated with placental functioning and UC parameters.[7,15] Oxygen and nutrient transfer capacity of the placenta is highly associated with the vascular network within the chorionic villi. Abnormal UC insertion is associated with a smaller placenta[15] and lower placental vessel density.[16] The placental insufficiency and fetal growth are dependent on abnormal cord insertion which may increase the susceptibility to antenatal risk.[17,18] Optimal placentation will result in a central insertion of the UC which facilitates optimal growth of the fetus throughout gestation. Therefore, the aim of the present study was to evaluate the gross features of UC and correlate it to the newborn parameters and maternal parameters at term.

Materials and Methods

An observational, descriptive pilot study was carried out with 100 placentas. All ethical principles for human research were followed and ethical approval was obtained from the institutional ethics committee of the medical college from where data were collected. The inclusion criteria were the adequately preserved placenta with no gross abnormalities. Placenta belonging to hypertensive mothers and mothers with gestational diabetes were excluded.

Collection of specimens

We collected a total of 100 specimens (placenta with intact UC) obtained from the department of Obstetrics and Gynecology. Samples were preserved in buffered 10% neutral formalin and analyzed at the department of anatomy.

Method of study

Specimens were cleared, dissected, and observed carefully for umbilical parameters, namely insertion (central, eccentric, marginal, velamentous, and furcate) by measuring its distance from the placental margin, cord length (normal between 55 and 60 cm, long >60 cm, and short <40 cm), cord vessels (number of arteries and veins), placental weight (normal between 500 and 600 g, overweight >600 g, underweight <500 g), and cord design (normal, false knots, and true knots). Details were photographed, recorded, and analyzed.

Newborn parameters analyzed were baby weight (normal 2.5–4.2 kg, overweight >4.2 kg, and underweight <2.5 g), head circumference (normal 33–35 cm, more >37 cm, and less <31 cm), baby length (normal 50–52 cm, more >55 cm, and less <45 cm). Maternal blood groups were noted down for further correlations.

Results

The placental attachment of UC and the site of insertion were noted down for 100 samples. Among the samples, 53 placentas showed central insertion and 36 eccentrically insertions of cords. In three specimens, we found furcated insertion five specimens had velamentous insertion and three specimens showed marginal insertion [Figure 1a-e].

Normal cord length was seen in 89 cases with an average of 53.14 cm. Short cords were noted among 10 cases which had central and eccentric insertions. The single placenta had a long cord. Ninety-six cases showed normal cord vasculature were four cases showed abnormal vascular patterns with single umbilical artery (SUA) [Figure 1f]. Placental weight was normal in 70 cases, where 24 placentas weighed less than the normal attached by central and eccentric insertion to UC and 6 placentas had increased weight than normal which had furcate, velamentous, and eccentric insertions of UC. Normal design and pattern of UC were observed in 37 specimens with eccentric insertions predominantly. False knots were seen in 63 cords with central insertions [Figure 1g]. No cord exhibited a true knot.

Newborn parameters analysis showed that 89 infants had normal birth weight with an average of 2.88 Kg. No incidence of large date babies was observed. Eleven babies were underweight with their UC and had central and eccentric insertions. Head circumference and baby length of 96 infants were normal with an average of 33.7 cm and 48.4 cm, respectively. No incidence of large head circumference and increased baby length was observed. Among 4, babies with decreased head circumference and baby length had central and eccentric insertions of their UC attachment.

Maternal blood group analysis showed Rh^{+ve} and Rh^{-ve} mothers of all blood groups had central, eccentric, and marginal insertions. When velamentous insertion of the cord was taken into special consideration because of its complexities, we had four B^{+ve} mothers and a single O^{-ve} mother. Further investigations are required among this insertion to reach a conclusion for blood group correlations.

Discussion

The UC morphology and parameters and the deviations from optimal features under certain conditions can affect the fetus. A better understanding of cord function and design is essential for finding solutions to UC-related complications. Abnormal UC design can result in cord rupture, entanglement, complications during labor, and uterine malfunction.

The present study statistics showed 53% placentas with central insertion, 36% eccentric insertion, 3% furcated and marginal insertions each, and 5% specimens with velamentous insertion [Table 1]. Studies by Piloto *et al*.,[19] Rolschau[20], and Ebbing *et al*.[15] had also reported the highest prevalence of central followed by eccentric and marginal insertions. The study samples were more than the present study in other studies by different authors but the percentages of the aforementioned

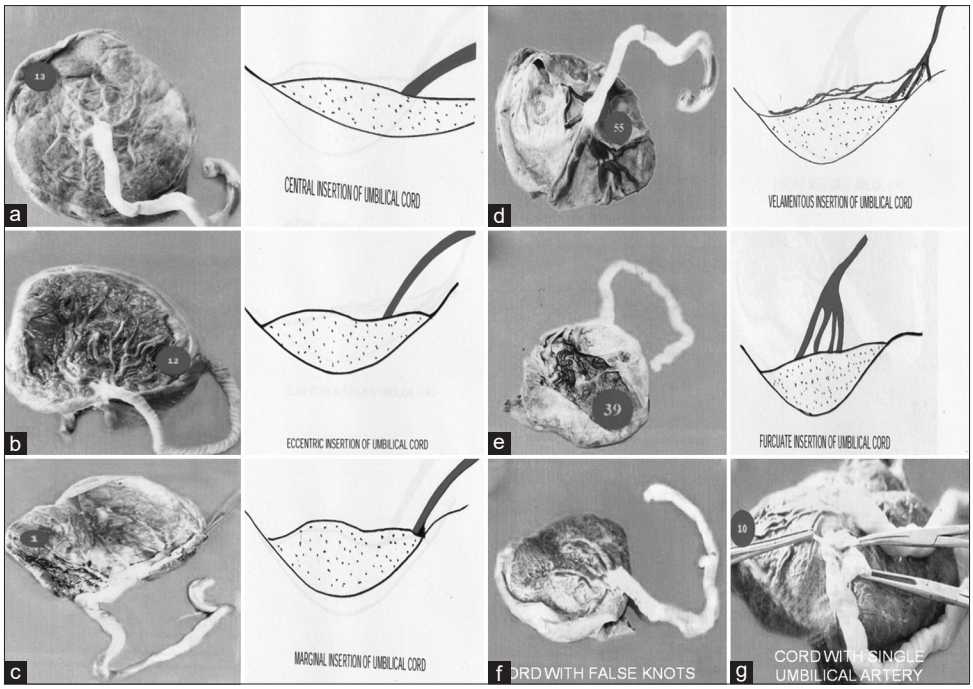

Figure 1: (a-e) Umbilical cord insertions, (f) Cord with false knots, (g) Cord with single umbilical artery

Table 1: Fetal organs and impaired maturation

Category parameters	Condition, *n* (%)				
	Central	Eccentric	Marginal	Furcate	Velamentous
UC insertion	53	36	3	3	5
UC length					
Normal	48	31	3	3	4
Long	0	1	0	0	0
Short	5	4	0	0	1
UC vasculature					
Normal	49	36	3	3	5
Abnormal	4	0	0	0	0
Placental weight					
Normal	35	26	3	2	4
More	0	4	0	1	1
Less	18	6	0	0	0
UC design					
Normal	12	24	1	0	0
False knots	41	12	2	3	5
True knots	0	0	0	0	0

UC: Umbilical cord

insertions were similar to the present study. Ranga MK and Sadanam SS report a higher prevalence for eccentric insertions than central insertions in their study.[21] None of the comparative studies had furcate insertion for UCs. When velamentous insertion was taken into account, the present study percentage for the same was more than the studies of Rolschau of 1.15% of velamentous insertions in studies. Ebbing *et al*. had 1.5% and Brouillet *et al*.[22] had 0.95% velamentous insertions in their sample populations. These percentages when compared to the present study show a decreased trend. In the present study, infant birth weight at term was reported within normal limits among central and peripheral UC insertions. Brouillet *et al*.[22] reported an association with fetal growth restriction in terms of low birth weight among UC insertion except for central insertion. This result suggests that central UC attachment is relevant for attaining optimal fetal parameters, i.e., fetal weight, and in peripheral cord insertions, there was a higher occurrence of fetal growth retardation.

In the present study, normal cord length was seen in 89 cases with an average of 53.14 cm. Short cords were noted among 10 cases that had central and eccentric insertions. The single placenta had a long cord. Abaidoo *et al*.[23] reported an average cord length of 47.04 cm and the study also reports 21.56% of short cords which is more than the present study which had only 10% of short cords. When the present study was compared to the studies of Appiah,[24] the percentage of short cords was higher in the compared study, i.e., 29.62%, where increased cord length percentages were similar to the present study.

While comparing with the previous study of UC vasculature, it was noted that the SUA was more significant in the present study. The present study had 4% of SUA against 1% in studies of Geipel *et al*. and 0.2%–1.1% in studies of Heredia and Jeanty.[25,26]

Newborn parameters analysis showed that 89 infants had normal birth weight with an average of 2.88 Kg. No incidence of large date babies was observed. Eleven babies were underweight with their UC and

had central and eccentric insertions. Thomson *et al*. reported that the placental weight and size were not directly proportional to the birth weight.[27] In contrast to this, Shanklin.[28] reports low birth weight when the cord is inserted marginally or velamentously. Grbesa and Durst-Zivković[29] reported low birth weight when the cord was inserted eccentrically which is similar to the present study but increased birth weight was seen in babies with marginal insertion of cord to the placenta. This is not observed in the present study.

Conclusion

Correlation between the UC morphology with maternal and fetal parameters has been highlighted in our study. Extensive studies are required to better understand the physiopathological mechanisms that facilitate the difference in the pattern of UC insertions. To improve neonatal outcomes and avoid maternal complications during delivery, adequate antenatal checkups and ultrasound monitoring for UC abnormalities are inevitable. Further investigations are required among velamentous insertion to reach a conclusion for maternal blood group correlations.

Limitations

We could not perform a placental immunohistochemical study to correlate partial regression of the chorionic villi with UC insertion.

Ethical approval

We have obtained consents from parents of the newborns involved in this study.

Authors' contributions

All authors have equal contribution towards the study.

Acknowledgments

All authors appreciate the great effort of anatomy lab technicians of AIIMS BBSR, Yenepoya Medical College, Mangalore for their timely help and assistance in the conduction of this study.

Financial support and sponsorship

Nil.

Conflicts of interest

There are no conflicts of interest.

References

1. Redline RW. The clinical implications of placental diagnoses. Semin Perinatol 2015;39:2-8.
2. Tantbirojn P, Saleemuddin A, Sirois K, Crum CP, Boyd TK, Tworoger S, *et al.* Gross abnormalities of the umbilical cord: Related placental histology and clinical significance. Placenta 2009;30:1083-8.
3. Robinson LK, Jones KL, Benirschke K. The nature of structural defects associated with velamentous and marginal insertion of the umbilical cord. Am J Obstet Gynecol 1983;146:191-3.
4. Liu CC, Pretorius DH, Scioscia AL, Hull AD. Sonographic prenatal diagnosis of marginal placental cord insertion: Clinical importance. J Ultrasound Med 2002;21:627-32.
5. Räisänen S, Georgiadis L, Harju M, Keski-Nisula L, Heinonen S. Risk factors and adverse pregnancy outcomes among births affected by velamentous umbilical cord insertion: A retrospective population-based register study. Eur J Obstet Gynecol Reprod Biol 2012;165:231-4.
6. Pinar H, Carpenter M. Placenta and umbilical cord abnormalities seen with stillbirth. Clin Obstet Gynecol 2010;53:656-72.
7. Redline RW. Clinical and pathological umbilical cord abnormalities in fetal thrombotic vasculopathy. Hum Pathol 2004;35:1494-8.
8. Monie IW. Velamentous insertion of the cord in early pregnancy. Am J Obstet Gynecol 1965;93:276-81.
9. Benirschke K, Kaufmann P, Benirschke K, Kaufmann P. Multiple pregnancy. Pathology of the human placenta. 2000. p. 790-902.
10. Singh L, Pal GP. Human Embryology in the Placenta. 8th ed. India: Macmillan Publishers India Ltd.; 2009. p. 59-75.
11. McLennan JE. Implications of the eccentricity of the human umbilical cord. Am J Obstet Gynecol 1968;101:1124-30.
12. Uyanwah-Akpom P, Fox H. The clinical significance of marginal and velamentous insertion of the cord. Br J Obstet Gynaecol 1977;84:941-3.
13. Gavriil P, Jauniaux E, Leroy F. Pathologic examination of placentas from singleton and twin pregnancies obtained after *in vitro* fertilization and embryo transfer. Pediatr Pathol 1993;13:453-62.
14. Luo G, Redline RW. Peripheral insertion of umbilical cord. Pediatr Dev Pathol 2013;16:399-404.
15. Ebbing C, Kiserud T, Johnsen SL, Albrechtsen S, Rasmussen S. Prevalence, risk factors and outcomes of velamentous and marginal cord insertions: A population-based study of 634,741 pregnancies. PLoS One 2013;8:e70380.
16. Misra DP, Salafia CM, Miller RK, Charles AK. Non-linear and gender-specific relationships among placental growth measures and the fetoplacental weight ratio. Placenta 2009;30:1052-7.
17. Burton GJ, Jauniaux E. Placental oxidative stress: From miscarriage to preeclampsia. J Soc Gynecol Investig 2004;11:342-52.
18. Burton GJ, Jauniaux E, Watson AL. Maternal arterial connections to the placental intervillous space during the first trimester of human pregnancy: The Boyd collection revisited. Am J Obstet Gynecol 1999;181:718-24.
19. Piloto RF, Magna LA, Beiguelman B. Factors influencing human birth weight in normal pregnancy: A prospective study in a Brazilian university hospital. Rev Bras Genét 1993. p. 457-69.
20. Rolschau J. The relationship between some disorders of the umbilical cord and intrauterine growth retardation. Acta Obstet Gynecol Scand 1978;57:15-21.
21. Ranga MK, Sadanam SS, Vellarada. Morphological variations of umbilical cord in human placenta. Int J Anat Res 2019;7:6786-9.
22. Brouillet S, Dufour A, Prot F, Feige JJ, Equy V, Alfaidy N, *et al.* Influence of the umbilical cord insertion site on the optimal individual birth weight achievement. Biomed Res Int 2014;2014:341251.
23. Abaidoo CS, Boateng KA, Warren MA. Morphological variations of the "Baby's supply line". J Sci Technol (Ghana) 2008;28:1-9.
24. Appiah PK. Relationship between the Morphology of the Placenta Umbilical Cord and Perinatal Outcome (Doctoral Dissertation).
25. Geipel A, Germer U, Welp T, Schwinger E, Gembruch U. Prenatal diagnosis of single umbilical artery: Determination

of the absent side, associated anomalies, Doppler findings and perinatal outcome. Ultrasound Obstet Gynecol 2000;15:114-7.
26. Heredia F, Jeanty P. Umbilical Cord Anomalies. Women's Health Alliance; 2002. p. 1149. Available from: www. thefetus. net/http:// sonoworld. com/fetus/page. aspx? [Last accessed on 2023 Aug 08].
27. Thomson AM, Billewicz WZ, Hytten FE. The weight of the placenta in relation to birthweight. J Obstet Gynaecol Br Commonw 1969;76:865-72.
28. Shanklin DR. The influence of placental lesions on the newborn infant. Pediatr Clin North Am 1970;17:25-42.
29. Grbesa D, Durst-Zivković B. Neonatal and placental factors in relation to the mode of umbilical cord insertion. Stereological analysis of chorionic villi. Pflugers Arch 1996;431:R205-6.

Original Article

Topographic Radioanatomical Analysis of the Singular Canal: Computed Tomography Study

Berin Tuğtağ Demir[1], Ali Köksal[2,3], Fatih Çankal[1,4]

[1]Department of Anatomy, Faculty of Medicine, Ankara Medipol University, [2]Department of Radiology, Ankara Bayindir Private Hospital, [3]Department of Radiology, Vocational School of Health Services, Atilim University, [4]Department of Radiology, Pursaklar State Hospital, Ankara, Türkiye

Abstract

Purpose: The singular canal (SC) is where the singular nerve, a branch of the inferior vestibular nerve, which carries afferent information from the posterior semicircular canal (PSCC), passes and is important in the surgical approach of the presigmoid retrolabyrinthine. This study was carried out to evaluate the visibility of the SC on standard computed tomography (CT) images, its distance to the surrounding structures, and to investigate the variations of its anatomy and its relationship with the meatus acusticus internus. **Materials and Methods:** The study was carried out retrospectively using images of 194 temporal bones on temporal bone CT scans of 44 men and 53 women aged 18–65. In the study, various measurements were made, especially the presence of the SC, its length, its angle with the internal acoustic canal (IAC), and the distance between the internal acoustic pore (IAP) and the singular foramen. In addition, the presence of the high jugular bulb and PSCC dehiscence images were investigated. **Results:** The SC was detected in 85.1% of the analyzed images. The mean canal length was 3.93 ± 1.22 mm, the angle between the SC and the IAC was 22.68° ±3.60°, and the distance between the SC and the IAP was 7.70 ± 0.83 mm. While no difference was found between the sides, it was determined that the length and diameter of the SC did not differ according to gender. **Conclusion:** Detailed morphometric analysis of the SC and a thorough understanding of its relationship with the IAC, vestibulum, and PSCC will help to accurately define the posterior and lateral borders of the dissection for this region.

Keywords: *Computed tomography, internal acoustic canal, singular canal, vestibulum*

Introduction

The singular canal (SC) is located posteroinferior to the lower vestibular nerve and in the pars petrosa of the temporal bone and lies between the ampulla of the posterior semicircular canal (PSCC) and the internal acoustic canal (IAC).[1] The singular nerve, a branch of the inferior vestibular nerve, also known as the posterior ampullar nerve, carries afferent information from the PSCC and passes through it.[1,2]

SC begins from the posteroinferior direction of the fundus of the IAC, medial to the lower vestibular area. The existing hole here is called foramen singulare (FS) (Morgagni foramen). This canal in the temporal bone ends in the ampulla of the PSCC and has a total length of 4–5 mm.[3] Determining the importance of the relationship between this critical landmark and the labyrinth is extremely important anatomically and radiologically when planning appropriate surgical procedures. SC is accepted as a surgical guide point during the retrosigmoid and transmeatal approach to the IAC with singular neurectomy.[4,5] In addition, since this canal can be confused with temporal bone fracture, it is particularly important in radiological evaluations.[3,4] The canal can be seen in clinical computed tomography (CT) studies, and its identification will help distinguish it from, for example, a fracture.

Another feature that makes SC important is the singular neurectomy, the basic surgical procedure for treating paroxysmal positional vertigo. This approach is unique because it is the only procedure, in which a retrolabyrinthine structure (the posterior ampullar nerve) can be manipulated transmeatally with minimal surgical intervention. Since the operation area is close to the inner ear structures, the operation requires sensitive surgical techniques.[6] Therefore, the spatial anatomy of this region is of primary importance for the surgeons undertaking the operation. Despite the importance of the procedure, there is little quantitative anatomical information regarding the optimal

How to cite this article: Demir BT, Köksal A, Çankal F. Topographic radioanatomical analysis of the singular canal: Computed tomography study. J Anat Soc India 2024;73:133-7.

Article Info

Received: 13 February 2023
Accepted: 02 February 2024
Available online: 27 June 2024

Address for correspondence:
Dr. Berin Tuğtağ Demir, Department of Anatomy, Faculty of Medicine, Ankara Medipol University, Ankara, Türkiye.
E-mail: berrintugtag@hotmail.com

Access this article online

Website: https://journals.lww.com/joai

DOI: 10.4103/jasi.jasi_14_23

Quick Response Code:

approach for this operation.[5,6] Although most surgeons learn the complex temporal bone anatomy by cutting cadaver temporal bones for relevant field operations, only a limited number of temporal bones are usually present. Unfortunately, precise three-dimensional (3D) measurements that can guide the procedure cannot be made at temporal bones during dissection. Although temporal bone anatomy can also be studied by a conventional histological study of two-dimensional slides, it can be difficult to relate this information to 3D anatomy. This study aims to present morphometric results that can guide singular neurectomy.

We planned to study this not-overworked part of the temporal bone, an extremely important structure in clinical anatomy, otolaryngology, and radiology education, which may be helpful. Until now, meatus acusticus internus has been studied in detail in anatomical and clinical studies, but the details of fundus morphology have remained in the background due to the small and complex structure of the relevant region. Studies have been done with small sample groups (n = 8–15 etc.,) with cadavers or micro-CT images.[3-6] This study aims to evaluate the visibility of SC on CT examination, its distance from surrounding structures, and to investigate its anatomical variations and its relationship with the meatus acusticus internus. This study aimed to contribute to the literature by evaluating the anatomical and radiological features of SC and presenting clinical and morphological data for other surgical approaches related to this region, especially the presigmoid retrolabyrinthine approach.

Materials and Methods

Study design and eligibility criteria

Among 145 patients who underwent temporal bone CT examination in our imaging center between January 2020 and August 2022, 97 patients (44 males and 53 females) aged between 18 and 65 years and did not meet the exclusion criteria were included in the study. Exclusion criteria were any trauma or surgical operation to this region, an inflammatory process causing changes in bone structure, and any acquired or congenital anatomical anomaly.

Imaging method and evaluation

The study was retrospective, and the images were obtained with a 32-detector multislice CT device with a section thickness of 0.625 mm in the axial plane.

Images of 194 temporal bones belonging to 97 patients were evaluated together by three researchers, one of whom is a radiologist, the second is an anatomist with knowledge of cross-sectional anatomy, and the other is also a radiologist and clinical anatomist. Image evaluations were made with the licensed RadiAnt DICOM Viewer 2022.1 BETA.

Research parameters

First, the presence of SC was investigated in the images, and in the cases found, the distance between the posterior wall of the internal acoustic pore (IAP) and the SC distance (IAP-SC), the angle of the SC with the IAC, the length of the SC, and the diameter of the SC were measured. Measurements were made from 2 points related to the SC diameter. The first measurement was made from the point where the SC enters the IAC (FS), and the second point is from the point where it exits the vestibulum. The SC angle was made from the point where the canal enters the IAC [Figure 1]. In addition, IAC length, vestibulum length and width, and transverse diameter of the PSCC ampulla were also measured. In addition, the presence of the high jugular bulb (HJB) and PSCC dehiscence was also evaluated.

Statistical analysis

After all measurements were completed, data analysis was performed with SPSS (IBM SPSS Statistics for Windows, Version 22.0. Armonk, NY: IBM Corp). Data on continuous variables are reported as mean ± standard deviation. Statistical significance was defined as a $P < 0.05$. The groups were then assessed by the independent t-test.

Results

Temporal CT images of 44 men and 53 women were included in the study. A total of 194 temporal CT images were analyzed. All images were evaluated separately as right and left sides. While SC was not detected in 14.9% (n = 29) of the analyzed images, SC was detected in 85.1% (n = 165). While 28.9% (n = 56) had HJB, PSCC dehiscence was found in 29.9% (n = 58) [Table 1].

It was determined that IAP-SC distance (IAP posterior wall and SC distance), SC length, vestibulum length, width, and transverse diameter of PSCC ampulla differed according to gender, and these parameters were longer in women than in men ($P < 0.05$). The diameter of the SC at the IAC inlet was measured as 0.59 ± 0.15 mm, and the diameter of the SC at the vestibulum outlet was measured as 0.97 ± 0.09 mm. The mean SC angle was measured as 22.68° ±3.60°. No statistical significance was found between the genders

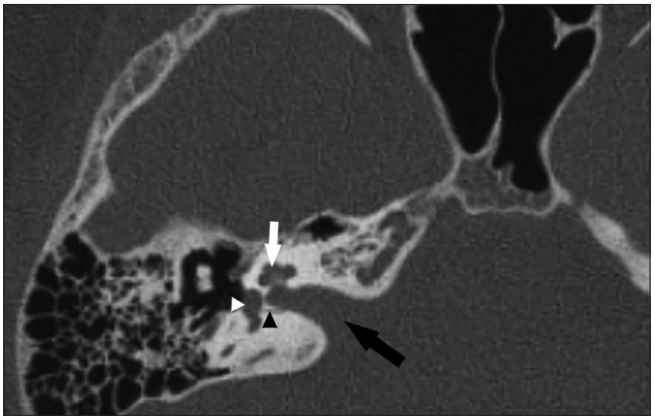

Figure 1: Axial computed tomography scan with bone window-weighting. Black arrow: Internal acoustic porus, black arrowhead: Singular canal, white arrow: Cochlea, white arrowhead: Vestibule

($P > 0.05$) [Table 2]. All these measurements were also analyzed by distinguishing the right and left sides. However, statistical significance was not determined between the sides for any measurements ($P > 0.05$).

The relationship between the presence of HJB and dehiscence and SC and vestibulum morphology is given in Table 3. It was determined that the SC and IAC were longer and the SC angle was smaller in individuals without HJB. It was determined that IAC, vestibulum length, width, and PSCC amp transverse diameter were larger in individuals without PSCC dehiscence ($P < 0.05$).

Figure 1 summarizes whether IAC length, vestibulum width, length, and transverse diameter of the PSCC ampulla differ according to the presence of SC. Accordingly, only the vestibulum length was longer in those without SC, which was statistically significant [Figure 2].

Table 1: Presence of singular canal, high jugular bulb, and posterior semicircular canal dehiscence

	Right, *n* (%)	Left, *n* (%)
SC		
Yes	85 (51.5)[a]	80 (48.5)[a]
No	12 (41.4)[a]	17 (58.6)[a]
HJB		
Yes	29 (29.9)[a]	27 (27.8)[a]
No	68 (70.1)[a]	70 (72.2)[a]
PSCC deh		
Yes	32 (33.0)[a]	26 (26.8)[a]
No	65 (67.0)[a]	71 (73.2)[a]

Chi-square, $P<0.05$, same letters indicate no significance. *n*=Frequency, SC: Singular canal, HJB: High jugular bulb, PSCC Deh: Posterior semicircular canal dehiscence

Discussion

Most inner ear structures have high variations in the topographic position, making them unreliable for the precise location of the underlying labyrinth structures. Many opinions discuss the anatomical limitations of various approaches, such as retrosigmoid transcranial surgery for the petroclival area, which requires extensive extradural drilling of the posterior pyramid, and reporting that the structures in this region should be well defined.[7,8] In this study, the morphology of the canal length, diameter, vestibulum, and PSCC ampulla diameter were investigated radiologically, with particular reference to SC surgery. In addition, in this study, although it was investigated whether the HJB and PSCC dehiscence were associated with SC morphology, no significance was found.

Table 2: Singular canal morphology by gender

Parameters	Mean	Female		Male		*t*	*P*
		Mean±SD	Minimum–maximum	Mean±SD	Minimum–maximum		
IAP-SC distance (mm)	7.70±0.83	7.98±0.57	5.90–9.81	7.46±1.05	4.90–9.07	4.06	0.00
SC length (mm)	3.93±1.22	4.10±1.50	1.78–5.82	3.67±0.50	2.12–4.12	2.31	0.02
SC diameter (IAC inlet) (mm)	0.59±0.15	0.58±0.10	0.33–0.99	0.61±0.20	0.23–1.19	0.84	0.39
SC diameter (vestibulum outlet) (mm)	0.97±0.09	0.97±0.06	0.67–1.10	0.98±0.12	0.56–1.10	0.99	0.32
SC angle (°)	22.68±3.60	22.94±4.29	19.10–56.80	22.28±2.11	19–28.90	0.84	0.45
IAC length (mm)	11.29±1.20	11.18±1.21	8.40–14.20	11.46±1.31	8.35–14.20	1.42	0.15
Vestibulum length (mm)	6.55±0.61	6.74±0.65	4.79–7.82	6.41±0.55	5.53–7.82	3.39	0.00
Vestibulum width (mm)	3.41±0.62	3.69±0.43	2.32–4.41	2.99±0.63	2.32–4.14	8.69	0.00
PSCC amp transverse diameter (mm)	1.37±0.39	1.47±0.35	0.59–2.03	1.24±0.41	0.59–1.92	3.80	0.00

Independent t-test, $P<0.05$. SC: Singular canal, IAP: Internal acoustic pore, IAC: Internal acoustic canal, PSCC: Posterior semicircular canal, SD: Standard deviation

Table 3: The relationship between the presence of high jugular bulb and dehiscence with measurements such as diameter, length, and angle

Parameters	HJB		*t*	*P*	PSCC dehiscence		*t*	*P*
	Yes	No			Yes	No		
IAP-SC distance (mm)	7.89±0.69	7.71±0.89	1.26	0.20	7.75±1.10	7.78±0.70	0.21	0.81
SC length (mm)	2.89±0.89	4.42±1.02	9.38	0.00	3.82±0.35	3.97±1.42	0.68	0.49
SC diameter (IAC inlet) (mm)	0.64±0.13	0.56±0.16	3.01	0.00	0.57±0.18	0.60±0.14	1.10	0.27
SC diameter (vestibulum outlet) (mm)	0.96±0.07	0.98±0.09	1.68	0.09	0.97±0.18	0.98±0.08	0.33	0.74
SC angle (between IAC-SC) (°)	23.90±2.56	22.12±3.91	3.03	0.00	22.07±1.88	22.95±4.05	1.38	0.16
IAC length (mm)	10.91±0.86	11.48±1.42	2.82	0.00	11.15±1.20	11.70±1.47	2.76	0.00
Vestibulum length (mm)	6.60±0.57	6.67±0.66	0.01	0.98	6.43±0.56	6.98±0.64	5.88	0.00
Vestibulum width (mm)	3.50±0.44	3.33±0.69	1.77	0.07	3.18±0.73	3.46±0.57	2.91	0.00
PSCC amp transverse diameter (mm)	1.32±0.36	1.39±0.41	1.03	0.30	1.17±0.41	1.45±0.36	4.72	0.00

Independent t-test, $P<0.05$. SC: Singular canal, IAP: Internal acoustic pore, IAC: Internal acoustic canal, HJB: High jugular bulb, PSCC deh: Posterior semicircular canal dehiscence

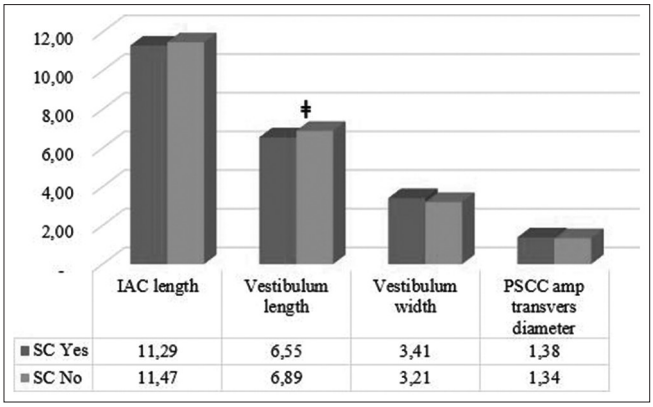

Figure 2: Relationship between the presence of singular canal and vestibulum and posterior semicircular canal ampulla. IAC: Internal acoustic canal, PSCC: Posterior semicircular canal, SC: Singular canal

SC may remain below the fenestra cochlea (FC) or may not be detected radiologically because it is very thin. Even when a singular neurectomy is desired for benign paroxysmal positional vertigo, surgery may fail because SC cannot be detected in 3%–8.3% of patients.[6] While Gacek (1984) reported that the SC was completely invisible behind the FC in 13.6% of the patients who were examined by CT,[9] Silverstein *et al*., according to the results of the high cranial tomography (HCT) examination of 21 temporal bones they dissected, in all of the cases, reported the presence of SC in all of the cases.[5] Muren *et al*. (1991) reported that on CT imaging, the rate of SC is 93% in the axial and 78% in the coronal.[10] In our research, we detected the presence of the SC canal at a rate of 85.1%. There are limited studies on SC and topographic anatomy in the literature, especially with radiological methods. Therefore, SC morphology and its relationship with inner ear structures are important in the region's surgery.

Krombach *et al*., in their study on CT, stated that care should be taken to avoid the PSCC and suggested that the bone lateral to the transverse crest should not be removed.[11] Scerrati *et al*. defined a microsurgical technique to approach the posterior half of the IAC by measuring a series of topographic points on five cadaver heads, but they reported that the SC dimensions should be known first for this.[12] When the SC is used as a landmark, more bone can be safely removed from the internal acoustic meatus (IAM) without fear of drilling the labyrinth.[13] In a study, in which SC was investigated using cone-beam CT, the canal length was determined as 4.16 ± 0.87 mm, and the mean angle was 19.1°. The diameters of the inner ear canal opening of SC, central turning area, and posterior ampulla opening have been reported as 0.98 ± 0.51, 0.36 ± 0.05, and 0.38 ± 0.06 mm, respectively.[14] Takahashi and Sando (1992) reported the SC length as 4.9 ± 0.6 mm and the mean SC angle (with the transmeatal approach) as 49°.[6] We determined the length of the SC to be 3.93 ± 1.22 mm, the diameter of the SC at the IAC inlet and the vestibule outlet as 0.59 ± 0.15 mm and 0.97 ± 0.09 mm, respectively, and the SC angle (the angle between IAC-SC) as 22.68° ±3.60°. Paying attention to the distances specified in the interventions to be made to IAM is recommended.

Labyrinth signs and relationships with structures encountered during surgical dissection should be noted. The SC is separated from the vestibule by 1–2 mm, consistent with the bone.[15] It is recommended that the singular nerve should not be approached more than 2 mm to prevent injury to the vestibule or ampulla of the PSCC.[5,16] In the retrosigmoid approach, if the transverse crest is accepted as the distal margin of the bony IAM dissection, drilling 3–4 mm lateral to the IAM will not be safe; in this case, the probability of drilling the labyrinth is 90%.[13] Agirdir *et al*. (2001) examined 10 dry 10 cadaver temporal bones by HCT. Using the SC as a landmark, the researchers reported that lateral drilling could be attempted from the posterior wall of the IAC after exposing 6–6.5 mm of the IAC.[17] They also emphasized that drilling can be done safely to a minimum depth of 4–5 mm from the posterior surface and 2–3 mm lateral to the Subarcuate fossa (SF). We found that the singular nerve opened 7.70 ± 0.83 mm from the IAP and the total length of the IAC was 11.29 ± 1.20 mm. When evaluated with the literature findings, it should not be forgotten that the singular nerve can be found after 6.00 mm from the IAP in interventions to the inner ear. Silverstein *et al*. reported that SC is valuable as a landmark in preventing fenestration of the labyrinth during surgery with the retrosigmoid IAC approach.[5] In this context, the aperture of the SC facing the IAC may be a useful indicator for estimating the distance to the fundus during IAC surgery since many investigators have reported that the length of the lateral portion of the IAC is relatively constant throughout life.[5,15,16]

When applying the retrosigmoid transmeatal approach in labyrinthine surgery, the most important guide point for safe access to the IAC has been stated as the medial of the SC.[7] Therefore, the position of SC in IAC is important. SC will be an important landmark in the inferolateral part of the IAC due to the proximity of the SC to the ampulla of the PSCC laterally.[15] In our study, it was determined that the transverse diameter of the PSCC ampulla was 1.32 ± 0.36 mm, the canal was oriented toward the IAC from the inferior of the ampulla and was connected to the IAC with an angulation of approximately 22°.

Although the semicircular canals and the relationship of the vestibular nerve with other bony elements are known in posterior meatal interventions, Silverstein *et al*. advocated using the PSCC to mark the lateral dimension of the drilling without disturbing the labyrinth.[16] Kartush *et al*. also advocated identifying the vestibular canal and the necessity of following the cochlear canal up to the circular canal to protect the vestibule.[13] Moreover, the location of the SC represents an important landmark during the retrosigmoid approach to vestibular schwannomas

because the identification of SC has a critical role in preventing labyrinth injury.[9] While Hou and Wang reported the vestibule length as 5.89 ± 0.34 mm and width as 2.47 ± 0.36 mm in the axial plane.[18] We determined the vestibulum length as 6.55 ± 0.61 mm and width as 3.41 ± 0.62 mm.

One of our study's most striking results was that the vestibulum length was longer in those without SC, which was statistically significant. It should be kept in mind that the vestibulum may be long and, therefore, should be protected when attempting to intervene in the labyrinth in individuals in whom SC cannot be detected. In addition, our study found that the SC and IAC were longer, and the SC angle was smaller in individuals without HJB. It was determined that IAC, vestibulum length, width, and PSCC ampulla transverse diameter were greater in individuals without PSCC dehiscence.

Conclusion

The posterior and lateral borders of the dissection can be accurately defined with a thorough understanding of the SC dimensions and the relationship of the SC with the IAC, vestibulum, and PSCC. While the retrosigmoid and posterior fossa transmeatal approach provides an opportunity to preserve hearing, topographic markings of the posterior part of the petrous pyramid are extremely valuable during surgical dissection. This study tried to prevent perforation of the labyrinth and to reveal the importance of SC in the relationship between IAC and labyrinth. It is anticipated that the use of intraoperative 3D imaging systems of the petrous pyramid alongside endoscopes to visualize the labyrinth with the IAC will be valuable in the future.

Financial support and sponsorship

Nil.

Conflicts of interest

There are no conflicts of interest.

References

1. Brackmann DE, Shelton C, Arriaga MA. Chapter 36 – Retrolabyrinthine and retrosigmoid vestibular neurectomy. In: Otologic Surgery. Elsevier Health Sciences, Amsterdam; 2018.
2. Kozerska M, Skrzat J. Anatomy of the fundus of the internal acoustic meatus – Micro-computed tomography study. Folia Morphol (Warsz) 2015;74:352-8.
3. Muren C, Wadin K, Dimopoulos P. Radioanatomy of the singular nerve canal. Eur Radiol 1991;1:65.
4. Kwong Y, Yu D, Shah J. Fracture mimics on temporal bone CT: A guide for the radiologist. AJR Am J Roentgenol 2012;199:428-34.
5. Silverstein H, Norrell H, Smouha E, Haberkamp T. The singular canal: A valuable landmark in surgery of the internal auditory canal. Otolaryngol Head Neck Surg 1988;98:138-43.
6. Takahashi H, Sando I. Three-dimensional computer-aided reconstruction and measurement of the temporal bone for singular neurectomy. Eur Arch Otorhinolaryngol 1992;249:74-8.
7. Rennert RC, Brandel MG, Steinberg JA, Friedman RA, Couldwell WT, Fukushima T, *et al*. Maturation of the internal auditory canal and posterior petrous bone with relevance to lateral and posterolateral skull base approaches. Sci Rep 2022;12:3489.
8. Day JD, Kellogg JX, Fukushima T, Giannotta SL. Microsurgical anatomy of the inner surface of the petrous bone: Neuroradiological and morphometric analysis as an adjunct to the retrosigmoid transmeatal approach. Neurosurgery 1994;34:1003-8.
9. Gacek RR. Cupulolithiasis and posterior ampullary nerve transection. Ann Otol Rhinol Laryngol Suppl 1984;112:25-30.
10. Muren C, Wadin K, Dimopoulos P. Radioanatomy of the singular nerve canal. Eur Radiol 1991;1:65-9.
11. Krombach GA, van den Boom M, Di Martino E, Schmitz-Rode T, Westhofen M, Prescher A, *et al*. Computed tomography of the inner ear: Size of anatomical structures in the normal temporal bone and in the temporal bone of patients with Menière's disease. Eur Radiol 2005;15:1505-13.
12. Scerrati A, Lee JS, Zhang J, Ammirati M. Microsurgical anatomy of the internal acoustic meatus as seen using the retrosigmoid approach. Otol Neurotol 2016;37:568-73.
13. Kartush JM, Telian SA, Graham MD, Kemink JL. Anatomic basis for labyrinthine preservation during posterior fossa acoustic tumor surgery. Laryngoscope 1986;96:1024-8.
14. Zhang ZY, Wang Z, Yin GX, Wang ZC. A study of quantitative measurement of singular nerve canal with cone-beam computed tomography. Zhonghua Yi Xue Za Zhi 2018;98:2978-81.
15. Haberkamp TJ, Meyer GA, Fox M. Surgical exposure of the fundus of the internal auditory canal: Anatomic limits of the middle fossa versus the retrosigmoid transcanal approach. Laryngoscope 1998;108:1190-4.
16. Silverstein H, Norrell H, Haberkamp T. A comparison of retrosigmoid IAC, retrolabyrinthine, and middle fossa vestibular neurectomy for treatment of vertigo. Laryngoscope 1987;97:165-73.
17. Agirdir BV, Sindel M, Arslan G, Yildirim FB, Balkan EI, Dinç O. The canal of the posterior ampullar nerve: An important anatomic landmark in the posterior fossa transmeatal approach. Surg Radiol Anat 2001;23:331-4.
18. Hou KY, Wang ZC. Measurements of the vestibule of normal inner ear on volume CT. Chin J Radiol (China) 2013;47:500-4.

Original Article

Normal Elbow Angles in Saudi Population: Radiographic Study

Sara M. Alharbi, Hamza M. Alrabai[1], Ahmed Fathalla El Fouhil, Mohammed Z. Aldalati[1], Banan S. Alqadi[2]

Departments of Anatomy, [1]Orthopedics and [2]College of Medicine, King Saud University, Riyadh, Saudi Arabia

Abstract

Background: In this study, we aimed to measure normal elbow radiographic angles in the Saudi population and compare the normal range of elbow angles between Saudi males and females, as well as those previously measured in other populations. **Methods:** Anteroposterior and lateral plain radiographs of 304 normal elbows from 153 females and 151 males from the Saudi population, aged > 18 years, were assessed. Radiographs, 174 right elbows, and 130 left elbows were studied retrospectively, between 2018 and 2023 in our institute. Only normal elbow radiographs with acceptable quality were included. The standard radiographic elbow measurements were collected. Data analysis was conducted with Student's *t*-test for parametric data and Wilcoxon Mann–Whitney *U* test for nonparametric data. Two certified orthopedic surgeons performed the measurements independently. Interobserver and intraobserver errors were measured. **Results:** All the radiographic elbow measurements in Saudis did not show any significant sexual dimorphism or difference between sides. The radiographic angles obtained on the anteroposterior view appeared more reliable than lateral view angles. Unlike carrying angle (CA), measurements of radiographic elbow angles in Saudis were inconsistent with previously published values. **Conclusions:** The elbow radiographic anatomical parameters of the Saudi population were not consistent with previously published values except for CA. The presence of a significant impact of geographical or racial variation on elbow radiographic anatomy requires additional investigations.

Keywords: *Carrying angle, elbow angles, radiographic studies, Saudi population*

Introduction

Understanding the anatomical variations in elbow joints is essential for the successful management of elbow pathologies.[1,2] Variations or alterations in elbow joint anatomy can be visualized on radiographs. Elbow radiographic anatomy has been studied with more focus on sex differences,[3] fracture outcomes,[4-7] and ossification patterns.[8] Radiographically, the elbow structural elements are typically silhouetted as consistent lines, curves, semicircles, and angles. These characteristics could be identified, described, and measured. Based on that, various radiographic qualitative and quantitative measurements have been proposed and proved to be useful for research and clinical purposes.[7,9,10] The physicians used to observe these radiographic features for identification, confirmation of elbow abnormalities, and development of appropriate treatment plans in multiple conditions such as congenital malformations, injuries, and arthrosis.[11]

Despite the valuable role of the elbow radiographic features and angles in clinical practice, there may be some degree of variation among people of different racial or geographical backgrounds. Zhao *et al*. observed that elbow prostheses, which were developed in the Western population, do not properly fit Chinese subjects.[12] To date, no studies have been conducted to determine the normal range of elbow joint angles in the Saudi population. This study aimed to evaluate the radiographic anatomical variations in elbow joint angles and establish their normal ranges in the Saudi population and compare the elbow joint angles between Saudi males and females. The present study also intended to compare the radiographic elbow measurements of Saudi patients with previously published data.

Methods

Patients

In this retrospective study, the authors reviewed 304 elbow radiographs collected from the radiology database, between 2018

How to cite this article: Alharbi SM, Alrabai HM, El Fouhil AF, Aldalati MZ, Alqadi BS. Normal elbow angles in Saudi population: Radiographic study. J Anat Soc India 2024;73:138-44.

Article Info

Received: 25 December 2023
Revised: 14 April 2024
Accepted: 12 May 2024
Available online: 27 June 2024

Address for correspondence:
Dr. Hamza M. Alrabai, Department of Orthopedics, College of Medicine, King Saud University, Riyadh, Saudi Arabia.
E-mail: halrabai@ksu.edu.sa

Access this article online

Website: https://journals.lww.com/joai

DOI: 10.4103/jasi.jasi_140_23

Quick Response Code:

and 2023. The study proposal was approved by the Institutional Review Board. Of these radiographs, 153 were from females and 151 were from males; 174 were from the right side and 130 were from the left side. All Saudi patients with normal elbow radiographs taken at 18 years and older were included in this study. The exclusion criteria were non-Saudi and elbow radiographs of patients with congenital deformities or with a history of trauma or surgery. The patients' demographic data, including age, sex, and side, were collected.

Radiographic assessment

The standard elbow radiography set consisted of anteroposterior and lateral views. Elbow anteroposterior radiographic images were taken at maximum elbow extension, whereas lateral images were obtained at a 90° flexed elbow position. For assessment of interobserver error, all the elbow radiographs were examined by two independent orthopedic-certified specialists. Two weeks later, the same team of independent orthopedic investigators reexamined the images to evaluate intraobserver error. The commonly used elbow radiographic angles and morphologic features were tested based on Goldfarb *et al*.'s[9] study assessment methods. The built-in tools of digital picture archiving and communication system software (GE Healthcare, Chicago, IL) were utilized to create, adjust, and measure angles and circles for radiographic measurement purposes.

Anteroposterior radiographic measurements

(1) The radial neck shaft angle (RNSA) represents the angle subtended between the longitudinal axis of the radial shaft and the radial neck long axis and is also a right angle to the articular surface of the radial head [Figure 1a]
(2) The articular surface angle is the angle between the joint line of the distal humerus and the long axis of the humerus [Figure 1b]
(3) The carrying angle (CA) is made by the intersection of the long axis of the distal humerus with the long axis of the proximal ulna [Figure 1c]
(4) The trochlear notch angle (TNA) refers to the angle between two tangential lines delineating the medial and lateral surfaces of the trochlear notch [Figure 1d]
(5) The articular surface assessment was conducted based on Goldfarb *et al*.[9] method which is consisted of qualitative and quantitative domains.

Qualitative assessment

Three distinct groups of distal humerus morphology were described based on the degree of development of the lateral trochlear ridge (LTR), trochlear sulcus (TS), and trochleocapitellar sulcus (TCS) [Figure 2]. Type 1 indicates a relatively flat-surfaced distal humerus where the LTR is poorly formed, and subsequently, the adjacent sulci appears ill-defined. Type 2 refers to the distal humerus version with underdeveloped LTR and a shallow sulcus on either side. Type 3 is characterized by a prominent ridge and deep adjacent sulci.

Quantitative assessment

The depth of the LTR, TS, and TCS relative to the distal humerus articular horizontal line was measured in millimeters [Figure 3].

Lateral radiographic measurements

(1) The anterior humeral capitellar line runs along the anterior cortex of the distal humerus and continues distally across the capitellum [Figure 4a]. The capitellum is divided into anterior, central, and posterior thirds. The zone, in which the AHCL falls is identified
(2) Radiocapitellar alignment was assessed by a line drawn along the radial neck and extended through the capitellum [Figure 4b]. The capitellar zone, in which this line passes, is observed. The capitellum is divided into superior, central, and inferior thirds
(3) Anterior angulation of the articular surface of the distal humerus was estimated by measuring the angle between the anterior cortical line of the distal humerus and a line representing the long axis of the distal humerus condylar segment [Figure 4c]

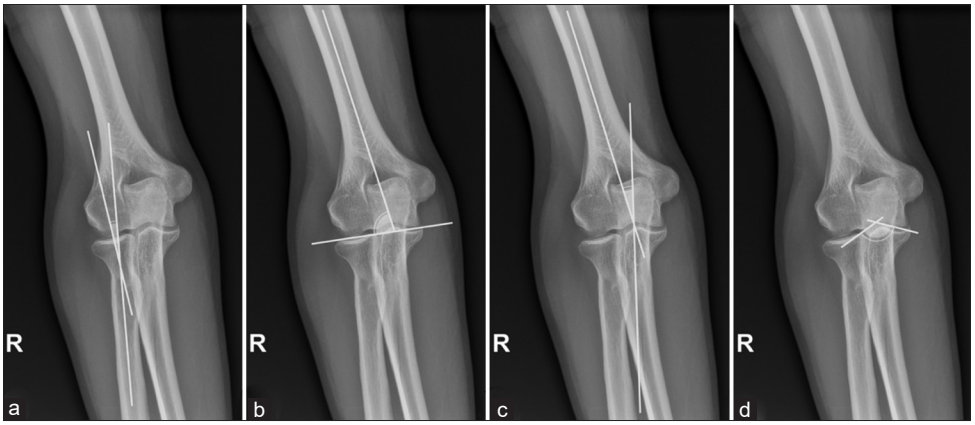

Figure 1: Standard elbow radiographic angles on the anteroposterior view. (a) Radial neck angle, (b) Articular surface angle, (c) Carrying angle, (d) Trochlear notch angle

Figure 2: Articular surface morphological classification. (a) Type 1 flat contour, (b) Type 2 small ridge and shallow sulci, (c) Type 3 prominent ridge and deep sulci

Figure 3: Quantitative assessment of the depth of anatomical landmarks of the distal humerus relative to the horizontal joint line

Figure 4: Standard elbow radiographic angles on the lateral view. (a) Anterior humeral capitellar line, (b) Radiocapitellar alignment, (c) Anterior angulation of the articular surface of the distal humerus, (d) Olecranon coronoid angle

Figure 5: The greater sigmoid notch circle is delineated with a dashed circle

(4) The olecranon coronoid angle is the angle between the ulnar shaft axis line and a line connecting the tips of the olecranon and coronoid processes [Figure 4d]
(5) The greater sigmoid notch angle (GSNA) was measured by fitting a circle in the greater sigmoid notch and drawing two lines linking this circular center to the olecranon tip and coronoid tip, respectively. The wide angle formed about the center is the angle of interest [Figure 5].

Statistical analysis

The continuous variables were represented as means and standard deviations for normally distributed data and medians and interquartile ranges for nonnormally distributed data. Categorical variables were expressed as frequencies and proportions. Comparisons of continuous data were conducted using the Student's *t*-test for normally distributed data and the Wilcoxon Mann–Whitney *U* test for nonnormally distributed data. $P < 0.05$ indicated statistical significance. The agreement between the two observers' measurements of the quantitative variables was assessed with the Pearson correlation coefficient. The degree of interobserver agreement for categorical data was calculated using Cohen's kappa. The kappa values were interpreted as 0 for poor agreement, 0–0.20 for slight agreement, 0.21–0.40 for fair agreement, 0.41–0.60 for moderate agreement, 0.61–0.80 for substantial agreement, and 0.81–1.00 for almost perfect agreement.[13]

Results

In the present study, 304 elbow radiographic studies met the eligibility criteria. Nearly half of the elbows were male (151; 49.67%), while the other half were female (153;

50.33%). There were 174 (57.24%) right-sided elbows and 130 (42.76%) left-sided elbows [Table 1].

Anteroposterior radiographic analysis revealed that the RNSA was 10.90° ±2.93°. The average ASA score was 82° ±3.88°. The CA measurement was 18.32° ±5.04°. The TNA was 132.32° ±9.20°. No significant difference was demonstrated based on sex or side [Table 2]. Regarding the morphology of the distal humerus, type II was the most common type encountered (178; 58.55%), followed by type I (88; 28.95%). Type III was the least common type (38; 12.50%). Based on the horizontal joint line, the TS was located approximately 4.58 mm ± 0.94 proximally, the LTR was situated at 1.84 mm ± 0.62, and the TCS was 2.64 mm ± 0.55 [Table 3].

On the lateral images, the AHCL predominantly crossed the central third of the capitellum in 255 elbows (83%), the anterior capitellar third in 45 elbows (14.80%), and the posterior third in 4 elbows (1.32%). The RCA was lined up with the central capitellar third in 195 elbows (64.14%). The RCA crossed the inferior third in 108 elbows (35.53%). Only one elbow (0.33%) had a superior third RCA [Table 4]. The angular measurements showed an AAASDH of 46.26° ±8.11°, an OCA of 25.02° ±4.20°, and a GSNA of 169.04° ±5.56°. Neither sex-based differences nor side-based differences were statistically significant [Table 5].

The reliability of the radiographic elbow measurements showed remarkable variability, as presented in Table 6. Substantial interobserver reliability was noted for the ASA, CA, TS, LTR, TCS, and OCA parameters. Moderate interobserver and intraobserver reliability were observed for the RNSA and TNA, as well as for subjective judgment of distal humerus morphological types. Fair interobserver and intraobserver reliability were observed for the AHCL and RCA. Both the AAASDH and GSNA scores had poor interobserver reliability and slight intraobserver reliability.

Compared to the findings of Goldfarb *et al*.,[9] our measurements of the radiographic elbow angles showed statistically significant differences for RNSA, ASA, and TNA. CA measurements were consistent between our study

Table 1: Patient demographic characteristics

Variable	Total, *n* (%)	Male, *n* (%)	Female, *n* (%)
Patients	304 (100)	151 (49.67)	153 (50.33)
Age (SD)	37.76 (14.79)	34.06 (15.18)	41.41 (13.49)
Right	174 (57.24)	85 (56.29)	89 (58.17)
Left	130 (42.76)	66 (43.71)	64 (41.83)

SD: Standard deviation

Table 2: Radiographic angle measurements on anteroposterior elbow radiographs

Measurement (°)	All (*n*=304)	Gender		*P*	Side		*P*
		Male (*n*=151)	Female (*n*=153)		Right (*n*=174)	Left (*n*=130)	
RNSA	10.90±2.93	10.99±2.93	10.82±2.94	0.601	11.00±2.91	10.78±2.97	0.514
ASA	82±3.88	81.72±3.88	82.27±3.86	0.209	82.14±3.91	81.81±3.84	0.462
CA	18.32±5.04	18.48±5.14	18.16±4.94	0.588	18.22±5.19	18.45±4.84	0.702
TNA	132.32±9.20	133.04±8.92	132.83±9.49	0.843	133.30±8.98	132.45±9.84	0.428

ASA: Articular surface angle, CA: Carrying angle, RNSA: Radial neck shaft angle, TNA: Trochlear notch angle

Table 3: Radiographic qualitative and quantitative assessment of the distal humerus morphology on anteroposterior elbow radiographs

Type	Total, *n* (%)	Male, *n* (%)	Female, *n* (%)	Right, *n* (%)	Left, *n* (%)	TS (mm)	LTR (mm)	TCS (mm)
Type I	88 (28.95)	42 (47.73)	46 (52.27)	51 (57.95)	37 (42.05)	4.58±0.94	2.50±0.60	2.13±0.53
Type II	178 (58.55)	88 (49.44)	90 (50.65)	97 (54.49)	81 (45.51)	4.22±0.79	1.84±0.66	2.58±0.65
Type III	38 (12.50)	21 (55.26)	17 (44.74)	26 (68.42)	12 (31.58)	3.62±0.85	1.26±0.62	2.64±0.55

LTR: Lateral trochlear ridge, TCS: Trochleocapitellar sulcus, TS: Trochlear sulcus

Table 4: Analysis of the anterior humeral capitellar line and radiocapitellar alignment on lateral elbow radiographs

Alignment	Total, *n* (%)	Male, *n* (%)	Female, *n* (%)	Right, *n* (%)	Left, *n* (%)
AHCL					
Anterior one-third	45 (14.80)	29 (9.54)	16 (5.26)	25 (8.22)	20 (6.58)
Central one-third	255 (83.88)	120 (39.47)	135 (44.41)	148 (48.68)	107 (35.20)
Posterior one-third	4 (1.32)	2 (0.66)	2 (0.66)	1 (0.33)	3 (0.99)
RCA					
Superior one-third	1 (0.33)	0	1 (0.33)	1 (0.33)	0
Central one-third	195 (64.14)	94 (30.92)	101 (33.22)	114 (37.50)	81 (26.64)
Inferior one-third	108 (35.53)	57 (18.75)	51 (16.78)	59 (19.41)	49 (16.12)

AHCL: Anterior humeral capitellar line, RCA: Radiocapitellar alignment

Table 5: Radiographic angle measurements on lateral elbow radiographs

Measurement (°)	All (*n*=304)	Gender		*P*	Side		*P*
		Male (*n*=151)	Female (*n*=153)		Right (*n*=174)	Left (*n*=130)	
AAASDH	46.26±8.11	45.89±8.23	46.61±8.01	0.440	45.57±8.91	45.83±7.98	0.788
OCA	25.02±4.20	25.11±4.12	24.94±4.30	0.733	24.86±4.20	25.24±4.21	0.441
GSNA	169.04±5.56	169.36±5.72	168.73±5.40	0.318	169.32±5.58	168.68±5.55	0.322

AAASDH: Anterior angulation of the articular surface of the distal humerus, OCA: Olecranon-coronoid angle, GSNA: Greater sigmoid notch angle

Table 6: Interobserver and intraobserver reliability of elbow radiographic measurements

Measurement	Interobserver reliability	Intraobserver reliability observer 1	Intraobserver reliability observer 2
Radial neck shaft angle	0.42	0.55	0.62
Articular surface angle	0.71	0.83	0.89
Carrying angle	0.78	0.80	0.84
Trochlear notch angle	0.59	0.59	0.47
Type of distal humerus morphology*	0.58	0.60	0.45
Trochlear sulcus depth	0.86	0.88	0.81
Lateral trochlear ridge height	0.80	0.89	0.83
Trochleocapitellar sulcus depth	0.82	0.78	0.85
Anterior humeral capetillar line*	0.32	0.30	0.38
Radiocapitellar alignment*	0.38	0.37	0.40
Anterior angulation of the articular surface of the distal humerus	0.13	0.33	0.26
Olecranon coronoid angle	0.74	0.87	0.90
Greater sigmoid notch angle	0.18	0.35	0.38

*Cohen's kappa was used to estimate reliability

Table 7: Comparison of radiographic angle measurements between the present study and Goldfarb *et al*.'s study[9]

Measurement	Present study (*n*=304)	Goldfarb *et al*.'s study (*n*=53)	*P*
RNSA (°)	10.90±2.93	12±2	<0.001*
ASA (°)	82±3.88	84±3	<0.001*
CA (°)	18.32±5.04	16±4	3.737
TNA (°)	132.32±9.20	125±8	<0.001*
AAASDH	46.26±8.11	121.7 (117.7–125.0)**	-
OCA	25.02±4.20	23.0 (21.0–25.7)**	-
GSNA	169.04±5.56	183.7 (177.0–191.7)**	-

*Statistically significant, **Median (IQR). AAASDH: Anterior angulation of the articular surface of the distal humerus, ASA: Articular surface angle, CA: Carrying angle, GSNA: Greater sigmoid notch angle, OCA: Olecranon coronoid angle, RNSA: Radial neck shaft angle, TNA: Trochlear notch angle, IQR: Interquartile range

and Goldfarb *et al*. report.[9] Further comparisons were not possible due to incoherent data variables [Table 7].

Discussion

Elbow anatomical peculiarities have attracted researchers to thoroughly study the elbow. The RNSA defines the anatomical relationship between the proximal and distal radial segments around the radial tuberosity. Clinically, excessive angulation in this region, irrespective of the cause, could lead to defective radiocapitellar articulation. This concept formed the foundation of radial neck fracture classification systems such as the Judet classification system and O'Brien classification system as well as the Metaizeau outcome scale.[14-16] A statistically significant difference was observed in the RNSA measurements among the Saudi population (10.90° ±2.93°) compared to the findings of Goldfarb *et al*.(12° ±2°).[9] The RSNA demonstrated moderate reliability in the intraobserver and interobserver error domains. Compared to those of the Goldfarb *et al*.'s study, the ASA measurements of Saudi participants (82° ±3.88°) were significantly different (84° ±3°). ASA measurements showed substantial intraobserver and interobserver reliability. The ASA is useful for assessing the frontal plane alterations in the distal humerus. Comparison with the contralateral normal side can be helpful.[17]

In the present study, there was no significant difference between the CAs of the Saudi population and those of the American population measured by Goldfarb *et al*. (18.32° ±5.04° versus 16° ±4°).[9] The CA also demonstrated substantial intraobserver and interobserver reliability. Our findings did not affirm any sex or side predilection associated with CA. There are inconsistent data in the literature regarding whether CA differs based on sex or side.[18-22] Restoration of the normal CA has been used as an indicator of acceptable elbow alignment in addition to its protective potential against ulnar neuropathy.[23] The

TNA was 132.32° ±9.20° in Saudi subjects. A significant difference existed between the TNA measurements in our study and those in Goldfarb *et al*.'s study.[9] The TNA may play a role in elbow stability and biomechanics.[24] The degree to which sulci and ridges develop on the distal humeral articular surface may play an undefined role in elbow mobility and stability. Like Goldfarb *et al*., we observed that type 2 represented the most common type encountered.

The central zone of the capitellar profile appeared to be the most common territory traversed by the AHCL and RCA in our study, as did that of Goldfarb *et al*.[9] We found that the lateral angular measurements of the elbow were inconsistent and less reliable than anteroposterior radiographic measurements. These observations could be related to the technical difficulty of obtaining ideal lateral elbow radiographs and ill-defined delineation of circular and linear shadows of the target structures.

Like other radiographic studies, this study is limited by the variability of the radiographic shooting angle when obtaining elbow radiographs.[25] Therefore, this study applied rigorous criteria to minimize this effect and included only acceptable quality elbow radiographs in terms of proper projection and resolution. In the same context, nomenclature and methodology variability exist between studies. Certain parameters were named differently, and some studies used similar terms to refer to different entities. Some parameters were measured using different methods. For that reason, the authors opted to follow the terminology and methodology of Goldfarb *et al*. throughout the text.[9]

Conclusion

Understanding normal elbow radiographic anatomy by clinicians is essential. Radiographic elbow parameters are of considerable clinical value in detecting elbow abnormalities and subsequent proper management. Moreover, the radiographic anatomy of the elbow may show some variation among subjects from different racial or geographical backgrounds.

Financial support and sponsorship

Nil.

Conflicts of interest

There are no conflicts of interest.

References

1. Aquilina AL, Grazette AJ. Clinical anatomy and assessment of the elbow. Open Orthop J 2017;11:1347-52.
2. Liman MN, Avva U, Ashurst JV, Butarbutar JC. Elbow trauma. In: StatPearls. Treasure Island (FL): StatPearls Publishing; 2023.
3. Gianakos AL, George N, Pinninti A, Kwan S, LaPorte D, Mulcahey MK. Sex- and gender-specific analysis in orthopaedic studies. Clin Orthop Relat Res 2020;478:1482-8.
4. Guitton TG, Doornberg JN, Raaymakers EL, Ring D, Kloen P. Fractures of the capitellum and trochlea. J Bone Joint Surg Am 2009;91:390-7.
5. Falciglia F, Giordano M, Aulisa AG, Di Lazzaro A, Guzzanti V. Radial neck fractures in children: Results when open reduction is indicated. J Pediatr Orthop 2014;34:756-62.
6. Stavrakakis IM, Ntontis Z, Kastritsi O, Chaniotakis C, Alpantaki K, Kastanis G. Distal humerus fracture malunion in adults: A case report and a review of the literature. Case Rep Orthop 2022;2022:1-5.
7. Sadacharan CM, Alikhan SB, Packirisamy V, Murlimanju BV. Carrying angle of the elbow joint in young Caucasian and Indian American population: A descriptive cross-sectional study. J Anat Soc India 2022;71:42-6.
8. Subramanian S, Kemp AK, Viswanathan VK. Bone cyst. In: StatPearls. Treasure Island (FL): StatPearls Publishing; 2023.
9. Goldfarb CA, Patterson JM, Sutter M, Krauss M, Steffen JA, Galatz L. Elbow radiographic anatomy: Measurement techniques and normative data. J Shoulder Elbow Surg 2012;21:1236-46.
10. Eren MB, Aşçı M, Bilgiç E, Güneş T, Balta O, Öztürk T. A practical method for obtaining true lateral elbow x-rays in a paediatric age group: Lateral elbow X-ray in the standing salute position. Indian J Orthop 2021;55:125-9.
11. Martinez Catalan N, Sanchez Sotelo J. Primary elbow osteoarthritis: Evaluation and management. J Clin Orthop Trauma 2021;19:67-74.
12. Zhao W, Guo Y, Xu C, Pei G, Basnet S, Pei Y, *et al.* Distal humerus morphological analysis of Chinese individuals: A statistical shape modeling approach. Orthop Surg 2022;14:2730-40.
13. Landis JR, Koch GG. The measurement of observer agreement for categorical data. Biometrics 1977;33:159-74.
14. Judet J, Judet R, Lefranc J. Fracture of the radial head in the child. Ann Chir 1962;16:1377-85.
15. O'Brien PI. Injuries involving the proximal radial epiphysis. Clin Orthop Relat Res 1965;41:51-8.
16. Metaizeau JP, Lascombes P, Lemelle JL, Finlayson D, Prevot J. Reduction and fixation of displaced radial neck fractures by closed intramedullary pinning. J Pediatr Orthop 1993;13:355-60.
17. Chen G, Cui L, Shi J, Zhang P, Li J, Wang Z, *et al.* Humerus trochlear angle (HTa)-a possible alternative for Baumann angle in the reduction of supracondylar humerus fractures. BMC Musculoskelet Disord 2021;22:950.
18. Allouh MZ, Abu Ghaida JH, Jarrar AA, Khasawneh RR, Mustafa AG, Bashaireh KM. The carrying angle: Racial differences and relevance to inter-epicondylar distance of the humerus. Folia Morphol (Warsz) 2016;75:388-92.
19. Bhattacharyya T, Roy R, Islam M, Agarwal B, Roy SJ. Racial variation of carrying angle of elbow in North-East Indian population: A clinico-radiological study. Indian J Orthop 2022;56:457-63.
20. Alsubael MO, Hegazy AM. Radiographic evaluation of the normal elbow carrying angle in adults. J Med Sci 2010;10:40-4.
21. Ismatsara M, Khalil M, Mannan S, Alam MT, Rahman MM, Ahmed Z, *et al.* Correlation of stature with foot length in 5-10 years aged Bangladeshi children. Mymensingh Med J 2017;26:519-24.
22. Yilmaz E, Karakurt L, Belhan O, Bulut M, Serin E, Avci M.

Variation of carrying angle with age, sex, and special reference to side. Orthopedics 2005;28:1360-3.
23. Chang CW, Wang YC, Chu CH. Increased carrying angle is a risk factor for nontraumatic ulnar neuropathy at the elbow. Clin Orthop Relat Res 2008;466:2190-5.
24. Chin K, Hussain S, Mazis G, Arya A. Clinical anatomy and biomechanics of the elbow. J Clin Orthop Trauma 2021;20:101485.
25. McCann F, Canet F, Sandman E, Petit Y, Rouleau DM. Does radiographic beam angle affect the radiocapitellar ratio measurement of subluxation in the elbow? Clin Orthop Relat Res 2013;471:2556-62.

Original Article

Hip Joint Angular Values in Children with Bilateral Spastic Cerebral Palsy: A Comparison between Ambulatory and Nonambulatory Groups According to the Gross Motor Functional Classification System

Abstract

Objective: The aim of this study was to compare the migration index (MI), femoral inclination angle (FIA), lateral center-edge angle (LCEA), and acetabular index (AI) values measured from hip joint radiographs of children with bilateral spastic cerebral palsy (CP) divided into ambulatory and nonambulatory groups according to the Gross Motor Functional Classification System with functional levels of children, and to examine their relationship with anthropometric measurements of the lower extremities. **Materials and Methods:** The present investigation encompassed the evaluation of 30 children afflicted with CP, through the conduction of hip joint radiographic assessments, which involved the right and left hip joints, the acquisition of images using MI, FIA, LCEA, and AI parameters, as well as measurement of lower-extremity anthropometric data. **Results:** A significant difference was found between ambulatory and nonambulatory groups in the left MI, FIA, and LCEA ($P < 0.05$). In comparison of anthropometric measurements to height ratios, no significant difference was found, except for left ankle circumference and bi-iliac diameter measurements ($P > 0.05$). **Conclusion:** The hip joint angular values of the ambulatory group were found to be within normal limits compared to those of the nonambulatory group. Although there were significant differences between hip joint angles in the two groups, there was no significant correlation with lower-extremity anthropometric measurements. It was concluded that hip joint angles were more pathological and prone to hip displacement in the nonambulatory group. This study revealed the importance of strategies to maintain and improve the functional capacity of children with CP.

Keywords: *Acetabular index, cerebral palsy, femur inclination angle, hip joints, lateral central edge, migration index, radiography*

Buket Rende, Ayla Tekin Orha[1]

Department of Vocational Studies, European Vocational School, Kocaeli Health and Technology University, [1]Department of Anatomy, Faculty of Medicine, Kocaeli University, Kocaeli, Turkey

Introduction

Cerebral palsy (CP) is a neurological disorder characterized by abnormalities in movement, posture, and motor function resulting from incomplete brain development during prenatal, perinatal, and postnatal periods. The etiology of CP is multifactorial, with potential causes including hypoxia, infections, maternal fever, trauma, brain edema, neonatal shock, hyperbilirubinemia, and hypoglycemia.[1] In addition, orthopedic, cognitive, emotional, sensory, and behavioral disorders, as well as seizures, can occur in patients with CP.[2,3] The disease is categorized based on the area of the brain that is affected, the degree of involvement in the extremities, and alterations in muscle tone. There are several classifications of CP, including spastic, dyskinetic, ataxic, hypotonic, and mixed types.[4] Of these, the spastic type of CP is the most prevalent clinical form, distinguished by increased muscle tone. The involvement of the spastic type can be either symmetrical or asymmetrical, and it accounts for 70%–80% of all cases of CP.[4,5] In children with CP who have normal hip joint angles at birth, hip region lesions may occur as they age, making routine pelvic radiography necessary for monitoring the condition of at-risk hips.[6] Children with CP may experience a greater load on their hips compared to typically developing children, potentially leading to changes in weight distribution within the body and balance problems.[7] The incidence of hip subluxation and dislocation is lower in children with CP who can perform weight-bearing, standing, and walking activities at an early stage, compared to those who are unable to do so.[8]

How to cite this article: Rende B, Orha AT. Hip joint angular values in children with bilateral spastic cerebral palsy: A comparison between ambulatory and nonambulatory groups according to the Gross Motor Functional Classification System. J Anat Soc India 2024;73:145-51.

Article Info

Received: 20 December 2023
Accepted: 12 May 2024
Available online: 27 June 2024

Address for correspondence:
Dr. Buket Rende, European Vacational School, Kocaeli Health and Technology University, Kocaeli 41001, Turkey.
E-mail: buketrnd@gmail.com

Access this article online

Website: https://journals.lww.com/joai

DOI: 10.4103/jasi.jasi_137_23

Quick Response Code:

The parameters most frequently utilized in the evaluation of hip joints are migration index (MI), femoral inclination angle (FIA), acetabular index (AI), and lateral center-edge angle (LCEA) in CP.[6,9,10] The MI, considered the gold standard for detecting hip dysplasia, is critical in indicating whether forces applied by the femoral head on the developing acetabulum are within normal limits.[11,12] An MI value below 20% is considered normal, between 20% and 32% indicates hip joint is at risk, an MI value between 33% and 99% signifies hip subluxation, and a value of 100% indicates a disrupted relationship between the femoral head and acetabulum, indicating hip joint dislocation.[7,9,13] The FIA, which assesses the geometry of the proximal part of the femur and hip joint, typically ranges from 120° to 145°.[13,14] When this angle deviates from its physiological limits by narrowing, it is referred to as "coxa vara," and when it widens, it's called "coxa valga." Such pathological conditions can lead to deviations in the loading line of the lower extremity.[13] The AI is a measurement method used to assess the shape and development of the acetabulum. In newborns, this angle is typically measured around 27.5°, but by the age of two, it can decrease to as low as 20°.[15] The AI of weight-bearing region is typically <15°.[16] AI evaluates the inclination and depth of the acetabulum in the frontal plane.[17] The LCEA, defined by Wiberg, generally indicates hip dysplasia when it is <20°.[18]

Hip joint dysplasia is a common issue found in people with CP, often occurring gradually due to muscle and bone problems, which may lead to mild dislocation risk or severe pain from a dislocated hip.[19] It has been established that there is a strong relationship between hip stability in children with CP and their ambulation level.[20] While the frequency of hip lateralization and dislocation is approximately 10% in children with CP who can walk independently, this rate increases to 70% in children with whole-body involvement.[21,22] Anterior-posterior hip radiography is absolutely required for early diagnosis of risky hips.[23] The principal aim of our research was to assess the MI, FIA, AI, and LCEA values, which are the most commonly analyzed parameters, obtained from hip joint radiographs of children with bilateral spastic CP and categorized as ambulatory or nonambulatory according to the Gross Motor Functional Classification System (GMFCS). Our investigation aimed to establish a relationship between these values and children's functional levels, as well as lower-extremity anthropometric measurements.

Materials and Methods

Study design

Our study was ethically approved by the Non-Invasive Clinical Research Ethics Committee of Kocaeli University in accordance with the principles of the Helsinki Declaration, on October 17, 2018, with decision number 2018/16.14. The study population was composed of patients with bilateral spastic CP aged 5–12 years, who had bilateral extremity involvement and were receiving regular physiotherapy and rehabilitation. The study was conducted on a prospective basis, utilizing measurable data, and patients who had undergone surgical interventions related to the hip joint or received botulinum toxin injections or intrathecal baclofen within the past 6 months were excluded. Due to the negligible differences in growth and development between genders within the 5–12 age range, gender distinctions were not made in our study. Before commencing measurements on 30 children with CP participating in the study, informed consent was obtained from their families, children, and institutional officials, following the provision of information about the study. In our investigation, participants with CP were classified based on the GMFCS, which comprises five levels and includes the following main classifications: Level 1 – walking unaided, Level 2 – walking with assistance, Level 3 – walking with a hand-held mobility device, Level 4 – walking with a wheelchair or other mobility device, and Level 5 – unable to walk independently.[24,25] Fifteen ambulatory individuals and 15 nonambulatory individuals with spastic bilateral involvement of CP were included in the study.

In the present investigation, children afflicted with CP were classified as ambulatory if they fell within levels 2–3, and as nonambulatory if they fell within levels 4–5, on the GMFCS. Radiographic imaging of the hip joint was utilized to perform anatomical measurements on the children, with individuals being positioned in a supine posture with the hip and knee joints extended to ensure clear image acquisition. Anatomical measurements of the hip joint, including MI, FIA, AI, and LCEA, were performed. The radiological measurements were conducted using the MicroDicom program (MicroDicom Ltd., Sofia, Bulgaria). The anthropometric measurements of children involved in the study were conducted using standardized methods. The height of participants was measured using a double-sided measuring tape in centimeters (cm), and their body weights were recorded using a digital scale sensitive to 0,1 kg. The lower extremities of participants were evaluated by measuring the thigh, leg, and foot lengths, as well as the thigh, leg, and ankle circumferences using a measuring tape. Bi-iliac and bitrochanteric diameters were obtained using calipers, and knee and ankle diameters were measured using the same caliper, in centimeters (cm). All measurements were recorded with great precision using a digital scale sensitive to 0,1 kg.

Measurements of radiographic parameters

Migration index measurement

In the coronal plane, the portion of the lateral cortex of the femoral head (caput femoris) that lies outside the outer rim of the acetabulum (a) was calculated as the ratio of the diameter of caput femoris (b) (a/b × 100) [Figure 1a].[13,15]

Acetabular index measurement

The angle between the line drawn from the upper lateral aspect of the acetabulum and Hilgenreiner line was calculated and measured [Figure 1b].[15]

Femoral inclination angle (FIA) measurement

The angle between the femoral head, neck, and femoral shaft was calculated and measured [Figure 1c].[26]

Lateral center-edge angle measurement

The angular value between the line drawn from the center of the femoral head parallel to the longitudinal axis of the femoral shaft and the line drawn from the femoral head to the outermost lateral point of the acetabulum was measured [Figure 1d].[18]

Statistical analysis

In the current study, a sample of 30 children with bilateral lower-extremity involvement in spastic diplegic CP, aged between 5 and 12 years, who received routine physiotherapy sessions, was selected. The data were analyzed using SPSS 22.0 software, and descriptive statistics (mean and standard deviation) were used for numerical variables, whereas frequencies and percentages were used for categorical variables. The independent samples *t*-test and Mann–Whitney *U*-test were conducted based on the assumption of normal distribution to compare differences between groups. The Chi-square test was used to examine the relationship among categorical variables, and the Pearson and Spearman correlation tests were used to investigate the relationship among numerical variables according to the appropriateness of normal distribution. Statistical significance was set at $P < 0.05$.[27]

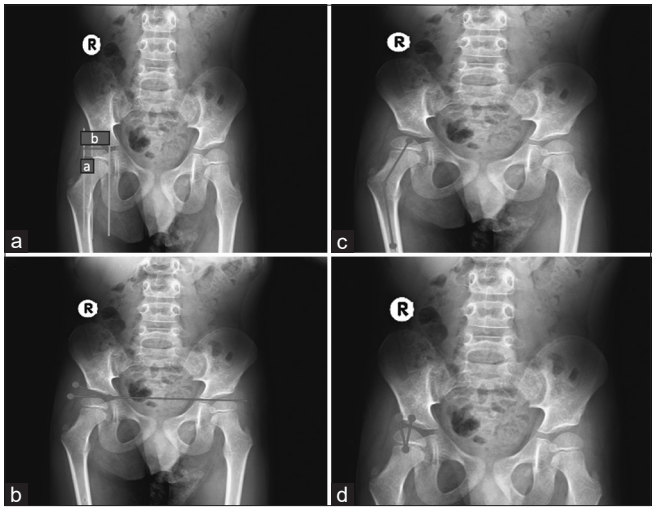

Figure 1: Measurements of radiographic parameters. (a) Measurement of the right hip migration index, (b) measurement of the right hip acetabular index, (c) measurement of the right hip FIA, and (d) measurement of the right hip lateral center-edge angle. FIA: Femoral inclination angle

Results

In the present study, 15 children with CP who were ambulatory (levels 2 and 3 according to GMFCS) and 15 children with CP who were nonambulatory (levels 4 and 5 according to GMFCS) were evaluated to investigate whether there was a significant relationship between these parameters in children with different functional levels by comparing the anatomical measurements of articular coxae and anthropometric measurements of the lower extremities in ambulatory and nonambulatory children with CP. A total of 30 children with CP, comprising 14 boys and 16 girls, participated in the study. The mean age of children who were ambulatory was 9.0 ± 2.4 years, the mean height was 119.1 ± 14.5 cm, and the mean weight was 25.9 ± 9.1 kg, while the mean age of children who were nonambulatory was 8.0 ± 2.0 years, the mean height was 113.9 ± 13.2 cm, and the mean weight was 20.5 ± 5.8 kg [Table 1]. These findings indicate that children who were unable to walk were, on average, slightly younger and shorter in height and weight than those who were able to walk.

In the comparison of hip joint measurements of ambulatory and nonambulatory children with CP on the right and left sides, no statistically significant difference was found in the measurements of MI, FIA, LCEA, and AI in the right hip and the AI angle in the left hip ($P > 0.05$). However, a statistically significant difference was noticed in the left hip's MI, FIA, and LCEA measurements between the two groups ($P < 0.05$) [Table 2].

When percentages of angular values of the hip joint above the normal limits in ambulatory and nonambulatory children with CP were analyzed, 26.6% of the ambulatory group had right MI, 6% had left MI, 33% had right FIA, 13.3% had left FIA, 40% had right AI, 20% had left AI, and 6.6% had right and left LCEA. In the nonambulatory group, 40% of patients had right and left MI, 60% had right FIA, 80% had left FIA, 46.6% had right and left AI, 26.6% had right LCEA, and 33.3% had left LCEA [Table 3].

The comparison of anthropometric measurements, including length, circumference, and diameter, between ambulatory and nonambulatory children with CP revealed that while the

Table 1: Age, height, and body weight findings

Variables	Mean±SD
Age (years)	
Ambulatory	9.0±2.4
Nonambulatory	8.0±2.0
Height (cm)	
Ambulatory	119.1±14.5
Nonambulatory	113.9±13.2
Body weight (kg)	
Ambulatory	25.9±9.1
Nonambulatory	20.5±5.8

SD: Standard deviation

Table 2: Comparison of angular values of the hip joint in children with cerebral palsy

Measurements	Mean±SD		*P*
	Ambulatory	Nonambulatory	
Right - MI (%)	26.37±14.61	29.79±11.90	0.285
Left - MI (%)	20.80±13.40	34.12±19.20	**0.023***
Right - FIA	152.03±7.44	156.24±4.51	0.071
Left - FIA	148.64±7.90	158.35±6.42	**0.001***
Right - LCEA	28.33±7.47	24.52±7.73	0.180
Left - LCEA	30.82±8.34	22.89±8.69	**0.010***
Right - AI	21.86±5.91	22.55±3.51	0.702
Left - AI	21.13±3.41	23.04±6.63	0.328

*Statistically significant differences were presented in bold.
P: Level of statistical significance, LCEA: Lateral center-edge angle, FIA: Femoral inclination angle, AI: Acetabular index, MI: Migration index, SD: Standard deviation

Table 3: Comparison of the percentages of the angular values of the hip joint above the normal limits in children with ambulatory and nonambulatory cerebral palsy

Measurements	Ambulatory (*n*=15), *n* (%)	Nonambulatory (*n*=15), *n* (%)
R - MI (%)	4 (26.6)	6 (40)
L - MI (%)	1 (6.6)	6 (40)
R - FIA	5 (33.3)	9 (60)
L - FIA	2 (13.3)	12 (80)
R - LCEA	6 (40)	7 (46.6)
L - LCEA	3 (20)	7 (46.6)
R - AI	1 (6.6)	4 (26.6)
L - AI	1 (6.6)	5 (33.3)

n: Number of patients, LCEA: Lateral center-edge angle, FIA: Femoral inclination angle, AI: Acetabular index, MI: Migration index

values of the ambulatory group were higher, they did not reach a statistically significant level ($P > 0.05$). Significant differences were observed in measurements of bi-iliac diameter and left ankle circumference ($P < 0.05$) [Table 4].

Discussion

CP is a nonprogressive disorder that affects movement, posture, and motor function, and is caused by lesions in the developing fetal or infant brain.[28] The hips of children with CP appear normal at birth, but pathologies emerge gradually with age.[29] In a study, it was reported that hip pathologies were less common in the ambulatory group with levels 1–2–3 according to the GMFCS compared to those with levels 4–5.[8] In our research, we conducted an analysis of measurements related to the hip joints in children with bilaterally affected spastic type CP at GMFCS levels 2–3–4–5. Our aim was to evaluate the significance of differences in angular values on hip radiographs in functionally ambulatory and nonambulatory children. This investigation compared the anatomical measurements of the hip joints in ambulatory and nonambulatory children with CP and determined the relationship with lower-extremity anthropometric measurements. Our findings indicate that angular values in the hip joints of ambulatory children, classified as level 2 and 3 according to the GMFCS, were within normal limits when compared to nonambulatory children. However, coxa vara and genu valgum were present in all children in both groups. There is a lack of literature regarding the relationship between anatomical and anthropometric measurements of the hip joint in children with CP. Although there were significant differences in hip joint angles between the two groups, there was no significant correlation with the anthropometric measurements of the lower extremities. In children with CP who have normal hip joint angles at birth, hip lesions also occur with increasing age. Therefore, pelvic radiography should be routinely performed in the follow-up of children with CP who are at risk for hip conditions.[6,30] Furthermore, hip subluxation and dislocation were found to be less frequent in children with CP who could perform weight transfer, standing, and walking activities in the early period than in those who could not perform these activities.[8]

Our study found that nonambulatory children often have hip angles outside the standard range, especially on the left side with significant differences in MI, FIA, and LCEA angles, possibly due to unequal weight transfer affecting both lower extremities, with one side more severely impacted. MI > 33% might indicate hip subluxation and help identify at-risk children for hip problems.[14] It has been reported that the severity of hip dysplasia is associated with higher GMFCS levels and MI is the key radiographic measure of hip dysplasia.[10,31] In our study, the percentages of MI in both groups were found to be outside the normal limits and the percentages in the nonambulatory group were within the riskier limits. In addition, 26.6% of the ambulatory group had right MI, 6.6% had left MI, and 40% of the nonambulatory group had right and left MI above 33%. Although MI values were within the risk value in both groups, the nonambulatory group had higher MI values. It was found that 24.3% of 235 children with CP at levels IV and V according to the GMFCS had at least one hip with an MI above 40%.[32] This shows the effect of functional level and MI on the risk of hip dysplasia in children with CP. In this context, the likelihood of hip dysplasia increases in children who cannot stand or walk functionally since the hip will not take weight. It was found that 24.3% of 235 children with CP who had levels IV and V according to the GMFCS had at least one hip with an MI above 40%.[32,33] This showed the effect of functional level and MI on the risk of hip dysplasia in children with CP. Therefore, hip subluxation and dislocation are more likely to develop in children who do not transfer weight to the hip joint, cannot stand, or are nonambulatory.

During our research, the mean FIA for children with CP in the specified age range was not determined. However, the FIA

Table 4: Comparison of lower-extremity anthropometric measurements and height ratios of children with ambulatory and nonambulatory cerebral palsy

Anthropometric measurements (cm/height cm)	Mean±SD		*P*
	Ambulatory	Nonambulatory	
Right - SIAS - medial malleolus length	52.66±4.60	50.87±2.67	0.203
Left - SIAS - medial malleolus length	52.84±4.47	50.25±2.55	0.062
Right - umbilicus - medial malleolus length	56.55±4.51	55.43±2.45	0.404
Left - umbilicus - medial malleolus length	56.73±4.42	55.10±2.51	0.225
Right - thigh length	22.91±2.08	22.54±1.44	0.579
Left - thigh length	22.96±2.11	22.06±1.36	0.179
Right - leg length	23.03±2.08	21.83±1.38	0.165
Left - leg length	23.11±2.06	21.78±1.23	0.071
Right - foot length	14.93±2.11	14.15±1.24	0.225
Left - foot length	14.94±2.02	14.18±1.27	0.232
Right - thigh circumference	24.58±4.00	23.51±3.51	0.444
Left - thigh circumference	24.58±4.17	22.81±3.80	0.235
Right - leg circumference	17.75±3.34	16.76±2.51	0.370
Left - leg circumference	17.95±3.52	16.42±2.72	0.330
Right - ankle circumference	13.84±2.29	12.55±1.26	0.171
Left - ankle circumference	13.93±2.34	12.27±1.53	**0.030***
Bi-iliac diameter	19.57±2.87	17.02±3.50	**0.038***
Bitrochanteric diameter	21.95±3.34	19.96±3.56	0.127
Right - knee diameter	5.87±0.88	5.52±0.82	0.286
Left - knee diameter	5.93±0.92	5.47±0.84	0.166
Right - ankle diameter	4.00±0.69	3.80±0.73	0.470
L - ankle diameter	3.92±0.70	3.59±0.83	0.256

*Statistically significant differences were presented in bold. *P*: Level of statistical significance, SD: Standard deviation, SIAS: Spina iliaca anterior superior

averages were found to be outside the normal limits for both groups, indicating coxa vara and genu valgum were present in the children. It has been reported that FIA found outside the normal limits may lead to dysplasia in the hips.[13] It was reported that FIA was higher in those who could not walk, and in this case, their hips may become more dysplastic. The right FIA angle of 33.3% and left FIA angle of 13.3% of the group who were ambulatory and the right FIA angle of 60% and left FIA angle of 80% of the group who were nonambulatory were found to be higher than normal limits. It has been reported that MI influenced acetabular anteversion; more prominent acetabular changes were found in the hip as MI increased; and thus, the acetabular tilt angle was found to be higher in children with hip dislocation.[34,35] The AI angle values of both groups were found in the upper limits, and this was interpreted as no significant difference between the groups because the children had an existing acetabular obliquity regardless of their functional level compared with normal children. It is seen that the risk of hip dysplasia is more common in nonambulatory children, and angular values are related to their functionality.

There are limited studies in which anthropometric measurements were performed in children with bilateral spastic type (diplegic and quadriplegic). In our study, in children with CP who were ambulatory; right thigh circumference 23.51 ± 3.51, left thigh circumference 22.81 ± 3.80, right leg circumference 16.76 ± 2.51, left leg circumference 16.42 ± 2.72, biliac diameter 19.57 ± 2.87, right knee diameter 5.87 ± 0.88, left knee diameter 5.93 ± 0.92, right thigh circumference was 25.37 ± 3.63, left thigh circumference was 25.40 ± 3.78, right leg circumference was 17.40 ± 2.19, left leg circumference was 17.44 ± 2.27, biliac diameter was 17.02 ± 3.50, right knee diameter was 5.52 ± 0.82, left knee diameter was 5.47 ± 0.84 in children with CP who were nonambulatory [Table 4]. In our investigation, we assessed the height ratios of lower-extremity anthropometric values in children with ambulatory and nonambulatory CP. Our investigation revealed that while anthropometric values were higher in the ambulatory group compared to the nonambulatory group, the difference was not statistically significant. However, a statistically significant difference was observed in left ankle circumference and bi-iliac diameter measurements. In addition, a significant difference in bi-iliac diameter measurement was found to be associated with the body structure of children. As body structure changes may also be influenced by genetic factors, it was not considered a value solely related to functionality. Similarly, the significant difference in anthropometric measurements around the left ankle was attributed to more atrophic musculature observed in nonambulatory children around the ankle, and predominant left-side involvement was higher in the nonambulatory group.

Conclusion

In our study, we discovered that the angular values of the hip joint in the ambulatory CP group were within the normal range when compared to those in the nonambulatory group. These values were found to be influenced by individuals' functional levels, and it was determined that the increase in hip joint angles was more pronounced in the nonambulatory group and was associated with a predisposition to hip displacement. Our findings highlight the importance of rehabilitation in maintaining and improving the functional capacity of children with CP, particularly the importance of positioning training for equal weight transfer to the hips. It is assumed that anatomical straightness of the hip is crucial, and changes in angular values should be monitored through regular hip follow-up. In addition, we recommend that future studies involving larger sample sizes and groups according to each level in the GMFCS be conducted to determine hip angular values and their clinical equivalence.

Financial support and sponsorship

This study was financially supported through a project (KOU-BAP: project no 2018/296) of the Kocaeli University Scientific Research Projects Coordination Unit.

Conflicts of interest

There are no conflicts of interest.

References

1. Paul S, Nahar A, Bhagawati M, Kunwar AJ. A review on recent advances of cerebral palsy. Oxid Med Cell Longev 2022;2022:2622310.
2. Novak I, Morgan C, Adde L, Blackman J, Boyd RN, Brunstrom-Hernandez J, *et al*. Early, accurate diagnosis and early intervention in cerebral palsy: Advances in diagnosis and treatment. JAMA Pediatr 2017;171:897-907.
3. Foster T, Rai AI, Weller RA, Dixon TA, Weller EB. Psychiatric complications in cerebral palsy. Curr Psychiatry Rep 2010;12:116-21.
4. Vitrikas K, Dalton H, Breish D. Cerebral palsy: An overview. Am Fam Physician 2020;101:213-20.
5. Hägglund G, Hollung SJ, Ahonen M, Andersen GL, Eggertsdóttir G, Gaston MS, *et al*. Treatment of spasticity in children and adolescents with cerebral palsy in Northern Europe: A CP-North registry study. BMC Neurol 2021;21:276.
6. Graham HK, Rosenbaum P, Paneth N, Dan B, Lin JP, Damiano DL, *et al.* Cerebral palsy. Nat Rev Dis Primers 2016;2:15082.
7. Macias-Merlo L, Bagur-Calafat C, Girabent-Farrés M, A Stuberg W. Effects of the standing program with hip abduction on hip acetabular development in children with spastic diplegia cerebral palsy. Disabil Rehabil 2016;38:1075-81.
8. Aroojis A, Mantri N, Johari AN. Hip displacement in cerebral palsy: The role of surveillance. Indian J Orthop 2021;55:5-19.
9. Wordie SJ, Robb JE, Hägglund G, Bugler KE, Gaston MS. Hip displacement and dislocation in a total population of children with cerebral palsy in Scotland. Bone Joint J 2020;102-B: 383-7.
10. Shrader MW, Wimberly L, Thompson R. Hip surveillance in children with cerebral palsy. J Am Acad Orthop Surg 2019;27:760-8.
11. Doruk Analan P, Aslan H. Association between the elasticity of hip muscles and the hip migration index in cerebral palsy. J Ultrasound Med 2019;38:2667-72.
12. Craven A, Pym A, Boyd RN. Reliability of radiologic measures of hip displacement in a cohort of preschool-aged children with cerebral palsy. J Pediatr Orthop 2014;34:597-602.
13. Scorcelletti M, Reeves ND, Rittweger J, Ireland A. Femoral anteversion: Significance and measurement. J Anat 2020;237:811-26.
14. Reimers J. The stability of the hip in children. A radiological study of the results of muscle surgery in cerebral palsy. Acta Orthop Scand Suppl 1980;184:1-100.
15. Shore BJ, Shrader MW, Narayanan U, Miller F, Graham HK, Mulpuri K. Hip surveillance for children with cerebral palsy: A survey of the posna membership. J Pediatr Orthop 2017;37:e409-14.
16. Horberg JV, Bailey JR, Mikesell TA, Graham RD, Allan DG. Assessing the weight-bearing surface in dysplastic acetabulae: The sourcil index. Arthroplast Today 2021;11:56-61.
17. Tannast M, Hanke MS, Zheng G, Steppacher SD, Siebenrock KA. What are the radiographic reference values for acetabular under- and overcoverage? Clin Orthop Relat Res 2015;473:1234-46.
18. Wiberg G. Shelf operation in congenital dysplasia of the acetabulum and in subluxation and dislocation of the hip. J Bone Joint Surg Am 1953;35-A: 65-80.
19. Judd H, Hyman JE. Operative treatment of the young cerebral palsy hip. J Pediatr Rehabil Med 2022;15:13-7.
20. Saisongcroh T, Shrader MW, Lennon N, Church C, Sees JP, Miller F. Residual deformity and outcome of ambulatory adults with cerebral palsy: A long-term longitudinal assessment. J Pediatr Orthop 2022;42:215-21.
21. Robb JE, Hägglund G. Hip surveillance and management of the displaced hip in cerebral palsy. J Child Orthop 2013;7:407-13.
22. Dohin B. The spastic hip in children and adolescents. Orthop Traumatol Surg Res 2019;105:S133-41.
23. Canavese F, Marengo L, de Coulon G. Results and complications of percutaneous pelvic osteotomy and intertrochanteric varus shortening osteotomy in 54 consecutively operated GMFCS level IV and V cerebral palsy patients. Eur J Orthop Surg Traumatol 2017;27:513-9.
24. Palisano RJ, Hanna SE, Rosenbaum PL, Russell DJ, Walter SD, Wood EP, *et al*. Validation of a model of gross motor function for children with cerebral palsy. Phys Ther 2000;80:974-85.
25. Sadowska M, Sarecka-Hujar B, Kopyta I. Cerebral palsy: Current opinions on definition, epidemiology, risk factors, classification and treatment options. Neuropsychiatr Dis Treat 2020;16:1505-18.
26. Amen J, Perkins O, Kafchitsas K, Reed D, Norman-Taylor F, Kokkinakis M. Bony hip reconstruction for displaced hips in patients with cerebral palsy: Is postoperative immobilization indicated? J Child Orthop 2023;17:268-75.
27. Serrano R, Blair JA, Watson DT, Infante AF Jr., Shah AR, Mir HR, *et al.* Cephalomedullary nail fixation of intertrochanteric femur fractures: Are two proximal screws better than one? J Orthop Trauma 2017;31:577-82.
28. Patel DR, Neelakantan M, Pandher K, Merrick J. Cerebral palsy in children: A clinical overview. Transl Pediatr 2020;9:S125-35.
29. Asma A, Howard JJ, Ulusaloglu AC, Rogers KJ, Miller F, Shrader MW. Identification of risk factors for reconstructive hip surgery after intrathecal baclofen therapy in children with cerebral palsy. Acta Orthop Traumatol Turc 2023;57:104-8.
30. Öztürk O, Salami F, Musagara AR, Demirbüken İ, Polat MG,

Wolf SI, *et al*. Functional hip joint centre determination in children with cerebral palsy. Gait Posture 2021;90:185-9.

31. Demir N, Demirel M, Turna Ö, Yildizlar D, Demirbaş Ö, Sağlam Y. Effect of clinician's experience and expertise on the inter- and intra-observer reliability of hip migration index in children with cerebral palsy: A strobe-compliant retrospective study. Medicine (Baltimore) 2021;100:e24538.
32. Poirot I, Laudy V, Rabilloud M, Roche S, Iwaz J, Kassaï B, *et al*. Patterns of hip migration in non-ambulant children with cerebral palsy: A prospective cohort study. Ann Phys Rehabil Med 2020;63:400-7.
33. Hägglund G. Association between pelvic obliquity and scoliosis, hip displacement and asymmetric hip abduction in children with cerebral palsy: A cross-sectional registry study. BMC Musculoskelet Disord 2020;21:464.
34. Cho Y, Park ES, Park HK, Park JE, Rha DW. Determinants of hip and femoral deformities in children with spastic cerebral palsy. Ann Rehabil Med 2018;42:277-85.
35. Jóźwiak M, Rychlik M, Szymczak W, Grzegorzewski A, Musielak B. Acetabular shape and orientation of the spastic hip in children with cerebral palsy. Dev Med Child Neurol 2021;63:608-13.

Original Article

Gender Prediction Using Cone-Beam Computed Tomography Measurements from Foramen Incisivum: Application of Machine Learning Algorithms and Artificial Neural Networks

Deniz Senol, Yusuf Secgin[1], Oguzhan Harmandaoglu[2], Seren Kaya[3], Suayip Burak Duman[4], Zülal Oner[5]

Department of Anatomy, Faculty of Medicine, Düzce University, Düzce, [1]Department of Anatomy, Faculty of Medicine, Karabük University, Karabük, [2]Department of Therapy and Rehabilitation, Çatalzeytin Vocational School, Kastamonu University, Kastamonu, [3]Department of Anatomy, Faculty of Medicine, Istanbul Beykent University, Istanbul, [4]Department of Oral and Maxillofacial Radiology, Faculty of Dentistry, Inönü University, Malatya, [5]Department of Anatomy, Faculty of Medicine, Izmir Bakırçay University, İzmir, Turkey

Abstract

Introduction: This study aims to predict gender using parameters obtained from images of the foramen (for.) incisivum through cone-beam computed tomography (CBCT) and employing machine learning (ML) algorithms and artificial neural networks (ANN). **Materials and Methods:** This study was conducted on 162 individuals in total. Precise measurements were meticulously extracted, extending from the foramen incisivum to the arcus alveolaris maxillaris, through employment of CBCT. The ML and ANN models were meticulously devised, allocating 20% for rigorous testing and 80% for comprehensive training. **Results:** All parameters that are evaluated, except for the angle between foramen palatinum majus and foramen incisivum-spina nasalis posterior (GPFIFPNS-A), exhibited a significant gender difference. ANN and among the ML algorithms, logistic regression (LR), linear discriminant analysis (LDA), and random rorest (RF) demonstrated the highest accuracy (Acc) rate of 0.82. The Acc rates for other algorithms ranged from 0.76 to 0.79. In the models with the highest Acc rates, 14 out of 17 male individuals and 13 out of 16 female individuals in the test set were correctly predicted. **Conclusion:** LR, LDA, RF, and ANN yielded high gender prediction rates for the measured parameters, while decision tree, extra tree classifier, Gaussian Naive Bayes, quadratic discriminant analysis, and K-nearest neighbors algorithm methods provided lower predictions. We believe that the evaluation of measurements extending from foramen incisivum to arcus alveolaris maxillaris through CBCT scanning proves to be a valuable method in gender prediction.

Keywords: *Artificial intelligence, foramen incisivum, forensic anthropology, gender prediction, machine learning, maxilla*

Introduction

The examination of anthropometric characteristics holds significance in issues pertaining to individual identification.[1] Determining gender is a classical forensic procedure and a crucial step in postmortem profiling.[2] Due to the recent surge in criminal cases involving modern offenses, there has been an increased demand in the legal realm for gender determination.[3] When it becomes necessary to identify skeletal remains, visual examination, anatomical measurement, and the precise measurement of bone dimensions stand among the radiological contributions. The skull, particularly, proves to be the most utilitarian region for comparative radiography. Radiography is employed, especially in cases of fragmented or charred bodies, to diagnose an individual in forensic pathology.[4] The skull, pelvis, and long bones emerge as the most advantageous in radiological gender determination.[2] Hence, employing the thicker and more robust bones, which often remain relatively intact, will yield reliable results in gender estimation. Even in cases of incineration, the zygomatic and maxillary bones tend to endure without severe damage. The maxilla exhibits variations in shape and size among individuals, genders, and diverse populations. They stabilize after the second decade of life, thereby allowing for reliable measurements on radiographic images.[5] Bilaterally, the foramen incisivum, a funnel-shaped aperture located behind the incisor teeth, can be observed in the sagittal plane at the junction where the anterior portions of the processus palatinus, contributing to the formation of the palatine, converge in the maxilla.[6,7]

How to cite this article: Senol D, Secgin Y, Harmandaoglu O, Kaya S, Duman SB, Oner Z. Gender prediction using cone-beam computed tomography measurements from foramen incisivum: Application of machine learning algorithms and artificial neural networks. J Anat Soc India 2024;73:152-9.

Article Info

Received: 10 December 2023
Revised: 12 May 2024
Accepted: 12 May 2024
Available online: 27 June 2024

Address for correspondence:
Assoc. Prof. Deniz Senol, Department of Anatomy, Faculty of Medicine, Düzce University, Düzce, Turkey.
E-mail: denizanatomi@gmail.com

Access this article online

Website: https://journals.lww.com/joai
DOI: 10.4103/jasi.jasi_129_23
Quick Response Code:

The dimensions of this aperture, in terms of distances to reference points such as the spina nasalis posterior, foramen palatinum majus, dens incisivus, and dens molaris, exhibit variations based on genders.[8-11] Consequently, owing to these distinctive attributes, the maxilla can serve as a reference bone for gender estimation.

In dentistry, imaging constitutes a pivotal diagnostic adjunct in the clinical evaluation of patients.[12] Digital imaging, encompassing computed tomography (CT), magnetic resonance imaging (MRI), positron emission tomography, and cone-beam computed tomography (CBCT), has undergone significant refinement. With the advent of CBCT, dentistry has transitioned from two-dimensional to three-dimensional (3D) imaging of the maxillofacial region, thereby facilitating access to and manipulation of 3D data.[13] This technology, in tandem with its high resolution, affords the capacity for reliable 3D measurements of the maxilla. In addition, it boasts a lower radiation dose relative to CT scans and is more cost-effective compared to MRI. These advantages have propelled CBCT technology into the echelons of being an efficacious tool in gender determination.[14] In extant literature, studies employing CBCT technology, or other imaging modalities, to predict gender based on sinus frontalis, sinus maxillaris, and craniofacial bones can be discerned.[1,3,5,15,16] However, no study has hitherto ventured into examining measurements extending from foramen incisivum to arcus alveolaris maxillaris through CBCT technology.

Through the prism of data analysis, data mining, the process of unearthing novel insights from pre-existing data, emerges as a pivotal predictive instrument within the domain of computer science.[17] Algorithms and methodologies serve to bolster the applications of machine learning (ML) within the purview of health care.[18] It is envisaged that ML techniques will traverse substantial ground in expeditiously processing and evaluating copious repositories of intelligent data, thereby laying the foundation for their expeditious integration within the realm of health care.[19] Besides, it is possible to observe a plethora of applications for ML and artificial neural network (ANN), encompassing clustering, classification, prediction, character recognition, speech processing, image processing, shape optimization, and data filtration.[20] Within the realm of health care, a notable domain for the application of ML and ANN lies in gender prediction.[21-25] Observationally, it is discernible that in gender prediction, distinct algorithms wield varying degrees of efficacy, thereby underscoring the pertinence of juxtaposing their respective performance metrics.[21,22,25-28] Within the domain of forensic anthropology, where accurately predicting gender holds paramount significance, it is crucial to meticulously consider methods with a high predictive precision. Therefore, it is logical to conclude that the results concerning the effectiveness of various approaches should be duly acknowledged in academic discussions.

This study was carried out to predict gender using ML algorithms and ANNs using measurements from the for. incisivum to the arcus alveolaris maxillaris obtained from CIBT scans.

Materials and Methods

Study sample, cone-beam computed tomography process, and image processing

The sample for this study comprised 80 female and 82 male individuals, aged between 19 and 54 years. CBCT images, obtained for various reasons, were retrieved from the hospital archive system in a randomized and retrospective manner. Individuals exhibiting any fracture, pathology, or surgical intervention in the maxilla were excluded from the study. The study received approval from the Local Ethics Committee of Düzce University under the reference number 2023/4357, dated January 24, 2023. CBCT images were acquired using the NewTom 5G device (Verona, Italy) with a scanning protocol of 110 kVp, 1–11 mA, and a 3.6 s exposure.

Images obtained from the hospital archive system were transferred to the RadiAnt Digital Imaging and Communications in Medicine (DICOM) Viewer program in DICOM format. Subsequently, measurements were conducted using the 3D volume rendering console of the program [Figure 1].

1. Width of foramen incisivum (IF-W)
2. Length of foramen incisivum (IF-L)
3. Right distance between foramen incisivum and foramen palatinum majus (RIFGPF-L)
4. Left distance between foramen incisivum and foramen palatinum majus (LIFGPF-L)
5. Right distance between foramen incisivum and third dens molaris serotinus
6. Left distance between foramen incisivum and third dens molaris serotinus (LIFDMS-L)
7. Distance between foramen incisivum and spina nasalis posterior (IFPNS-L)
8. Distance between foramen incisivum and sutura palatina transversa (IFTPS-L)
9. Distance between foramen incisivum and foramen palatinum majus (IFGPF-L)
10. Angle between foramen palatinum majus, foramen incisivum, and spina nasalis posterior (GPFIFPNS-A)

Furthermore, utilizing the 3D multiplanar reconstructions console of the program, the images were transformed into 3D representations, namely, sagittal, axial, and coronal. The sections in the axial image were superimposed to obtain the measurement image.

The following parameters were measured based on this acquired image:

11. Distance to the bone in front of foramen incisivum
12. Distance between foramen incisivum on the right and the closest point of dens incisivus medialis (RIFMID-L)

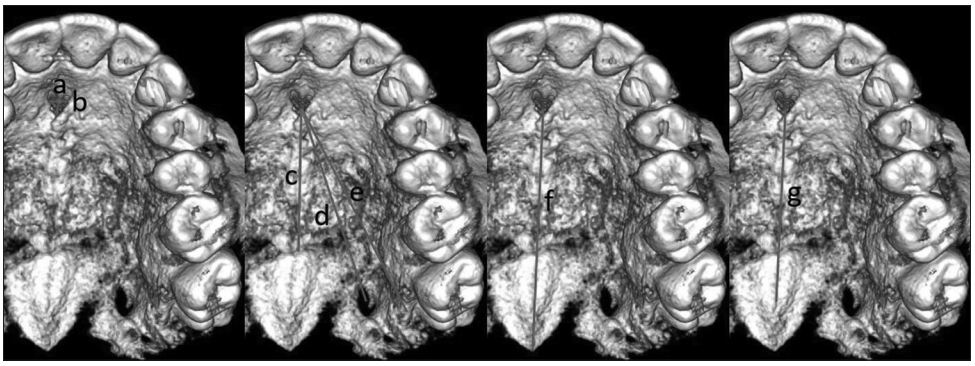

Figure 1: Demonstration of three-dimensional volume rendering measurements. a: Length of foramen incisivum, b: Width of foramen incisivum, c: Distance between foramen incisivum and spina nasalis posterior, d: Left distance between foramen incisivum and foramen palatinum majus, e: Left distance between foramen incisivum and 3rd dens molaris serotinus, f: Distance between Foramen incisivum and spina nasalis posterior, g: Distance between Foramen incisivum and foramen palatinum majus

13. Distance between foramen incisivum on the left and the closest point of dens incisivus medialis (LIFMID-L) [Figure 2].

Application of machine learning algorithms and artificial neural networks

The ML and ANN modeling processes were conducted using a computer equipped with an 8 GB RAM and an i5 operating system by Monster. For modeling, the Python 3.9 programming language and the scikit-learn 1.1.1 framework were employed. Models were developed with an 80% training data and a 20% testing data split. In the ML model, the following algorithms were employed: linear discriminant analysis (LDA), quadratic discriminant analysis (QDA), logistic regression (LR), extra tree classifier (ETC), decision tree (DT), random forest (RF), K-nearest neighbors algorithm (k-NN), and Gaussian Naive Bayes (GaussianNB). For the ANN model, a multilayer perceptron classifier (MLCP) was utilized, consisting of two hidden layers (the first with 10 and the second with 15 neurons), 14 input layers, and 2 output layers. The topology of the MLCP was established through 100, 500, and 1000 iterations of training. The performance of the models was tested using accuracy (Acc), specificity (Spe), sensitivity (Sen), and F1 score (F1).

$$\text{Acc}=\frac{\text{TP}}{\text{TP+FN+FP+TN}}$$

$$\text{Sen}=\frac{\text{TP}}{\text{TP+FN}}$$

$$\text{Spe}=\frac{\text{TN}}{\text{TN+FP}}$$

$$\text{F1}=2\frac{\text{Precision}\times\text{Recall}}{\text{Precision+Recall}}$$

Equation 1 (TP: True positive, TN: True negative, FP: False positive, FN: False negative).

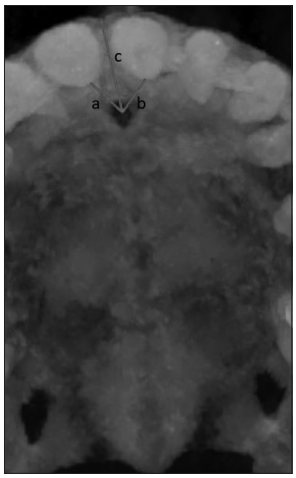

Figure 2: Demonstration of three-dimensional multiplanar reconstructions measurements. a: Distance between foramen incisivum on the right and the closest point of dens incisivus medialis, b: Distance between foramen incisivum on the left and the closest point of dens incisivus medialis, c: Distance to the bone in front of foramen incisivum

Statistical analysis

For data exhibiting a normal distribution in the descriptive statistics of parameters, the mean ± standard deviation was provided, while for nonnormally distributed data, the median (minimum–maximum) values were presented. For the conformity of the data with normal distribution, the Anderson–Darling test was conducted. If the data demonstrated normal distribution, the two-sample *t*-test was employed; otherwise, the Mann–Whitney *U*-test was applied. The statistical analyses were conducted using the Minitab 17 software package.

Results

In this study encompassing 162 individuals within the age range of 19–54 years, the ages of male individuals were found to be 39 (19–54), whereas for female individuals, they were 35 (19–54). There was a significant difference in ages between genders ($P = 0.003$). Following the normality test, it was determined that all parameters, with the exception of

the IFTPS-L parameter, did not exhibit a normal distribution. The IFTPS-L parameter was identified as 2.736 ± 0.332 for male individuals and 2.496 ± 0.278 for female individuals. A significant difference based on gender was observed according to the two-sample *t*-test ($P = 0.000$). Except for the GPFIFPNS-A parameter, all other parameters exhibited a significant difference in terms of gender according to the Mann–Whitney *U*-test [Table 1] ($P < 0.005$).

As a result of the ML algorithms, the highest Acc ratio was found to be 0.82 with the LR, LDA, and RF algorithm. The Acc ratio of the other algorithms ranged between 0.76 and 0.79 [Table 2].

Among the models with the highest Acc rates, 14 out of 17 male individuals and 13 out of 16 female individuals were correctly predicted in the test set [Figure 3].

To evaluate the predictive power of parameters in determining gender, the SHapley Additive exPlanations explainer of the RF algorithm was employed and it was found that the five highest contributions were RIFMID-L, IF-L, RIFGPF-L, IFTPS-L, and LIFMID-L parameters, respectively [Figure 4].

The data were also tested with the MLCP model of the ANN, resulting in an Acc rate of 0.79 after 100 iterations, 0.82 after 500 iterations, and 0.73 after 1000 iterations [Table 3].

Table 1: Descriptive statistics and gender-based comparison table for nonnormally distributed data

Parameters	Gender	Median (minimum–maximum)	*P*
IF-W	Male	0.347 (0.085–0.678)	0.004
	Female	0.274 (0.094–0.632)	
IF-L	Male	0.365 (0.112–0.610)	0.000
	Female	0.228 (0.076–0.553)	
RIFGPF-L	Male	3.750 (3.060–4.650)	0.000
	Female	3.525 (3.020–4.230)	
LIFGPF-L	Male	3.735 (2.810–4.640)	0.000
	Female	3.520 (3.020–4.300)	
RIFDMS-L	Male	4.015 (3.330–5.050)	0.002
	Female	3.860 (3.290–4.760)	
LIFDMS-L	Male	4.075 (3.120–4.850)	0.001
	Female	3.820 (3.300–4.720)	
IFPNS-L	Male	4.160 (3.520–4.980)	0.000
	Female	3.845 (3.240–4.780)	
IFTPS-L	Male	2.685 (1.790–3.810)	0.000
	Female	2.495 (1.830–3.240)	
IFGPF-L	Male	3.540 (2.140–4.320)	0.000
	Female	3.255 (2.860–3.960)	
GPFIFPNS-A	Male	23.750 (13.800–30.400)	0.054
	Female	24.300 (20.100–30.200)	
AIF-L	Male	1.002 (0.157–1.540)	0.035
	Female	0.951 (0.358–1.530)	
RIFMID-L	Male	0.616 (0.248–1.130)	0.000
	Female	0.459 (0.176–1.010)	
LIFMID-L	Male	0.611 (0.356–1.200)	0.000
	Female	0.544 (0.238–1.070)	

IF-W: Width of foramen incisivum, IF-L: Length of foramen incisivum, RIFGPF-L: Distance between right foramen incisivum and foramen palatinus major, LIFGPF-L: Distance between left foramen incisivum and foramen palatinus major, RIFDMS-L: Distance between right foramen incisivum and third dens molaris serotinus, LIFDMS-L: Distance between left foramen incisivum and 3rd dens molaris serotinus, IFPNS-L: Distance between foramen incisivum and spina nasalis posterior, IFTPS-L: Distance between foramen incisivum and sutura palatina transversa, IFGPF-L: Distance between foramen incisivum and foramen palatinum majus, GPFIFPNS-A: Angle between foramen palatinum majus, foramen incisivum, and spina nasalis posterior, AIF-L: Distance to the bone in front of foramen incisivum, RIFMID-L: Distance between right foramen incisivum and the closest point of dens incisivus medialis, LIFMID-L: Distance between left foramen incisivum and the closest point of dens incisivus medialis

Discussion

In the field of forensic medicine and forensic sciences, the evaluation of bones holds significant importance for initial information gathering, particularly in determining gender. While the cranial and pelvic regions are commonly assessed due to their display of sexual dimorphism, estimations of gender are also derived from bones of other body regions such as ulna, radius, humerus, femur, tibia, patella, vertebrae, and tarsal bones. Gender can be estimated in the cranial region by measuring points like foramen magnum, palatinum durum, gonion, pterion, as well as nasal and orbital data, arcus zygomaticus, paranasal sinuses, and mandibular measurements.[8,23,29-33] In gender estimation, particularly in cases of peripheral measurement points being compromised, as in burn cases, it becomes evident that measurements taken from more resilient and deeper structures like palatinum durum, which are more resistant to heat, hold greater significance.[8] In this context, the present study achieved a gender prediction Acc of 0.82 through morphometric data pertaining to foramen incisivum within the palatinum durum, along with distances to anatomical neighbors such as foramen palatinum

Table 2: Performance values obtained from machine learning algorithms

Algorithms	Acc	Spe	Sen	F1
LR	0.82	0.82	0.82	0.82
LDA	0.82	0.82	0.82	0.82
RF	0.82	0.82	0.82	0.82
DT	0.79	0.79	0.79	0.79
ETC	0.79	0.79	0.79	0.79
Gaussian NB	0.79	0.79	0.79	0.79
QDA	0.76	0.76	0.76	0.76
k-NN (k=10)	0.76	0.76	0.76	0.76

DT: Decision tree, RF: Random forest, ETC: Extra tree classifier, LR: Logistic regression, LDA: Linear discriminant analysis, QDA: Quadratic discriminant analysis, Acc: Accuracy, Spe: Specificity, Sen: Sensitivity

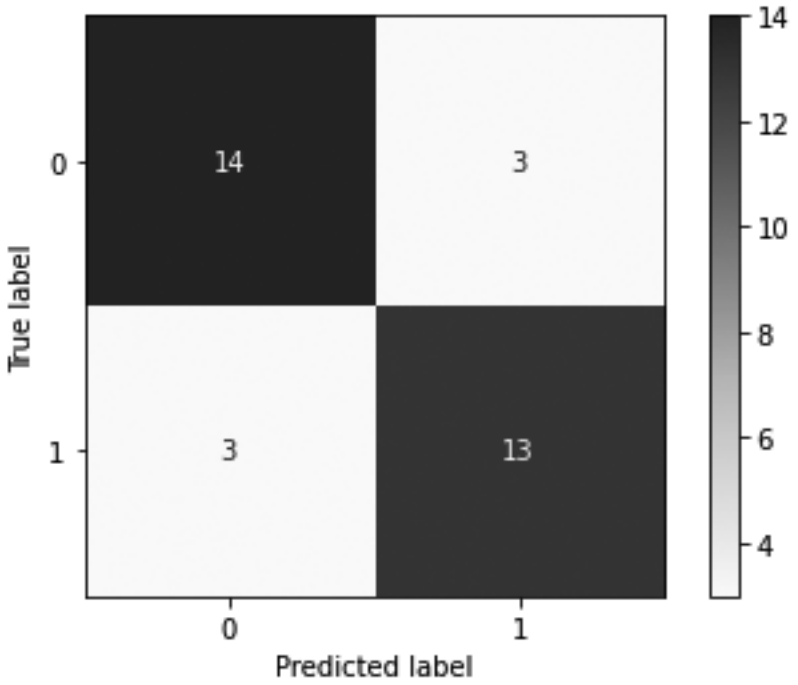

Figure 3: Confusion matrix table for models with the highest accuracy rates

Table 3: Performance values obtained based on the training iterations of artificial neural network

Number of Trainings	Acc	Spe	Sen	F1
100	0.79	0.80	0.79	0.79
500	0.82	0.82	0.82	0.82
1000	0.73	0.73	0.73	0.73

Acc: Accuracy, Spe: Specificity, Sen: Sensitivity

majus, dens molaris, spina nasalis, and sutura palatina transversa, employing ML methods such as LR, LDA, RF, and ANN. Since sex estimation is accepted between 80-90% in forensic medicine, the accuracy rate obtained is an acceptable rate.[34] However, it was observed that DT, ETC, GaussianNB methods were not as sufficient as other methods in terms of sex determination in our study due to the accuracy rates of 0.79, 0.76 of QDA, k-NN methods.

ANN is an advantageous method as it provides fast results without being dependent on the person who automatically evaluates the classification after training on the data.[35,36] Moreover, in gender determination, ANN exhibits superior performance compared to alternative methods in instances where a nonlinear relationship among variables is present.[36] Within the ANN's MLCP model, error rates are minimized through both forward and backward propagation, thereby necessitating reevaluation to the most minimal extent. In this context, efficacy is further augmented through adjustments in training iterations, layer count, and a surplus of data.[37,38] In a study by Oner *et al*., employing the ANN method through sternum, adjustments in the numbers of the first and second hidden layers, along with subjecting the data to 500 rounds of training, were made to achieve the highest performance

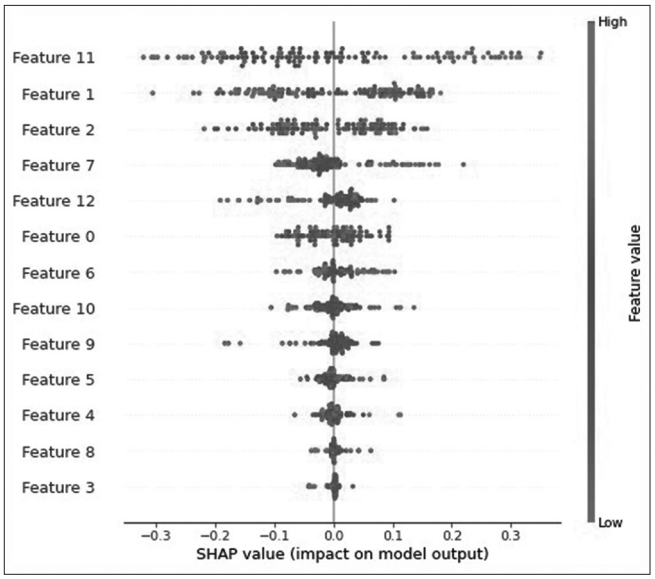

Figure 4: SHAP analyzer (Feature. 0: Width of foramen incisivum, 1: Length of Foramen incisivum, 2: Right distance between foramen incisivum and foramen palatinum majus, 3: Left distance between foramen incisivum and foramen palatinum majus, 4: Right distance between foramen incisivum and 3rd dens molaris serotinus, 5: Left distance between foramen incisivum and 3rd dens molaris serotinus, 6: Distance between Foramen incisivum and spina nasalis posterior, 7: Distance between Foramen incisivum and spina nasalis posterior, 8: Distance between Foramen incisivum and foramen palatinum majus, 9: GPFIFPNS-A, 10: Distance to the bone in front of foramen incisivum, 11: Distance between Foramen incisivum on the right and the closest point of dens incisivus medialis, 12: Distance between Foramen incisivum on the left and the closest point of dens incisivus medialis)

values, resulting in Acc values of 0.97 and 0.83, respectively.[36] In another study comparing discriminant analysis and ANN methods for gender prediction over the femur, the Acc rates of femoral head circumference and transverse diameter were found to be higher in the ANN method.[39] In this study, the maximum Acc value was reached with 500 trainings using the MLCP model in ANN. The highest ACC value obtained was 0.82, demonstrating similarity to the algorithms LR, LDA, and RF employed in other ML methods. In comparison to methods such as DT, ETC, GaussianNB, QDA, and k-NN, it exhibited superior performance.

Studies on gender prediction can be designed based on measurements taken from cadavers as well as radiographic images. Kamath *et al*., in their study on gender prediction utilizing measurements of palatinum durum taken with calipers on dry skulls, identified that the length between for. incisivum and spina nasalis posterior held the highest predictability at an 0.87 ratio among the evaluated lengths.[8] Another study, similar to ours predicted gender through skull parameters, including RIFGPF-L, LIFGPF-L, and IFGPF-L, and alternatively, the distance between the basion-for. incisivum, through conventional statistical evaluation. In this study, the most significant difference was found in the distance between the basion-for. incisivum and secondly in the LIFGPF-L value, specifically. However, it was determined that the reliability was 63% and 65%, respectively. However, their reliabilities were identified at 63% and 65%, respectively.[9] In our evaluation of radiographically obtained measurements using ML algorithms, RIFGPF-L and IFPNS-L lengths were found to rank 3rd and 6th, respectively, in terms of predicting gender among all evaluated values. The values of RIFMID-L, IF-L, RIFGPF-L, IFTPS-L, and LIFMID-L were observed to provide stronger data for gender identification.

Among the evaluated parameters, IF-L is a significant contributor to gender prediction between females and males, holding the second highest position. Conversely, IF-W, while showing a significant difference between genders, was found to have a lesser impact on gender prediction compared to IF-L. Similarly, studies have identified significant differences in gender based on measurements of anteroposterior diameter and lateral edges in the axial plane and sagittal length of for. incisivum.[10,11,40,41] In contrast, Nasseh *et al*. did not observe significant differences in gender in the sagittal diameter.[42] In addition, while Kim *et al*. found both axial and sagittal diameters to be higher in males, they were unable to detect a statistically significant difference between them.[43] Similarly, Soumya *et al*. found no significant difference between genders in both axial and sagittal dimensions of for. incisivum.[44] In our study, a significant difference in gender was identified in the distance from for. incisivum to the anterior bone, similar to the findings of Al Amery *et al*.[45] However, this parameter did not contribute significantly to gender prediction in comparison to the other evaluated parameters. In their study, Gönül *et al*. found no significant difference in the distance from for. incisivum to the anterior bone when evaluating CT scans of 100 patients. Similarly, in the same study, they found no significant difference in the distance from the anterior apex of dens incisivus to canalis nasopalatinus, which continues from for. incisivum in axial sections.[46] Costa *et al*. observed no significant difference in the distance between the roots of for. incisivum and dens incisivus based on gender, facial shape, or skeletal class.[11] While our study found significant gender differences in the evaluated parameters RIFMID-L and LIFMID-L, they were found to contribute to gender prediction to a lesser extent.

Concerning the assessed parameter GPFIFPNS-A, no noteworthy distinction emerged between females and males concerning the angle, implying a limited influence on gender prediction. Correspondingly, within the existing literature examining the relevance of this angle during anesthesia administration, an average range of 21°–23° has been reported.[47-49] However, it remains unassessed whether gender disparities exist within the context of these studies, as this facet has not been explicitly addressed within the available literature.

It is observed that within the realm of forensic anthropology, a subset of artificial intelligence known as ML is employed for gender prediction using various algorithms.[50] In a study where gender prediction was conducted using patella morphometric data, the methods yielded the highest Acc value in RF, followed by ETC, both surpassing LDA.[21] In a study where gender prediction was conducted using patella morphometric data, the methods yielded the highest Acc value in RF, followed by ETC, both surpassing LDA.[21] In an analysis of gender using antropometric measurements of the axis vertebrae from cervical, the algorithms ETC and LDA demonstrated the highest performance values in terms of Acc. Specifically, in the relevant study, ETC and LDA yielded accuracies of 0.89, followed by RF and K-NN with 0.88, QDA with 0.87, and DT and GaussianNB with 0.84.[28] In Senol *et al*.'s study, which predicted gender based on maxilla molar and canine tooth parameters, among ML algorithms, RF yielded the highest Acc rate (0.77) compared to DT, ETC, RF, LDA, LR, and QDA, which showed Acc rates ranging from 0.67 to 0.71.[26] In our study, while LDA and RF were equivalent in terms of Acc, ETC exhibited a slightly lower performance. DT, ETC, and GaussianNB demonstrated similar performances, whereas QDA and K-NN algorithms outperformed them.

This study presents an evaluation of the effectiveness of different algorithms using the same dataset. Similar to the study focused on gender prediction based on patella morphometric data, adjustments made to a single algorithm can significantly impact performance, potentially leading to higher prediction rates.[51] In this study, we compared the performance of various algorithms. We believe that

by refining a single algorithm within similar datasets, higher prediction rates for gender can be achieved. This, however, necessitates further investigation in future studies.

In both ML and ANN, a larger dataset can enhance the Acc of results, albeit at the cost of extended training time in this study, we also believe that the performance of the methods may be higher if the sample size is larger. Nevertheless, this is acknowledged as a limitation of our study. The higher volume of data can potentially extend the training period, delaying the acquisition of results.

Conclusion

In this study, gender prediction with significant implications in forensic anthropology was conducted through the application of ML algorithms and ANN using morphometric data pertaining to for. incisivum from CBCT images. When assessed through the MLCP model of YSA, algorithms such as LR, LDA, RF, and ANN demonstrated higher performance values, resulting in an Acc of 0.82. Throughout this study, attempts were made to achieve the highest performance values by modifying the number of training iterations in the application of ANN. In future studies, Acc, specificity, sensitivity, and F1 score values can be evaluated with the utilization of a larger sample size and adjustments in the number of hidden layers through the MLCP model. This would potentially offer insights into achieving even higher levels of Acc in gender prediction within the domain of forensic anthropology.

Financial support and sponsorship

Nil.

Conflicts of interest

There are no conflicts of interest.

References

1. Ono I, Ohura T, Narumi E, Kawashima K, Matsuno I, Nakamura S, *et al.* Three-dimensional analysis of craniofacial bones using three-dimensional computer tomography. J Craniomaxillofac Surg 1992;20:49-60.
2. Robling AG, Ubelaker DH. Sex estimation from the metatarsals. J Forensic Sci 1997;42:1062-9.
3. Saccucci M, Cipriani F, Carderi S, Di Carlo G, D'Attilio M, Rodolfino D, *et al.* Gender assessment through three-dimensional analysis of maxillary sinuses by means of cone beam computed tomography. Eur Rev Med Pharmacol Sci 2015;19:185-93.
4. Asala SA. Sex determination from the head of the femur of South African whites and blacks. Forensic Sci Int 2001;117:15-22.
5. Sharma S, Jehan M, Kumar A. Measurements of maxillary sinus volume and dimensions by computed tomography scan for gender determination. J Anat Soc India 2014;63:36-42.
6. Gänsslen A, Grechenig S, Nerlich M, Müller M. Standard approaches to the acetabulum part 1: Kocher-langenbeck approach. Acta Chir Orthop Traumatol Cech 2016;83:141-6.
7. Fukuda M, Matsunaga S, Odaka K, Oomine Y, Kasahara M, Yamamoto M, *et al.* Three-dimensional analysis of incisive canals in human dentulous and edentulous maxillary bones. Int J Implant Dent 2015;1:12.
8. Kamath V, Asif M, Shetty R, Avadhani R. Binary logistic regression analysis of hard palate dimensions for sexing human crania. Anat Cell Biol 2016;49:151-9.
9. Nascimento Correia Lima N, Fortes de Oliveira O, Sassi C, Picapedra A, Francesquini L Jr, Daruge E Jr. Sex determination by linear measurements of palatal bones and skull base. J Forensic Odontostomatol 2012;30:37-43.
10. Bahşi I, Orhan M, Kervancıoğlu P, Yalçın ED, Aktan AM. Anatomical evaluation of nasopalatine canal on cone beam computed tomography images. Folia Morphol (Warsz) 2019;78:153-62.
11. Costa ED, de Oliveira Reis L, Gaêta Araujo H, Martins LA, Oliveira Santos C, Freitas DQ. Comparison of distance of upper central incisor root and incisive canal in different sagittal and vertical skeletal patterns and sex: A retrospective CBCT study. Int Orthod 2021;19:462-70.
12. Scarfe WC, Farman AG. What is cone-beam CT and how does it work? Dent Clin North Am 2008;52:707-30, v.
13. Kau CH, Bozic M, English J, Lee R, Bussa H, Ellis RK. Cone-beam computed tomography of the maxillofacial region – An update. Int J Med Robot 2009;5:366-80.
14. Urooge A, Patil BA. Sexual dimorphism of maxillary sinus: A morphometric analysis using cone beam computed tomography. J Clin Diagn Res 2017;11:C67-70.
15. Şimşek HA, Gültekin T, Bilecenoğlu B, Kolsuz ME, Atakan C. Sex Determination from the maxillary sinus by cone beam computed tomography. Turkiye Klinikleri Journal of Dental Sciences 2021;27:364-71.
16. Şimşek HA, Gültekin T, Bilecenoğlu B, Kolsuz ME, Atakan C. Morphological sex determination using frontal sinus by cone-beam computed tomography. Turkiye Klinikleri J Foren Sci Leg Med 2020;17:117-21.
17. George T, Rufus E, Alex Z. Simulation of microwave induced thermo-acoustical imaging technique for cancer detection. ARPN J Eng Appl Sci 2015;10:9424-8.
18. Islam MM, Ferdousi R, Rahman S, Bushra H. Likelihood prediction of diabetes at early stage using data mining techniques. Computer Vision and Machine Intelligence in Medical Image Analysis 2020. p. 113-25.
19. Ogurtsova K, da Rocha Fernandes JD, Huang Y, Linnenkamp U, Guariguata L, Cho NH, *et al.* IDF diabetes atlas: Global estimates for the prevalence of diabetes for 2015 and 2040. Diabetes Res Clin Pract 2017;128:40-50.
20. Shi Z, He L. Application of neural networks in medical image processing. Proceedings of the Second International Symposium on Networking and Network Security. 2010. p. 2-4.
21. Bidmos MA, Olateju OI, Latiff S, Rahman T, Chowdhury ME. Machine learning and discriminant function analysis in the formulation of generic models for sex prediction using patella measurements. Int J Legal Med 2023;137:471-85.
22. Erkartal HŞ, Tatlı M, Secgin Y, Toy S, Duman S. Gender estimation with parameters obtained from the upper dental arcade by using machine learning algorithms and artificial neural networks. Eur J Ther 2023;29:352-8.
23. Kartal E, Etli Y, Asirdizer M, Hekimoglu Y, Keskin S, Demir U, *et al.* Sex estimation using foramen magnum measurements, discriminant analyses and artificial neural networks on an Eastern Turkish population sample. Leg Med (Tokyo) 2022;59:102143.
24. Ortega RF, Irurita J, Campo EJ, Mesejo P. Analysis of the performance of machine learning and deep learning methods for sex estimation of infant individuals from the analysis of 2D

images of the ilium. Int J Legal Med 2021;135:2659-66.
25. Secgin Y, Oner Z, Turan MK, Oner S. Gender prediction with the parameters obtained from pelvis computed tomography ımages and machine learning algorithms. J Anat Soc India 2022;71:204.
26. Senol D, Secgin Y, Duman BS, Toy S, Oner Z. Sex and age estimation with machine learning algorithms with parameters obtained from cone beam computed tomography images of maxillary first molar and canine teeth. Egypt J Forensic Sci 2023;13:27.
27. Şenol D, Seçgin Y, Toy Ş, Öner S, Öner Z. Can typical cervical vertebrae be distinguished from one another by using machine learning algorithms? Radioanatomic new markers. Konuralp Med J 2023;15:210-8.
28. Yenigül H. A study on gender determination with machine learning algorithms by making anthropometric measurements of the second cervical vertebra. Master's thesis. Karabuk University; 2021.
29. Gao H, Geng G, Yang W. Sex determination of 3D skull based on a novel unsupervised learning method. Comput Math Methods Med. 2018; 25: 4567267.
30. Hekimoglu Y, Sasani H, Etli Y, Keskin S, Tastekin B, Asirdizer M. Sex estimation from the paranasal sinus volumes using semiautomatic segmentation, discriminant analyses, and machine learning algorithms. Am J Forensic Med Pathol 2023;44:311-20.
31. Navega D, Vicente R, Vieira DN, Ross AH, Cunha E. Sex estimation from the tarsal bones in a Portuguese sample: A machine learning approach. Int J Legal Med 2015;129:651-9.
32. Nogueira L, Santos F, Castier F, Knecht S, Bernardi C, Alunni V. Sex assessment using the radius bone in a French sample when applying various statistical models. Int J Legal Med 2023;137:925-34.
33. Özdemir M. Age and gender determination by cranial metric measurements and paranasal sinus measurements from brain computerized tomography in patients aged 10-65. Master thesis. Marmara University Faculty of Medicine, Department of Forensic Medicine; 2022.
34. Toneva DH, Nikolova SY, Agre GP, Zlatareva DK, Hadjidekov VG, Lazarov NE. Data mining for sex estimation based on cranial measurements. Forensic Sci Int 2020;315:110441.
35. Bewes J, Low A, Morphett A, Pate FD, Henneberg M. Artificial intelligence for sex determination of skeletal remains: Application of a deep learning artificial neural network to human skulls. J Forensic Leg Med 2019;62:40-3.
36. Oner Z, Turan MK, Oner S, Secgin Y, Sahin B. Sex estimation using sternum part lenghts by means of artificial neural networks. Forensic Sci Int 2019;301:6-11.
37. Ataseven B. Forecasting by using artificial neural networks. Oneri Journal 2013;10:101-15.
38. Ari A, Berberler ME. Interface design for solving prediction and classification problems with artificial neural networks. Acta Infologica 2017;1:55-73.
39. Alunni V, Jardin PD, Nogueira L, Buchet L, Quatrehomme G. Comparing discriminant analysis and neural network for the determination of sex using femur head measurements. Forensic Sci Int 2015;253:81-7.
40. Tözüm TF, Güncü GN, Yıldırım YD, Yılmaz HG, Galindo Moreno P, Velasco Torres M, *et al.* Evaluation of maxillary incisive canal characteristics related to dental implant treatment with computerized tomography: A clinical multicenter study. J Periodontol 2012;83:337-43.
41. Acar B, Kamburoğlu K. Morphological and volumetric evaluation of the nasopalatinal canal in a Turkish population using cone-beam computed tomography. Surg Radiol Anat 2015;37:259-65.
42. Nasseh I, Aoun G, Sokhn S. Assessment of the nasopalatine canal: An anatomical study. Acta Inform Med 2017;25:34-8.
43. Kim YT, Lee JH, Jeong SN. Three-dimensional observations of the incisive foramen on cone-beam computed tomography image analysis. J Periodontal Implant Sci 2020;50:48-55.
44. Soumya P, Koppolu P, Pathakota KR, Chappidi V. Maxillary incisive canal characteristics: A radiographic study using cone beam computerized tomography. Radiol Res Pract 2019;27:6151253.
45. Al Amery SM, Nambiar P, Jamaludin M, John J, Ngeow WC. Cone beam computed tomography assessment of the maxillary incisive canal and foramen: Considerations of anatomical variations when placing immediate implants. PLoS One 2015;10:e0117251.
46. Gönül Y, Bucak A, Atalay Y, Beker Acay M, Çalişkan A, Sakarya G, *et al.* MDCT evaluation of nasopalatine canal morphometry and variations: An analysis of 100 patients. Diagn Interv Imaging 2016;97:1165-72.
47. Saralaya V, Nayak SR. The relative position of the greater palatine foramen in dry Indian skulls. Singapore Med J 2007;48:1143-6.
48. Chrcanovic BR, Custódio AL. Anatomical variation in the position of the greater palatine foramen. J Oral Sci 2010;52:109-13.
49. Wu B, Li H, Fan Y, Wang X, Li W, Zhong S, *et al.* Clinical and anatomical study of foramen locations in jaw bones and adjacent structures. Medicine (Baltimore) 2020;99:e18069.
50. Nikita E, Nikitas P. On the use of machine learning algorithms in forensic anthropology. Leg Med (Tokyo) 2020;47:101771.
51. Öner S, Turan M, Öner Z. Estimation of gender by using decision tree, a machine learning algorithm, with patellar measurements obtained from MDCT ımages. Med Records 2021;3:1-9.

Original Article

A Comparative Study of Fresh versus Frozen Embryo Transfer and their Outcomes in Patients with Polycystic Ovarian Syndrome

Anupama Sawal, Geetanjali Yadgire[1], Preeti Thute, Kirti Chaudhary, Pradeep Bokariya[2], Darshana Fulmali

Department of Anatomy, Jawaharlal Nehru Medical College, [2]Department of Anatomy, Mahatma Gandhi Institute of Medical Sciences, Wardha, [1]Department of Anatomy, PDMMC, Amravati, Maharashtra, India

Abstract

Background: In *in vitro* fertilization (IVF)/assisted reproductive technology, fresh embryo transfer is generally preferred over frozen embryo transfer (FET). Still, some research shows that FET could increase the childbirth rate which reduces the amount of ovarian hyperstimulation syndrome (OHSS) and pregnancy problems in females with polycystic ovarian syndrome (PCOS). There is a high risk of aberrant pregnancies, incorrect placentation, and other issues when a fresh embryo is transferred. They are more likely to get OHSS. Fresh embryo transfer reduces the chances to get pregnant as the stimulatory effect will be there for long time, and the endometrium is less receptive for the embryos and vice versa in the case of FET. For IVF, the transfer of fresh embryos is typically preferred over the transfer of frozen embryos. However, some research suggests that the transfer of frozen embryos may increase the live birth rate and decrease the rates of OHSS and pregnancy complications in women with polycystic ovary syndrome. One of the most prevalent endocrine illnesses in women of reproductive age is PCOS. Chronic anovulation, hyperandrogenemia, and clinical signs of hyperandrogenism are hallmarks of polycystic ovary syndrome in the absence of additional diseases such as congenital adrenal hyperplasia, androgen-producing tumors, or Cushing syndrome. Despite the fact that some patients are discovered to be clomiphene citrate (CC) resistant, CC is still the first line of treatment for anovulatory infertility caused by PCOS. Numerous treatments, such as the usage of metformin, ovarian drilling, and gonadotropin therapy, may be taken into consideration in these people. **Materials and Methods:** Fifty women in all ranging in age from 25 to 45 participated in the study. Half of the study participants are from Wardha, and the other half are from rural areas close to Wardha. Participants were chosen from patients who sought medical attention for issues relating to infertility. We have taken consent from all the patients with the mutual understanding that their medical is being used for a comparative study. All the patients in our study are subjected to IVF following embryo transfer. We have taken $n = 50$ in which all the patients are PCOS patients with AMH noticeably higher than others. Out of them, we have taken 25 patients who are allocated for fresh Day 5 transfer and 25 of them are allocated for Day 5 FET. We have collected data for a total of 50 patients and compared the β-human chorionic gonadotropin values whether it is positive or negative in each case. We have done a comparative study by comparing the results of patients undergoing fresh versus FET with their ages ranging from 25 to 45 years. **Results:** The data of fresh Day 5 embryo and frozen Day 5 transfer and their outcome were noted. We concluded that FET has good results compared to fresh embryo transfer.

Keywords: *Embryo transfer, frozen embryo transfer, hormonal imbalance, ovarian stimulation, polycystic ovarian syndrome*

Article Info

Received: 01 November 2023
Revised: 01 May 2024
Accepted: 12 May 2024
Available online: 27 June 2024

Address for correspondence:
Dr. Pradeep Bokariya, Department of Anatomy, Mahatma Gandhi Institute of Medical Sciences, Sevagram, Wardha - 442 102, Maharashtra, India.
E-mail: pradeepbokariya@mgims.ac.in

Access this article online

Website: https://journals.lww.com/joai
DOI: 10.4103/jasi.jasi_114_23
Quick Response Code:

Introduction

A hormonal condition in women called polycystic ovarian syndrome (PCOS) results in larger ovaries with tiny cysts on the borders.[1] A woman with PCOS produces more than the required levels of androgen, a male hormone. These hormonal imbalances result in irregular menses, thus making it difficult for them to get pregnant.[2]

The cause of PCOS is not well understood, but it can be either genetic or environmental factors, or sometimes both. Metabolism is one of the most critical processes in our body by which the food we eat break down into nutritious juices.[3] Improper metabolism produces a highly toxic sticky mucus-like substance called antimitochondrial antibody. It reaches up to the ovaries and disturbs the process of ovulation which results in the trapping of eggs in the ovaries and forming multiple cysts, which are medically stated as polycystic in ovaries.[4]

The other cause can be the higher production of male androgen hormones,

How to cite this article: Sawal A, Yadgire G, Thute P, Chaudhary K, Bokariya P, Fulmali D. A comparative study of fresh versus frozen embryo transfer and their outcomes in patients with polycystic ovarian syndrome. J Anat Soc India 2024;73:160-6.

which do not allow ovaries to produce eggs conventionally. Too much androgen production can be one of the significant reasons as it is associated with various factors such as genes, insulin resistance, and inflammation.[5]

PCOS is present in about 85% of all female patients with insulin resistance. Severe stress and anxiety are some other possible causes of PCOS. It can be determined by testing serum cortisol levels in patients suffering from PCOS. Experts think genetics can be the major reason for developing PCOS.[6]

The effects of PCOS can be severe and life longing. Woman with PCOS experiences drastic hair fall, acne, pimples, and weight gain, and they are difficult to type 2 diabetes, high BP, heart diseases, and endometrial cancer.[7]

One of the most disturbing effects of PCOS is infertility. It not only disturbs the fertility of the life of a woman physically but also it turns her out mentally. Going through PCOS does not mean a woman cannot get pregnant.[8] The problem arises when due to PCOS, women have difficulty producing eggs due to the barring of hormonal imbalances with emergence, maturation, and liberation of the ovum from ovaries.[9]

Women with PCOS goes through a lot in their life. The most disturbing factor is that women face social stigma if they are infertile. We know that infertility can be experienced by both male as well as female partners, but men do not have to face social stigma as compared to women.[10]

Nowadays, people with infertility do not have to worry much as so many assisted reproductive techniques are there to help such people get pregnant, whether infertility lies in males or females. Talking women with PCOS face many difficulties in getting pregnant naturally. In such cases, assisted reproductive technology (ART) can be the best solution for such a couple.[11]

Semen analysis, egg retrieval techniques, *in vitro* fertilization (IVF), intracytoplasmic sperm injection, and other treatments make up ART. Currently, patients suffering from PCOS are treated with IVF, and the results are overwhelming. IVF is a boon to people suffering from who have infertility with PCOS facing infertility are recommended to go through IVF so that the problem with the ovaries cannot interfere with the implantation of the embryo and help the patient conceive properly.[12] In this procedure, the sperm and eggs are collected from the couple and fertilized in a dish in the laboratory. Then, the embryo is placed in the endometrium for implantation. The procedure is known as "embryo transfer." Fresh embryo transfer is when the embryos are transferred on the same day as the egg retrieval; frozen embryo transfer (FET), also known as frozen-thawed embryo transfer, is when frozen embryos are transplanted. Proper implantation is achieved by scraping the endometrium to increase its thickness before 2 days of embryo transfer.[13] The reason for carrying out embryo transfer in PCOS patients is the ovaries with polycystic interfere with the implantation of the embryo and hence do not help in conceiving. When fresh embryos are transferred instead of frozen-thawed embryos, the same issue arises. There is a high risk of aberrant pregnancies, incorrect placentation, and other issues if fresh embryo transfer is used. They are more susceptible to developing ovarian hyperstimulation syndrome (OHSS).[14]

Regarding this, patients who have undergone fresh embryo transfer have the lowest risk of OHSS and exhibit higher rates of live birth and successful pregnancies than patients who have not undergone fresh embryo transfer.[15]

Studies also demonstrate that fresh embryo transfer outperforms FET in terms of outcomes; nevertheless, the main disadvantage of this technique is the significant risk of OHSS that patients face after undergoing fresh embryo transfer.[16] Transferring fresh embryos is a routine practice in most IVF centers when they are accessible. In some circumstances, all the embryos can be cryopreserved without a new embryo transfer, usually to avoid OHSS when there has been significant follicle growth.[17] Frozen embryos or blastocysts are thawed and transplanted to the female uterus after a closely watched physiological hormone replacement cycle is complete to prime the endometrium for the restoration of ovarian function. Both the ovarian stimulation medications and the subsequent supraphysiologic sex steroids may alter the endometrial receptivity, which may hinder trophoblastic invasion and placentation.[18]

Objectives

- To evaluate the patient with PCOS
- To observe the outcomes of fresh embryo transfer in patients with PCOS
- To observe the outcomes of FET on patients with PCOS
- To compare the outcomes of fresh versus FET in patients with PCOS.

Materials and Methods

Fifty women in all ranging in age from 25 to 45 participated in the study.

Half of the study participants are from Wardha, and the other half are from rural areas close to Wardha. Participants were chosen from patients who sought medical attention for issues relating to infertility. We have taken consent from all the patients with mutual understanding that their medical is being used for a comparative study.

All the patients in our study are subjected to IVF following embryo transfer.

We have taken $n = 50$ in which all the patients are PCOS patients with AMH noticeably higher than others. Out of them, we have taken 25 patients who are allocated for fresh Day 5 transfer and 25 of them are allocated for Day 5 FET.

We have collected data for a total of 50 patients and compared the β-human chorionic gonadotropin values whether it is positive and negative in each case.

We have done a comparative study by comparing the results of patients undergoing fresh versus FET with their age ranging from 25 to 45 years.

Inclusion criteria

- Patients who are suffering from infertility due to PCOS
- Patients with PCOS who are planning embryo transfer
- PCOS patients undergoing fresh Day 5 embryo transfer
- PCOS patients undergoing frozen Day 5 embryo transfer.

Exclusion criteria

- Patients suffering from infertility due to some reasons other than PCOS
- Patients not willing to give consent to be a part of the study.

Results

We have taken data of fresh Day 5 embryo transfer and its outcome of 25 patients in total.

We have distributed negative and positive results and calculated its percentage. The outcome is shown in Table 1 and depicted in Figure 1.

As shown above, if we see out of 25 patients, there are only eight patients with positive pregnancy results, whereas the number of patients with negative pregnancy results is 17 which if we calculate in percentage then out of 100% there are only 32% positive outcomes of fresh Day 5 embryo transfer and the percentage of negative results are 68%.

Furthermore, we have taken the data of frozen Day 5 embryo transfer of 25 patients in total.

We have distributed positive and negative pregnancy outcomes and calculated its percentage. The outcome is shown in Table 2 and depicted in Figure 2.

As shown above, the number of patients with positive pregnancy results in frozen Day 5 embryo transfer is 15 and the number of patients with negative pregnancy outcome is 10 which if we calculate in the percentage out of 100%, the percentage of positive outcomes is 60% and that of negative outcomes is 40%.

Comparative study of fresh and frozen embryo transfer

We compared both the results of fresh Day 5 embryo transfer and frozen Day 5 embryo transfer and we observed that the rate of positive pregnancy outcomes in patients undergoing frozen Day 5 embryo transfer is 28% higher than in patients undergoing fresh Day 5 embryo transfer. Hence, as we have mentioned in this study, we concluded that FET has good results compared to fresh embryo transfer. The bar showing both positive and negative results of fresh and frozen Day 5 embryo transfer is shown in Figure 3.

Table 1: The outcome of negative and positive results of fresh on Day 5 embryo

Sample size	Age band (years)	Embryo (days)	Embryo transfer	BHCG
25 patients	25–45	D5	Fresh	Negative cases - 17 Positive cases - 8

BHCG: Beta-Human Chorionic Gonadotropin

Table 2: The outcome of negative and positive results of frozen on Day 5 embryo

Sample size	Age band (years)	Embryo (days)	Embryo transfer	BHCG
25 patients	25–45	D5	Frozen	Negative cases - 10 Positive cases - 15

BHCG: Beta-Human Chorionic Gonadotropin

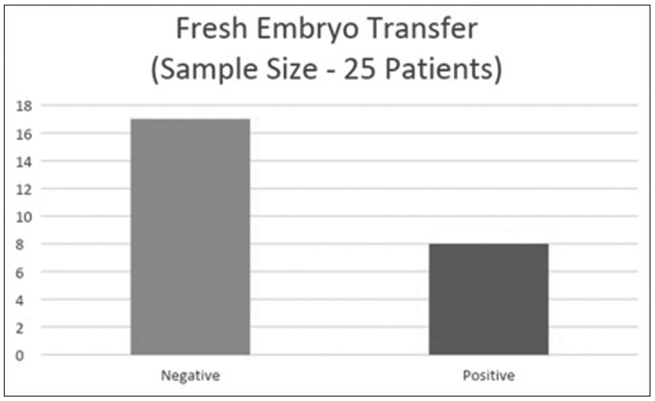

Figure 1: The bar graph showing positive and negative pregnancy outcomes of patients with fresh Day 5 embryo transfer

Discussion

In a comprehensive examination of infertile women with PCOS, the incidence of successful live deliveries and singleton live births following FET was notably higher than the rates observed after fresh embryo transfers.[19] The disparity between these two groups was primarily influenced by the substantially reduced rate of miscarriages in the FET group. The occurrence of OHSS significantly diminished with FET, despite an elevated risk of preeclampsia.[20]

Although OHSS, an iatrogenic side effect of ovulation induction medication, is less prevalent nowadays, it still poses a considerable threat to patients' health, potentially leading to fatal outcomes. A previous observational study, comparing outcomes within the same population, reported that FET was associated with a higher incidence of hypertension in comparison to fresh embryo transfer.[21]

Conversely, FET offers the advantage of allowing the ovaries to recover from the effects of ovarian stimulation.

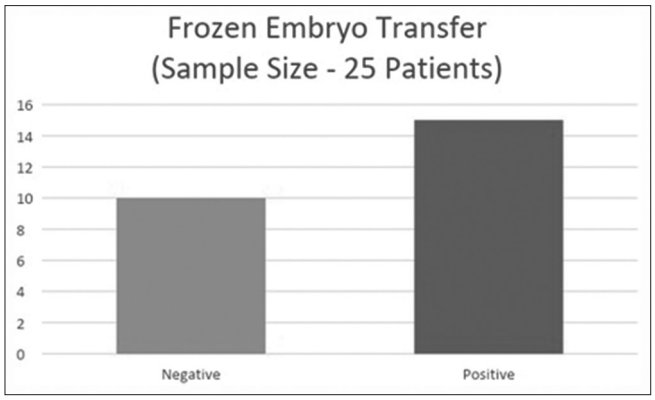

Figure 2: The bar graph showing positive and negative pregnancy outcomes of patients with frozen Day 5 embryo transfer

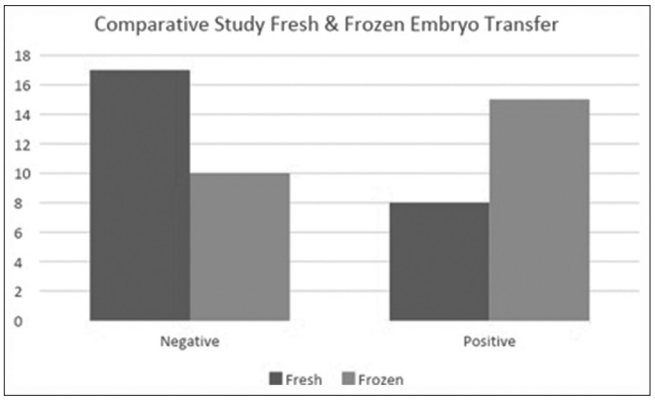

Figure 3: The bar showing both positive and negative results of fresh and frozen Day 5 embryo transfer

The exposed endometrial lining is shed, symbolizing a fresh beginning.[22] Given that our study focused on women with PCOS, a group with a higher susceptibility to OHSS and pregnancy complications, our findings may not be directly applicable to all women undergoing IVF. We found that FET resulted in a greater number of live births compared to fresh embryo transfer in a randomized study of infertile women with PCOS, and this difference was linked to a lower miscarriage risk.[23] In line with the frozen embryo group, preeclampsia was more prevalent, whereas OHSS was less common. A previous meta-analysis indicated that PCOS patients are at a higher risk of experiencing pregnancy and neonatal complications, including pregnancy-induced hypertension, preeclampsia, gestational diabetes, and preterm delivery, all of which can impact the likelihood of successful live births. It remains unclear whether these risks stem from inherent PCOS traits, underlying infertility issues, disrupted steroid levels, or a combination of these factors.[24]

Multiple observational studies have suggested that pregnancies resulting from the transfer of thawed frozen embryos tend to have better obstetric and perinatal outcomes when compared to fresh embryo transfers.[25] A prior randomized, controlled study included infertile women with PCOS and aimed to assess whether freezing embryos instead of using fresh embryos increased the live birth rate while reducing treatment-related and postpartum pregnancy complications.[26]

Although the preferred outcome in infertility trials, live birth rates were not previously reported in randomized trials comparing fresh and FETs. In our study, women with PCOS in both groups exhibited similar clinical pregnancy rates, but FET was associated with a higher incidence of live births, highlighting the importance of prioritizing live birth as the primary outcome.[27] In a prior randomized trial involving women expected to respond well to ovarian stimulation (defined as having more than 15 antral follicles observed on baseline ultrasonography), there was no significant difference in clinical pregnancy rates between the two embryo transfer procedures. However, a different study from the same group found that the rate of clinical pregnancy after FET was higher than that after fresh embryo transfer among women expected to have a normal response.[28]

The frozen embryo group displayed a higher frequency of preeclampsia, consistent with earlier studies that investigated this outcome. An observational study comparing outcomes within the same group revealed that FET was associated with a higher occurrence of hypertensive issues compared to fresh embryo transfer. Congenital abnormality rates in our study were comparable to those seen after IVF and did not significantly differ between the two groups.[29]

A meta-analysis of eleven observational studies yielded similar results, with clinical and ongoing pregnancy rates being approximately 15%–30% higher after FET compared to fresh embryo transfer, as observed in two smaller randomized trials that compared the two methods. However, the presence or absence of polycystic ovary syndrome was not recorded.[30,31] Our study's examination of subsequent pregnancy rates did not reveal discernible differences between the groups. We employed gonadotropin-releasing hormone (GnRH) antagonist techniques for ovarian stimulation, in line with the two earlier smaller trials.[32] In a recent large randomized trial comparing FET with fresh embryo transfer in PCOS-affected women undergoing IVF with the transfer of two embryos, there was no significant difference in ongoing pregnancy rates between the groups. However, the live birth rate was significantly higher with FET due to a lower rate of pregnancy loss in the second trimester. In addition, the incidence of OHSS was reduced in the group that utilized frozen embryos.[33]

Women with PCOS, given their increased risk of OHSS and pregnancy complications, may derive more benefits from a frozen embryo procedure. However, it is important to note that the confidence intervals in this study overlap with those published for women with PCOS, indicating that our results are not necessarily inconsistent with the previous findings.[34]

In one study, when blastocysts frozen on Day 6 were transferred on Day 5 of a freeze-thaw cycle, researchers observed no significant difference in the ongoing pregnancy rate between frozen embryo and fresh embryo transfers. This suggests that differences in endometrial and embryo development timing during the fresh embryo cycle may contribute to lower success rates.[35] Unlike earlier studies involving women with PCOS, we did not find a significant decrease in OHSS rates in the frozen embryo group compared to the fresh embryo group. Notably, the complication rate was quite low in our study. To reduce the risk of ovarian hyperstimulation, we typically administered gonadotropin-releasing hormone agonists to women with more than 15 follicles for egg maturation. This practice was a requirement for exclusion in our study, which excluded women at high risk for OHSS. Interestingly, all three stillbirths in the study occurred in the fresh embryo group, although the number of stillbirths was limited.[36]

Other observational studies have reported an increase in the proportion of large-for-gestational-age newborns following FET. However, a retrospective Japanese study found that FET was associated with improved perinatal outcomes compared to fresh embryo transfer. In a large cohort study, there was no discernible difference in the occurrence of congenital abnormalities between the two groups.[37]

A recent study surprisingly indicated a higher overall incidence of preeclampsia in pregnancies following the transfer of frozen embryos rather than fresh ones. This was unexpected, given that transferring frozen embryos was intended to create a more favorable intrauterine environment for placentation, potentially lowering the risk of preeclampsia.[38] Notably, the majority of the increased preeclampsia risk was linked to twin pregnancies following FET, and twin pregnancies had a higher preeclampsia risk compared to singleton pregnancies. This suggests that preeclampsia in twin pregnancies may have different underlying mechanisms compared to singleton pregnancies and may be less associated with "ischemic placenta." According to a large registry data study, twin pregnancies after FET had a higher risk of hypertensive disorders than twin pregnancies after fresh embryo transfer, whereas twin pregnancies after spontaneous conception had a lower risk of these disorders. In an intriguing finding, several studies also revealed that preeclampsia was more likely to develop in twin pregnancies resulting from oocyte donation without ovarian stimulation for recipients than in twin pregnancies arising from autologous oocytes.[39]

The study's strengths included randomization, ensuring comparability between the two groups, and the use of multi-center data sources, which enhanced the generalizability of our findings. Nevertheless, there were certain limitations to this study. First, despite pooling data from three randomized trials and having a sample size of 1508 individuals, which exceeded the meta-analysis comparing fresh versus FETs, this study may not have been able to detect differences in low-incidence issues.[40] A future meta-analysis could incorporate the results of this study to arrive at a more comprehensive conclusion. Second, the pragmatic design of this study limited its ability to elucidate the underlying reasons for the difference in pregnancy outcomes between frozen and fresh embryo transfers. Therefore, caution should be exercised when extrapolating these results to a non-PCOS population, as women with PCOS often exhibit enhanced ovarian responses and higher risks of maternal complications. In addition, since the study population was relatively young, the results may not be readily applicable to older patients, who may be more prone to obstetric difficulties than their younger counterparts.[41]

In observational studies, data regarding the likelihood of preterm delivery following frozen and fresh embryo transfers have yielded inconsistent results. While some studies have reported a reduction in premature births after FET, others have not. Patients who underwent fresh embryo transfer in addition to preserving extra embryos may fare better in observational studies than patients who exclusively underwent fresh embryo transfer. In our study, where patients were randomly assigned to receive either frozen or fresh embryo transfers, there were no significant differences in the risks of extremely preterm delivery and preterm birth for both singleton and twin pregnancies between the two groups. In most IVF clinics, the transfer of fresh embryos is the standard procedure when such embryos are available. In cases of excessive follicle development, all embryos may be cryopreserved, bypassing fresh embryo transfer to avoid OHSS. After ovarian recovery, embryos are thawed and transferred to the uterus, following a predetermined hormone replacement cycle to prepare the endometrium. Observational studies have indicated that singleton pregnancy rates are higher following FET than after fresh embryo transfer. Differences in the drugs used for ovarian stimulation or subsequent sex steroid levels may affect endometrial receptivity during fresh embryo transfer and negatively impact trophoblastic invasion or placental development. A *post hoc* analysis of two small randomized studies revealed no differences in gestational ages at birth for singletons or twin pregnancies between the groups receiving fresh or FETs.[42-44]

The study's outcomes included macrosomia (birth weight over 4000 g), gestational diabetes mellitus, preeclampsia, gestational age at birth, very preterm birth, preterm birth, small for gestational age (SGA), large for gestational age (LGA), and neonatal hospitalization exceeding 3 days. Extremely preterm births were defined as those occurring before 32 complete weeks of pregnancy, and premature births were defined as births before 37 complete weeks of pregnancy. The 3rd, 10th, and 90th percentiles of gender-specific birth weight reference values for the Chinese population were used as cutoff values for very

SGA, SGA, and LGA outcomes. The term "vanishing twins" referred to situations where two intrauterine gestational sacs were present at conception, but only one child was born.[45]

This study had certain limitations. Despite delaying randomization until the day of oocyte retrieval to reduce the risk of nonadherence, approximately 10% of patients in each group deviated from the protocol, most commonly by failing to take prescribed medications. Such variations were expected to reduce the differences between groups in the intention-to-treat analysis. In addition, the outcomes of the per-protocol analysis were consistent with those of the intention-to-treat study. Since our study focused exclusively on women with PCOS, a group with a higher risk of experiencing OHSS and pregnancy complications, the findings may not be directly applicable to other women undergoing IVF.

Conclusion

In this study, we found that the likelihood of a pregnancy through FET is higher than the likelihood of a pregnancy through fresh embryo transfer and the likelihood of a pregnancy through fresh embryo transfer is higher than the likelihood of a pregnancy through FET. Therefore, we came to the conclusion that choosing FET over a fresh one is preferable for PCOS patients. FET has been shown to be beneficial for achieving better pregnancy outcomes because we are aware of all the factors that can affect the implantation rate in fresh embryo transfer, and because the patient's body is not sufficiently prepared for the fresh transfer. In addition, numerous studies have demonstrated that frozen thawed embryos have a good implantation rate in PCOS patients.

Financial support and sponsorship

Nil.

Conflicts of interest

There are no conflicts of interest.

References

1. Ndefo UA, Eaton A, Green MR. Polycystic ovary syndrome: A review of treatment options with a focus on pharmacological approaches. *P* T 2013;38:336-55.
2. Rosenfield RL, Ehrmann DA. The pathogenesis of polycystic ovary syndrome (PCOS): The hypothesis of PCOS as functional ovarian hyperandrogenism revisited. Endocr Rev 2016;37:467-520.
3. Goldzieher JW, Green JA. The polycystic ovary. I. Clinical and histologic features. J Clin Endocrinol Metab 1962;22:325-38.
4. Lauritsen MP, Bentzen JG, Pinborg A, Loft A, Forman JL, Thuesen LL, *et al*. The prevalence of polycystic ovary syndrome in a normal population according to the Rotterdam criteria versus revised criteria including anti-mullerian hormone. Hum Reprod 2014;29:791-801.
5. Lin LH, Baracat MC, Maciel GA, Soares JM Jr., Baracat EC. Androgen receptor gene polymorphism and polycystic ovary syndrome. Int J Gynaecol Obstet 2013;120:115-8.
6. Khan MJ, Ullah A, Basit S. Genetic basis of polycystic ovary syndrome (PCOS): Current perspectives. Appl Clin Genet 2019;12:249-60.
7. Keen MA, Shah IH, Sheikh G. Cutaneous manifestations of polycystic ovary syndrome: A cross-sectional clinical study. Indian Dermatol Online J 2017;8:104-10.
8. Brady C, Mousa SS, Mousa SA. Polycystic ovary syndrome and its impact on women's quality of life: More than just an endocrine disorder. Drug Healthc Patient Saf 2009;1:9-15.
9. Dennett CC, Simon J. The role of polycystic ovary syndrome in reproductive and metabolic health: Overview and approaches for treatment. Diabetes Spectr 2015;28:116-20.
10. Nasiri Amiri F, Ramezani Tehrani F, Simbar M, Mohammadpour Thamtan RA, Shiva N. Female gender scheme is disturbed by polycystic ovary syndrome: A qualitative study from Iran. Iran Red Crescent Med J 2014;16:e12423.
11. Ombelet W, Cooke I, Dyer S, Serour G, Devroey P. Infertility and the provision of infertility medical services in developing countries. Hum Reprod Update 2008;14:605-21.
12. Melo AS, Ferriani RA, Navarro PA. Treatment of infertility in women with polycystic ovary syndrome: Approach to clinical practice. Clinics (Sao Paulo) 2015;70:765-9.
13. Simon A, Laufer N. Assessment and treatment of repeated implantation failure (RIF). J Assist Reprod Genet 2012;29:1227-39.
14. Shi Y, Wei D, Liang X, Sun Y, Liu J, Cao Y, *et al*. Live birth after fresh embryo transfer versus elective embryo cryopreservation/ frozen embryo transfer in women with polycystic ovary syndrome undergoing IVF (FreFro-PCOS): Study protocol for a multicenter, prospective, randomized controlled clinical trial. Trials 2014;15:154.
15. Liu C, Li Y, Jiang H, Liu Y, Song X. The clinical outcomes of fresh versus frozen embryos transfer in women≥40 years with poor ovarian response. Obstet Gynecol Sci 2021;64:284-92.
16. La Marca A, Sunkara SK. Individualization of controlled ovarian stimulation in IVF using ovarian reserve markers: From theory to practice. Hum Reprod Update 2014;20:124-40.
17. Zaat T, Zagers M, Mol F, Goddijn M, van Wely M, Mastenbroek S. Fresh versus frozen embryo transfers in assisted reproduction. Cochrane Database Syst Rev 2021;2:CD011184.
18. Teh WT, McBain J, Rogers P. What is the contribution of embryo-endometrial asynchrony to implantation failure? J Assist Reprod Genet 2016;33:1419-30.
19. Chen ZJ, Shi Y, Sun Y, Zhang B, Liang X, Cao Y, *et al*. Fresh versus frozen embryos for infertility in the polycystic ovary syndrome. N Engl J Med 2016;375:523-33.
20. Blazquez A, García D, Vassena R, Figueras F, Rodriguez A. Risk of pre-eclampsia after fresh or frozen embryo transfer in patients undergoing oocyte donation. Eur J Obstet Gynecol Reprod Biol 2018;227:27-31.
21. Alper MM, Smith LP, Sills ES. Ovarian hyperstimulation syndrome: Current views on pathophysiology, risk factors, prevention, and management. J Exp Clin Assist Reprod 2009;6:3.
22. Yang L, Wang R, Wang F, Wang F, Zou L. Ovarian hyperstimulation syndrome in a frozen-thawed embryo transfer pregnancy: A rare case report. BMC Pregnancy Childbirth 2020;20:313.
23. Vuong LN, Dang VQ, Ho TM, Huynh BG, Ha DT, Pham TD, *et al*. IVF transfer of fresh or frozen embryos in women without polycystic ovaries. N Engl J Med 2018;378:137-47.
24. Lin J, Huang J, Wang N, Kuang Y, Cai R. Effects of pre-pregnancy body mass index on pregnancy and perinatal

outcomes in women with PCOS undergoing frozen embryo transfer. BMC Pregnancy Childbirth 2019;19:487.
25. Maheshwari A, Pandey S, Amalraj Raja E, Shetty A, Hamilton M, Bhattacharya S. Is frozen embryo transfer better for mothers and babies? Can cumulative meta-analysis provide a definitive answer? Hum Reprod Update 2018;24:35-58.
26. Wang X, Wu H, He X, Jiang H, Wu L, Xu Y, *et al*. Retrospective study to compare frozen-thawed embryo transfer with fresh embryo transfer on pregnancy outcome following intracytoplasmic sperm injection for male infertility. Med Sci Monit 2018;24:2668-74.
27. Harbin Consensus Conference Workshop Group, Conference Chairs, Legro RS, Wu X, Scientific Committee, Barnhart KT, *et al*. Improving the reporting of clinical trials of infertility treatments (IMPRINT): Modifying the CONSORT statement. Hum Reprod 2014;29:2075-82.
28. Shapiro BS, Daneshmand ST, Garner FC, Aguirre M, Hudson C, Thomas S. Evidence of impaired endometrial receptivity after ovarian stimulation for *in vitro* fertilization: A prospective randomized trial comparing fresh and frozen-thawed embryo transfer in normal responders. Fertil Steril 2011;96:344-8.
29. Davies MJ, Moore VM, Willson KJ, Van Essen P, Priest K, Scott H, *et al.* Reproductive technologies and the risk of birth defects. N Engl J Med 2012;366:1803-13.
30. Belva F, Henriet S, Van den Abbeel E, Camus M, Devroey P, Van der Elst J, *et al.* Neonatal outcome of 937 children born after transfer of cryopreserved embryos obtained by ICSI and IVF and comparison with outcome data of fresh ICSI and IVF cycles. Hum Reprod 2008;23:2227-38.
31. Healy DL, Breheny S, Halliday J, Jaques A, Rushford D, Garrett C, *et al.* Prevalence and risk factors for obstetric haemorrhage in 6730 singleton births after assisted reproductive technology in Victoria Australia. Hum Reprod 2010;25:265-74.
32. Pelkonen S, Koivunen R, Gissler M, Nuojua-Huttunen S, Suikkari AM, Hydén-Granskog C, *et al*. Perinatal outcome of children born after frozen and fresh embryo transfer: The Finnish cohort study 1995-2006. Hum Reprod 2010;25:914-23.
33. Emeksiz HC, Bideci A, Nalbantoğlu B, Nalbantoğlu A, Çelik C, Yulaf Y, *et al.* Anxiety and depression states of adolescents with polycystic ovary syndrome. Turk J Med Sci 2018;48:531-6.
34. Sterling L, Liu J, Okun N, Sakhuja A, Sierra S, Greenblatt E. Pregnancy outcomes in women with polycystic ovary syndrome undergoing *in vitro* fertilization. Fertil Steril 2016;105:791-7.e2.
35. Shapiro BS, Daneshmand ST, Restrepo H, Garner FC, Aguirre M, Hudson C. Matched-cohort comparison of single-embryo transfers in fresh and frozen-thawed embryo transfer cycles. Fertil Steril 2013;99:389-92.
36. Pelkonen S, Hartikainen AL, Ritvanen A, Koivunen R, Martikainen H, Gissler M, *et al*. Major congenital anomalies in children born after frozen embryo transfer: A cohort study 1995-2006. Hum Reprod 2014;29:1552-7.
37. Ishihara O, Araki R, Kuwahara A, Itakura A, Saito H, Adamson GD. Impact of frozen-thawed single-blastocyst transfer on maternal and neonatal outcome: An analysis of 277,042 single-embryo transfer cycles from 2008 to 2010 in Japan. Fertil Steril 2014;101:128-33.
38. Sibai BM, Hauth J, Caritis S, Lindheimer MD, MacPherson C, Klebanoff M, *et al*. Hypertensive disorders in twin versus singleton gestations. National institute of child health and human development network of maternal-fetal medicine units. Am J Obstet Gynecol 2000;182:938-42.
39. Chantanahom N, Phupong V. Clinical risk factors for preeclampsia in twin pregnancies. PLoS One 2021;16:e0249555.
40. Roque M, Lattes K, Serra S, Solà I, Geber S, Carreras R, *et al*. Fresh embryo transfer versus frozen embryo transfer in *in vitro* fertilization cycles: A systematic review and meta-analysis. Fertil Steril 2013;99:156-62.
41. Roos N, Kieler H, Sahlin L, Ekman-Ordeberg G, Falconer H, Stephansson O. Risk of adverse pregnancy outcomes in women with polycystic ovary syndrome: Population based cohort study. BMJ 2011;343:d6309.
42. Maheshwari A, Pandey S, Shetty A, Hamilton M, Bhattacharya S. Obstetric and perinatal outcomes in singleton pregnancies resulting from the transfer of frozen thawed versus fresh embryos generated through *in vitro* fertilization treatment: A systematic review and meta-analysis. Fertil Steril 2012;98:368-77.e1.
43. Shapiro BS, Daneshmand ST, Bedient CE, Garner FC. Comparison of birth weights in patients randomly assigned to fresh or frozen-thawed embryo transfer. Fertil Steril 2016; 106:317-21.
44. Rallis A, Tremellen K. Controlled ovarian hyper-stimulation during IVF treatment does not increase the risk of preterm delivery compared to the transfer of frozen-thawed embryos in a natural cycle. Aust N Z J Obstet Gynaecol 2013;53:165-9.
45. Dai L, Deng C, Li Y, Zhu J, Mu Y, Deng Y, *et al.* Birth weight reference percentiles for Chinese. PLoS One 2014;9:e104779.

Original Article

Morphology and Morphometry of the Anterior Clinoid Process in a Select South African Population

Nomthandazo Magcaba, Samuel Oluwaseun Olojede[1], Sodiq Kolawole Lawal[2], Carmen Rennie, Onyemaechi Okpara Azu[3], Edwin Coleridge Naidu

Discipline of Clinical Anatomy, School of Laboratory Medicine and Medical Sciences, Nelson R. Mandela School of Medicine, University of KwaZulu-Natal, Durban, [1]Division of Human Anatomy, Department of Human Biology, Faculty of Medicine and Health Sciences, Walter Sisulu University, [3]Department of Medical Biosciences, University of the Western Cape, Bellville, South Africa, [2]School of Nursing, Faculty of Health Sciences, University of Botswana, Gaborone, Botswana

Abstract

Background: Clinoid space is revealed when the anterior clinoid process (ACP) is removed, and it makes anterior vertical segment of the internal carotid artery (ICA) visible. Also, the presence of Carotico-clinoid foramen (CCF) makes the ICA from the cavernous sinus emerges through it and endangers the artery during anterior clinoidectomy which necessitates understanding the variable dimensions of ACP. **Aim and Objectives:** This study intended to investigate the morphology and morphometry of the ACP and to document the prevalence of the CCF in a select group of the South African population. **Materials and Methods:** The study was carried out on a total of 32 open crania (n=64 ACP) obtained from the University of KwaZulu-Natal, Nelson Mandela School of Medicine, Discipline of Clinical Anatomy using digital vernier caliper to measure the dimensions of the ACP. **Results:** The mean length, basal width, and thickness of the ACP on the right were10.18±1.34mm, 10.27±0.73mm, and 5.81±0.80mm and the left side was 10.89±0.94mm, 11.63±0.90mm, and 4.78±0.64mm respectively. The left ACP was significantly longer, wider, and thinner than the right ACP. Type I (short and broad) ACP was the most prevalent type, occurring in 53.13% of the studied population. Out of the 32 skulls studied, the CCF was observed in 6 (18.75%) cases. Five out of the six skulls (83.33%) had a bilateral complete CCF, and 1 (16.67%) had a unilaterally incomplete CCF. **Conclusion:** The ACP in our setting differs from other populations in terms of type, dimensions, and prevalence of the CCF and these should be considered when interpreting skull base radiographs and planning anterior clinoidectomy.

Keywords: *Anterior clinoid process, caroticoclinoid foramen, morphology, morphometry, South Africa*

Introduction

The sella turcica is a saddle-shaped depression on the body of the sphenoid bone's intracranial surface. There are three clinoid processes on either side of the sella turcica. The medial and anterior prolongations of the lesser wing of the sphenoid bone combine to form the anterior clinoid processes (ACPs).[1] The ACP has a pyramidal shape with a tip and a 3-point fixation base. It is attached to the planum sphenoidale medially, the lesser sphenoid wing laterally, and the optic strut inferomedially.[2,3] The posterior clinoid processes (PCPs) can be found at the dorsum sellae, and the middle clinoid process (MCP) is present on either side of the tuberculum sellae.[1] The caroticoclinoid ligament, which connects the anterior and MCPs, can ossify and form the caroticoclinoid foramen (CCF). The CCF is a bony bridge between the tip of the MCP and the ACP, first described by Henle, in 1855. It changes the end of the carotid groove into a bony ring called a foramen.[4] Through this closed, usually circular ring of bone, the internal carotid artery (ICA) emerges forward and medially from the cavernous sinus.[5,6] The presence of the CCF causes compression of the clinoid segment of the ICA and increases the risk of hemorrhage when dealing with paraclinoid aneurysms and tumors in this region.[7] The interclinoid osseous bridge connects the ACP to the PCP. During development, the CCF and interclinoid osseous bridge are formed by the ossification of the caroticoclinoid and interclinoid ligament.[4] These bridges are related to the cavernous sinus, ICA, and pituitary gland. The presence of a bony or osseous CCF may result in compression, tightening, or stretching of the ICA, particularly the clinoidal segment. It may lead to complications during regional surgery.

How to cite this article: Magcaba N, Olojede SO, Lawal SK, Rennie C, Azu OO, Naidu EC. Morphology and morphometry of the anterior clinoid process in a select South African population. J Anat Soc India 2024;73:167-71.

Article Info

Received: 27 November 2023
Revised: 13 April 2024
Accepted: 29 April 2024
Available online: 27 June 2024

Address for correspondence:
Dr. Samuel Oluwaseun Olojede, Division of Human Anatomy, Department of Human Biology, Faculty of Medicine and Health Sciences, Walter Sisulu University, Nelson Mandela Drive, Mthatha 5099, South Africa.
E-mail: olojedesamuelo@gmail.com

Access this article online

Website: https://journals.lww.com/joai
DOI: 10.4103/jasi.jasi_121_23
Quick Response Code:

The morphology of the ACP shows significant population-specific variations in its dimensions and prevalence of the CCF.[2,8,9] To ensure optimal neurovascular control during the surgical operation, pathologic lesions located at or near the anterior and middle skull base may necessitate the removal of the ACP; anterior clinoidectomy necessitates a thorough understanding of the anterior and middle skull base neuroanatomy.[10] Removal of the ACP supply improved exposure of structures in and around the ACP and mobilization of ICA and optic nerve, also minimizing chances of brain retraction.[2] The morphology of the ACP, which is usually removed during the surgical removal of sellar region tumors or aneurysms, is clinically (surgically) significant.[11] Variations in the sellar region, such as the dimensions of the ACP and the presence of CCF, may make clinoidectomy procedures more difficult, particularly in the presence of an aneurysm and in surgical management when dealing with vascular, neoplastic, or traumatic lesions of the central skull base.[1] Although the ACP is a relatively small structure, its removal provides an enormous gain in facilitating the management of lesions, either tumors or aneurysms, in the paraclinoid region and upper basilar artery.[2,12] Owing to variations in the dimensions and complexity of the associated structures, investigating the morphology and morphometry of the ACP will contribute to the existing anatomical information on the ACP and guide in surgical procedures. Although anatomical variations in the dimensions of the ACP and prevalence of the CCF have been documented, this is the first report in a South African sample.

Materials and Methods

Ethical approval

The ethical approval for this study was obtained from the Biomedical Research Ethics Committee of the University of KwaZulu-Natal with reference number BREC: 00002996/2021.

Sample size

This study was carried out on a total of 32 open crania (n = 64 ACP) obtained from the University of KwaZulu-Natal Nelson Mandela School of Medicine, Department of Clinical Anatomy.

Inclusion and exclusion criteria

Only skulls with erupted third molars and without any visible deformations in the paraclinoid region were used. More than 100 skulls were rejected due to deformations in the paraclinoid region.

Morphometric parameters

The dimensions of the ACP, i.e., its length, width, and thickness, were measured using a digital Vernier caliper. All measurements were recorded in millimeters to 1 decimal place.

In the middle cranial fossa, the ACP was identified. The presence of CCF was determined through observation. The number of skulls in which the CCF was found present was recorded and expressed as a percentage.

Using a modification of the criteria provided by Cecen *et al*. (2016), the ACP was classified into four types based on dimensions. The categorization is as follows: Type I is short (10.5 mm) and broad (>8.14 mm), Type II is long (10.5 mm) and narrow (8.14), Type IIIa is short (10.5 mm) and thin (8.14 mm), and Type IIIb is long (10.5 mm) and wide (>8.14 mm). The length was measured from the base to the tip of the ACP, while the width was measured at the base. These reference points are based on a study by Sibuor *et al*. (2018). The thickness was measured on the body of the ACP. The data were collected by a single observer, with all the measurements repeated three times using the digital Vernier caliper and an arithmetic average taken to minimize intra-observer bias.

Statistical analysis

The data were analyzed using SPSS version 29.0.x (SPSS IBM version 29.0.x, Armonk, NY, United States of America). The means, standard deviations, and ranges were calculated. To determine statistically significant differences in means between the right and left ACP, the paired Student's t-test was used. $P \leq 0.05$ was considered statistically significant.

Results

Prevalence of the caroticoclinoid foramen

The CCF was present in 6 (18.75%) of the 32 skulls [Table 1]. Five out of the six skulls (83.33%) had a bilateral complete CCF, and 1 (16.67%) had a unilateral incomplete CCF as observed in Figure 1.

Dimensions of the anterior clinoid process

Statistically significant side differences were observed in the dimensions of the ACP [Table 2]. The mean length of the ACP on the right was 10.18 ± 1.34 mm (range: 7.54–12.40 mm, and it was 10.89 ± 0.94 mm (range: 8.15–12.94 mm) on the left. The mean width on the right was 10.27 ± 0.73 mm (range: 8.79–11.70 mm), and it was 11.63 ± 0.90 mm (range: 9.75–13.70 mm) on the left. The mean thickness of the ACP on the right was 5.81 ± 0.80 mm (range: 3.63–7.74 mm), and it was

Table 1: Comparison of the caroticoclinoid foramen between different populations

Population	Sample size (%)
Nepalese[9]	35 (20.00)
Indian[13]	223 (37.19)
European[14]	200 (16.75)
Brazilian[15]	597 (14.20)
Kenyan[8]	51 (17.60)
South African	32 (18.75)

4.78 ± 0.64 mm (range: 2.98–6.64 mm) on the left. There are statistically significant differences between the right and the left ACP in length, width, and thickness [Figure 2].

Type of the anterior clinoid process

The most common type of ACP was found to be Type I, observed in 53.13% of the ACPs studied. Type IIIb ACP was observed in 45.31%. Type IIIa had the lowest prevalence. It was seen in only 1.56% of ACPs. Type II ACPs were absent [Figure 3].

Discussion

The importance of removing the ACP from the lesser wing of the sphenoid has been emphasized in reports on surgical treatment of tumors such as meningiomas or dissection of parasellar and suprasellar aneurysms using the pterional approach.[2,16] Drilling through bone to access lesions in the parasellar and paraclinoid regions carries the risk of damaging nearby vessels and nerves or causing an aneurysm.[17] Bony prominences in the region can obstruct visualization of vital neurovascular structures and make safe exposure of lesions difficult. The optic nerve and the ICA are directly overlain and obscured by the ACP, which is one of the region's most significant prominences.[18] This necessitates a thorough understanding of the morphology and morphometry of the ACP. This study was conducted by collecting data from a South African sample.

The CCF was found in 18.75% of the South Africa population studied [Figure 4]. This prevalence was comparable to that found in other populations [Table 3], such as Kenyan,[8] Nepalese,[9] and European.[14] The incidence of the caroticoclinoid in this study was higher than that found in the Brazilian population,[15] and lower than that reported in the Indian population.[13] The majority had bilateral complete CCF. These studies were conducted across various ethnic groups, implying a possible ethnic difference in ACP morphology. Furthermore, the prevalence of CCF in the current study, which is 18.75%, is comparable to that found in the Kenyan population,[8] which was found to be 17.60%. Both these population groups are in Africa. This suggests that these variations could also

Table 2: Dimensions of the anterior clinoid process

Dimensions (mm)	Mean±SD		*P*
	Right (mm)	Left (mm)	
Length	10.18±1.34	10.89±0.94	<0.001
Width	10.27±0.7	11.63±0.90	<0.001
Thickness	5.81±0.80	4.78±0.64	<0.001

SD: Standard deviation

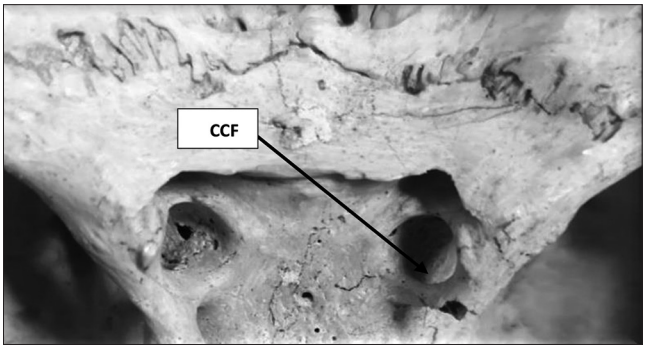

Figure 1: Caroticoclinoid foramen. CCF: Caroticoclinoid foramen

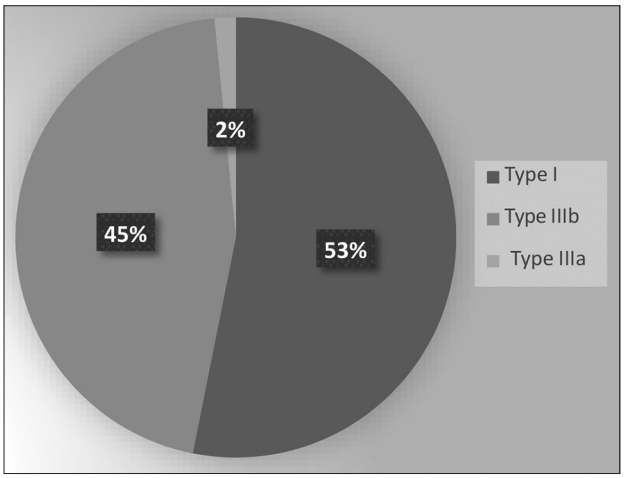

Figure 3: Prevalence of different types of anterior clinoid processes in the select South African population. ACP's: Anterior clinoid process

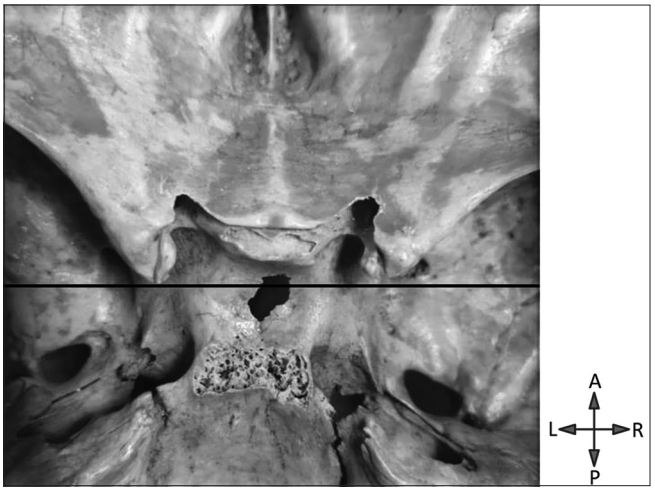

Figure 2: Difference in length between the right and the left anterior clinoid process

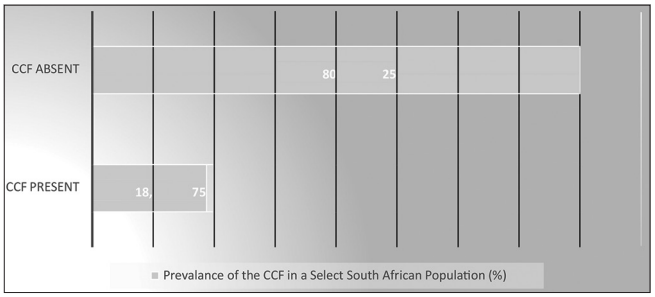

Figure 4: Prevalence of the caroticoclinoid foramen. CCF: Caroticoclinoid foramen

Table 3: Dimensions of the anterior clinoid process in different populations

Population	Length (mm)	Width (mm)	Thickness (mm)	Methodology
Nepalese[9]	10.74±2.37	10.83±1.20	5.13±1.03	Dry bone measurement
Indian[19]	10.68±1.90	12.40±2.58	6.88±1.09	Dry bone measurement
European[14]	9.90±1.60	9.40±1.40	-	Dry bone measurement
Brazilian[15]	10.31±2.10	7.70±1.73	-	CT scans
Kenyan[8]	10.92±2.79	10.43±2.67	5.43±2.02	Dry bone measurement
South African	10.18±1.34	10.27±0.73	5.81±0.80	Dry bone measurement

CT: Computed tomography

be due to epigenetic differences between populations. The ossified ligament forming the CCF forms an extra fixation point for the ACP. Failure to recognize it during anterior clinoidectomy results in incomplete ACP mobilization and, as a result, inappropriate ICA retraction.

This could result in an ICA rupture, which would be fatal.[14] Knowledge of the prevalence of CCF assists during the interpretation of skull base radiographs and anterior clinoidectomy to help avoid the associated complications.

The dimensions of the ACP obtained in this study are comparable to those of other populations [Figure 5 and Table 3]. The length of the ACP in the study population was similar to that of the Nepalese,[9] Kenyan,[8] Brazilian,[15] Indian,[13] and European.[14] However, The ACP in our study was shorter than that of the Korean population.[10] Unlike the Kenyan and Korean populations, there was a significant difference in dimensions and thickness between the ACP on the left-hand side and the ACP on the right-hand side when compared to the Nepalese population. The average mean length of the ACP was significantly longer on the left-hand side and shorter on the right [Figure 3]. However, there were very few cases where the length on the right-hand side was longer than that on the left. This was observed in 2 out of the 32 skulls investigated in this study.

The average thickness of the ACP was comparable to the Kenyan, Korean, and Nepalese populations and smaller than that of the Indian population. Unlike the length and the basal width, the thickness of the ACP was greater on the right-hand side (5.81 ± 0.80 mm) compared to the left-hand side (4.78 ± 0.64 mm). The above-mentioned variations in the ACP could be due to genetic factors. Nevertheless, methodological factors should not be ignored. The average mean width of the ACP was comparable to that of the Indian population; however, it was wider than that of the Kenyan, Brazilian, European, Korean, and Nepalese populations. The basal width of the ACP in this study was significantly wider on the left-hand side, 11.63 ± 0.90 mm, and narrower on the right, 10.27 ± 0.73 mm. These results were comparable to that of the Nepalese population.

The ACP's length and width influence its type, which influences the surgical techniques used during anterior clinoidectomies. Based on the criteria used by Sibuor *et al*., in 2018, the majority of the ACP in our population is Type I (short and wide), unlike in the Kenyan population in which the majority of the population was Type IIIb (long and wide). Type IIIb was only observed in 45.31% of the population. The intricate anatomy surrounding the ACP is critical for surgical approaches to the cavernous sinus.[20] When the ACP is removed, a clinoid space is revealed, and an anterior vertical segment of the ICA located medially can be identified.[10] The clinoid space is the space exposed following anterior clinoidectomy, and its dimensions vary with the ACP dimensions.[15] This necessitates surgeons being aware of the variable dimensions of the ACP within a population and between different populations to avoid surgical complications during anterior clinoidectomies.

Figure 5: Dimensions of the anterior clinoid process

Conclusion

The current study advances our understanding of the varied morphology of the ACP in the South African population. It is clinically significant for neurosurgeons who work in the parasellar region. The ACP in our setting differs in terms of the presence of the CCF and the type of ACP. There is also a significant difference between the ACP on the right and that on the left. These characteristics should be considered when interpreting skull base radiographs and planning anterior clinoidectomy. However, this same study on the South African population can be improved using a larger sample size and looking into the morphology and morphometry of the ACP between males and females separately to see if there are any significant differences between the two.

Acknowledgments

The authors acknowledge the College of Health Science, University of KwaZulu-Natal, National Research Foundation, as well as the technical support received from

the members of staff of Discipline of Clinical Anatomy, University of KwaZulu-Natal.

Authors contributions

NM, SOO, SKL, CR, OOA, and ECN conceived and designed the research; NM, SOO, and SKL performed the study and acquired the data; NM, OOA, ECN, CR, SOO, and SKL analyzed the data, performed statistical analyses, and wrote the manuscript. NM, ECN, OOA, CR, SOO, and LSK proofread and edited the manuscript.

Financial support and sponsorship

This study was funded by the National Research Foundation (NRF).

Conflicts of interest

There are no conflicts of interest.

References

1. Muthukumar V, Nanjundaiah K, Shetty S. Study of carotico clinoid foramen in dry human skulls. Int J Anat Res 2017;5:4630-4.
2. Menasinkai SB, Savitha V. Morphometric analysis of anterior clinoid process and optic strut: A cadaveric study. IJARS 2022;4:AO11-4.
3. Cecen A, Celigoklue E, Is M, Kale AC, Eroglu BT. Pre-operative measurement of the morphometry and angles of the anterior clinoid process (ACP) for aneurysm surgery. Int J Morphol 2016;34:1333-8.
4. Erturk M, Kayalioglu G, Govsa F. Anatomy of the clinoidal region with special emphasis on the caroticoclinoid foramen and interclinoid osseous bridge in a recent Turkish population. Neurosurg Rev 2004;27:22-6.
5. Souza AD, Ankolekar VH, Nayak N, Hosapatna M, Souza AS. Morphometric study of anterior clinoid process and optic strut and the ossification of carotico-clinoid ligament with their clinical importance. J Clin Diagn Res 2016;10:C05-7.
6. Cheng Y, Wang C, Yang F, Duan Y, Zhang S, Wang J. Anterior clinoid process and the surrounding structures. J Craniofac Surg 2013;24:2098-102.
7. Bansode SA, Devadas P, Vinila BS. Study of incidence of the carotico-clinoid foramen in the South Indian dry adult skulls: A cross-sectional study. Int J Anat Res 2017;5:4051-5.
8. Sibour W, Cheruiot I, Munguti J, Kigera J, Gikenye G. Morphology of the anterior clinoid process in a select Kenyan population. Anat J Afr 2018;7:1132-7.
9. Gupta N, Ray B, Ghosh S. A study on anterior clinoid process and optic strut with emphasis on variations of caroticoclinoid foramen. Nepal Med Coll J 2005;7:141-4.
10. Lee HW, Park HS, Yoo KS, Kim KU, Song YJ. Measurement of critical structures around paraclinoidal area: A cadaveric morphometric study. J Korean Neurosurg Soc 2013;54:14-8.
11. Noguchi A, Balasingam V, Shiokawa Y, McMenomey SO, Delashaw JB Jr. Extradural anterior clinoidectomy. Technical note. J Neurosurg 2005;102:945-50.
12. Froelich SC, Aziz KM, Levine NB, Theodosopoulos PV, van Loveren HR, Keller JT. Refinement of the extradural anterior clinoidectomy: Surgical anatomy of the orbitotemporal periosteal fold. Neurosurgery 2007;61:179-85.
13. Desai S, Sreepadma S. Study of carotico clinoid foramen in dry human skulls of North Interior Karnataka. Natl J Basic Med Sci 2012;1:60-4.
14. Kapur E, Mehić A. Anatomical variations and morphometric study of the optic strut and the anterior clinoid process. Bosn J Basic Med Sci 2012;12:88-93.
15. Da costa MD, De Olivera Santos BF, Araujo Paz DE, Rodrigues TP, Abdala N, Centeno RS, *et al*. Anatomical variations of the anterior clinoid process: A study of 597 skull base computerized tomography scans. Oper Neurosurg 2016;12:289-97.
16. Dagtekin A, Avci E, Uzmansel D, Kurtoglu Z, Kara E, Uluc K, *et al*. Microsurgical anatomy and variations of the anterior clinoid process. Turk Neurosurg 2014;24:484-93.
17. Boyan N, Ozsahin E, Kizilkanat E, Tekdemir I, Soames R, Oguz O. Surgical importance of the morphometry of the anterior clinoid process, optic strut, caroticoclinoid foramen, and interclinoid osseous bridge. Neurosurg Q 2011;21:133-6.
18. Dhakal A, Mehta UK, Sah SK, Chaudhary RK. Morphological variation of anterior clinoid process in dry human skulls. Birat J Health Sci 2019;4:813-7.
19. Hunnargi S, Ray B, Pai SR, Siddaraju KS. Metrical and non-metrical study of anterior clinoid process in South Indian adult skulls. Surg Radiol Anat 2008;30:423-8.
20. Avci E, Bademci G, Ozturk A. Microsurgical landmarks for safe removal of anterior clinoid process. Minim Invasive Neurosurg 2005;48:268-72.

Original Article

A Radioanatomical Evaluation of the Plantaris Tendon with Magnetic Resonance Imaging Method and a Review of the Literature in the Light of Our Findings

Fatih Çankal[1,2], Hilal Melis Altıntaş[1], Dilara Patat[1], Mustafa Kaya[3]

[1]Department of Anatomy, Faculty of Medicine, Ankara Medipol University, [2]Department of Radiology, Pursaklar Public Hospital, [3]Department of Radiology, Faculty of Medicine, Gazi University, Ankara, Turkey

Abstract

Introduction: Variations of the plantaris muscle and tendon are common. Ultrasonography and magnetic resonance imaging (MRI) are radiological methods for evaluating the plantaris tendon. This study aimed to perform a radioanatomical evaluation of the plantar tendon using MRI and to compare our findings with the literature data. **Materials and Methods:** The presence of the plantaris tendon in 155 ankle magnetic resonance studies of 139 patients, its diameter, its course, the localization of the calcaneal attachment of the tendon, and its relationship with the Achilles tendon were evaluated. Student's *t*-test was used for those with normal distribution in numerical data, and the Mann–Whitney *U* test was used for those who did not. Pearson Chi-square test was used in the evaluation of categorical data, depending on the assumptions. $P < 0.05$ was considered statistically significant. **Results:** A total of 139 patients, 89 (67.74%) females, and 50 (32.26%) males were included in the study. In 115 (74.2%) of 142 cases in which the plantaris tendon was imaged, the plantaris tendon was inserted into the calcaneus separately from the Achilles tendon and was joining the Achilles tendon at various levels in 27 cases (17.41%). In 27 cases where the plantaris tendon joined with the Achilles tendon, the distance from the junction point to the calcaneal insertion was 15 ± 9.90 cm. **Conclusion:** Our study is one of the limited number of studies in the literature to examine the thickness and termination levels of the plantaris tendon. We believe that our measurements will contribute to future radioanatomical meta-analyses.

Keywords: *Achilles tendon, ankle magnetic resonance imaging, plantaris muscle, plantaris tendon*

Introduction

The plantaris muscle is a short, thin spindle-shaped muscle with a long tendon. The muscular part measures 10 cm × 1.5 cm.[1-3] It originates between the posterosuperior of the supracondylar ridge of the femur and the lateral head of the gastrocnemius muscle. The tendon of the muscle moves across proximally medial to the soleus and gastrocnemius muscles. It then lays on the medial to the Achilles tendon and terminates in the calcaneus or Achilles tendon.[1,2,4-8]

The plantaris muscle participates in plantar flexion of the foot.[4] Its role in plantar flexion is to contribute to motor function rather than strength.[9] Its participation rate in plantar flexion is 0.7%.[10] Its proprioceptive function is more prominent compared to plantar flexion.[11]

The plantaris tendon may also be damaged in Achilles tendon pathologies that cause limitation of movement due to serious injuries.[12] The course and endpoint of the plantaris tendon are an important factor in Achilles middle segment tendinopathies.[10]

It can be used as a graft in the repair of the patellar tendon, palmaris longus tendon, coracoclavicular ligament, and atrioventricular valve.[1,10,13,14]

Variations of the plantaris muscle and tendon are common.[7,8,12] It is thought that its contribution to Achilles tendinopathy may be related to these variations.[1,12] In recent years, there has been an increased interest in this tendon in patients with mid-portion Achilles chronic pain. A thick tendon has been associated with pain in some patients, and it has been reported that the complaints of some patients, some of whom are elite athletes, disappear after surgical removal.[15-17] However, there are still opinions that its clinical significance is not taken seriously enough.[10]

How to cite this article: Çankal F, Altıntaş HM, Patat D, Kaya M. A radioanatomical evaluation of the plantaris tendon with magnetic resonance imaging method and a review of the literature in the light of our findings. J Anat Soc India 2024;73:172-7.

Article Info

Received: 09 November 2023
Revised: 12 April 2024
Accepted: 08 May 2024
Available online: 27 June 2024

Address for correspondence:
Dr. Hilal Melis Altıntaş, Hacıbayram Mahallesi, Talatpaşa Bulvarı, Ankara Medipol Üniversitesi, No. 2, Altındağ, Ankara 06050, Turkey. E-mail: hilalmelisaltintas@gmail.com

Access this article online

Website: https://journals.lww.com/joai
DOI: 10.4103/jasi.jasi_117_23
Quick Response Code:

Ultrasonography and magnetic resonance imaging (MRI) are radiological methods for evaluating the plantaris tendon. The plantaris tendon can also be easily evaluated in the MRI examination used in ankle-related disorders.[18] In the detection of the plantaris tendon, the sensitivity of MRI is 92.8% and the specificity is 100%. The incidence of the tendon in MRI examinations was found to be 62.8% and 97.5% in cadavers. It has been reported that section thickness below 5 mm will increase sensitivity.[4]

We aimed to evaluate this structure, which has limited studies in the literature, in routine ankle MRI examinations in detail and to contribute to the literature.

Materials and Methods

Ethics

This study was planned as a retrospective study. At all stages, the 1964 Declaration of Helsinki, national research committee standards, and ethical guidelines were meticulously complied with. This study was approved by a local noninterventional research ethics committee (September 23, 2021, Decision No: 38).

Study design and patient selection criteria

Between January 2020 and July 2021, 284 examinations of 249 patients who underwent ankle MRI at the imaging center were evaluated retrospectively. Patients who had undergone surgery, patients with infection, abscess, fracture, hematoma, Achilles tendinopathy, malignant mass, and patients younger than 18 years of age were excluded from the study group. One hundred and fifty-five ankle MRI of the remaining 139 patients were included in the study. The flowchart showing the exclusion criteria is presented in Figure 1.

MRI examinations were performed using 1.5 T (Tesla) (Signa Explorer, GE Healthcare, USA) MRI scanners.

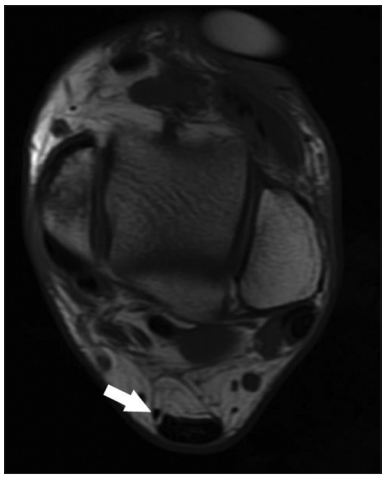

Figure 1: Plantar tendon is observed separately. Axial T1W image. White arrow: Plantaris tendon

Routine sequences included in the standard protocol were taken in MRI examinations. The retrieved sequences and their properties are given in Table 1.

The presence of the plantaris tendon, its diameter, its course separately or together with the Achilles tendon, the localization of the calcaneal attachment of the tendon, the distances between the plantar tendon and the endpoints of the Achilles tendon, the distance of the junction of the plantar tendons joining the Achilles tendon to the calcaneal ending level of the Achilles tendon were evaluated. Plantar tendon thickness was measured at its thickest part in the axial section. Images in the collection environment of the center were examined on two separate dates by a radiologist with 23 years of experience using the picture archiving and communication system. Distance measurements were made using maximum magnification.

Statistical analysis

Mean ± standard deviation was given for numerical variables, and number (n) and percentage (%) were given for categorical variables. Student's *t*-test was used for those with normal distribution in numerical data, and the Mann–Whitney *U* test was used for those who did not. Pearson Chi-square test was used in the evaluation of categorical data, depending on the assumptions. Data were analyzed using IBM SPSS Statistics for Windows Version 22 (IBM Corp., Armonk, New York, USA). $P < 0.05$ was considered statistically significant. Intraobserver reliability was tested using the Cohen kappa test.

Results

A total of 155 individuals, 105 (67.74%) females, and 50 (32.26%) males were included in the study. While the mean age of the total individuals is (44.28 ± 14.72), the mean age of women is (46.80 ± 12.75) and the mean age of men is (38.98 ± 16.99) [Table 2].

The plantaris tendon was visualized in 142 (91, 61%) of 155 cases. The cases where the plantaris tendon is absent/cannot be visualized are 13 (8.39%). In 115 (74.2%) of 142 cases in which the plantaris tendon was imaged, the plantaris tendon was inserted into the calcaneus separately from the Achilles tendon, while it was joining the Achilles tendon at various levels in 27 cases (17.41%). In 94 (60.65%) cases that terminate separately, the plantaris tendon ends in the anterior of the Achilles tendon, and in 21 (13.55%), it ends medially [Table 2 and Figures 2-4].

There was no statistical difference between the plantaris tendon joining or separating, ending anteriorly or medially, and the age and gender of the cases ($P = 0.548$, $P = 0.379$, respectively) [Table 3].

In the intraobserver reliability study using the Cohen kappa test, the results were between 0.87 and 0.95 and were accepted as reliable.

Table 1: Average values of routine sequences in the magnetic resonance imaging examination of the ankle

	TR (ms)	TE (ms)	FOV	Matrix	ST (mm)	SS (gap) (mm)
Axial T2W	7691	85	14–16	352×224	4.0	1.0
Axial T1W	421	15.2	14–16	320×256	4.0	1.0
Sagittal T2W	3522	111	16–18	320×256	3.0	1.0
Sagittal STIR	4209	93.6	16–18	320×224	3.0	1.0
Coronal T1W	700	14	14	256×256	3.0	1.0
Coronal T2 TSE FS	3400	50	14	256×256	3.0	1.0

TR: Repetition time, TE: Echo time, FOV: Field of view, ST: Slice Thickness, SS: Slice Spacing, STIR: Short tau inversion recovery

Table 2: Age and number distribution of the subjects in the study

	Number of cases *n* (%)	Total	The average age (mean±SD)	Total
Women				
Anterior	62 (40)	95 (61.29)	46.56±12.49	46.80±12.75
Medial	13 (8.39)		45.32±11.59	
Combined	20 (12.9)		44.95±12.99	
Absent	10 (6.45)	10 (6.45)	54.00±12.91	
Men				
Anterior	32 (20.65)	47 (30.33)	37.94±16.07	36.98±16.99
Medial	8 (5.16)		50.13±19.54	
Combined	7 (4.52)		33.71±14.87	
Absent	3 (1.93)	3 (1.93)	32.67±8.50	
Total	155 (100)	155 (100)		44.28±14.72

Values are given as mean±SD and *n* (%). SD: Standard deviation

Table 3: Distribution of the plantar tendon being separate or combined (position) by age and gender

	Anterior + medial	Combined	*P*
Age	44.26±14.64	42.04±14.35	0.548, >0.05
Gender, *n* (%)	115 (74.2)	27 (17.41)	0.379, >0.05

Mann-Whitney U Test. $P<0.05$

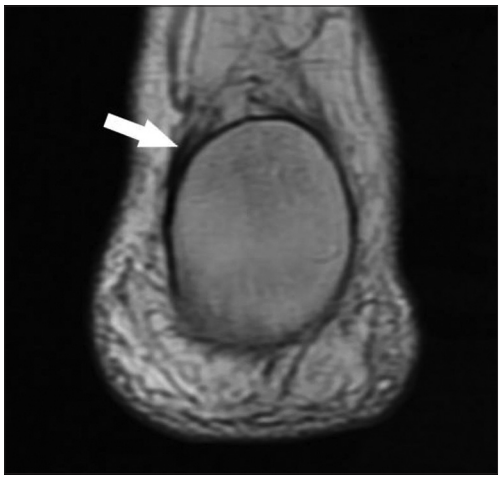

Figure 2: The plantar tendon ends separately on the calcaneus. Coronal T1W image. White arrow: Plantaris

Diameter

Within the scope of this study, the diameter measurement of the plantaris tendon was also made. The mean diameter of the tendon in all cases was 2.77 ± 0.90 mm (2.64 ± 0.82 mm in women, 3.04 ± 1.00 mm in men). The diameter of the anteriorly located plantaris tendon is 2.83 ± 0.87 mm (2.68 ± 0.80 mm in women, 3.11 ± 0.93 mm in men). The diameter of the medially located plantaris tendon was 3.19 ± 0.96 mm (3.12 ± 0.82 mm in women, 3.30 ± 1.15 mm in men). In cases where the Achilles tendon and plantaris tendon joined, the plantaris tendon diameter was measured as 2.24 ± 0.72 mm (2.18 ± 0.64 mm in women, 2.41 ± 0.87 mm in men) [Table 4].

When the mean diameters of tendons were compared between men and women, the measured diameter value was found to be statistically higher in men than in women (P = 0.021). When the diameter of the anteriorly located plantaris tendon was compared between the sexes, this diameter value was found to be higher in men than in women, and this value was statistically significant (P = 0.035) [Table 5].

The diameters of the medial and confluent plantaris tendons were compared between men and women, and no significant difference was found between the sexes in this value (P = 0.716, P = 0.551, respectively) [Table 5].

The diameters of the anterior and medial plantaris tendons were compared with each other, and no statistically significant difference was found between them (P = 0.136) [Table 6].

The diameters of the anterior and medial ending tendons and the plantaris tendon with the fused ending were compared with each other, and the diameters of the anterior and medial terminated plantaris tendons were found to be statistically higher than those of the conjoined tendons (P = 0.001, P = 0.001, respectively) [Table 6].

Distance

The mean distances of anterior and medial tendons to the Achilles endpoint were measured as 2.80 ± 2.85 mm (2.80 ± 2.89 mm in women, 2.80 ± 2.81 mm in men) in all cases. This distance was found to be 2.19 ± 2.32 mm in cases where the plantaris tendon terminated anterior to the Achilles tendon, and 5.51 ± 3.35 mm in cases where it terminated medially [Table 2].

When the distances of the anterior and medial plantaris tendons to the Achilles tendon are compared with each

Figure 3: The plantar tendon terminates separately anteriorly. Sagittal T1W image. White arrow: plantaris tendon

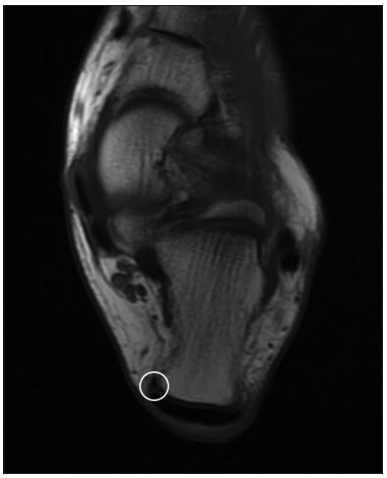

Figure 4: Axial T1W image. In the marked area (white circle), the plantaris tendon is difficult to distinguish from the Achilles tendon

Table 4: Diameter and distance values of the plantar tendon

	Diameter (mean/mm)				Distance (mean/mm)		
	Anterior	Medial	Combined	Total	Anterior	Medial	Total
Woman	2.68±0.80	3.12±0.82	2.18±0.64	2.64±0.82	2.26±2.58	5.33±2.86	2.80±2.89
Man	3.11±0.93	3.30±1.15	2.41±0.87	3.04±1.00	2.06±1.70	5.74±4.01	2.80±2.81
Total	2.83±0.87	3.19±0.96	2.24±0.72	2.77±0.90	2.19±2.32	5.51±3.35	2.80±2.85

Table 5: Distribution of diameter values by gender

	Woman	Man	*P*
Anterior diameter	2.6 (1.3–5.5)	2.9 (1.5–5.0)	0.035, <0,05*
Medial diameter	3.2 (1.8–4.3)	2.95 (1.8–5.1)	0.716, >0.05
Combined diameter	2.2 (1–3.8)	2.8 (2.2–4.6)	0.551, >0.05
Total diameter	2.6 (1–5.5)	2.9 (1.5–5.1)	0.021, <0,05*

*Mann-Whitney U Test. $P<0.05$

Table 6: Comparison of plantar tendon diameters in different positions with each other

Anterior	Medial	Combined	*P*
2.7 (1.3–5.5)	3.1 (1.8–5.1)	-	0.136, >0.05
2.7 (1.3–5.5)	-	2.3 (1.0–4.6)	0.001, <0,05*
-	3.1 (1.8–5.1)	2.3 (0.5–4.6)	0.001, <0.05*

*Mann-Whitney U Test. $P<0.05$

other, the distance of the medial plantaris tendon to the Achilles tendon is greater than the anterior location, and this value is statistically significant ($P < 0.05$ $P = 0.000$) [Table 7].

The distance of the anterior and medial-ending plantaris tendon to the Achilles tendon was compared between the genders, and no statistically significant difference was found ($P = 0.148$, $P = 0.818$, respectively) [Table 8].

Joining location

The distance from the junction of the plantaris tendon to the calcaneal insertion in 27 cases where it joined with the Achilles tendon was measured, and this distance was found to be 15 ± 9.90 cm (15.4 ± 9.53 cm in women, 13.9 ± 10.81 cm in men) in all cases.

When the distances of the merging plantaris tendon to the calcaneus were compared between men and women, no statistically significant difference was found in this value ($P = 0.789$).

Discussion

The presence, origin, course, relationship with neurovascular structures, and insertion of the plantaris tendon show various variations. Its absence and unilateral or bilateral pairing have been reported.[7,10,12,19-25]

The absence of plantaris tendon has been reported between 0% and 19% in the literature.[5,12,26,27] In our study, the tendon was observed in 91.61% of cases, which is consistent with the literature data. In cadaveric studies, the rate of tendon detection increases in studies involving proximal dissection.[1] We agree with this finding. Therefore, we think that the possibility of the tendon joining the Achilles tendon proximally should not be ignored in patients in whom the plantaris tendon is not observed in the ankle MRI.

Plantaris tendon termination also shows wide variations.[6,12,28]

Daseler and Anson reported that in 750 lower extremity dissections, the plantaris tendon was independent of Achilles in 80%, Nayak *et al*. in 1/3 of cases, and van Sterkenburg *et al*. in 89.7%.[5,6,28] The rate we found in our study was 74.2%.

Table 7: Comparison of anterior and medial plantar tendon distances

Anterior	Medial	*P*
1.45 (0.3–12)	5.5 (1.3–12)	0.000, <0.05*

*Mann-Whitney U Test. *P*<0.05

Table 8: Comparison of anterior and medial plantar tendon distances by gender

	Woman	Man	*P*
Anterior	1.25 (0.3–12)	1.8 (2–10)	0.148, >0.05
Medial	5.5 (1.3–9.4)	5.85 (0.6–12)	0.818, >0.05

Mann-Whitney U Test. *P*<0.05

Although there are a few anatomical studies about the plantaris tendon in the literature, there are very few size measurements.[1] Average tendon thicknesses vary between 1.9 mm and 4.1 mm and can reach 7 mm.[1,19] In our study, we measured the average tendon diameter of 2.77 ± 0.90 mm. We believe that our measurements will contribute to future radio-anatomical meta-analyses. The data provided in cadaveric and radiological studies are consistent with our study. However, in our study, it was found that the tendon thickness was higher in men than in women, and the diameter of the tendons ending in the calcaneus was greater than the tendons joining with the Achilles tendon.

In our study, it was difficult to determine that the plantaris tendon often ended differently from the Achilles tendon in the normal evaluation. Examination at maximum magnification and in all three orthogonal planes could detect that these two tendons terminate at different points.

There are different typings in terms of plantaris tendon shape and endpoint. However, we think that the use of these typings in radiological evaluation and reporting is incompatible with the ordinary flow of daily life. Therefore, in our study, we chose data that can be easily evaluated in practical use.

There were some limitations of our study such as the retrospective nature of the study, the lack of sufficient data about the clinical manifestations of the patients, and the measurements being made in a single center and by a single radiologist. However, since the study is a radioanatomical study rather than a clinical one, it is hoped that the results will contribute to the literature.

The ankle has a complex biomechanical function. There are studies showing a relationship between Achilles paratenon thickness and Achilles tendinitis and plantar fasciitis.[29,30] In this case, the protective or triggering effects of a well-developed plantar tendon, which indirectly affects the Achilles paratenon thickness, in the development of Achilles tendonitis or plantar fasciitis need to be investigated. Again, we think that the possible protective or triggering effect of a well-developed plantar tendon with susceptibility to ankle lateral collateral ligament injuries is worth investigating.

Conclusion

We believe that our measurements will contribute to future radio-anatomical meta-analyses. We think that the plantaris tendon developmental differences and the predisposing or protective effects of other tendinous/ligamentous pathologies are worth investigating.

Financial support and sponsorship

Nil.

Conflicts of interest

There are no conflicts of interest.

References

1. Spang C, Alfredson H, Docking SI, Masci L, Andersson G. The plantaris tendon: A narrative review focusing on anatomical features and clinical importance. Bone Joint J 2016;98-B: 1312-9.
2. White WL. The unique, accessible and useful plantaris tendon. Plast Reconstr Surg Transplant Bull 1960;25:133-41.
3. Allard JC, Bancroft J, Porter G. Imaging of plantaris muscle rupture. Clin Imaging 1992;16:55-8.
4. Saxena A, Bareither D. Magnetic resonance and cadaveric findings of the incidence of plantaris tendon. Foot Ankle Int 2000;21:570-2.
5. Daseler EH, Anson BJ. The plantaris muscle: An anatomical study of 750 specimens. J Bone Joint Surg 1943;25:822-7.
6. van Sterkenburg MN, Kerkhoffs GM, Kleipool RP, Niek van Dijk C. The plantaris tendon and a potential role in mid-portion Achilles tendinopathy: An observational anatomical study. J Anat 2011;218:336-41.
7. Unilateral MP, Anatómica UR. Unilateral double plantaris muscle: A rare anatomical variation. Int J Morphol 2010;28:1097-9.
8. Sugavasi R, Latha K, Devi I, Jetti R, Sirasanagandla SR, Gorantla VR. A case report of variant insertion of plantaris muscle and its morphological and clinical implications. J Morphol Sci 2013;30:304-5.
9. Kannus P. Structure of the tendon connective tissue. Scand J Med Sci Sports 2000;10:312-20.
10. Gonera B, Kurtys K, Karauda P, Olewnik Ł, Polguj M. Possible effect of morphological variations of plantaris muscle tendon on harvesting at reconstruction surgery – Case report. Surg Radiol Anat 2020;42:1183-8.
11. Peck D, Buxton DF, Nitz A. A comparison of spindle concentrations in large and small muscles acting in parallel combinations. J Morphol 1984;180:243-52.
12. Olewnik Ł, Wysiadecki G, Podgórski M, Polguj M, Topol M. The plantaris muscle tendon and its relationship with the Achilles tendinopathy. Biomed Res Int 2018;2018:9623579.
13. Unglaub F, Bultmann C, Reiter A, Hahn P. Two-staged reconstruction of the flexor pollicis longus tendon. J Hand Surg Br 2006;31:432-5.
14. Shuhaiber JH, Shuhaiber HH. Plantaris tendon graft for atrioventricular valve repair: A novel hypothetical technique. Tex Heart Inst J 2003;30:42-4.
15. Calder JD, Freeman R, Pollock N. Plantaris excision in the treatment of non-insertional Achilles tendinopathy in elite athletes. Br J Sports Med 2015;49:1532-4.
16. Steenstra F, van Dijk CN. Achilles tendoscopy. Foot Ankle Clin 2006;11:429-38, viii.

17. Alfredson H. Midportion Achilles tendinosis and the plantaris tendon. Br J Sports Med 2011;45:1023-5.
18. Jain R, Shetty S, Radhika PM. Morphometric study of plantaris muscle in South Indian population and its clinical importance. Int J Curr Res Rev 2020;12:46-50.
19. Olewnik Ł, Gonera B, Kurtys K, Podgórski M, Polguj M, Topol M. A proposal for a new classification of the fibular (lateral) collateral ligament based on morphological variations. Ann Anat 2019;222:1-11.
20. Sharma S, Sharma GD, Bhardwaj S. Absence of plantaris muscle. Nov Sci Int J Med Sci 2012;1:300-4.
21. Sawant SP, Shaikh ST, More RM. Cadavrevic case report on variant heads of plantaris muscle. Int J Health Sci Res 2012;2:117-22.
22. Srimani P, Meyur R, de Bose A, Kundu B, Sadhu A. Unilateral variation of plantaris muscle: A case report. J Evol Med Dent Sci 2014;3:618-22.
23. Rana KK, Das S, Verma R. Double plantaris muscle: A cadaveric study with clinical importance. Int J Morphol 2006;24:495-8.
24. Kumar A. Bicipital origin of plantaris muscle – A case report. Int J Anat Var 2011;4:177-9.
25. Kwinter DM, Lagrew JP, Kretzer J, Lawrence C, Malik D, Mater M, *et al*. Unilateral Double Plantaris Muscle: A Rare Anatomical Variation. Int J Morphol 2010;28:1097-9.
26. Jain R, Radhika PM, Shailaja S. Morphometric study of plantaris muscle in South Indian population and its clinical importance. Int J Curr Res Rev 2020;12:46.
27. Cummins EJ, Anson BJ. The structure of the calcaneal tendon (of Achilles) in relation to orthopedic surgery, with additional observations on the plantaris muscle. Surg Gynecol Obstet 1946;83:107-16.
28. Nayak SR, Krishnamurthy A, Prabhu LV, Madhyastha S. Additional tendinous origin and entrapment of the plantaris muscle. Clinics (Sao Paulo) 2009;64:67-8.
29. Stecco C, Corradin M, Macchi V, Morra A, Porzionato A, Biz C, *et al.* Plantar fascia anatomy and its relationship with Achilles tendon and paratenon. J Anat 2013;223:665-76.
30. van Sterkenburg MN, van Dijk CN. Mid-portion Achilles tendinopathy: Why painful? An evidence-based philosophy. Knee Surg Sports Traumatol Arthrosc 2011;19:1367-75.

Original Article

Application of Machine Learning Algorithms for Carpal Tunnel Syndrome

Yıldız Yener[1,2], Elif Sarıca Darol[3], Süleyman Uzun[4], Murat Alemdar[5], Tuncay Çolak[1]

[1]Department of Anatomy, Faculty of Medicine, Kocaeli University, Kocaeli, [2]Department of Therapy and Rehabilitation, Vocational School of Health Services, Sakarya University, [3]Department of Neurology, Training and Research Hospital, [4]Department of Computer Engineering, Faculty of Technology, Sakarya Applied Sciences University, [5]Department of Neurology, Sakarya University Faculty of Medicine, Sakarya, Turkey

Abstract

Introduction: Median nerve entrapment is commonly related to alterations in the anatomy of the surrounding tissues in the carpal tunnel. Carpal tunnel syndrome (CTS) is the most prevalent form of peripheral entrapment neuropathy. Machine learning (ML) is utilized in a variety of fields. After conferring with a physician, ML enables doctors to conduct the necessary examinations and make an early diagnosis. Methods based on artificial intelligence have the potential to be utilized in clinical practice as a supplementary instrument for accurate evaluation of median nerve entrapment. Despite the rise in ML-based medical research, median nerve entrapment has received less attention. The purpose of this study was to evaluate the performance of classification approaches with ML algorithms in CTS patients utilizing electromyography test data from patients exhibiting varied CTS symptoms and indications. **Materials and Methods:** Our study includes message and demographic information derived from the electromyography results of 315 individuals. In classification procedures, the logistic regression, support vector machine (SVM), K-nearest neighbor, and naïve Bayes algorithms from ML techniques were utilized. **Results:** As a result of the classification, performance values for accuracy, precision, sensitivity, specificity, and F1-score were obtained. As a result of our research, the SVM algorithm achieved a 96% success rate. **Conclusion:** ML algorithms are an emerging method of analysis. The diagnosis and treatment of diseases are gradually gained by clinicians through observation and experience. Therefore, categorization systems can aid in the accurate and timely diagnosis of median nerve entrapment by clinicians.

Keywords: *Electromyography, machine learning, median nerve, nerve conduction studies*

Introduction

The deep fascia thickens on the front of the wrist and forms the flexor retinaculum (transverse carpal ligament). This ligament is joined to the pisiform and hamate bones on inside, and the scaphoid and trapezium bones on outside. The anatomical groove between this ligament and the carpal bones is called as carpal tunnel (wrist canal). The carpal tunnel contains nine flexor tendons and the median nerve. Underneath the flexor retinaculum, the median nerve is the most superficial structure. The motor branch of the median nerve most commonly branches from the proximal part of the retinaculum flexorum and provides innervation to the thenar muscles. The median nerve extends from the carpal tunnel into the palm and separates into branches that innervate the thumb, index finger, middle finger, and radial half of the ring finger with sensory fibers.[1,2] Because it is associated with alterations in the normal anatomy of the nerve environment, median nerve compression is of clinical significance.[3] When the median nerve is squeezed or compressed in the carpal canal, the most frequent entrapment neuropathy of the upper extremity, carpal tunnel syndrome (CTS), occurs.[4-6]

CTS is a neurological disorder associated with work-related strain and repetitive motion in affected individuals.[7] It can be acute or chronic, with chronic being far more prevalent. CTS symptoms can vary from patient to patient. Consequently, they are classified as mild, moderate, and severe.[8] Compressive stresses on the median nerve result in microvascular nerve and myelin sheath damages.[7] Therefore, pain, numbness, and tingling are experienced in places where the median nerve is widely distributed. Obesity, monotonous wrist activity, pregnancy, genetic inheritance, and rheumatoid inflammation are the most prevalent risk factors for CTS. CTS is more prominent among women than men. It is reported that the risk is particularly elevated between the ages of 45 and 54 in women, and 75 and 84 in males.[2,8] It is a significant cause of

How to cite this article: Yener Y, Darol ES, Uzun S, Alemdar M, Çolak T. Application of machine learning algorithms for carpal tunnel syndrome. J Anat Soc India 2024;73:178-83.

Article Info

Received: 01 August 2022
Revised: 04 December 2023
Accepted: 29 April 2024
Available online: 27 June 2024

Address for correspondence:
Dr. Yıldız Yener,
Department of Anatomy, Faculty of Medicine, Kocaeli University, Kocaeli, Turkey.
E-mail: yildizece@sakarya.edu.tr

Access this article online

Website: https://journals.lww.com/joai
DOI: 10.4103/jasi.jasi_108_22
Quick Response Code:

work disability, affecting around 3% of the population.[7] This makes CTS a common issue among employees who actively utilize their hands.[8] CTS treatment should be initiated urgently.[4,6]

In recent years, techniques based on machine learning (ML) have found extensive usage in health care and revolutionized the field of medical diagnostics.[9-11] Artificial intelligence (AI) technologies have the potential to be employed in clinical practice as an auxiliary tool for the high-accuracy assessment of CTS.[12]

ML is a subfield of AI that refers to an algorithm's ability to learn patterns in vast datasets.[13] One of the most essential characteristics of ML is that it can generate accurate and high-performance predictions using nonlinear and extremely complex data sets.[14] Given sufficient data, an ML algorithm is able to learn to make predictions or solve problems, such as identifying objects in images or winning certain games.[15] ML develops data analytics algorithms to extract features from data. Inputs to ML algorithms include patient "characteristics" and occasionally medical outcomes of interest. Typically, a patient's characteristics consist of fundamental information such as age, gender, and disease history, as well as disease-specific information such as diagnostic imaging, physical examination results, clinical symptoms, and medications.[16]

ML algorithms use a variety of statistical, probabilistic, and optimization techniques to detect useful patterns in vast, unstructured, and complex datasets by learning from past experience.[17] Utilizing algorithms with a high predictive capability and high success rate increases the likelihood of early diagnosis and treatment. The research on this topic and the success of the applied devices highlight the significance of ML in the medical field. There are numerous classification methods for ML.[14] In this investigation, the ML algorithms logistic regression (LR), support vector machine (SVM), K-nearest neighbor (KNN), and naive Bayes were utilized.

Materials and Methods

CTS is frequently diagnosed solely on clinical symptoms; nevertheless, electromyography (EMG) is recommended for making a diagnosis.[3] Transcarpal sensory conduction abnormalities or transcarpal sensory and motor conduction abnormalities of median nerve in the presence of normal ipsilateral ulnar nerve conduction are the main indicators of CTS in a nerve conduction study (NCS). Sensory NCSs are more sensitive in the electrodiagnosis of CTS than motor NCSs. The diagnosis of carpal tunnel syndrome is made based on these criteria. Another typical finding is the prolonged distal motor latency on the wrist-to-thenar muscle segment in the presence of normal median nerve motor conduction velocity in the forearm segment. In a normal adult, the median nerve distal motor latency varies between 2.0 and 4.5 ms. Motor distal latency prolongation over 4.4 ms is considered significant for CTS. In the differential diagnosis of CTS, it is necessary to examine the ipsilateral ulnar nerve in all cases. We also used the parameter of motor distal latency difference recorded from the second lumbrical (median nerve) and interosseous muscle (ulnar nerve) in confirmation of CTS. Prolongation of the motor distal latency difference recorded from the second lumbrical-interosseous muscle (>0.4 ms) by stimulating the median and ulnar nerves from an equal distance at the wrist has a sensitivity of 73%–98% for baseline CTS.[17] Patients with cervical radiculopathy; patients previously operated due to CTS; patients with a history of sequelae, trauma, or surgery in the upper extremity; and patients diagnosed with myopathy and polyneuropathy were not included in the study. Our study included the message and demographic data acquired from the EMG test of 315 individuals with a prediagnosis of CTS whose EMG was performed. In nerve conduction studies performed with an electromyography device, motor and sensory latency, amplitude and velocity values of the median and ulnar nerves, gender, age, height, weight, dominant side, and body mass index data were used in Table 1.

The experimental investigation employed AI to classify CTS data into two categories: CTS and no CTS. In

Table 1: Dataset

Attribute	Definition
Average age	46,4
Gender	Male/female
Height	cm
Weight	kg
Dominant hand	Right/left
Side	Right/left
BMI	BMI
BMI group	<18.5: Thin (underweight) 18.6–25: Normal 25.1–30: Overweight 30.1–35: First-degree obese 35.1–40: Second-degree obese Over 40.1: Third-degree obese
Median sensory nerve action potentials	>6 mV
Median sensory nerve conduction velocities	>49 m/s
Median motor distal latency	<4.20 m/s
Median compound muscle action potential	>4.5 mV
Median mean corpuscular volume	>50 m/s
Ulnar sensory nerve action potentials	>4 mV
Ulnar sensory nerve conduction velocities	>49 m/s
Ulnar motor distal latency	<4.0 m/s
Ulnar compound muscle action potential	>5.0 mV
CTS	Yes/no

BMI: Body mass index, CTS: Carpal tunnel syndrome

classification procedures, ML algorithms LR, SVM, KNN, and naïve Bayes (NB) were utilized.

LR is a strong and well-established classification technique. Using a logistic function, the LR model expresses the link between many input features (independent variables) and a categorical dependent variable (outcome variable) and estimates the probability of a given outcome variable.[18-20]

SVM is a learning algorithm that is based on statistical learning theory.[21] SVM can categorize both linear and nonlinear data. Each data item is initially mapped to an *n*-dimensional attribute space, where *n* is the number of attributes. It then specifies the hyperplane that divides the data points into two classes, maximizing the marginal distance for both classes while reducing classification errors. The marginal distance for a class is the distance between the decision hyperplane and the member of that class with the nearest instance. To perform the classification, we must locate the hyperplane with the greatest margin between the two classes.[14,18]

KNN is the simplest and most fundamental algorithm as well as a supervised learning algorithm.[14,18] In order to select the nearest features in the procedure, an integer value *k* is determined.[18] The Euclidean, Manhattan, Chebyshev, Minkowski, or Hamming distance is utilized to calculate the distance between the test data and the training data.[14] The algorithm operates under the assumption that adjacent data points belong to the same class. Due to its simplicity and resistance to complex training data, it is one of the most favored ML algorithms.[22]

NB is a theorem-based classification method. This theorem can be used to characterize the likelihood of an event given prior knowledge of its associated conditions. This classifier considers that a feature within a class is not directly related to any other characteristic, but that features within the class may have dependency among themselves.[18] It estimates probabilities one-by-one for each data set element and classifies according to the probability with the highest value. A large amount of training data yield accurate results, although a high success rate can be attained with fewer data. If data in the test set cannot be found in the training set, or if data in the training set cannot be found in the test set, then the probability cannot be calculated because it cannot be estimated, and "0" probability is returned.[21]

The study was approved by the non-Interventional Ethics Committee of the Faculty of Medicine at Sakarya University, dated March 2, 2022, and numbered 91.

Simulation results and performance evaluation

The data set is divided into 80% training and 20% testing. During the training phase, no validation methods were undertaken, and the learning rate was determined to be 0.1. After the training operations, the utilized ML algorithms were evaluated with a test data set they had never seen, and training performance was acquired.

As a result of the categorization, performance values for accuracy, precision, sensitivity, specificity, and F1-score were obtained. To better explain these results, receiver operating characteristic (ROC) curves were generated graphically. The confusion matrix is used to calculate performance metrics [Table 2].

Equations 1, 2, 3, 4, and 5 provide mathematical equations for the performance metrics utilized in the study.

$$\text{Accuracy} = \frac{TP + TN}{TP + TN + FP + FN} \quad (1)$$

$$\text{Precision} = \frac{TP}{TP + FP} \quad (2)$$

$$\text{Sensitivity} = \frac{TP}{TP + FN} \quad (3)$$

$$\text{Specificity} = \frac{TN}{TN + FP} \quad (4)$$

$$F1\text{-score} = \frac{2 * TP}{2 * TP + FP + FN} \quad (5)$$

Figure 1 depicts the confusion matrix developed as a result of the investigation. In this matrix, the proportion of successfully and incorrectly identified "with CTS" and "no CTS" classes for each algorithm is displayed.

SVM is the ML algorithm that best classifies whether or not there is CTS. In both classes, 96% accuracy was achieved with a single misclassification of data. The LR algorithm, on the other hand, misclassified 3 of 32 non-CTS data as having CTS, and 93% accuracy was achieved by incorrectly stating that there is no CTS in 1 data, despite the presence of CTS. On the other hand, the NB algorithm misclassified it, stating that there are CTSs when there are only 2, and that there are none when there are 3. On the other hand, the KNN algorithm misclassified it as there being no CTS in 1 data, but there being no CTS in 4 data.

The performance results of the CTS data were calculated using the numerical values obtained from the confusion matrix given in Figure 1 and substituting them in Equations 1, 2, 3, 4, and 5 [Table 3].

In Table 3, the SVM algorithm had the highest performance with a 96% success rate. This is followed by LR with 93%, NB with 92%, and KNN with 92%.

Figure 2 depicts the CTS ROC curves. In this graph, the classification performance of classification algorithms is clearly displayed.

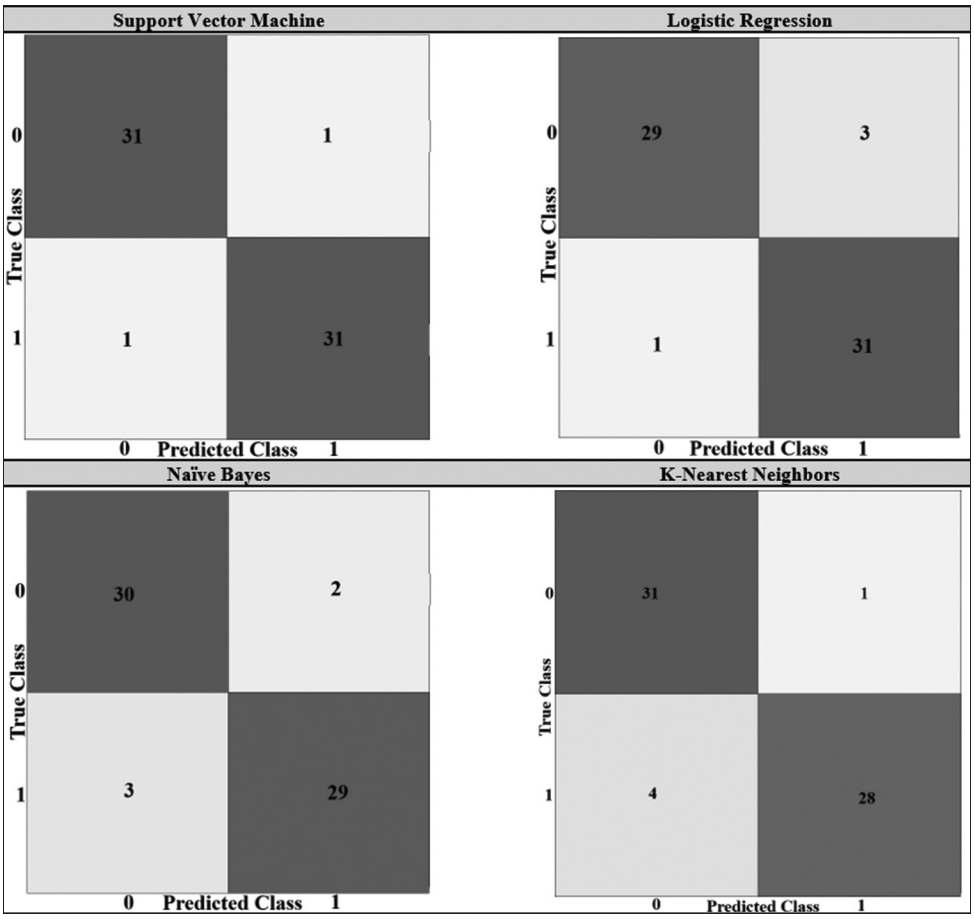

Figure 1: Confusion matrix obtained from the study

Table 2: Confusion matrix

Predicted class	Actual class	
	Positive	Negative
True	TP	TN
False	FP	FN

TP: True positive, FP: False positive, TN: True negative, FN: False negative

On the ROC curve graph, a separate graph displaying the performance of the algorithms, SVM has the largest area. This is then followed by LR, NB, and KNN, respectively.

Discussion

ML algorithms are an emerging method of analysis. These strategies have been utilized in other nations, including our own. Recent years have seen an increase in the application of AI algorithms to effectively identify musculoskeletal disorders using medical imaging without human error.[3] The diagnosis and treatment of diseases are gradually gained by clinicians through observation and experience.[23] There are studies showing that nerve conduction speed decreases asymptomatically over time due to the multitude of movements that may cause a decrease in nerve conduction speed, wrong sports and wrong ergonomic approaches.[24,25] Utilizing computer-assisted techniques in medical practice can aid in reducing cost, time, human expertise, and medical error.[26] There are similar studies that have recently begun to be used to classify diseases at the diagnosis stage.[27]

In Bilgin's study, they utilized multilayer perceptual neural networks, SVM, decision tree, ensemble learning algorithms, linear discriminant analysis, and KNN techniques to the data of 520 patients to evaluate the risk of diabetes in the early period using ML algorithms. As a result of the analysis, he concluded that the KNN algorithm achieved the best level of accuracy, 99.81%.[14]

ML algorithms are a prevalent classification technique that has been recently applied to the classification of neurological illnesses.[27] Algorithms based on ML are suitable for disease classification, decision-making, and the development of novel therapeutics. Despite the surge in medical research employing ML, less research has been conducted on CTS.

Sayin *et al*. used four ML algorithms (SVM, NB, tree, and artificial neural network) to diagnose CTS in 67 of 109 CTS patients with CTS and 42 patients without CTS. The greatest success rate was found to be 91.04% for NB. SVM came in second with 89.55%.[27]

CTS classification was made using ML algorithms LR, SVM, KNN, and NB. As a result of the classification, the SVM

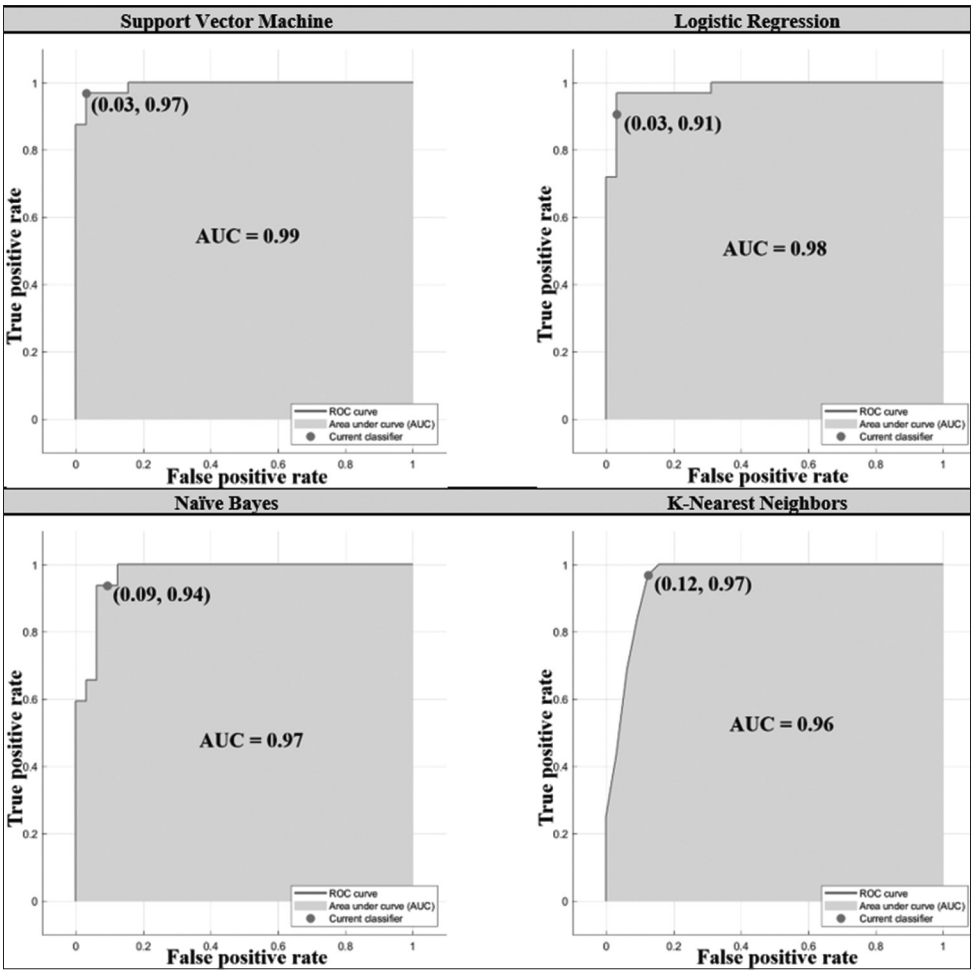

Figure 2: Carpal tunnel syndrome receiver operating characteristic curve graph

Table 3: Carpal tunnel syndrome performance results of the classification

Classifier	Accuracy (%)	Precision (%)	Sensitivity (%)	Specificity (%)	F1-score (%)
SVM	0.96	0.96	0.96	0.96	0.96
LR	0.93	0.96	0.90	0.96	0.93
NB	0.92	0.90	0.93	0.90	0.92
KNN	0.92	0.88	0.96	0.87	0.92

LR: Logistic regression, KNN: K-nearest neighbor, NB: Naïve Bayes, SVM: Support vector machine

algorithm achieved the highest success rate at 96%. This is followed by LR with 93%, NB with 92%, and KNN with 92%.

Faeghi *et al*. examined the precision of CTS diagnosis based on ML modeling by performing segmentation procedures to the wrist-level sonographic images of 65 patients, 57 individuals with an equal number of controls and CTS wrists, and 228 individuals from 57 controls. As a result, they reported that computer-assisted diagnosis improved the diagnostic accuracy of radiologists.[3]

In Tsamis *et al*.'s NCS, ML algorithms with five classifiers (LR, SVM, KNN, tree, and NB) were employed, and the findings were compared to neurophysiological and clinical diagnoses. Automatic identification between patients and controls using SVM, the most accurate classifier, achieved 0.9513 accuracy compared to NCS and 0.8906 accuracy compared to clinical diagnosis.[7]

Ardakani *et al*. used SVM and convolutional neural network for the diagnosis and grading of CTS utilizing morphometry and shear-wave elastography on 200 wrists, 100 of which were KTS and 100 of which were control wrists. They discovered that SVM performed the best with an AUC of 0.94.[12]

In our investigation, SVM performed the best, with an AUC of 0.99, followed by LR (0.98), NB (0.97), and KNN (0.96).

Conclusion

Consistent with previous research, our findings indicated that ML algorithms were able to produce more accurate

predictions. Utilizing reliable classification methods can aid doctors in making an accurate and rapid diagnosis of CTS. We believe that studies in this field will provide useful information for future researchers and physicians.

Financial support and sponsorship

Nil.

Conflicts of interest

There are no conflicts of interest.

References

1. Wright AR, Atkinson RE. Carpal tunnel syndrome: An update for the primary care physician. Hawaii J Health Soc Welf 2019;78:6-10.
2. Koyama T, Sato S, Toriumi M, Watanabe T, Nimura A, Okawa A, *et al*. A screening method using anomaly detection on a smartphone for patients with carpal tunnel syndrome: Diagnostic case-control study. JMIR Mhealth Uhealth 2021;9:e26320.
3. Faeghi F, Ardakani AA, Acharya UR, Mirza Aghazadeh Attari M, Abolghasemi J, Ejtehadifar S, *et al.* Accurate automated diagnosis of carpal tunnel syndrome using radiomics features with ultrasound images: A comparison with radiologists' assessment. Eur J Radiol 2021;136:109518.
4. Zaralieva A, Georgiev GP, Karabinov V, Iliev A, Aleksiev A. Physical therapy and rehabilitation approaches in patients with carpal tunnel syndrome. Cureus 2020;12:e7171.
5. Ghasemi Rad M, Nosair E, Vegh A, Mohammadi A, Akkad A, Lesha E, *et al*. A handy review of carpal tunnel syndrome: From anatomy to diagnosis and treatment. World J Radiol 2014;6:284-300.
6. Watanabe T, Koyama T, Yamada E, Nimura A, Fujita K, Sugiura Y. The accuracy of a screening system for carpal tunnel syndrome using hand drawing. J Clin Med 2021;10:4437.
7. Tsamis KI, Kontogiannis P, Gourgiotis I, Ntabos S, Sarmas I, Manis G. Automatic electrodiagnosis of carpal tunnel syndrome using machine learning. Bioengineering (Basel) 2021;8:181.
8. Genova A, Dix O, Saefan A, Thakur M, Hassan A. Carpal tunnel syndrome: A review of literature. Cureus 2020;12:e7333.
9. Richens JG, Lee CM, Johri S. Improving the accuracy of medical diagnosis with causal machine learning. Nat Commun 2020;11:3923.
10. Esteva A, Robicquet A, Ramsundar B, Kuleshov V, DePristo M, Chou K, *et al*. A guide to deep learning in healthcare. Nat Med 2019;25:24-9.
11. Bhavsar KA, Abugabah A, Singla J, AlZubi AA, Bashir AK, Gurov N. A comprehensive review on medical diagnosis using machine learning. Comput Mater Contin 2021;67:1997-2014.
12. Ardakani AA, Afshar A, Bhatt S, Bureau NJ, Tahmasebi A, Acharya UR, *et al*. Diagnosis of carpal tunnel syndrome: A comparative study of shear wave elastography, morphometry and artificial intelligence techniques. Pattern Recogn Lett 2020;133:77-85.
13. Schwartz JT, Gao M, Geng EA, Mody KS, Mikhail CM, Cho SK. Applications of machine learning using electronic medical records in spine surgery. Neurospine 2019;16:643-53.
14. Bilgin G. Investigation of the risk of diabetes in early period using machine learning algorithms. J Intell Syst Theory Appl 2021;4:55-64.
15. Pedersen M, Verspoor K, Jenkinson M, Law M, Abbott DF, Jackson GD. Artificial intelligence for clinical decision support in neurology. Brain Commun 2020;2:fcaa096.
16. Jiang F, Jiang Y, Zhi H, Dong Y, Li H, Ma S, *et al.* Artificial intelligence in healthcare: Past, present and future. Stroke Vasc Neurol 2017;2:230-43.
17. Sheean GL, Houser MK, Murray NM. Lumbrical-interosseous latency comparison in the diagnosis of carpal tunnel syndrome. Electroencephalogr Clin Neurophysiol 1995;97:285-9.
18. Uddin S, Khan A, Hossain ME, Moni MA. Comparing different supervised machine learning algorithms for disease prediction. BMC Med Inform Decis Mak 2019;19:281.
19. Wu YT, Zhang CJ, Mol BW, Kawai A, Li C, Chen L, *et al.* Early prediction of gestational diabetes mellitus in the Chinese population via advanced machine learning. J Clin Endocrinol Metab 2021;106:e1191-205.
20. Yang WJ, Wu L, Mei ZM, Xiang Y. The application of artificial neural networks and logistic regression in the evaluation of risk for dry eye after vitrectomy. J Ophthalmol 2020;2020:1024926.
21. Ece Y, Çolak T, Uzun S, Sağıroğlu AO. Classification of artificial intellingence based coronary artery stenosis. Pak J Med Health Sci 2022;16:548-54.
22. Subasi A. Medical decision support system for diagnosis of neuromuscular disorders using DWT and fuzzy support vector machines. Comput Biol Med 2012;42:806-15.
23. Eslami S, Fadaei B, Baniasadi M, Yavari P. Clinical presentation of carpal tunnel syndrome with different severity: A cross sectional study. Am J Clin Exp Immunol 2019;8:32-6.
24. Bamac B, Colak S, Dundar G, Selekler HM, Taşkiran Y, Colak T, *et al*. Influence of the long term use of a computer on median, ulnar and radial sensory nerves in the wrist region. Int J Occup Med Environ Health 2014;27:1026-35.
25. Colak T, Bamaç B, Alemdar M, Macit Selekler H, Ozbek A, Colak S, *et al.* Nerve conduction studies of the axillary, musculocutaneous and radial nerves in elite ice hockey players. J Sports Med Phys Fitness 2009;49:224-31.
26. Kunhimangalam R, Ovallath S, Joseph PK. A novel fuzzy expert system for the identification of severity of carpal tunnel syndrome. Biomed Res Int 2013;2013:846780.
27. Sayin R, Keskin S, Hamamci M. Evaluation of several classification methods in carpal tunnel syndrome. J Pak Med Assoc 2017;67:1654-7.

Case Report

Prostatic Carcinosarcoma: Report of a Case with Immunohistochemical Characterization

Abstract

Carcinosarcoma of the prostate is a rare neoplasm characterized by a sarcomatoid component coexisting with an adenocarcinoma. This tumor has a poor outcome and presents usually with distant metastasis. Immunohistochemically, the epithelial and mesenchymal components are different, and on a molecular basis, the presence of mutations of TP53 and phosphate and tensin homolog (PTEN) supports the role of epithelial-mesenchymal transition in the pathogenesis of this entity. We report the case of a 63-year-old man presented with advanced prostate carcinosarcoma showing a negative reaction for PTEN and a positive staining for P53 in both components by immunohistochemical study.

Keywords: *Carcinosarcoma, p53, PTEN*

Mehdi Karimi-Shahri, Farnaz Torabian, Mehdi Montazer

Department of Pathology, Mashhad University of Medical Sciences, Mashhad, Iran

Introduction

Carcinosarcoma is a rare neoplasm representing <1% of all prostatic neoplasms. It is composed of an adenocarcinoma admixed with a sarcoma and usually arises from a high-grade acinar adenocarcinoma.[1]

Different theories have been suggested for the development of this tumor but recent molecular data are more in favor of the transition of epithelial to mesenchymal cells.[2] The prognosis is usually poor, although the localized tumor can be effectively treated by surgery and/or radiotherapy.[1]

We report a case of a 63-year-old man with advanced prostate carcinosarcoma.

Case Report

Our case is a 63-year-old man presenting with gross hematuria, frequency, and urinary retention. He has a previous history of prostate acinar adenocarcinoma of Gleason 4 + 4 with extensive perineural and fat invasions, diagnosed on a 12-core biopsy during a workup for erectile dysfunction 19 months earlier. Multiple vertebral bone metastasis and several pelvic lymph node involvements had been discovered as well. He received hormonal therapy. One year later, he experienced a recurrence with low back pain, multiple bone metastases, and rise of prostate-specific antigen (PSA) plasma levels to 32.35 ng/mL. After androgen deprivation therapy and radiotherapy, the pain was relieved and PSA levels fell down to 6.75 ng/mL. Now in his current presentation, a large hard prostatic lobe was found in rectal examination. Total serum PSA was 4.27 ng/mL. Ultrasound study showed bladder wall thickening and huge heterogeneous prostate bulging into the bladder and a postvoid residual volume of 600 mL. Urethral catheterization and transurethral resection of the prostate (TURP) were performed.

The histopathologic examination of the TURP specimen showed a mixture of an adenocarcinoma of acinar type with a Gleason score of 5 + 4, admixed with atypical pleomorphic giant cells and spindle cells with foci of fascicular pattern [Figure 1].

Immunohistochemically, P504S and vimentin were positive in the epithelial and mesenchymal cells, respectively. Both components showed diffuse and strong immunoreactivity for p53 and complete nuclear loss of PTEN tumor suppressor protein [Figure 2]. The results of immunostainings are summarized in Table 1.

The abdominal computed tomographic scan showed multiple pelvic and hepatic

How to cite this article: Karimi-Shahri M, Torabian F, Montazer M. Prostatic carcinosarcoma: Report of a case with immunohistochemical characterization. J Anat Soc India 2024;73:184-6.

Article Info

Received: 11 February 2022
Revised: 01 June 2023
Accepted: 01 February 2024
Available online: 27 June 2024

Address for correspondence:
Dr. Mehdi Montazer, Department of Pathology, Mashhad University of Medical Sciences, Mashhad, Iran.
E-mail: montazermhm@gmail.com

Access this article online

Website: https://journals.lww.com/joai
DOI: 10.4103/jasi.jasi_30_22
Quick Response Code:

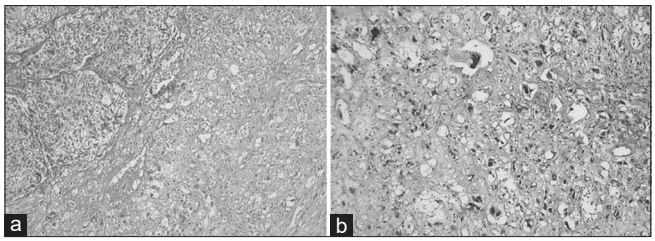

Figure 1: Microscopic examination of the specimen shows a mixture of epithelial and mesenchymal components (a). The mesenchymal component is composed of atypical pleomorphic giant cells and spindle cells (b). H and E staining, ×100 original magnification

metastatic sites. The patient decided to receive palliative care, and unfortunately, he could survive only 4 months.

Discussion

Carcinosarcoma is one of the rarest neoplasms of the prostate and presents with symptoms such as frequency, urgency, and nocturia at a mean age of 70 years. A nodular, enlarged, and hard prostate gland on digital rectal examination can be found.[3] The PSA levels in the serum may not rise proportionately to the tumor volume.[4] Distant metastasis develops in half of the patients at the time of diagnosis or afterward.[5]

At least half the cases arise from a previous adenocarcinoma after a wide-ranged interval, reported from 2 months to many years.[3,6] During this interval, more than 50% of cases receive radiation or hormonal therapy. It has been suggested that radiation may make prone prostate adenocarcinoma to the development of carcinosarcoma but a definite association has not been proved.[1] The proceeded adenocarcinoma is usually of acinar type with a Gleason score ranged from 6 to 10.[5]

Histologically, the tumor is biphasic; an adenocarcinoma that is usually of an acinar type and a sarcoma. Rarely, other types of carcinoma such as ductal adenocarcinoma, squamous or adenosquamous carcinomas, basal cell carcinoma, and mixed urothelial-squamous components are on record.[5] The sarcomatoid component is usually undifferentiated. It may compose of pleomorphic spindle cells or bizarre giant cells in sheets or with a fascicular pattern, with variable cellularity and mitotic activity. Various types of differentiation may be found such as osteosarcoma, chondrosarcoma, rhabdomyosarcoma, malignant fibrous histiocytoma, and fibrosarcoma.[5,6]

Immunohistochemically, the epithelial cells may show immunoreactivity for cytokeratin, PSA, prostate-specific acid phosphatase (PSAP), P504S, NKX3.1, and androgen receptor (AR).[1,3,6,7] In a retrospective review of a large series, 91% of the concurrent adenocarcinomas in prostate carcinosarcomas were negative for PSA and the remaining 9% were only focally positive.[1] The mesenchymal cells are reactive with vimentin and may show positivity for actin, desmin, S-100 protein, and Myo-D1, based on

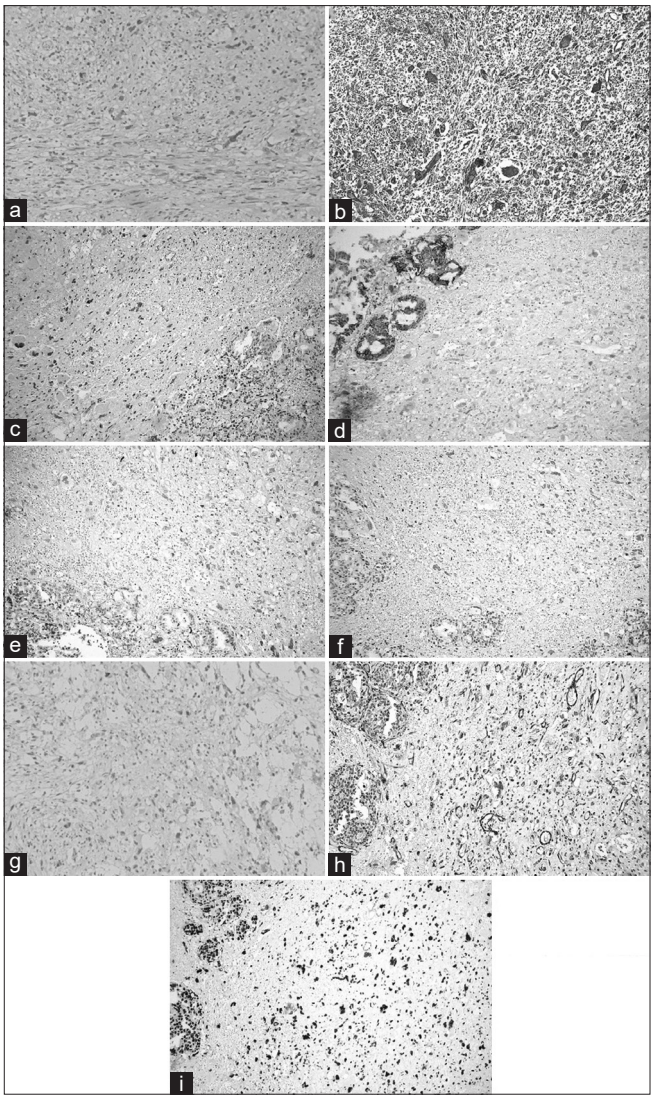

Figure 2: Immunohistochemical study shows the negative reaction of mesenchymal cells for CK (a), positive staining of mesenchymal cells for vimentin (b), negativity of prostate-specific antigen (c), positive reaction of epithelial cells for P504S (d) and negativity of CK7 (e), CK 20 (f), and S 100 protein (g). PTEN is lost in neoplastic cells (h) and P53 is diffusely positive (i). ×100

the present heterogeneous differentiation lines.[6,7] The sarcomatous areas are typically negative for PSA but may be focally positive for keratins and PSAP.[5] Similarly, our case of prostate carcinosarcoma was not immunoreactive for PSA, whereas epithelial cells stained with P504S and both components were negative for cytokeratins.

Increased levels of p53 expression have been observed in the sarcomatoid carcinoma compared to the proceeding adenocarcinoma.[8] In our case, both epithelial and mesenchymal cells showed strong and diffuse positivity for p53. In addition, PTEN showed a loss of nuclear expression on both components. Deletion of these two tumor suppressors has been proposed to have roles in epithelial-mesenchymal transition. In a study on PTEN knockout mice, carcinosarcoma was one of the most

Table 1: Immunohistochemical study results of our prostatic carcinosarcoma case

Antibody (clone)	Reactivity (cell types)
Vimentin (DACO, V9)	Positive (mesenchymal)
P504S (DACO, 13H4)	Positive (epithelial)
S100 (DACO, polyclonal)	Negative
Cytokeratin cocktail (Master Diagnostica AE1/AE3)	Negative
PSA (DACO, polyclonal)	Negative
Cytokeratin 7 (Master Diagnostica, 0VTL 12/30)	Negative
Cytokeratin 20 (Master Diagnostica, KS 20.8)	Negative
p53 (DACO, D-0-7)	Positive (epithelial and mesenchymal)
PTEN (Diagnostic Biosystems, 6H2.1)	Negative

PSA: Prostate-specific antigen, PTEN: Phosphatase and tensin homolog

frequent cytokeratin-negative prostate malignancies.[9] In another study on mice, loss of PTEN and TP53 showed to lead to the transformation of multipotential progenitors and epithelial to mesenchymal transition.[10]

The treatment options are limited and include surgical resection, adjuvant chemotherapy, and radiotherapy together with palliative attempts. However, the optimal treatment strategy is still unknown. In case of early diagnosis, localized tumors can be treated by surgery and/or radiation.[1] Moreover, this neoplasm fails to respond to androgen deprivation therapy. This might be due to a lower amount of AR and no expression of phosphorylated AR in the sarcomatoid component compared to the adenocarcinomatous part.[4]

The prognosis is dismal in the majority of cases. In a series of 21 cases, the 5- and 7-year overall survival (OS) rates were 41% and 14%, respectively.[6] In a retrospective study on 45 cases, the OS was 9 months in cases with bladder invasion and 7.1 months in patients with lymph node involvement, although, in local diseases, the survival was more than 5 years.[1] In another study of 42 cases, the actual risk of death at 1 year after diagnosis was 20% and no correlation was found between OS and morphologic features.[5] Receiving palliative care, our patient survives only 4 months after the diagnosis of carcinosarcoma.

Financial support and sponsorship

Nil.

Conflicts of interest

There are no conflicts of interest.

References

1. Markowski MC, Eisenberger MA, Zahurak M, Epstein JI, Paller CJ. Sarcomatoid carcinoma of the prostate: Retrospective review of a case series from the Johns Hopkins hospital. Urology 2015;86:539-43.
2. Pang A, Carbini M, Moreira AL, Maki RG. Carcinosarcomas and related cancers: Tumors caught in the act of epithelial-mesenchymal transition. J Clin Oncol 2018;36:210-6.
3. Mazzucchelli R, Lopez-Beltran A, Cheng L, Scarpelli M, Kirkali Z, Montironi R. Rare and unusual histological variants of prostatic carcinoma: Clinical significance. BJU Int 2008;102:1369-74.
4. Salvi S, Casadio V, Martignano F, Gurioli G, Tumedei MM, Calistri D, *et al*. Carcinosarcoma of the prostate: Case report with molecular and histological characterization. Int J Biol Markers 2018;33:540-4.
5. Hansel DE, Epstein JI. Sarcomatoid carcinoma of the prostate: A study of 42 cases. Am J Surg Pathol 2006;30:1316-21.
6. Dundore PA, Cheville JC, Nascimento AG, Farrow GM, Bostwick DG. Carcinosarcoma of the prostate. Report of 21 cases. Cancer 1995;76:1035-42.
7. Zizi-Sermpetzoglou A, Savvaidou V, Tepelenis N, Galariotis N, Olympitis M, Stamatiou K. Sarcomatoid carcinoma of the prostate: A case report. Int J Clin Exp Pathol 2010;3:319-22.
8. Zhang Z, Wang Y, Zhao Q, Li G, Zhao X, Li J, *et al*. Mixed adenocarcinoma, sarcomatoid carcinoma and adenosquamous carcinoma of the prostate: A case report. Oncol Lett 2014;8:2325-7.
9. Korsten H, Ziel-van der Made AC, van Weerden WM, van der Kwast T, Trapman J, Van Duijn PW. Characterization of heterogeneous prostate tumors in targeted pten knockout mice. PLoS One 2016;11:e0147500.
10. Martin P, Liu YN, Pierce R, Abou-Kheir W, Casey O, Seng V, *et al*. Prostate epithelial Pten/TP53 loss leads to transformation of multipotential progenitors and epithelial to mesenchymal transition. Am J Pathol 2011;179:422-35.

Case Report

Triple Anterior Horn Insertion of the Medial Meniscus Combined with Posterior Horn Hypertrophy: A Rare Case and Brief Literature Review

Abstract

Anomalies of the medial meniscus (MM) are uncommon. The most frequently occurring anomaly is found in the anterior horn. This report describes for the first time a case of abnormal multiple insertions of the anterior horn of the MM (AHMM) combined with posterior horn hypertrophy, which was found incidentally during routine dissection of a separate left lower limb from an adult cadaver. The AHMM was found to have a standard attachment to the anterior surface of the tibia in addition to two additional bands. One of these bands was the anteromedial meniscofemoral ligament, which ran parallel and independent of the anterior cruciate ligament and ended at the intercondylar notch of the femur. The other band extended as the transverse ligament that connected the AHMM to the lateral meniscus. The posterior horn of MM was found to be hypertrophied. The clinical implications of these anomalies are discussed below along with a relevant literature review.

Keywords: *Anteromedial meniscofemoral, medial meniscus, multiple insertions ligament*

Waad Mohammed Assiri, Ahmed Fathalla Ibrahim El Fouhil, Khaleel I. Alyahya, Muhammad Atteya

Department of Anatomy, Clinical Anatomy Laboratory, College of Medicine, King Saud University, Riyadh, Saudi Arabia

Introduction

Congenital anomalies of the medial meniscus (MM) are rare when compared with anomalies of the lateral meniscus. Many types of MM anomalies are found and include medial discoid variations, meniscus hypoplasia, and abnormal anterior horn insertion.[1-3] An abnormal insertion of the anterior horn of the MM (AHMM) into the femoral intercondylar notch through an anteromedial meniscofemoral ligament (AMMFL) is highly unusual and considered extremely rare with a reported incidence of 0.5%–2.8%.[4] According to Kim and Joo,[3] no direct connection between AHMM and tibia exists in association with the presence of AMMFL. All previous cases described were identified unexpectedly during knee arthroscopic procedures and magnetic resonance imaging. Due to arthroscopy and imaging limitations, these occurrences have been insufficiently described, and lack relevant details.

In this report, we describe a case of abnormal multiple AHMM insertions combined with posterior horn hypertrophy. To the best of our knowledge, this abnormality has not been previously described in the literature. The report provides a detailed study of the morphological and histological features of such an anomaly along with its relevant clinical implications.

Case Report

During routine dissection of the knee joint in a separate left lower limb of an adult cadaver of unknown age and gender, multiple AHMM insertions were noticed. The AHMM is normally attached to the intercondylar region of the tibia in a position just anterior to the anterior cruciate ligament (ACL) insertion site. This attachment was wider and stronger than the usual one and measured about 28 mm in length. The anterior horn was then split into two bands. The posterior band or AMMFL is extended, parallel to, and independent of the ACL. The AMMFL was approximately 35 mm and attached to the posterolateral wall of the intercondylar notch of the femur at a position anterior to the ACL insertion site. The other anterior band was 30 mm long and 4 mm wide and extended as a thick transverse ligament (TL). This band connected the AHMM to the anterior horn of the lateral meniscus. The posterior horn of the MM was also hypertrophied as shown in Figure 1. The AMMFL was dissected and then studied histologically.

How to cite this article: Assiri WM, El Fouhil AF, Alyahya KI, Atteya M. Triple anterior horn insertion of the medial meniscus combined with posterior horn hypertrophy: A Rare case and brief literature review. J Anat Soc India 2024;73:187-9.

Article Info

Received: 11 December 2023
Revised: 15 April 2024
Accepted: 29 April 2024
Available online: 27 June 2024

Address for correspondence:
Prof. Ahmed Fathalla Ibrahim El Fouhil, Department of Anatomy, College of Medicine, King Saud University, Riyadh 11461, Saudi Arabia. E-mail: ahmedfathala@gmail.com

Access this article online

Website: https://journals.lww.com/joai
DOI: 10.4103/jasi.jasi_130_23
Quick Response Code:

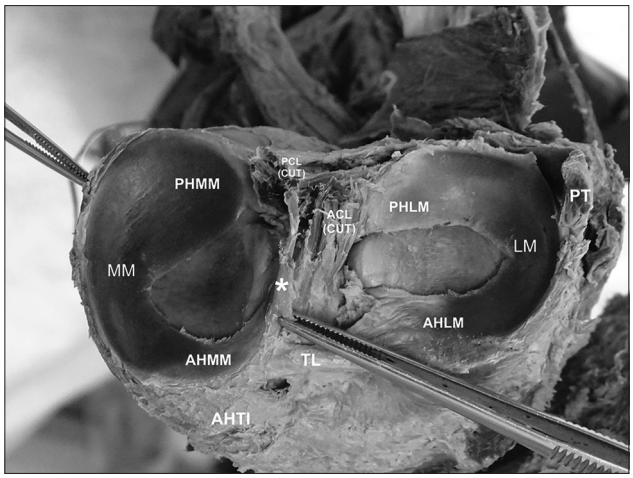

Figure 1: Top view of the proximal tibia with the femur removed. The anterior horn of the medial meniscus (AHMM) is attached to the intercondylar area of the tibia. The anterior horn of the medial meniscus is split into: the anteromedial meniscofemoral ligament (asterisk), anterior to the anterior cruciate ligament (ACL), and to the transverse ligament (TL). Notice the hypertrophy of the posterior horn of the medial meniscus (PHMM). MM: Medial meniscus; LM: lateral meniscus; AHMM: anterior horn tibial insertion; PCL: posterior cruciate ligament; PHLM: posterior horn of lateral meniscus; AHLM: anterior horn of lateral meniscus; PT: popliteus tendon; AHTI: Anterior horn tibial insertion

Samples were collected from the proximal and distal parts of this ligament. Regular dense parallel bundles of collagen fibers were separated by loose connective tissue in which many fibroblasts were observed in the proximal part [Figure 2]. In the distal part, the bundles of collagen fibers were separated by rows of chondrocytes enclosed in their lacunae [Figure 3].

Discussion

The AHMM is firmly and securely attached to the anterior intercondylar area of the tibial plateau, anterior to the tibial insertion of the ACL.[5] However, some variations regarding the insertion site of the AHMM exist. According to Berlet and Fowler,[6] the AHMM can be inserted either into a flat intercondylar area of the tibial plateau, into a downward slope from the medial articular plateau to the intercondylar region, into the tibial plateau anterior slope, or with no firm bony insertion. Based on studies conducted by Ohkoshi *et al*.[7] it was found that AHMM may have no bony attachment; however, the AHMM may be attached to the TL, the ACL, the coronary ligament, or the infrapatellar synovial fold in order of prevalence. In addition, McCormack and McGrath,[8] described for the first time that the AMMFL connecting the AHMM to the posterolateral wall of the femoral intercondylar notch. This ligament runs anterior to the ACL and has no bony attachment to the tibia plateau. In the present case, the AHMM has a standard tibial attachment to the intercondylar area in a position anterior to the ACL, the anterior horn then splits into two ligamentous bands. One of them extended anteriorly to continue as the TL that connected the AHMM to the anterior horn of

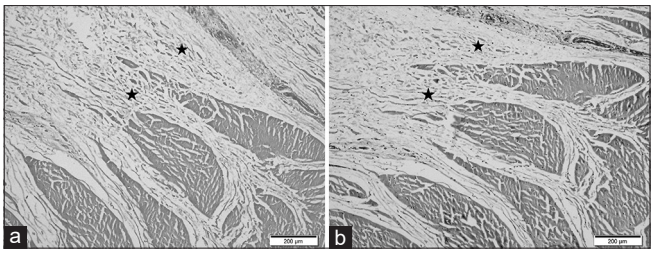

Figure 2: Histological sections through (a and b) Proximal attachment of the anteromedial meniscofemoral ligament (to the femur) showing collagen bundles interspersed with parallel rows of fibroblasts, typical of a ligamentous tissue structure, and separated by bands of loose fibrous connective tissue (asterisks). (a: H and E,; b: Masson's trichrome stain; scale bars, 200 μm)

the lateral meniscus. The other band emerged from the posterior aspect of the AHMM and was attached to the posterolateral wall of the femoral intercondylar notch. This band was similar to that described by McCormack and McGrath.[8] Thus, it was named the AMMFL. While this anomaly shared a portion of the synovial membrane with ACL, the AMMFL was gradually converted into a separate bundle of ligamentous tissue, which was clearly distinct from the ACL. Compared to the ACL, the AMMFL was shorter, thinner, oriented horizontally rather than vertically, and continuous with the anterior root of MM. The histological structure of AMMFL has been previously studied, but most of the studies focused on the ligamentous core and not on the proximal and distal ends. Several authors describe the AMMFL as a completely fibrocartilaginous structure resembling the meniscus.[9-11] In the present study, the proximal part of AMMFL was attached to the posterolateral wall of the intercondylar notch of the femur and contained parallel collagen bundles separated by loose connective tissue with many fibroblasts, which is typical of ligamentous tissue. Its distal part emerged from the AHMM and showed a gradual change into a fibrocartilaginous structure similar to MM as characterized by the presence of collagen bundles separated by rows of chondrocytes in their lacunae. Previous studies reported that AMMFL is an anatomical anomaly that occurs when the AHMM is not attached to the tibia and confirmed the rarity of the existence of multiple insertions of AHMM whenever it is attached to the tibia.[3,7] In the current case, the presence of tibial attachment of AHMM associated with AMMFL and TL contradicts those reports. However, the current case is the first to report multiple AHMM insertions. It is uncertain whether abnormal meniscus insertions that run to either the ACL or intercondylar notch are relevant to meniscus injuries. Some authors reported that anomalies of AHMM may cause anterior knee pain and increase the risk of injury to the meniscus.[3,6,7] Santi and Richardson[12] explained that the mechanical impingement of the AMMFL against the femoral condyle during knee extension could be the reason for anterior knee pain. In our opinion, multiple insertions of AHMM

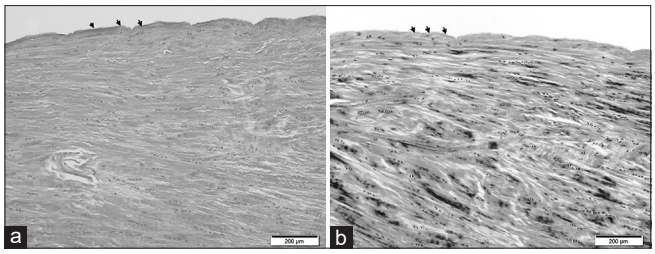

Figure 3: Histological sections through (a and b) Distal attachment of the anteromedial meniscofemoral ligament (to the anterior horn of the medial meniscus) showing collagen bundles interspersed with parallel rows of chondrocytes in their lacunae, typical of a fibrocartilaginous structure, and covered with a synovial membrane (arrow), compatible with medial meniscus tissue. (a: H and E,; b: Masson's trichrome stain; scale bars, 200 μm)

might further restrict the movement of MM. Considering its ligamentous nature, Anderson *et al*.[13] suggested that the AMMFL anchors the AHMM. Therefore, when an external force acts suddenly on the knee, the MM fails to coordinate with the femoral condyle, leading to a meniscus injury.[14,15] In general, abnormalities at AHMM insertions are asymptomatic. They are normally found incidentally during knee arthroscopic procedures or imaging following routine tests for other reasons. The treatment of AMMFL should be chosen according to the pain severity and clinical condition.[6,13,15] Chen *et al*.[4] reported that if no symptoms related to an anomalous AHMM insertion are present, no need for special treatment exists. Finally, this report presents a case of multiple AHMM insertions with posterior horn hypertrophy, which has not been reported previously. The report also provides the first histological description of AMMFL. Anomalies of AHMM are extremely rare, but they should be considered during diagnostic procedures to avoid misdiagnosis.

Financial support and sponsorship

Nil.

Conflicts of interest

There are no conflicts of interest.

References

1. Twyman RS, Ferris BD. Congenital hypoplasia of the medial meniscus: A report of two cases. Arthroscopy 1991;7:148-50.
2. Yang X, Shao D. Bilateral discoid medial Meniscus: Two case reports. Medicine (Baltimore) 2019;98:e15182.
3. Kim YM, Joo YB. Anteromedial meniscofemoral ligament of the anterior horn of the medial meniscus: Clinical, magnetic resonance imaging, and arthroscopic features. Arthroscopy 2018;34:1590-600.
4. Chen P, Huang P, Ren Y, Jiang G, Zhang W, Zhang X. Anomalous insertion of the anterior horn of the medial meniscus combined with anterior horn hypertrophy and a synovial cyst: Case report and literature review. J Int Med Res 2021;49:0300060520981538. [doi: 10.1177/0300060520981538].
5. Fox AJ, Bedi A, Rodeo SA. The basic science of human knee menisci: Structure, composition, and function. Sports Health 2012;4:340-51.
6. Berlet GC, Fowler PJ. The anterior horn of the medical meniscus. An anatomic study of its insertion. Am J Sports Med 1998;26:540-3.
7. Ohkoshi Y, Takeuchi T, Inoue C, Hashimoto T, Shigenobu K, Yamane S. Arthroscopic studies of variants of the anterior horn of the medical meniscus. Arthroscopy 1997;13:725-30.
8. McCormack D, McGrath J. Antero-medial menisco-femoral ligament. Clin Anat 1992;5:485-7.
9. Shea KG, Westin C, West J. Anomalous insertion of the medial meniscus of the knee. A case report. J Bone Joint Surg Am 1995;77:1894-6.
10. Coulier B, Himmer O. Anteromedial meniscofemoral ligament of the knee: CT and MR features in 3 cases. JBR-BTR 2008;91:240-4.
11. Nakajima T, Nabeshima Y, Fujii H, Ozaki A, Muratsu H, Yoshiya S. Symptomatic anomalous insertion of the medial meniscus. Arthroscopy 2005;21:629.
12. Santi MD, Richardson AB. Bilaterally painful anomalous insertion of the medial meniscus in a volleyball player with Marfanoid features. Arthroscopy 1993;9:217-9.
13. Anderson AF, Awh MH, Anderson CN. The anterior meniscofemoral ligament of the medial meniscus: Case series. Am J Sports Med 2004;32:1035-40.
14. Soejima T, Murakami H, Tanaka N, Nagata K. Anteromedial meniscofemoral ligament. Arthroscopy 2003;19:90-5.
15. Arjun S, Takahashi S, Tang Y, Nakane N, Yonemitsu H. MR appearance of anomalous insertion of the medial meniscus. A case report. Acta Radiol 1998;39:554-6.

The Editorial Process

A manuscript will be reviewed for possible publication with the understanding that it is being submitted to Journal of the Anatomical Society of India alone at that point in time and has not been published anywhere, simultaneously submitted, or already accepted for publication elsewhere. The journal expects that authors would authorize one of them to correspond with the Journal for all matters related to the manuscript. All manuscripts received are duly acknowledged. On submission, editors review all submitted manuscripts initially for suitability for formal review. Manuscripts with insufficient originality, serious scientific or technical flaws, or lack of a significant message are rejected before proceeding for formal peer-review. Manuscripts that are unlikely to be of interest to the Journal of the Anatomical Society of India readers are also liable to be rejected at this stage itself.

Manuscripts that are found suitable for publication in Journal of the Anatomical Society of India are sent to two or more expert reviewers. During submission, the contributor is requested to provide names of two or three qualified reviewers who have had experience in the subject of the submitted manuscript, but this is not mandatory. The reviewers should not be affiliated with the same institutes as the contributor/s. However, the selection of these reviewers is at the sole discretion of the editor. The journal follows a double-blind review process, wherein the reviewers and authors are unaware of each other's identity. Every manuscript is also assigned to a member of the editorial team, who based on the comments from the reviewers takes a final decision on the manuscript. The comments and suggestions (acceptance/ rejection/ amendments in manuscript) received from reviewers are conveyed to the corresponding author. If required, the author is requested to provide a point by point response to reviewers' comments and submit a revised version of the manuscript. This process is repeated till reviewers and editors are satisfied with the manuscript.

Manuscripts accepted for publication are copy edited for grammar, punctuation, print style, and format. Page proofs are sent to the corresponding author. The corresponding author is expected to return the corrected proofs within three days. It may not be possible to incorporate corrections received after that period. The whole process of submission of the manuscript to final decision and sending and receiving proofs is completed online. To achieve faster and greater dissemination of knowledge and information, the journal publishes articles online as 'Ahead of Print' immediately on acceptance.

Clinical trial registry

Journal of the Anatomical Society of India favors registration of clinical trials and is a signatory to the Statement on publishing clinical trials in Indian biomedical journals. Journal of the Anatomical Society of India would publish clinical trials that have been registered with a clinical trial registry that allows free online access to public. Registration in the following trial registers is acceptable: http://www.ctri.in/; http://www.actr.org.au/; http://www.clinicaltrials.gov/; http://isrctn.org/; http://www.trialregister.nl/trialreg/index.asp; and http://www.umin.ac.jp/ctr. This is applicable to clinical trials that have begun enrollment of subjects in or after June 2008. Clinical trials that have commenced enrollment of subjects prior to June 2008 would be considered for publication in Journal of the Anatomical Society of India only if they have been registered retrospectively with clinical trial registry that allows unhindered online access to public without charging any fees.

Authorship Criteria

Authorship credit should be based only on substantial contributions to each of the three components mentioned below:

1. Concept and design of study or acquisition of data or analysis and interpretation of data;
2. Drafting the article or revising it critically for important intellectual content; and
3. Final approval of the version to be published.

Participation solely in the acquisition of funding or the collection of data does not justify authorship. General supervision of the research group is not sufficient for authorship. Each contributor should have participated sufficiently in the work to take public responsibility for appropriate portions of the content of the manuscript. The order of naming the contributors should be based on the relative contribution of the contributor towards the study and writing the manuscript. Once submitted the order cannot be changed without written consent of all the contributors. The journal prescribes a maximum number of authors for manuscripts depending upon the type of manuscript, its scope and number of institutions involved (vide infra). The authors should provide a justification, if the number of authors exceeds these limits.

Contribution Details

Contributors should provide a description of contributions made by each of them towards the manuscript. Description should be divided in following categories, as applicable: concept, design, definition of intellectual content, literature search, clinical studies, experimental studies, data acquisition, data analysis, statistical analysis, manuscript preparation, manuscript editing and manuscript review. Authors' contributions will be printed along with the article. One or more author should take responsibility for the integrity of the work as a whole from inception to published article and should be designated as 'guarantor'.

Conflicts of Interest/ Competing Interests

All authors of must disclose any and all conflicts of interest they may have with publication of the manuscript or an institution or product that is mentioned in the manuscript and/or is important to the outcome of the study presented. Authors should also disclose conflict of interest with products that compete with those mentioned in their manuscript.

Submission of Manuscripts

All manuscripts must be submitted on-line through the website https://review.jow.medknow.com/jasi. First time users will have to register at this site. Registration is free but mandatory. Registered authors can keep track of their articles after logging into the site using their user name and password.

- If you experience any problems, please contact the editorial office by e-mail at editor@jasi.org.in

The submitted manuscripts that are not as per the "Instructions to Authors" would be returned to the authors for technical correction, before they undergo editorial/ peer-review. Generally, the manuscript should be submitted in the form of two separate files:

[1] Title Page/First Page File/covering letter:

This file should provide

1. The type of manuscript (original article, case report, review article, Letter to editor, Images, etc.) title of the manuscript, running title, names of all authors/ contributors (with their highest academic degrees, designation and affiliations) and name(s) of department(s) and/ or institution(s) to which the work should be credited, . All information which can reveal your identity should be here. Use text/rtf/doc files. Do not zip the files.
2. The total number of pages, total number of photographs and word counts separately for abstract and for the text (excluding the references, tables and abstract), word counts for introduction + discussion in case of an original article;
3. Source(s) of support in the form of grants, equipment, drugs, or all of these;
4. Acknowledgement, if any. One or more statements should specify 1) contributions that need acknowledging but do not justify authorship, such as general support by a departmental chair; 2) acknowledgments of technical help; and 3) acknowledgments of financial and material support, which should specify the nature of the support. This should be included in the title page of the manuscript and not in the main article file.
5. If the manuscript was presented as part at a meeting, the organization, place, and exact date on which it was read. A full statement to the editor about all submissions and previous reports that might be regarded as redundant publication of the same or very similar work. Any such work should be referred to specifically, and referenced in the new paper. Copies of such material should be included with the submitted paper, to help the editor decide how to handle the matter.
6. Registration number in case of a clinical trial and where it is registered (name of the registry and its URL)
7. Conflicts of Interest of each author/ contributor. A statement of financial or other relationships that might lead to a conflict of interest, if that information is not included in the manuscript itself or in an authors' form
8. Criteria for inclusion in the authors'/ contributors' list
9. A statement that the manuscript has been read and approved by all the authors, that the requirements for authorship as stated earlier in this document have been met, and that each author believes that the manuscript represents honest work, if that information is not provided in another form (see below); and
10. The name, address, e-mail, and telephone number of the corresponding author, who is responsible for communicating with the other authors about revisions and final approval of the proofs, if that information is not included on the manuscript itself.

[2] Blinded Article file: The main text of the article, beginning from Abstract till References (including tables) should be in this file. The file must not contain any mention of the authors' names or initials or the institution at which the study was done or acknowledgements. Page headers/ running title can include the title but not the authors' names. Manuscripts not in compliance with the Journal's blinding policy will be returned to the corresponding author. Use rtf/doc files. Do not zip the files. **Limit the file size to 1 MB.** Do not incorporate images in the file. If file size is large, graphs can be submitted as images separately without incorporating them in the article file to reduce the size of the file. The pages should be numbered consecutively, beginning with the first page of the blinded article file.

[3] Images: Submit good quality color images. **Each image should be less than 2 MB in size.** Size of the image can be reduced by decreasing the actual height and width of the images (keep up to 1600 x 1200 pixels or 5-6 inches). Images can be submitted as jpeg files. Do not zip the files. Legends for the figures/images should be included at the end of the article file.

[4] The contributors' / copyright transfer form (template provided below) has to be submitted in original with the signatures of all the contributors within two weeks of submission via courier, fax or email as a scanned image. Print ready hard copies of the images (one set) or digital images should be sent to the journal office at the time of submitting revised manuscript. High resolution images (up to 5 MB each) can be sent by email.

Contributors' form / copyright transfer form can be submitted online from the authors' area on https://review.jow.medknow.com/jasi.

Preparation of Manuscripts

Manuscripts must be prepared in accordance with "Uniform requirements for Manuscripts submitted to Biomedical Journals" developed by the International Committee of Medical Journal Editors (October 2008). The uniform requirements and specific requirement of Journal of the Anatomical Society of India are summarized below. Before submitting a manuscript, contributors are requested to check for the latest instructions available. Instructions are also available from the website of the journal (www.jasi.org.in) and from the manuscript submission site https://review.jow.medknow.com/jasi.

Journal of the Anatomical Society of India accepts manuscripts written in American English.

Copies of any permission(s)

It is the responsibility of authors/ contributors to obtain permissions for reproducing any copyrighted material. A copy of the permission obtained must accompany the manuscript. Copies of any and all published articles or other manuscripts in preparation or submitted elsewhere that are related to the manuscript must also accompany the manuscript.

Types of Manuscripts

Original articles:

These include randomized controlled trials, intervention studies, studies of screening and diagnostic test, outcome studies, cost effectiveness analyses, case-control series, and surveys with high response rate. The text of original articles amounting to up to 3000 words (excluding Abstract, references and Tables) should be divided into sections with the headings Abstract, Key-words, Introduction, Material and Methods, Results, Discussion and Conclusion, References, Tables and Figure legends.

An abstract should be in a structured format under following heads: **Introduction, Material and Methods, Results,** and **Discussion and Conclusion.**

Introduction: State the purpose and summarize the rationale for the study or observation.

Material and Methods: It should include and describe the following aspects:

Ethics: When reporting studies on human beings, indicate whether the procedures followed were in accordance with the ethical standards of the responsible committee on human experimentation (institutional or regional) and with the Helsinki Declaration of 1975, as revised in 2000 (available at http://www.wma.net/e/policy/17-c_e.html). For prospective studies involving human participants, authors are expected to mention about approval of (regional/ national/ institutional or independent Ethics Committee or Review Board, obtaining informed consent from adult research participants and obtaining assent for children aged over 7 years participating in the trial. The age beyond which assent would be required could vary as per regional and/ or national guidelines. Ensure confidentiality of subjects by desisting from mentioning participants' names, initials or hospital numbers, especially in illustrative material. When reporting experiments on animals, indicate whether the institution's or a national research council's guide for, or any national law on the care and use of laboratory animals was followed. Evidence for approval by a local Ethics Committee (for both human as well as animal studies) must be supplied by the authors on demand. Animal experimental procedures should be as humane as possible and the details of anesthetics and analgesics used should be clearly stated. The ethical standards of experiments must be in accordance with the guidelines provided by the CPCSEA and World Medical Association Declaration of Helsinki on Ethical Principles for Medical Research Involving Humans for studies involving experimental animals and human beings, respectively). The journal will not consider any paper which is ethically unacceptable. A statement on ethics committee permission and ethical practices must be included in all research articles under the 'Materials and Methods' section.

Study design:

Selection and Description of Participants: Describe your selection of the observational or experimental participants (patients or laboratory animals, including controls) clearly, including eligibility and exclusion criteria and a description of the source population. *Technical information*: Identify the methods, apparatus (give the manufacturer›s name and address in parentheses), and procedures in sufficient detail to allow other workers to reproduce the results. Give references to established methods, including statistical methods (see below); provide references and brief descriptions for methods that have been published but are not well known; describe new or substantially modified methods, give reasons for using them, and evaluate their limitations. Identify precisely all drugs and chemicals used, including generic name(s), dose(s), and route(s) of administration.

Reports of randomized clinical trials should present information on all major study elements, including the protocol, assignment of interventions (methods of randomization, concealment of allocation to treatment groups), and the method of masking (blinding), based on the CONSORT Statement (http://www.consort-statement.org).

Reporting Guidelines for Specific Study Designs

Initiative	Type of Study	Source
CONSORT	Randomized controlled trials	http://www.consort-statement.org
STARD	Studies of diagnostic accuracy	http://www.consort-statement.org/stardstatement.htm
QUOROM	Systematic reviews and meta-analyses	http://www.consort- statement.org/Initiatives/MOOSE/moose.pdf statement.org/Initiatives/MOOSE/moose.pdf
STROBE	Observational studies in epidemiology	http://www.strobe-statement.org
MOOSE	Meta-analyses of observational studies in epidemiology	http://www.consort- statement.org/Initiatives/MOOSE/moose.pdf

Statistics: Whenever possible quantify findings and present them with appropriate indicators of measurement error or uncertainty (such as confidence intervals). Authors should report losses to observation (such as, dropouts from a clinical trial). When data are summarized in the Results section, specify the statistical methods used to analyze them. Avoid non-technical uses of technical terms in statistics, such as 'random' (which implies a randomizing device), 'normal', 'significant', 'correlations', and 'sample'. Define statistical terms, abbreviations, and most symbols. Specify the computer software used. Use upper italics (*P* 0.048). For all *P* values include the exact value and not less than 0.05 or 0.001. Mean differences in continuous variables, proportions in categorical variables and relative risks including odds ratios and hazard ratios should be accompanied by their confidence intervals.

Results: Present your results in a logical sequence in the text, tables, and illustrations, giving the main or most important findings first. Do not repeat in the text all the data in the tables or illustrations; emphasize or summarize only important observations. Extra- or supplementary materials and technical detail can be placed in an appendix where it will be accessible but will not interrupt the flow of the text; alternatively, it can be published only in the electronic version of the journal.

When data are summarized in the Results section, give numeric results not only as derivatives (for example, percentages) but also as the absolute numbers from which the derivatives were calculated, and specify the statistical methods used to analyze them. Restrict tables and figures to those needed to explain the argument of the paper and to assess its support. Use graphs as an alternative to tables with many entries; do not duplicate data in graphs and tables. Where scientifically appropriate, analyses of the data by variables such as age and sex should be included.

Discussion: Include summary of *key findings* (primary outcome measures, secondary outcome measures, results as they relate to a prior hypothesis); *Strengths and limitations* of the study (study question, study design, data collection, analysis and interpretation); *Interpretation and implications* in the context of the totality of evidence (is there a systematic review to refer to, if not, could one be reasonably done here and now?, what this study adds to the available evidence, effects on patient care and health policy, possible mechanisms); *Controversies* raised by this study; and *Future research directions* (for this particular research collaboration, underlying mechanisms, clinical research).

Do not repeat in detail data or other material given in the Introduction or the Results section. In particular, contributors should avoid making statements on economic benefits and costs unless their manuscript includes economic data and analyses. Avoid claiming priority and alluding to work that has not been completed. New hypotheses may be stated if needed, however they should be clearly labeled as such. About 30 references can be included. These articles generally should not have more than six authors.

Review Articles:

These are comprehensive review articles on topics related to various fields of Anatomy. The entire manuscript should not exceed 7000 words with no more than 50 references and two authors. Following types of articles can be submitted under this category:

- Newer techniques of dissection and histology
- New methodology in Medical Education
- Review of a current concept

Please note that generally review articles are by invitation only. But unsolicited review articles will be considered for publication on merit basis.

Case reports:

New, interesting and rare cases can be reported. They should be unique, describing a great diagnostic or therapeutic challenge and providing a learning point for the readers. Cases with clinical significance or implications will be given priority. These communications could be of up to 1000 words (excluding Abstract and references) and should have the following headings: Abstract (unstructured), Key-words, Introduction, Case report, Discussion and Conclusion, Reference, Tables and Legends in that order.

The manuscript could be of up to 1000 words (excluding references and abstract) and could be supported with up to 10 references. Case Reports could be authored by up to four authors.

Letter to the Editor:

These should be short and decisive observations. They should preferably be related to articles previously published in the Journal or views expressed in the journal. They should not be preliminary observations that need a later

paper for validation. The letter could have up to 500 words and 5 references. It could be generally authored by not more than four authors.

Book Review: This consists of a critical appraisal of selected books on Anatomy. Potential authors or publishers may submit books, as well as a list of suggested reviewers, to the editorial office. The author/publisher has to pay INR 10,000 per book review.

Other:

Editorial, Guest Editorial, Commentary and Opinion are solicited by the editorial board.

References

References should be *numbered* consecutively in the order in which they are first mentioned in the text (not in alphabetic order). Identify references *in text*, tables, and legends by Arabic numerals in superscript with square bracket after the punctuation *marks. References cited only* in tables or figure legends should be numbered in accordance with the sequence established by the first identification in the text of the particular table or figure. Use the style of the examples below, which are based on the formats used by the NLM *in Index Medicus*. The titles of journals *should be abbreviated* according to the style used in Index Medicus. Use complete name of the journal for non-indexed journals. Avoid using abstracts as references. Information from manuscripts submitted but not accepted should be cited in the text as "unpublished observations" with written permission from the source. Avoid citing a "personal communication" unless it provides essential information not available from a public source, in which case the name of the person and date of communication should be cited in parentheses in the text. The commonly cited types of references are shown here, for other types of references such as newspaper items please refer to ICMJE Guidelines (http://www.icmje.org or http://www.nlm.nih.gov/bsd/uniform_requirements.html).

Articles in Journals

1. Standard journal article (for up to six authors): Parija S C, Ravinder PT, Shariff M. Detection of hydatid antigen in the fluid samples from hydatid cysts by co-agglutination. Trans. R.Soc. Trop. Med. Hyg.1996; 90:255–256.
2. Standard journal article (for more than six authors): List the first six contributors followed by *et al*.

Roddy P, Goiri J, Flevaud L, Palma PP, Morote S, Lima N. *et al*., Field Evaluation of a Rapid Immunochromatographic Assay for Detection of Trypanosoma cruzi Infection by Use of Whole Blood. J. Clin. Microbiol. 2008; 46: 2022-2027.

3. Volume with supplement: Otranto D, Capelli G, Genchi C: Changing distribution patterns of canine vector borne diseases in Italy: leishmaniosis vs. dirofilariosis. Parasites & Vectors 2009; Suppl 1:S2.

Books and Other Monographs

1. Personal author(s): Parija SC. Textbook of Medical Parasitology. 3rd ed. All India Publishers and Distributors. 2008.
2. Editor(s), compiler(s) as author: Garcia LS, Filarial Nematodes In: Garcia LS (editor) Diagnostic Medical Parasitology ASM press Washington DC 2007: pp 319-356.
3. Chapter in a book: Nesheim M C. Ascariasis and human nutrition. In Ascariasis and its prevention and control, D. W. T. Crompton, M. C. Nesbemi, and Z. S. Pawlowski (eds.). Taylor and Francis,London, U.K.1989, pp. 87–100.

Electronic Sources as reference

Journal article on the Internet: Parija SC, Khairnar K. Detection of excretory *Entamoeba histolytica* DNA in the urine, and detection of *E. histolytica* DNA and lectin antigen in the liver abscess pus for the diagnosis of amoebic liver abscess. *BMC Microbiology* 2007, **7**:41. doi:10.1186/1471-2180-7-41. http://www.biomedcentral.com/1471-2180/7/41

Tables

- Tables should be self-explanatory and should not duplicate textual material.
- Tables with more than 10 columns and 25 rows are not acceptable.
- Number tables, in Arabic numerals, consecutively in the order of their first citation in the text and supply a brief title for each.
- Place explanatory matter in footnotes, not in the heading.
- Explain in footnotes all non-standard abbreviations that are used in each table.
- Obtain permission for all fully borrowed, adapted, and modified tables and provide a credit line in the footnote.
- For footnotes use the following symbols, in this sequence: *, †, ‡, §, ‖,¶ , **, ††, ‡‡
- Tables with their legends should be provided at the end of the text after the references. The tables along with their number should be cited at the relevant place in the text

Illustrations (Figures)

- Upload the images in JPEG format. The file size should be within 1024 kb in size while uploading.
- Figures should be numbered consecutively according to the order in which they have been first cited in the text.
- Labels, numbers, and symbols should be clear and of uniform size. The lettering for figures should be large enough to be legible after reduction to fit the width of a printed column.
- Symbols, arrows, or letters used in photomicrographs

should contrast with the background and should be marked neatly with transfer type or by tissue overlay and not by pen.
- Titles and detailed explanations belong in the legends for illustrations not on the illustrations themselves.
- When graphs, scatter-grams or histograms are submitted the numerical data on which they are based should also be supplied.
- The photographs and figures should be trimmed to remove all the unwanted areas.
- If photographs of individuals are used, their pictures must be accompanied by written permission to use the photograph.
- If a figure has been published elsewhere, acknowledge the original source and submit written permission from the copyright holder to reproduce the material. A credit line should appear in the legend for such figures.
- Legends for illustrations: Type or print out legends (maximum 40 words, excluding the credit line) for illustrations using double spacing, with Arabic numerals corresponding to the illustrations. When symbols, arrows, numbers, or letters are used to identify parts of the illustrations, identify and explain each one in the legend. Explain the internal scale (magnification) and identify the method of staining in photomicrographs.
- Final figures for print production: Send sharp, glossy, un-mounted, color photographic prints, with height of 4 inches and width of 6 inches at the time of submitting the revised manuscript. Print outs of digital photographs are not acceptable. If digital images are the only source of images, ensure that the image has minimum resolution of 300 dpi or 1800 x 1600 pixels in TIFF format. Send the images on a CD. Each figure should have a label pasted (avoid use of liquid gum for pasting) on its back indicating the number of the figure, the running title, top of the figure and the legends of the figure. Do not write the contributor/s' name/s. Do not write on the back of figures, scratch, or mark them by using paper clips.
- The Journal reserves the right to crop, rotate, reduce, or enlarge the photographs to an acceptable size.

Protection of Patients' Rights to Privacy

Identifying information should not be published in written descriptions, photographs, sonograms, CT scans, etc., and pedigrees unless the information is essential for scientific purposes and the patient (or parent or guardian, wherever applicable) gives informed consent for publication. Authors should remove patients' names from figures unless they have obtained informed consent from the patients. The journal abides by ICMJE guidelines:

1. Authors, not the journals nor the publisher, need to obtain the patient consent form before the publication and have the form properly archived. The consent forms are not to be uploaded with the cover letter or sent through email to editorial or publisher offices.
2. If the manuscript contains patient images that preclude anonymity, or a description that has obvious indication to the identity of the patient, a statement about obtaining informed patient consent should be indicated in the manuscript.

Sending a revised manuscript

The revised version of the manuscript should be submitted online in a manner similar to that used for submission of the manuscript for the first time. However, there is no need to submit the "First Page" or "Covering Letter" file while submitting a revised version. When submitting a revised manuscript, contributors are requested to include, the 'referees' remarks along with point to point clarification at the beginning in the revised file itself. In addition, they are expected to mark the changes as underlined or colored text in the article.

Reprints and proofs

Journal provides no free printed reprints. Authors can purchase reprints, payment for which should be done at the time of submitting the proofs.

Publication schedule

The journal publishes articles on its website immediately on acceptance and follows a 'continuous publication' schedule. Articles are compiled in issues for 'print on demand' quarterly.

Copyrights

Checklist

Covering letter

- Signed by all contributors
- Previous publication / presentations mentioned
- Source of funding mentioned
- Conflicts of interest disclosed

Authors

- Last name and given name provided along with Middle name initials (where applicable)
- Author for correspondence, with e-mail address provided
- Number of contributors restricted as per the instructions
- Identity not revealed in paper except title page (e.g. name of the institute in Methods, citing previous study as 'our study', names on figure labels, name of institute in photographs, etc.)

Presentation and format

- Double spacing
- Margins 2.5 cm from all four sides
- Page numbers included at bottom
- Title page contains all the desired information
- Running title provided (not more than 50 characters)
- Abstract page contains the full title of the manuscript
- Abstract provided (structured abstract of 250 words for original articles, unstructured abstracts of about 150 words for all other manuscripts excluding letters to the Editor)
- Key words provided (three or more)
- Introduction of 75-100 words
- Headings in title case (not ALL CAPITALS)
- The references cited in the text should be after punctuation marks, in superscript with square bracket.
- References according to the journal's instructions, punctuation marks checked
- Send the article file without 'Track Changes'

Language and grammar

- Uniformly American English
- Write the full term for each abbreviation at its first use in the title, abstract, keywords and text separately unless it is a standard unit of measure. Numerals from 1 to 10 spelt out
- Numerals at the beginning of the sentence spelt out
- Check the manuscript for spelling, grammar and punctuation errors
- If a brand name is cited, supply the manufacturer's name and address (city and state/country).
- Species names should be in italics

Tables and figures

- No repetition of data in tables and graphs and in text
- Actual numbers from which graphs drawn, provided
- Figures necessary and of good quality (colour)
- Table and figure numbers in Arabic letters (not Roman)
- Labels pasted on back of the photographs (no names written)
- Figure legends provided (not more than 40 words)
- Patients' privacy maintained (if not permission taken)
- Credit note for borrowed figures/tables provided
- Write the full term for each abbreviation used in the table as a footnote

Journal of
The Anatomical Society of India

Salient Features:

- Publishes research articles related to all aspects of Anatomy and Allied medical/surgical sciences.
- Pre-Publication Peer Review and Post-Publication Peer Review
- Online Manuscript Submission System
- Selection of articles on the basis of MRS system
- Eminent academicians across the globe as the Editorial board members
- Electronic Table of Contents alerts
- Available in both online and print form.

The journal is registered with the following abstracting partners:
Baidu Scholar, CNKI (China National Knowledge Infrastructure), EBSCO Publishing's Electronic Databases, Ex Libris – Primo Central, Google Scholar, Hinari, Infotrieve, Netherlands ISSN center, ProQuest, TdNet, Wanfang Data

The journal is indexed with, or included in, the following:
SCOPUS, Science Citation Index Expanded, IndMed, MedInd, Scimago Journal Ranking, Emerging Sources Citation Index.

Impact Factor® as reported in the 2022 Journal Citation Reports® (Clarivate Analytics, 2023): 0.4

Editorial Office:
Dr. Vishram Singh, Editor-in-Chief, JASI
B5/3 Hahnemann Enclave, Plot No. 40, Sector 6,
Dwarka Phase – 2, New Delhi - 110 075, India.
Email: editorjasi@gmail.com
(O) | Website: www.asiindia.in

The journal is owned and run by The Anatomical Society of India